# Cell Journal (Yakhteh)

**Guide for Authors**

**Aims and Scope: The "Cell Journal (Yakhteh)"** is a peer review and monthly English publication of Royan Institute of Iran. The aim of the journal is to disseminate information through publishing the most recent scientific research studies on exclusively Cellular, Molecular and other related topics. **Cell J**, has been certified by the Ministry of Culture and Islamic Guidance since 1999 and also accredited as a scientific and research journal by HBI (Health and Biomedical Information) Journal Accreditation Commission since 2000 which is an open access journal. **This journal holds the membership of the Committee on Publication Ethics (COPE).**

## 1. Types of articles

The articles in the field of Cellular and Molecular can be considered for publications in **Cell J.** These articles are as below:

### A. Original articles

Original articles are scientific reports of the original research studies. The article consists of English Abstract (structured), Introduction, Materials and Methods, Results, Discussion, Conclusion, Acknowledgements, Author's Contributions, and References **(Up to 40).**

### B. Review articles

Review articles are the articles written by well experienced authors and those who have excellence in the related fields. The corresponding author of the review article must be one of the authors of at least three published articles appearing in the references. The review article consists of English Abstract (unstructured), Introduction, Conclusion, Author's Contributions, and References **(Up to 70).**

### C. Systematic Reviews

Systematic reviews are a type of literature review that collect and critically analyzes multiple research studies or papers. The Systematic reviews consist of English Abstract (unstructured), Introduction, Materials and Methods, Results, Discussion, Conclusion, Acknowledgements, Author's Contributions, and References **(Up to 70).**

### D. Short communications

Short communications are articles containing new findings. Submissions should be brief reports of ongoing researches. The short communication consists of English Abstract (unstructured), the body of the manuscript (should not hold heading or subheading), Acknowledgements, Author's Contributions, and References **(Up to 30).**

### E. Case reports

Case reports are short discussions of a case or case series with unique features not previously described which make an important teaching point or scientific observation. They may describe novel techniques or use equipment, or new information on diseases of importance. It consists of English Abstracts (Unstructured), Introduction, Case Report, Discussion, Acknowledgements, Author's Contributions, and References **(Up to 30).**

### F. Editorial

Editorials are articles should be written in relevant and new data of journals' filed by either the editor in chief or the editorial board.

### G. Imaging in biology

Images in biology should focus on a single case with an interesting illustration such as a photograph, histological specimen or investigation. Color images are welcomed. The text should be brief and informative.

### H. Letter to the editors

Letter to the editors are in response to previously published **Cell J** articles, and may also include interesting cases that do not meet the requirement of being truly exceptional, as well as other brief technical or clinical notes of general interest.

### I. Debate

Debates are articles which show a discussion of the positive and negative view of the author concerning all aspect of the issue relevant to scientific research.

## 2. Submission process

It is recommended to see the guidelines for reporting different kinds of manuscripts. This guide explains how to prepare the

manuscript for submission. Before submitting, we suggest authors to familiarize themselves with **Cell J** format and content by reading the journal via the website (www.celljournal.com). The corresponding author ensures that all authors are included in the author list and agree with its order, and they must be aware of the manuscript submission.

**A. Author contributions statements**

It is essential for authors to include a statement of responsibility in the manuscript that specifies the contribution of every one of them. This participation must include conception and design of the manuscript, data acquisition or data analysis and interpretation, drafting of the manuscript and/or revising it for critically important intellectual content, revision and final approval of the manuscript and statistical analysis, obtaining funding, administrative, technical, or material support, or supervision. Authors who do not meet the above criteria should be acknowledged in the **Acknowledgments section.**

**B. Cover letter and copyright**

Each manuscript should be accompanied by a cover letter, signed by all authors specifying the following statement: "The manuscript has been seen and approved by all authors and is not under active consideration for publication. It has neither been accepted for publication nor published in another journal fully or partially (except in abstract form). **Also, no manuscript would be accepted in case it has been pre-printed or submitted to other websites.** I hereby assign the copyright of the enclosed manuscript to **Cell J.**" Corresponding author must confirm the proof of the manuscript before online publishing. Also, it is needed to suggest three peer reviewers in the field of their manuscript.

**C. Manuscript preparation**

Authors whose first language is not English encouraged to consult a native English speaker in order to confirm his manuscripts to American or British (not a mixture) English usage and grammar. It is necessary to mention that we will check the plagiarism of your manuscript by iThenticate Software. The manuscript should be prepared in accordance with the "International Committee of Medical Journal Editors (ICMJE)". Please send your manuscript in two formats word and PDF (including: title, name of all the authors with their degree, abstract, full text, references, tables and figures) and also send tables and figures separately in the site. The abstract and text pages should have consecutive line numbers in the left margin beginning with the title page and continuing through the last page of the written text. Each abbreviation must be defined in the abstract and text when they are mentioned for the first time. Avoid using abbreviation in the title. Please use the international and standard abbreviations and symbols

It should be added that an essential step toward the integration and linking of scientific information reported in published literature is using standardized nomenclature in all fields of science and medicine. Species names must be italicized (*e.g., Homo sapiens*) and also the full genus and species written out in full, both in the title of the manuscript and at the first mention of an organism in a paper.

It is necessary to mention that genes, mutations, genotypes, and alleles must be indicated in italics. Please use the recommended name by consulting the appropriate genetic nomenclature database, e.g., HUGO for human genes. In another words; if it is a human gene, you must write all the letters in capital and italic (*e.g., OCT4, c-MYC*). If not, only write the first letter in capital and italic (*e.g., Oct4, c-Myc*). **In addition, protein designations are the same as the gene symbol but are not italicized.**

**Of note, Cell J** will only consider publishing genetic association study papers that are novel and statistically robust. Authors are advised to adhere to the recommendations outlined in the STREGA statement (http://www.strega-statement.org). The following criteria must be met for all submissions:

1. Hardy-Weinberg Equilibrium (HWE) calculations must be carried out and reported along with the P-values if applicable [see Namipashaki et al. 2015 (Cell J, Vol 17, N 2, Pages: 187-192) for a discussion].

2. Linkage disequilibrium (LD) structure between SNPs (if multiple SNPs are reported) must be presented.

3. Appropriate multiple testing correction (if multiple independent SNPs are reported) must be included.

Submissions that fail to meet the above criteria will be rejected before being sent out for review.

Each of the following manuscript components should begin in the following sequence:

**Authors' names** and order of them must be carefully considered (full name(s), highest awarded academic degree(s), email(s), and institutional affiliation(s) of all the authors in English. Also, you must send mobile number and full postal address of the corresponding author).

**Changes to Authorship** such as addition, deletion or rearrangement of author names must be made only before the manuscript has been accepted in the case of approving by the journal editor. In this case, the corresponding author must explain the reason of changing and confirm them (which has been signed by all authors of the manuscript). If the manuscript has already been published in an online issue, an erratum is needed.

**Title** is providing the full title of the research (do not use abbreviations in title).

**Running title** is providing a maximum of 7 words (no more than 50 characters).

**Abstract** must include Objective, Materials and Methods, Results, and Conclusion (no more than 300 words).

**Keywords,** three to five, must be supplied by the authors at the foot of the abstract chosen from the Medical Subject Heading (MeSH). Therefore; they must be specific and relevant to the paper.

The following components should be identified after the abstract:

**Introduction:** The Introduction should provide a brief background to the subject of the paper, explain the importance of the study, and state a precise study question or purpose.

**Materials and Methods:** It includes the exact methods or observations of experiments. If an apparatus is used, its manufacturer's name and address should be stipulated in parenthesis. If the method is established, give reference but if the method is new, give enough information so that another author can perform it. If a drug is used, its generic name, dose, and route of administration must be given. Standard units of measurements and chemical symbols of elements do not need to be defined.

**Statistical analysis:** Type of study and statistical methods should be mentioned and specified by any general computer program used.

**Ethical considerations*:*** Please state that informed consent was obtained from all human adult participants and from the parents or legal guardians of minors and include the name of the appropriate institutional review board that approved the project. It is necessary to indicate in the text that the maintenance and care of experimental animals complies with National Institutes of Health guidelines for the humane use of laboratory animals, or those of your Institute or agency.

**Clinical trial registration:** All of the Clinical Trials performing in Iran must be registered in Iranian Registry of Clinical Trials (www.irct.ir). The clinical trials performed abroad, could be considered for publication if they register in a registration site approved by WHO or www.clinicaltrials.gov. If you are reporting phase II or phase III randomized controlled trials, you must refer to the CONSORT Statement for recommendations to facilitate the complete and transparent reporting of trial findings. Reports that do not conform to the CONSORT guidelines may need to be revised before peer-reviewing.

**Results:** They must be presented in the form of text, tables, and figures. Take care that the text does not repeat data that are presented in tables and/or figures. Only emphasize and summarize the essential features of the main results. Tables and figures must be numbered consecutively as appeared in the text and should be organized in separate pages at the end of the manuscript while their location should be mentioned in the main text.

**Tables and figures:** If the result of your manuscript is too short, it is better to use the text instead of tables & figures. Tables should have a short descriptive heading above them and also any footnotes. Figure's caption should contain a brief title for the whole figure and continue with a short explanation of each part and also the symbols used (no more than 100 words). All figures must be prepared based on cell journal's guideline in color (no more than 6 Figures and Tables) and also in TIF format with 300 DPI resolution.

**Of Note: Please put the tables & figures of the result in the results section not any other section of the manuscript.**

**Supplementary materials** would be published on the online version of the journal. This material is important to the understanding and interpretation of the report and should not repeat material within the print article. The amount of supplementary material should be limited. Supplementary material should be original and not previously published and will undergo editorial and peer review with the main manuscript. Also, they must be cited in the manuscript text in parentheses, in a similar way as when citing a figure or a table. Provide a caption for each supplementary material submitted.

**Discussion:** It should emphasize the present findings and the variations or similarities with other researches done by other researchers. The detailed results should not be repeated in the discussion again. It must emphasize the new and important aspects of the study.

**Conclusion:** It emphasizes the new and important aspects of the study. All conclusions are justified by the results of the study.

**Acknowledgements:** This part includes a statement thanking those who contributed substantially with work relevant to the study but does not have authorship criteria. It includes those who provided technical help, writing assistance and name of departments that provided only general support. You must mention financial support in the study. Otherwise; write this sentence "There is no financial support in this study".

**Conflict of interest:** Any conflict of interest (financial or otherwise) and sources of financial support must be listed in the Acknowledgements. It includes providers of supplies and services from a commercial organization. Any commercial affiliation must be disclosed, regardless of providing the funding or not.

**Of Note:** If you have already any patent related to the subject of your manuscript, or you are going to apply for such a patent, it must be mentioned in this part.

**References:** The references must be written based on the Vancouver style. Thus the references are cited numerically in the text and listed in the bibliography by the order of their appearance. The titles of journals must be abbreviated according to the style used in the list of Journals Indexed in PubMed. Write surname and initials of all authors when there are six or less. In the case of seven or more authors, the names of the first six authors followed by "et al." must be listed. You can download Endnote file for Journal references style: endnote file

The reference of information must be based on the following order:

**Article:**

Surname(s) and first letter of name &middle name(s) of author(s) .Manuscript title. Journal title (abbr).publication date (year); Volume & Issue: Page number.

Example: Manicardi GC, Bianchi PG, Pantano S, Azzoni P, Bizzaro D, Bianchi U, et al. Presence of endogenous nicks in DNA of ejaculated human spermatozoa and its relationship to chromomycin A3 accessibility. Biol Reprod. 1995; 52(4): 864-867.

**Book:**

Surname(s) and first letter of name & middle name(s) of author(s).Book title. Edition. Publication place: publisher name; publication date (year); Page number.

Example: Edelman CL, Mandle CL. Health promotion throughout the lifespan. 2nd ed. ST Louis: Mosby; 1998; 145-163.

**Chapter of book:**

Surname(s) and first letter of name & middle name(s) of author(s).Chapter title. In: Surname(s) and first letter of name & middle name(s) of editor(s), editors. Book title. Edition. Publication place: publisher name; publication date (year); Page number.

Example: Phillips SJ, Whisnant JP. Hypertension and stroke. In: Laragh JH, Brenner BM, editors. Hypertension: pathophysiology, diagnosis, and management. 2nd ed. New York: Raven Press; 1995; 465-478.

**Abstract book:**

Example: Amini rad O.The antioxidant effect of pomegranate juice on sperm parameters and fertility potential in mice. Cell J. 2008;10 Suppl 1:38.

**Thesis:**

Name of author. Thesis title. Degree. City name. University. Publication date (year).

Example: Eftekhari Yazdi P. Comparison of fragment removal and co-culture with Vero cell monolayers on development of human fragmented embryos. Presented for the Ph.D., Tehran. Tarbiyat Modarres University. 2004.

**Internet references**

**Article:**

Example: Jahanshahi A, Mirnajafi-Zadeh J, Javan M, Mohammad-Zadeh M, Rohani M. Effect of low-frequency stimulation on adenosineA1 and A2A receptors gene expression in dentate gyrus of perforant path kindled rats. Cell J. 2008; 10 (2): 87-92. Available from: http://www.celljournal.org. (20 Oct 2008).

**Book:**

Example: Anderson SC, Poulsen KB. Anderson's electronic atlas of hematology.[CD-ROM]. Philadelphia: Lippincott Williams & Wilkins; 2002.

**D. Proofs** are sent by email as PDF files and should be checked and returned within 72 hours of receipt. It is the authors' responsibility to check that all the text and data as contained in the page proofs are correct and suitable for publication. **We are requested to pay particular attention to author's names and affiliations as it is essential that these details be accurate when the article is published.**

**E. Pay for publication:** Publishing an article in **Cell J** requires Article Processing Charges (APC) that will be billed to the submitting author following the acceptance of an article for publication. For more information please see www.celljournal.org.

**F. Ethics of scientific publication:** Manuscripts that have been published elsewhere with the same intellectual material will refer to duplicate publication. If authors have used their own previously published work or work that is currently under review, as the basis for a submitted manuscript, they are required to cite the previous work and indicate how their submitted manuscript offers novel contributions beyond those of the previous work. Research and publication misconduct is considered a serious breach of ethics.

The Journal systematically employs iThenticate, plagiarism detection and prevention software designed to ensure the originality of written work before publication. Plagiarism of text from a previously published manuscript by the same or another author is a serious publication offence. Some parts of text may be used, only where the source of the quoted material is clearly acknowledged.

**3. General information**

**A.** You can send your manuscript via online submission system which is available on our website. If the manuscript is not prepared according to the format of **Cell J**, it will be returned to authors.

**B.** The order of article appearance in the Journal is not demonstrating the scientific characters of the authors.

**C. Cell J** has authority to accept or reject the manuscript.

**D.** The received manuscript will be evaluated by associate editor. **Cell J** uses a single-blind peer review system and if the manuscript suits the journal criteria, we select the reviewers. If three reviewers pass their judgments on the manuscript, it will be presented to the editorial board of **Cell J.** If the editorial board has a positive judgment about the manuscript, reviewers' comments will be presented to the corresponding author (the identification of the reviewers will not be revealed). The executive member of journal will contact the corresponding author directly within 3-4 weeks by email. If authors do not receive any reply from journal office after the specified time, they can contact journal office. Finally, executive manager will respond promptly to authors' request.

**The Final Checklist**

The authors must ensure that before submitting the manuscript for publication, they have to consider the following parts:

**1.** The first page of manuscript should contain title, name of the author/coauthors, their academic qualifications, designation & institutions they are affiliated with, mailing address for future correspondence, email address, phone, and fax number.

**2.** Text of manuscript and References prepared as stated in the "guide for authors" section.

**3.** Tables should be on a separate page. Figures must be sent in color and also in JPEG (Jpg) format.

**4.** Cover Letter should be uploaded with the signature of all authors.

**5.** An ethical committee letter should be inserted at the end of the cover letter.

***The Editor-in-Chief: Ahmad Hosseini, Ph.D.***

***Cell Journal*** *(Yakhteh)*

***P.O. Box: 16635-148, Iran***

***Tel/Fax: + 98-21-22510895***

***Emails: Celljournal@royaninstitute.org***

***info@celljournal.org***

## IN THE NAME OF GOD

**Dr. Saeed Kazemi Ashtiani**

Gone But not Forgotten

In the memory of the late Director of Royan Institute, Founder of Stem Cells Research in Iran and Chairman of ***Cell Journal*** *(Yakhteh)*. May he rest in peace.


**OWNED:**
Royan Institute, Iranian Academic Center for Education Culture and Research (ACECR)

**CHAIRMAN:**
Hamid Gourabi, Ph.D., (Professor, Royan Institute, Tehran, Iran)

**EDITOR IN CHIEF:**
Ahmad Hosseini, Ph.D., (Professor, Shahid Beheshti Medical University, Tehran, Iran)

**EDITOR ASSOCIATE:**
Saeid Abroun, Ph.D., (Professor, Tarbiat Modares University, Tehran, Iran)

**EDITORIAL BOARD:**
Saeid Abroun, Ph.D., (Professor, Tarbiat Modares University, Tehran, Iran)
Kamran Alimoghadam, M.D.,(Associate Professor, Tehran Medical University, Tehran, Iran)
Alireza Asgari, Ph.D., (Professor, Baghyatallah University, Tehran, Iran)
Mohammad Kazem Aghaee Mazaheri, D.D.S., (Assistant Professor, ACECR, Tehran, Iran)
Mohamadreza Baghaban Eslaminejad, Ph.D., (Professor, Royan Institute, Tehran, Iran)
Gila Behzadi, Ph.D., (Professor, Shahid Beheshti Medical University, Tehran, Iran)
Hossein Baharvand, Ph.D., (Professor, Royan Institute, Tehran, Iran)
Marzieh Ebrahimi, Ph.D., (Professor, Royan Institute, Tehran, Iran)
Mary Familari, Ph.D., (Senior Lecturer, University of Melbourne, Melbourne, Australia)
Hamid Gourabi, Ph.D., (Professor, Royan Institute, Tehran, Iran)
Jurgen Hescheler, M.D., (Professor, Institute of Neurophysiology of University Zu Koln, Germany)
Ghasem Hosseini Salekdeh, Ph.D., (Professor, Agricultural Biotechnology Research Institute, Karaj, Iran)
Esmaiel Jabbari, Ph.D., (Associate Professor, University of South Carolina, Columbia, USA)
Suresh Jesuthasan, Ph.D., (Associate Professor, National University of Singapore, Singapore)
Bahram Kazemi, Ph.D., (Professor, Shahid Beheshti Medical University, Tehran, Iran)
Saadi Khochbin, Ph.D., (Professor, Inserm/Grenoble University, France)
Ali Khademhosseini, Ph.D., (Professor, Harvard Medical School, USA)
Kun Ping Lu, M.D., Ph.D., (Professor, Harvard Medical School, Boston, USA)
Navid Manuchehrabadi, Ph.D., (Angio Dynamics, Marlborough, USA)
Hosseinali Mehrani, Ph.D., (Professor, Baghyatallah University, Tehran, Iran)
Marcos Meseguer, Ph.D., (Clinical Embryology Laboratory IVI Valencia, Valencia, Spain)
Seyed Javad Mowla, Ph.D., (Professor, Tarbiat Modares University, Tehran, Iran)
Mohammad Hossein Nasr Esfahani, Ph.D., (Professor, Royan Institute, Tehran, Iran)
Toru Nakano, M.D., Ph.D., (Professor, Osaka University, Osaka, Japan)
Donald Newgreen, Ph.D., (Professor, Murdoch Children Research Institute, Melbourne, Australia)
Mojtaba Rezazadeh Valojerdi, Ph.D., (Professor, Tarbiat Modares University, Tehran, Iran)
Mohammad Hossein Sanati, Ph.D., (Associate Professor, National Institute for Genetic Engineering and Biotechnology, Tehran, Iran)
Eimei Sato, Ph.D., (Professor, Tohoku University, Sendai, Japan)
Andreas Serra, M.D., (Professor, University of Zurich, Zurich, Switzerland)
Abdolhossein Shahverdi, Ph.D., (Professor, Royan Institute, Tehran, Iran)
Michele Catherine Studer, Ph.D., (Institute of Biology Valrose, IBV University of Nice Sophia-Antipolis, France)
Peter Timashev, Ph.D., (Sechenov University, Moscow, Russia)
Daniela Toniolo, Ph.D., (Head, Unit of Common Disorders, San Raffaele Research Institute, Milano, Italy)
Christian van den Bos, Ph.D., Managing Director MARES Ltd, Greven, Germany
Catherine Verfaillie, Ph.D., (Professor, Katholie Universiteit Leuven, Leuven, Belgium)
Gianpaolo Zerbini, M.D., Ph.D., (San Raffaele Scientific Institute, Italy)
Shubing Zhang, Ph.D., ( Associate Professor, Central South University, China)
Daniele Zink, Ph.D., (Institute of Bioengineering and Nanotechnology, Agency for Science Technology & Science, Singapore)

**EXECUTIVE MANAGER:**
Farideh Malekzadeh, M.Sc., (Royan Institute, Tehran, Iran)

**EXECUTIVE BOARD:**
Parvaneh Afsharian, Ph.D., (Royan Institute, Tehran, Iran)
Reza Azimi, B.Sc., (Royan Institute, Tehran, Iran)
Reza Omani-Samani, M.D., (Royan Institute, Tehran, Iran)
Elham Amirchaghmaghi,M.D., Ph.D., (Royan Institute, Tehran, Iran)
Leila Daliri, M.Sc., (Royan Institute, Tehran, Iran)
Mahdi Lotfipanah, M.Sc., (Royan Institute, Tehran, Iran)
Faezeh Shekari, Ph.D., (Royan Institute, Tehran, Iran)

**ENGLISH EDITOR:**
Mitra Amiri Khabooshan, Ph.D., (Monash University, Victoria, Australia)
Sima Binaafar, M. Sc., (Royan Institute, Tehran, Iran)
Saman Eghtesad, Ph.D., (Royan Institute, Tehran, Iran)
Jane Elizabeth Ferrie, Ph.D., (University College of London, London, UK)
Vahid Ezzatizadeh, Ph.D., (Royan Institute, Tehran, Iran)
Kiana Kakavand, Ph.D., (University of Melbourne, Melbourne, Australia)
Farnaz Shapouri, Ph.D., (Memphasys Limited, NSW, Australia)
Kim Vagharfard, M.Sc., (Royan Institute, Tehran, Iran)
Maryam Vatani, M.Sc., (University of Calgary, Canada)

**GRAPHICS:**
Laleh Mirza Ali Shirvani, B.Sc., (Royan Institute, Tehran, Iran)

**PUBLISHED & SPONSORED BY:**
Publication of Royan Institute (ACECR)

**Indexed in:**
1. Thomson Reuters (ISI)
2. PubMed
3. PubMed Central (PMC)
4. National Library Medicine (NLM)
5. Biosis Preview
6. Index Medicus for the Eastern Mediterranean Region (IMEMR)
7. Regional Information Center for Sciences and Technology (RICeST)
8. Index Copernicus International
9. Cambridge Scientific Abstract (CSA)
10. EMBASE
11. Scopus
12. Cinahl Database
13. Google Scholar
14. Chemical Abstract Service (CAS)
15. Proquest
16. Directory of Open Access Journals (DOAJ)
17. Open Academic Journals Index (OAJI)
18. Directory of Research Journals Indexing (DRJI)
19. Scientific Information Database (SID)
20. Iranmedex
21. Islamic World Science Citation Center (ISC)
22. Magiran
23. Science Library Index
24. Biological Abstracts
25. Essential Science Indicators
26. EuroPub

**Copyright and license information:**
The **Cell Journal**$_{(Yakhteh)}$ is an open access journal which means the articles are freely available online for any individual author to download and use the providing address. The journal is licensed under a Creative Commons Attribution-Non Commercial 3.0 Unported License which allows the author(s) to hold the copyright without restrictions that is permitting unrestricted non-commercial use, distribution, and reproduction in any medium provided the original work is properly cited.

**Editorial Office Address (Dr. Ahmad Hosseini):**
Royan Institute, P.O.Box: 16635-148,
Tehran, Iran
Tel & Fax: (+9821)22510895
Website: www.celljournal.org
Emails: info@celljournal.org
celljournal@royaninstitute.org

**Printing Company:**
Naghshe e Johar Co.
No. 103, Fajr alley, Tehranpars Street,
Tehran, Iran.

Cell Journal(Yakhteh), Vol 24, No 7, July 2022, Serial Number: 102, Pages: 353-426

CONTENTS

## Review Article



## Original Articles



## Letter to The Editor

Review Article

# Cell-Free Treatments: A New Generation of Targeted Therapies for Treatment of Ischemic Heart Diseases

**Nahid Daneshi, M.D.[1], Nazila Bahmaie, Ph.D.[2, 3, 4, 5], Abdolreza Esmaeilzadeh, Ph.D.[6, 7, 8*]**

1. School of Medicine, Zanjan University of Medical Sciences, Zanjan, Iran
2. Department of Allergy and Immunology, Faculty of Medicine, Graduate School of Health Science, Near East University, Nicosia, Northern Cyprus, Cyprus
3. Private Baskent Hospital, Nicosia, Northern Cyprus, Cyprus
4. Pediatric Ward, Department of Allergy and Immunology, Near East University Affiliated Hospital, Nicosia, Northern Cyprus, Cyprus
5. Network of Immunity in Infection, Malignancy and Autoimmunity, Universal Scientific Education and Research Network, Tehran, Iran
6. Department of Immunology, School of Medicine, Zanjan University of Medical Sciences, Zanjan, Iran
7. Cancer Gene Therapy Research Centre, Zanjan University of Medical Sciences, Zanjan, Iran
8. Immunotherapy Research and Technology Group, Zanjan University of Medical Sciences, Zanjan, Iran

**Corresponding Address: P.O.Box: 4513956111, Department of Immunology, School of Medicine, Zanjan University of Medical Sciences, Zanjan, Iran*
*Email: a46reza@zums.ac.ir*

**Received: 28/May/2020, Accepted: 22/September/2020**

Abstract

Although recent progress in medicine has substantially reduced cardiovascular diseases (CVDs)-related mortalities, current therapeutics have failed miserably to be beneficial for all patients with CVDs. A wide array of evidence suggests that newly-introduced cell-free treatments (CFTs) have more reliable results in the improvement of cardiac function. The main regeneration activity of CFTs protocols is based on bypassing cells and using paracrine factors. In this article, we aim to compare various stem cell secretomes, a part of a CFTs strategy, to generalize their effective clinical outcomes for patients with CVDs. Data for this review article were collected from 70 published articles (original, review, randomized clinical trials (RCTs), and case reports/series studies done on human and animals) obtained from Cochrane, Science Direct, PubMed, Scopus, Elsevier, and Google Scholar) from 2015 to April 2020 using six keywords. Full-text/full-length articles, abstract, section of book, chapter, and conference papers in English language were included. Studies with irrelevant/insufficient/data, or undefined practical methods were excluded. CFTs approaches involved in growth factors (GFs); gene-based therapies; microRNAs (miRNAs); extracellular vesicles (EVs) [exosomes (EXs) and microvesicles (MVs)]; and conditioned media (CM). EXs and CM have shown more remarkable results than stem cell therapy (SCT). GF-based therapies have useful results as well as side effects like pathologic angiogenesis. Cell source, cell's aging and CM affect secretomes. Genetic manipulation of stem cells can change the secretome's components. Growing progression to end stage heart failure (HF), propounds CFTs as an advantageous method with practical and clinical values for replacement of injured myocardium, and induction of neovascularization. To elucidate the secrets behind amplifying the expansion rate of cells, increasing life-expectancy, and improving quality of life (QOL) for patients with ischemic heart diseases (IHDs), collaboration among cell biologist, basic medical scientists, and cardiologists is highly recommended.

***Keywords:*** Cardiovascular Diseases, Exosomes, Extracellular Vesicles, Gene Therapy, microRNAs

Cell Journal(Yakhteh), Vol 24, No 7, July 2022, Pages: 353-363

**Citation:** Daneshi N, Bahmaie N, Esmaeilzadeh A. Cell-free treatments: a new generation of targeted therapies for treatment of ischemic heart diseases. Cell J. 2022; 24(7): 353-363. doi: 10.22074/cellj.2022.7643.

This open-access article has been published under the terms of the Creative Commons Attribution Non-Commercial 3.0 (CC BY-NC 3.0).

## Introduction

According to the reports of World Health Organization (WHO), cardiovascular diseases (CVDs) have been among the leading causes of death worldwide for the last 15 years. In 2017, they accounted for a combined total of 17.8 million recorded deaths; being expected to exceed 22.2 million deaths by 2030 (1). Current approaches for treatment of ischemic heart diseases (IHDs) include procedures restoring blood flow, pharmacological treatments lessening cardiac remodeling, cardiovascular surgical interventions, and various immunopathophysiological strategies inducing revascularization (2). Unfortunately, current therapeutic strategies only postpone the progression from IHDs to heart failure (HF). In other words, those aforementioned therapeutic approaches lack the ability to completely reverse clinical manifestations in patients with CVDs. Therefore, loss of myocardial tissues with progression to HF remains as a problematic challenge in IHDs treatment (3). Those challenges have encouraged basic medical scientists to make a borderless and integrative collaboration by the usage of interdisciplinary frameworks aimed at seeking for more efficient approaches that are based on cellular and molecular immunopathophysiology which play an indispensable role in the microenvironment of CVDs. Accordingly, stem cell therapy (SCT) is considered as a recent, and promising strategy in myocyte replacement after a myocardial infarction (MI) (4).

In heart tissue regeneration through SCT, wide array of stem cells are used aimed at improving clinical outcomes to increase angiogenesis, decrease pathological cardiac remodeling, increase left ventricular ejection fraction (LVEF), amplify regional contractility, decrease scar tissue and infarct size, improve New York Heart Association (NYHA) classification, and improve quality of life (QOL) for patients with CVDs. However, for improving regenerative functions of an infarcted heart through SCT, there are many unresolved challenges like: selection of an optimal cell

type; possible ambiguities with specification of the cell dose, route and frequency of administration (5, 6); possibility of arrythmogenicity, complex cellular mechanisms of action, and low number of survived stem cells after transplantation in the infarct zone (7). Thus, SCT remains to be determined as the only responsible source for improvement of cardiac function (8). Various cellular and molecular mechanisms have been proposed to justify the immunobiological properties-derived clinical applications of SCT, including: i. differentiation of stem cells into heart muscle cells, ii. differentiation of stem cells into blood cells, iii. paracrine effects; and, iv. cell fusion (7). It has been demonstrated that paracrine mechanisms play indisputable roles for exacerbating the function of stem cells in regenerative medicine for treatment of MI. Paracrine effects, as cell-free treatments (CFTs), have attracted the attention of researchers because of their clinical potentials in heart tissue regeneration (9). In other words, CFTs have shown advantages through paracrine effects in heart regenerative medicine than SCT (10). Not only CFTs-based secretome and paracrine mechanisms can mimic the beneficial effects of SCT, but they also can reduce some of limitations and drawbacks regarding the clinical usages of SCT (8, 11).

In order to design paracrine mechanisms-based therapeutic approaches, properties of different stem cell-derived secretomes and agents influencing components of the secretome are of utmost importance for cell biologists. Optimization of cells obtained from cell culture medium and preparation of clinically-effective cells, are prime examples that should be specified for designation of the most therapeutic strategies in heart regeneration. So, comprehensive knowledge and outstanding understanding on molecular and immunobiological mechanisms of action related to CFTs-based regenerative activities [particularly genetically-remodeling exosomes (EXs)], as well as physiological cardiac remodeling can definitely open promising windows into recovery of the infarcted area, improvement of QOL, and increasing life-expectancy for patients with IHDs. Hence, through more collaborations between physicians, cellular cellular/molecular biologists, and laboratory scientists, preclinical and basic medical studies can simplify translation of laboratory-based data into the clinical settings, decipher secrets of more accurate medical decisions, make optimal clinical outcomes, and increase life-expectancy and QOL for patients with CVDs.

Here, we aim to summarize different mechanisms of action and functional roles of CFTs in research laboratories, highlight the role of data acquired from basic medical sciences, focus on their therapeutic applications for treatment of CVDs, and investigate the proficiency and clinical efficiency of these strategies to improve clinical outcomes for patients with CVDs.

## Types of cell-free treatment

The hypothesis, "main regeneration activities of stem cells are done indirectly through a paracrine manner" is traced back to the proposal for bypassing cells and simultaneous usage of supposedly-paracrine factors (12). Stem cell secretomes are considered as off-the-shelf therapeutic approaches that mitigate safety risks, overcome the risks of occlusion in microvasculature, and refrain from unregulated growth (particularly for administration of large amounts of viable cells). In clinical settings, the promising results acquired from mesenchymal stem cells (MSCs)-derived secretomes are similar to the results from transplantation of MSCs (13, 14).

In the CFTs method, heart tissues are regenerated by collaborative functions of growth factors (GFs), cytokines, microRNAs (miRNAs), involved genes, EXs, microvesicles (MVs), and conditioned media (CM)-derived from stem cells. Their presence in the surrounding tissues leads to the activation of intrinsic repairing mechanisms (15). This secretion regulates several procedures like: myocardial protection, neovascularization, cardiac remodeling, and induction of endogenic cardiac stem cells (CSCs) differentiation (16). Figure 1 lists the regulatory effects of MSCs secretomes in heart regeneration (17, 18).

Conclusively, since heart is not a post-mitotic organ, it seems that there is an imperative need to a comprehensive perception from secretomes and paracrine mechanisms to design new and practical therapeutic approaches aimed at heart tissue regeneration.

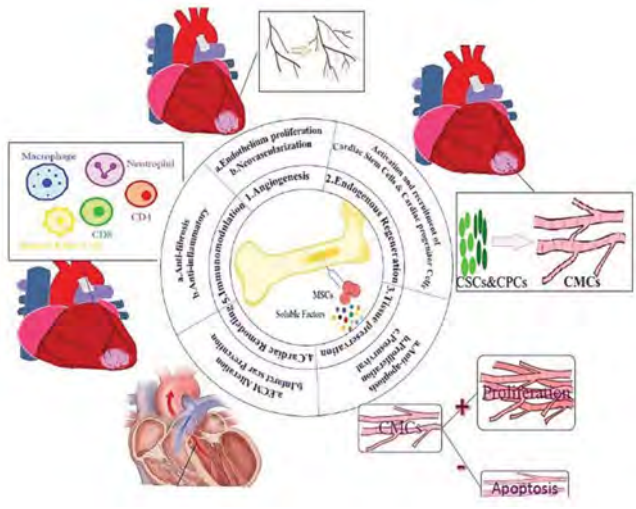


**Fig.1:** The effect of MSCs secretomes in heart tissue regeneration. MSCs secretomes show their regulatory properties through various paracrine processes. CMCs; Cardiomyocytes, CPCs; Cardiac progenitor cells, CSCs; Cardiac stem cells, and MSCs; Mesenchymal stem cells.

## Extracellular vesicles in ischemic heart diseases

Extracellular vesicles (EVs) include EXs and MVs. The components of MVs are 0.1-1 μm in size and they are shed from the cell surface of normal or damaged cells during membrane blebbing. EVs can 'hijack' both membrane components and engulfed cytoplasmic contents. They contain several structural proteins and lipids that are

similar to those in the membranes of the cells from which they are originated. Those EVs also contain intracellular proteins, messenger RNAs (mRNAs), regulatory miRNAs, and intact organelles such as mitochondria (10).

EXs have a diameter of 30-100 nm which are secreted by different cells through the assimilation of multi-vesicular bodies within the plasma membrane. They carry complex of proteins, RNAs and miRNAs, mediating cell signals such as immune responses, cell survival mechanisms, and intercellular communications (19). EXs can be obtained from three groups of cells, including stem cells [MSCs, CSCs, and embryonic stem cells (ESCs)]; mature cells present in heart tissues [cardiomyocytes (CMCs) and fibroblasts]; and from cells exposed to pathological conditions or genetically-modified cells (8). EXs are considered as acceptable therapeutic tools for heart regenerative medicine which are categorized into more functional members compared to MVs and apoptotic bodies. Structurally, the myocardial origin of CMCs-derived EXs is characterized by their specific protein cargo patterns which are affected by the cellular microenvironment. EXs released from cardiosphere derived cells (CDCs) show anti-apoptotic and proliferative properties on CMCs (20). The therapeutic potency of EXs is usually functionalized in the presence of a biologically-relevant protein or RNA in the EXs (21). In a study on a mouse model of ischemia/reperfusion (I/R), intravenous injection of MVs on ischemia had led to reduced myocardial injury, diminished infarct size, and lessened number of apoptotic CMCs which totally improved cardiac function (22).

The origin of EXs affects their biological behaviours in the microenvironment. CDCs-derived EXs with miR-146a in a MI model could improve cardiac function and decrease scar mass (11). Administration of MSCs-derived EXs increased the amount of miR-19a with anti-apoptotic properties in a rat MI model, which played indisputable roles in activation and differentiation of endogenous CSCs in the infarcted heart (8). Table 1 lists the functions of different particles in stem cell-derived Exs and their role in the treatment of IHDs. Table 2 lists a number of EXs that have been recently used in clinical studies on MI models. In addition, the age of the donor cells appears to be effective on the composition of secretomes. Sharma et al. (23) have reported that neonatal cardiac progenitor cells-derived conditioned medium (nCPCs-CM) were more effective than adult CPC-CM (aCPCs-CM). Surprisingly, nCPCs-CM were more effective than neonatal CPCs (nCPCs) and nCPC-EX.

Compared to other cell-based therapies used for heart regeneration, EXs are very stable and preservable. There is no aneuploidy risk, and also the possibility of immune rejections after *in vivo* allogeneic administrations is low (24). Adamiak et al. (25) compared the cardiac reparative capabilities of induced pluripotent stem cells (iPSCs)-derived EXs with iPSCs in a mouse model of reperfused MI. Their results showed that iPSCs-derived EVs induced superior cardiac repair in vivo compared to iPSCs. In their study, injections of iPSCs resulted in teratoma formation, whereas injections of iPSCs-derived EVs were safe. They concluded that iPSCs-EVs represented a feasible, and safer alternative for potential therapeutic applications of EVs in patients with ischemic myocardial damages.

**Table 1:** The function of different EXs and their effective particles in IHDs

| EX-derived cells | EX enriched particles | Function | References |
|---|---|---|---|
| Cardiac endothelial cells | miR-126 and miR-210 | Proangiogenic | (26) |
| CPCs | miR-144 | Cardioprotective | (26) |
| | miR-132, miR-146a, | Proangiogenic | |
| | miR-210 | | |
| | miR-29a | Anti-fibrotic | |
| | miR-132, miR-146a,miR-451, miR-210 | Cardioprotective, post-MI neovascularization, and healing of damaged heart tissues | |
| CDCs | miR-146a | Survival, angiogenesis, and CMCs proliferation | (15) |
| | miR-210, miR-132, miR-146a-3p | Survival | |
| | | Angiogenesis | |
| Sca-1$^{+}$, mouse | miR-451 | Survival | (15) |
| Cardiac myocytes | Hsp60 | Induction of CMCs apoptosis | (27) |
| Hypoxic CMCs | TNF-α | Triggers cell death in other CMCs | (27) |
| iPSCs | miR-21, miR-210 | Cardioprotective | (27) |
| MSCs | miR22 | Anti-apoptotic | (17) |
| | | Improvement of ischemic CMCs injuries | |
| | 20S proteasome subunits (PMSA 1-7) | Cardioprotective | |
| | miR-21 | Anti-apoptotic | (27) |

EX; Exosomes, IHD; Ischemic heart disease, CPCs; Cardiac progenitor cells, CMCs; Cardiomyocytes, MSCs; Mesenchymal stem cells, iPSCs; Induced pluripotent stem cells, and MI; Myocardial infarction.

**Table 2:** Comparison of different EXs used as therapeutic tools for different models of IHDs

| Type of EX | MI model | Outcome | Reference |
|---|---|---|---|
| CPCs-derived EX | Rat | Improved cardiac function, Less profound cardiac apoptosis, ↑ Intracardiac angiogenesis | (26) |
| SHH-containing EVs | Murine | Proangiogenic, anti-apoptotic, and vasculoprotective effects ↓ Infarct size | (26) |
| MSCs-derived EX | MIRI mouse model | Improved CMCs survival ↓ Cardiac fibrosis and apoptosis compared to hearts treated with control EX | (27) |
| MSCs-IPC EX | Mouse | | (27) |
| CDCs EX | Porcine AMI and CMI | ↓Scarring, halted adverse remodeling, improved LVEF | (28) |
| Akt-hucMSC derived EX | Acute MI rat model | Improved cardiac function, Promoted angiogenesis | (29) |
| ESCs derived EX | Acute MI mouse model | Enhanced neovascularization, augmented cardiac function after MI, reduced fibrosis, promoted CPC and myocyte survival and proliferation | (30) |
| iPSCs-derived EX | Reperfused MI in mice | Improved LV function, reduced apoptosis, promoted angiogenesis, attenuated LV hypertrophy, and iPSCs-EX injection was safe. | (25) |

EX; Exosomes, IHD; Ischemic heart disease, CPCs; Cardiac progenitor cells, SHH; Sonic hedgehog, EV; Extracellular vesicles, MSCs; Mesenchymal stem cells, IPC; Ischemic preconditioning, CDC; Cardiosphere derived cells, hucMSCs; Umbilical cord mesenchymal stem cells, iPSC; Induced pluripotent stem cells, ESC; Embryonic stem cells, iPSCs; Induced pluripotent stem cells, MIRI; Myocardial ischemia-reperfusion injury, AMI; Acute myocardial infarction, CMI; Chronic myocardial infarction, MI; Myocardial infarction, CMCs; Cardiomyocytes, and LVEF; Left ventricular ejection fraction.

From cellular aspects, it has been demonstrated that several cellular procedures indicate potential properties in EVs-based therapies aimed at regeneration of an infarcted heart. These aforesaid cellular processes mainly prevent from apoptosis by inducing autophagy via modulation of AMPK/mTOR, Akt/mTOR, and Wnt/β-catenin pathways. Hence, clinical usages of EVs lead to a wide range of improved clinical outcomes like increased survival rate of CMCs in ischemic lesions, neovascularization in the peri-infarcted myocardial zone, restrained pathological remodeling, and regulation of CMCs function (14). All in all, it sounds that cells used in SCT-based approaches now can be genetically altered by GFs, cytokines, and hypoxia-exposed stem cells under pathologic conditions. Eventually, secretomes derived from these genetically-altered stem cells can be used according to the pathophysiological stage of the patients with CVDs and optimized to treat them (10).

## Heart tissues-target therapy with exosomes

Most systemically-injected EXs are accumulated in organs such as the liver, kidneys, lungs, and bone marrow (BM). Despite the high efficacy observed in concentrated and pure doses of infused EXs, the therapeutic potentials of EXs mostly depend on their bio-distribution. Mostly-secreted EXs tend to be less specific to a particular cell type in the cellular microenvironment. EXs are mostly cleared by macrophages within the reticulonodular system, limiting their therapeutic applications in clinical trials. Therefore, the cardioprotective effects and specific/efficient delivery of administered EXs are not well-established (31, 32). To reduce systemic clearance of EXs and increase their numbers, as well as increase tropism of EXs in target tissues, altering the surface of these particles by creating ligands is highly recommended. Those ligands bind EXs to specific molecules or antibodies in target tissues. In an *in vivo* MI study done by Mentkowski and Lang (31), engineered CDCs expressing LAMP2-cardyomyocytes targeting peptide (LAMP2-CMP) on the membranes of secreted Exs, could increase the CMCs endocytosis potential of CDCs (which are originated from EXs). LAMP2, a membrane protein on the EXs surface, was fused to CMP (a CMC specific peptide). Intramyocardial injection of these biologically-engineered EXs showed that they were more likely to be absorbed by CMCs than the non-engineered types. In comparison with the non-engineered types, these engineered CDCs could significantly reduce apoptosis, increase the survival rate of CMCs and induce more cardiac retention.

Tian et al. (33) used cyclo (Arg-Gly-Asp-D-Tyr-Lys) peptide [c(RGDyK)] conjugated EXs, which were called EXs-c(RGDyK) to treat a mouse model of cerebral ischemia. Biologically, c(RGDyK) is a peptide that has a high affinity for binding to integrin $\alpha_v\beta_3$ of cerebrovascular endothelial cells after ischemia. The results of their study showed that intravenous infusion of this engineered EXs strongly suppressed the inflammatory responses, and lowered cell apoptosis in the lesion area of the cerebral ischemia.

As a result, engineered EXs provide a convenient and effective way to transfer therapeutic materials into different tissues. These engineered EXs could be enriched with angiogenic or protective substances to be delivered to specific target organs and tissues such as the heart in order to produce effective angiogenesis and increase CMCs survival for patients with IHDs.

## microRNAs in ischemic heart diseases

As non-coding RNAs, miRNAs are approximately 22 nucleotides in length, mediating regulatory effects on post-transcriptional gene expression (34). They were initially discovered in *Caenorhabditis elegans*

(*C. elegans*) two decades ago (35). miRNAs regulate various biological and physiologic pathways such as differentiation, proliferation, growth, and apoptosis, as well as pathological processes such as cancer, Alzheimer's and CVDs. miRNAs are found in tissues and body fluids such as the blood, urine, saliva, plasma and serum (36). Recently, circulating miRNAs can be used for diagnosis, prognosis, and therapeutic applications for a wide range of disorders. In case of MI, it has been speculated that heart tissue undergoes various pathological and physiological processes such as apoptosis, angiogenesis, tissue perfusion, and fibrosis. Generally, inhibition or activation of several families of miRNAs, including miRNAs-15, miRNAs-21, miRNAs-24, miRNAs-29, miRNAs-34, miRNAs-92a, miRNAs-101, miRNAs-133a, and miRNAs-320 leads to cardiac tissue repair and improved heart function (37, 38).

In terms of CVDs, Wang et al. (39) showed that knockdown of miR-16-5p increased cell viability and angiogenesis in human microvascular endothelial cells (HMVEC), and inhibited cell apoptosis by increasing insulin receptor substrate 1 (IRS1). Zhao et al. (40) tried to clarify the regulatory mechanisms of miR-132 in MI-induced myocardial remodeling. They reported that up-regulation of miR-132 increased LVEF and LV fractional shortening, and inhibited CMCs apoptosis to ameliorate myocardial remodeling through down-regulation of IL-1β.

## Growth factor therapy in ischemic heart diseases

Several GFs and cytokines have been used to treat CVDs in clinical and preclinical studies because of their direct and distinct effects on several cellular functions such as adhesion, proliferation, and migration. GFs can induce regenerative mechanisms that include anti-apoptotic pathways, angiogenic properties, positive remodeling of the ECM, CMCs proliferation, and CSC recruitment. The results of most studies indicate that daily subcutaneous injections of GF might have cardioprotective effects through up-regulation of the Akt pathway, and CPC differentiation (41, 42).

Induction of angiogenesis by GFs during coronary artery occlusion is an important mechanism that protects heart tissues against hypoxemic conditions. The process of angiogenesis is regulated by a various GFs, such as vascular endothelial growth factor (VEGF), fibroblast growth factor-2 (FGF-2), and platelet-derived growth factor (PDGF). VEGF is a major initiator of angiogenesis and recruitment factor for endothelial cells; FGF-2 is a mitogen of various cell types, recruitment factor for pericytes, and a producer of the ECM. PDGF is a recruitment factor for smooth muscle cells and a maturation factor for new vessels, playing an important role in angiogenic processes. As a result, these processes lead the microenvironment toward increased tissue perfusion, reduced inflammation and fibrosis, and ultimate improvement in heart muscle performance (41, 42).

Several GFs have been used to treat CVDs. Thavapalachandran et al. (43) in their experimental study evaluated the therapeutic effects of recombinant human platelet-derived growth factor-AB (rhPDGF-AB) protein in a clinically-relevant porcine model of myocardial ischemia-reperfusion injury (MIRI). They demonstrated that infusion of rhPDGF-AB promoted post-MI cardiac repair by altering the mechanics of the infarcted scar, being resulted in improved LVEF, myocardial contractility, and increased survival rate, as well as decreased ventricular arrhythmias. Furthermore, injection of stromal-derived factor-1 (SDF-1/CXCR4) in the myocardia of patients with IHDs was reported to be a safe and experimentally-feasible approach. Patients who received the highest doses (15 mg and 30 mg) of SDF-1 had shown improvement in QOL, the six-minute walking distance test, and NYHA class (44).

According to the reported side effects due to administration of high or inappropriate dosages of certain cytokine/GFs (like organization of aberrant and perforated vessels, hypotension, and tumour angiogenesis), there is an imperative need for further investigations on the proper clinical usage of GFs and cytokines for treatment of patients with CVDs (18).

## Conditioned media in ischemic heart diseases

As described earlier, secretomes consist of proteins, miRNAs, GFs, anti-oxidants, proteasomes, and EXs secreted by stem cells. Literally, those culture media which are conditioned by secretomes are called CM. A variety of paracrine factors, including VEGF, hepatocyte growth factor (HGF), insulin-like growth factor-1 (IGF-1), IGF-2 and SDF-1, are secreted into the cell culture medium during the cell culture processes. These factors are associated with physiological and pathophysiological processes like cell proliferation, apoptosis, inflammation, neovascularization, MI, angiogenesis, and fibrosis. It is presumed that addition of secretomes to the cell culture media of the damaged organs increases metabolic activities, oxygen supply, and remodeling the ECM in order to ultimately prevent from increased organ damage (45, 46).

In case of CVDs, CM can be used to induce clinically-advantageous effects on target tissues. For example, either CDC-derived CM or MSC-derived CM have the capability to increase the survival potential of CMCs against hypoxia (16, 19). Secretomes are the most functional unit of stem cells and EXs play an indispensable role in improving their therapeutic manifestation; however, Sharma et al. (23) reported that sole administration of EXs does not suffice and CM is needed for maximum clinical benefit. In addition, they reported that division of CM into EXs and EX-free fractions diminishes its capacity to recover myocardial function. MVs and CM derived from stem cells have the same pro-regenerative potentials as infusion of intact cells (10) which can replace the cells in SCT. Fortunately, the allogeneic CM method lacks ethical controversies and immune rejection. Then, it appears to be a perfect, and promising solution for immediate clinical applications with the ability to minimize the amount of surgeries invasiveness (47). Table 3 shows the effects of CMs that are originated from different stem cells in animal models of IHDs.

**Table 3:** Comparison of different CMs for treatment of IHD models

| Source of CM | Animal model | Outcome | Reference |
|---|---|---|---|
| hADSCs | SCID and C57BL/6 mice model of MI | Improved cardiac function<br>↓ Infarct size<br>↑ Reparative angiogenesis<br>↓ CMCs apoptosis (The observed effects of ADSCs application on the first three mentioned outcomes were superior to those reported from ADSC-CM.) | (48) |
| Human STRO-3-mesenchymal precursor cells | Athymic nude rat model of MI | ↑ Ventricular function<br>↓ Ventricular dilatation and infarct size<br>↑ Neovascularization | (48) |
| Human embryonic stem cell-derived MSCs | Porcine model of MI | ↑ Capillary density<br>↓ Infarct size<br>↑ Myocardial performance | (48) |
| Porcine peripheral blood endothelial progenitor cells | Porcine model of MI | ↑ Angiogenesis<br>↑ CMCs remodeling and contractility | (48) |
| Human MSCs | Porcine model of MI | ↑ Myocardial capillary density<br>↓ MI size, and preserved systolic and diastolic performance | (45) |
| SHED-CM | Mouse model of I/R | ↓ MI size<br>↓ Apoptosis<br>↓Inflammatory cytokine levels of TNF-α, IL-6, and IL-β<br>↑ Cardiac function<br>↑Survival of cardiac myocytes in response to hypoxia | (47) |
| nCPCs | Rodent model of MI | ↑ Recovering cardiac function<br>↑ Stimulation of neovascularization<br>↑ Myocardial remodeling | (23) |
| Hypoxic-ADMSCs | Rat model of MI | ↓ Infarct size, apoptosis index, and apoptosis related proteins | (49) |

HD; Ischemic heart disease, CM; Conditioned media, hADSCs; Human adipose tissue-derived stem cells, MSCs; Mesenchymal stem cells, ADMSCs: Adipose tissue-derived mesenchymal stem cells; SHED; Stem cells from human exfoliated deciduous teeth, CPCs; Cardiac progenitor cells, MI; Myocardial infarction, CMCs; Cardiomyocytes, I/R; Ischemia/reperfusion, ESCs; Embryonic stem cells, and nCPCs; Neonatal CPCs.

## Gene therapy in ischemic heart diseases

Although several GFs have been used to stimulate new vessel formation after MI, none of them could achieve significant results in phase I/II clinical trials of heart regeneration. A clinically-acceptable solution to overcome this problematic challenge is gene therapy that shows desired clinical outcomes. To date, plasmids with adenovirus vectors delivering VEGF, FGF and HGF for treatment of patients with severe coronary artery diseases (CADs) and MI have been the focus of investigation in several randomized controlled trials (RCTs). Researchers proposed that the combination

of gene-based therapies with SCT could significantly improve clinical outcomes in heart regeneration medicine (50).

Gene-based therapies are techniques that use biological carriers to simplify the insertion and expression of a therapeutic gene in target cells (51), in order to induce or inhibit synthesis of specific proteins and alter the structure and function of the cells in target tissues (52).

Gene-based therapies mainly refer to the utilization of genetically-altered cells as carriers for the genes and plasmids aimed at transferring these target genes to damaged heart tissues for treatment of patients with IHDs. These genetic changes in cells go back to the fact that they are measured out to increase the expressions of specific genes, GFs, and cytokines, affecting immunobiological processes such as angiogenesis, proliferation and differentiation of CSCs, apoptosis, remodeling, and ventricular function (51, 52).

Various carriers used to transfer the desired genes to the target cells include: i. Plasmid carriers for transportation of naked DNA, ii. Viral vectors such as Adenoviruses, Adeno-associated viruses, Retroviruses, and Lentiviruses (51); and iii. Gene-modified cells (52). Gene-modified cells with the ability to overexpress the transgenes act as transgene carriers, leading to reinforced/desired levels of therapeutic proteins in target tissues (52).

Despite substantial progress in novel therapeutics, there are still several types of disorders especially those which have not an efficient and successful treatment, leading basic medical scientists and clinical specialists toward novel therapeutic strategies like gene-based therapies. For instance, modified BM-MSCs that overexpress *IL-35* gene in an Imiquimod-induced psoriasis-like mouse model will most likely become an effective therapeutic approach for the worldwide problem of psoriasis (53). Lin et al. (54) investigated whether overexpression of the *IGF-1* gene could enhance BM-derived stem cell (BMSC) viability, migration, anti-apoptotic, and protective effects of CMCs in an acute MI (AMI) rat model. They reported that BMSCs that overexpressed *IGF-1* gene called BMSCs-IGF-1 could significantly rescue cardiomyoblasts from hypoxia-induced apoptosis, preserve cell viability under hypoxic conditions and reduce the infarct volume. Su et al. (55) in their study on an AMI rat model, loaded Adenoviruses that carried the *SDF-1α* gene onto microbubble carriers by ultrasound targeted destruction of these microbubbles. The results of their study suggested that ultrasound-mediated transduction of the exogenous *SDF-1α* genes into the AMI rats could effectively promote the homing of endogenous BMSCs into the infarcted heart.

Figure 2 shows a schematic presentation of novel strategies recruited by CFTs aimed at treatment of patients with CVDs.

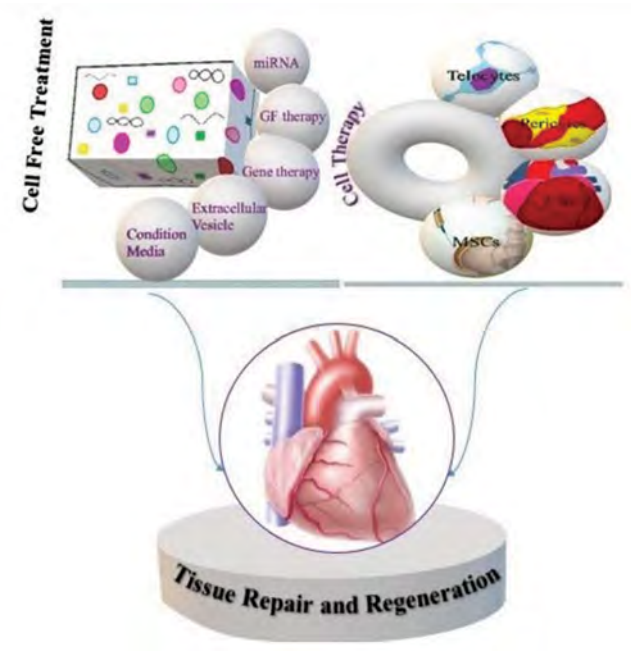


**Fig.2:** Schematic presentation of novel therapeutic strategies for CVDs. CFTs includes GFs, gene-based therapies, miRNAs, EVs, and CM. EX and CM usually have more remarkable results than stem cell therapy. CVDs; Cardiovascular diseases, CFTs; Cell-free treatments, CSCs; Cardiac stem cells, GF; Growth factor, miRNAs; microRNAs, EVs; Extracellular vesicles, EX; Exosomes, CM; Conditioned media, and MSCs; Mesenchymal stem cells.

## Route, time, and dosage of cell-free treatment administration

CFTs-based therapy for heart regeneration is administered by intravenous, intra-arterial, intramuscular, or intramyocardial injections of several recombinant angio-peptides such as VEGF, FGF, and HGF (56). To be more precise, for having an ideal route of administration of CFTs (GFs)-based therapies, time- and dose-dependent function/efficacy of recruited genes can be considered as a major hindrance for heart regeneration. Bauzá et al. (57) investigated whether optimized doses of high mobility group box 1 (HMGB1) would promote angiogenesis signaling, and expression of specific regenerative genes in sheep with acute MI. They reported that intramyocardial injection of high-dose (250 μg) HMGB1 had induced angio/arteriogenesis, reduced the infarct size, and improved LV function two months post-treatment.

Although delivery of angiogenic factors has the potential abilities to stimulate formation of new blood vessels both *in vivo* and *in vitro*, there are some limitations that should not be underestimated. Those limitations include the explosive or uncontrolled release of GFs that leads to high toxicity; decreased half-life of GFs; and elevated cost for purified GFs. One strategy for overcoming these challenges is delivery of the gene of the same factor in the cells for producing the required angiogenic GFs (58). Gene delivery strategies will be discussed in the following paragraphs.

Direct surgical injection, catheter-based intracardiac or intracoronary injections, pericardial delivery, the V-focus system, and surgical delivery strategies are used for

gene transferring and gene delivery to the myocardium. Although there is no unique delivery system or a virus serotype specifically-optimized for cardiac orientation that lacks simultaneous expression in other tissues. The molecular cardiac surgery with recirculating delivery (MCARD) vector-mediated gene is undoubtedly considered as one of the most promising gene transfer systems, providing very high expression levels with low morbidity, diminished immune responses, and minimal simultaneous expression (59).

Selection of the most proper transgenes, the most efficient routes of gene delivery, the type and quality of these recruited vectors for gene-based therapies, and dosage are all determining factors for optimal therapeutic outcomes in gene-based therapies of CVDs (60).

A meta-analysis conducted by Yang et al. (61) for a systematic review of the efficacy of EVs on MI in both small and large animals did not show any significant associations between efficacy and type of stem cells, ligation-to-injection interval, route of delivery, dosage, and follow-up period. However, Liu et al. (62) performed a meta-analysis to systematically review the efficacy of EVs in preclinical acute kidney injury (AKI) rodent models. They reported that the route of delivery, dosage, and cell origin of EVs were independent factors that influenced clinical effects of the EVs. For achieving maximum efficacy without adverse effects in EVs-based therapies, determining the optimal dosage, appropriate time window for administration of EXs, number of repeated dosages, and route of administration are considered as the most important issues to be resolved (63).

## Clinical trials of cell-free treatment in ischemic heart diseases

Effective results acquired from preclinical studies have encouraged scientists to continue experimental studies toward clinical trials. In recent decades, many clinical trials have been conducted aimed at CFTs-based therapies for patients with IHDs. These studies focused on the clinical usages of angiogenic genes such as *VEGF*, *FGF*, *HGF*, developmental endothelial locus-1 (*DEL-1*), and *SDF*. Meng et al. (64) performed intracoronary transplantation of Adenoviruses that carried the *HGF* gene (Ad-*HGF*) in patients with CADs. They concluded that long-term administration of Ad-*HGF* was safe that did not cause any adverse reactions or unwanted clinical manifestations (like tumors, prolonged fever, arrhythmia, and retinal vessel anomalies). The results of their study showed that intracoronary transplantation of Ad-*HGF* efficiently improved echocardiographic EF at the 36-month follow-up compared to the results acquired from baseline levels.

**Table 4:** The most important clinical trials with different GFs and gene therapies in patients with IHDs

| Author and year of publication | Vector or GF | Patients | Outcome measurements | Results |
|---|---|---|---|---|
| Anttila et al. (67), 2020 | Epicardial injection of AZD8601 (VEGF-A165 mRNA formulated in biocompatible citrate-buffered saline and optimized for high-efficiency VEGF-A expression with minimal innate immune response) | 24 patients with stable CADs and moderately decreased LVEF (30%-50%) who were undergoing coronary artery bypass graft surgery | The safety and tolerability of AZ8601, effect of AZD8601 on regional and global stress myocardial blood flow, LV end-diastolic volume, LV end-systolic volume, and LVEF, regional myocardial wall motion, NYHA class, change in troponin T and NT-proBNP levels in six months | Ongoing clinical trial |
| Greenberg et al. (68), 2016 | Intracoronary adeno-associated virus 1 / sarcoplasmic/endoplasmic reticulum $Ca^{2+}$-ATPase | 250 patients who had NYHA class II-IV HF and LVEF≤35% | Time to recurrent events, defined as hospital admission because of HF or ambulatory treatment for worsening HF in 12 months | No evidence of improvement in the clinical course and outcome |
| Chung et al. (69), 2015 | Endomyocardial injection of plasmid SDF-1 | 93 subjects with IHF on stable guideline-based medical therapy and LVEF ≤40% | Safety, efficacy, LV functional and structural measures were assessed | Attenuating LV remodeling and improving EF. Demonstrated safety |
| Penn et al. (70), 2013 | Endomyocardial injection of JVS-100 (a DNA plasmid encoding human SDF-1) | 17 subjects with ischemic cardiomyopathy, NYHA class III HF, and EF ≤40% on stable medical therapy | Major adverse cardiac events, QOL, NYHA class, six-minute walking distance, single photon emission computed tomography, NT-proBNP and safety over 12 months | All of the cohorts demonstrated improvements in six-minute walking distance, QOL, and NYHA class. The primary safety end point was met |

IHD; Ischemic heart disease, GFs; Growth factors, CADs; Coronary artery diseases, NYHA: New York Heart Association, IHF; Ischemic heart failure, NT-proBNP; N-terminal pro b-type natriuretic peptide, HF; Heart failure, QOL; Quality of life, EF; Ejection fraction, LV; Left ventricle, SDF-1; Stromal-derived factor-1, LVEF; Left ventricular ejection fraction, and VEGF-A; Vascular endothelial growth factor A.

Gross et al. (65) conducted a randomized, prospective, double-blind, and placebo-controlled clinical trial (SITAGRAMI) that included 174 patients with acute MI. Participants were treated with placebo (control group) or a 1:1 ratio of granulocyte-colony stimulating factor (G-CSF) plus sitagliptin (case group). The results of their study that included a 4.5 year follow-up, showed no significant differences in the incidence rate of major adverse cardiac and cerebrovascular events (MACCE) between both control and case groups. Treatment with sitagliptin did not have any significant effects on the clinical outcomes of patients with MI.

Kukuła et al. (66) conducted a double-blind clinical trial (NCT00620217) on 52 patients with CADs, who received intramyocardial injections of VEGF-A165/bFGF plasmid into the ischemic regions of the heart tissues. The control group received a placebo plasmid. The results of the 10 year follow-up showed that this vector was also safe and there was no evidence of increase in the prevalence of death or malignancies. They indicated that the incidence of stroke, MI, and cardiovascular-related mortalities were similar between both control and case groups.

Table 4 summarizes the most important clinical trials that used various GFs and gene-based therapies for patients with IHDs.

However, our search results could not find any reasonable clinical usage of EXs, CM, and miRNAs among current clinical trials of EVs for patients with IHDs. Although CFTs-based strategies are promising approaches for treatment of patients with CVDs, more preclinical studies are needed to evaluate the efficacy of CFTs as effective therapeutic approaches for IHDs. These studies should particularly be conducted with large animal models of IHDs, enabling progress toward more efficient and productive clinical trials.

## Conclusion

Despite substantial progress in the prognosis, diagnosis, and treatment of diseases, CVDs-related morbidities and mortalities still remain high. Hence, scientists are encouraged toward more practical methods to obtain better clinical outcomes. In this context, clinical applications of stem cell-derived secretomes as a missing piece in the puzzle of CVDs target therapy can be considered as off-the-shelf methods with controlled and predictable outcomes, decreased adverse effects, and reduced constrains of SCT. Neovascularization, differentiation, and proliferation of new CSCs are significant features that should not be underestimated for heart regenerative medicine, which may provide effective outcomes for treatment of patients with IHDs, and increase LV contractility in patients with HF.

According to the results acquired from current studies, EXs and CM have shown more practical effects among the various types of CFTs, as well as when compared to SCT. The usage of genetically-modified cell culture medium through neonatal cell-derived CM, and the components present in Exs, and CM allow us to expect cost-effective and optimized results for treatment of various clinical stages in CVDs. Despite the successful results acquired from clinical studies done on CVDs models, adverse effects such as hypotension, tumor angiogenesis, severe inflammatory reactions, arrhythmia, off-target responses, and poor gene transfer efficiency have been reported, complicating clinical applications of GF-based therapies in patients with CVDs. Although a myriad of preclinical and laboratory studies have used GFs and gene-based therapies for improvement of cardiovascular performance in patients with IHDs, they have failed to achieve much success in improving cardiac function and halting the MI process.

Totally, due to less adverse effects, CFTs can hopefully pave the way for providing more promising therapeutic approaches for patients with CVDs, reducing IHDs-related mortalities and morbidities rates, as well as diminishing hospitalization expenses for patients and the health system.

CFT, with a broad spectrum of profound regulatory effects on clinical outcomes of patients with CVDs is still in its infancy. Further investigations aimed at elimination of the ambiguities related to the clinical applications of this recently-introduced method are highly recommended for achievement of beneficial effects of CFTs. In order to reach this purpose, additional preclinical and clinical studies, and collaboration among cellular and molecular biologists, clinical laboratory scientists, immunobiologists, gene and cell therapists, clinical specialists, diseases-specific biomarker scientists, cardiologists, medical biotechnologists, and health science coordinators are unquestionably needed.

## Acknowledgements

There are no financial support, and conflicts of interest in this study.

## Authors' Contributions

A.E.; Supervision, project corresponding, and verification of the last version before submission. A.E., N.B.; Contribution to conceptualization, validation, and formal analysis. N.B.; Designation of main methodology, search strategy, academic/scientific/grammatical revision for important intellectual content, preparation, and main designation of the final draft of the manuscript. N.D., N.B.; Major conception, data extraction, and data interpretation. N.D.; Data gathering and preparation of first draft of manuscript, visualization, image/table designation. All of the authors attest to the validity and legitimacy of data, receiving an electronic copy of the final version, and published version of the manuscript.

## References

1. Virani SS, Alonso A, Benjamin EJ, Bittencourt MS, Callaway CW, Carson AP, et al. Heart disease and stroke statistics-2020 update: a report from the american heart association. Circulation. 2020:

141(9): e139-e596.
2. Duan B. Concise review: harnessing iPSC-derived cells for ischemic heart disease treatment. J Transl Int Med. 2020; 8(1): 20-25.
3. Cambria E, Steiger J, Günter J, Bopp A, Wolint P, Hoerstrup SP, et al. Cardiac regenerative medicine: the potential of a new generation of stem cells. Transfus Med Hemother. 2016; 43(4): 275-281.
4. Esmaeilzadeh A, Daneshi N, Erfanmanesh M. Evaluation of methods of cultivation, processing and improving of stem cell differentiation into cardiomyocytes. Journal of Laboratory and Diagnosis. 2017; 8(34): 39-47.
5. Sasse S, Skorska A, Lux CA, Steinhoff G, David R, Gaebel R. Angiogenic potential of bone marrow derived $CD133^+$ and $CD271^+$ intramyocardial stem cell trans- plantation post MI. Cells. 2020; 9(1): 78.
6. Turner D, Rieger AC, Balkan W, Hare JM. Clinical-based cell therapies for heart disease-current and future state. Rambam Maimonides Med J. 2020; 11(2): e0015.
7. Sanganalmath SK, Bolli R. Cell therapy for heart failure: a comprehensive overview of experimental and clinical studies, current challenges, and future directions. Circ Res. 2013; 113(6): 810-34.
8. Singla DK. Stem cells and exosomes in cardiac repair. Curr Opin Pharmacol. 2016; 27: 19-23.
9. Wernly B, Mirna M, Rezar R, Prodinger C, Jung C, Podesser BK, et al. Regenerative cardiovascular therapies: stem cells and beyond. Int J Mol Sci. 2019; 20(6): 1420.
10. Ratajczak MZ, Kucia M, Jadczyk T, Greco NJ, Wojakowski W, Tendera M, et al. Pivotal role of paracrine effects in stem cell therapies in regenerative medicine: can we translate stem cell-secreted paracrine factors and microvesicles into better therapeutic strategies? Leukemia. 2012; 26(6): 1166-1173.
11. Prathipati P, Nandi SS, Mishra PK. Stem cell-derived exosomes, autophagy, extracellular matrix turnover, and mirnas in cardiac regeneration during stem cell therapy. Stem Cell Rev Rep. 2017; 13(1): 79-91.
12. Cambria E, Pasqualini FS, Wolint P, Günter J, Steiger J, Bopp A, et al. Translational cardiac stem cell therapy: advancing from first-generation to next-generation cell types. NPJ Regen Med. 2017; 2: 17.
13. Tsao CR, Liao MF, Wang MH, Cheng CM, Chen CH. Mesenchymal stem cell derived exosomes: a new hope for the treatment of cardiovascular disease? Acta Cardiol Sin. 2014; 30(5): 395-400.
14. Harrell CR, Fellabaum C, Jovicic N, Djonov V, Arsenijevic N, Volarevic V. Molecular mechanisms responsible for therapeutic potential of mesenchymal stem cell-derived secretome. Cells. 2019; 8(5): 467.
15. Khanabdali R, Rosdah AA, Dusting GJ, Lim SY. Harnessing the secretome of cardiac stem cells as therapy for ischemic heart disease. Biochem Pharmacol. 2016; 113: 1-11.
16. Mirotsou M, Jayawardena TM, Schmeckpeper J, Gnecchi M, Dzau VJ. Paracrine mechanisms of stem cell reparative and regenerative actions in the heart. J Mol Cell Cardiol. 2011; 50(2): 280-289.
17. Gallina C, Turinetto V, Giachino C. A new paradigm in cardiac regeneration: the mesenchymal stem cell secretome. Stem Cells Int. 2015; 2015: 765846.
18. Ranganath SH, Levy O, Inamdar MS, Karp JM. Harnessing the mesenchymal stem cell secretome for the treatment of cardiovascular disease. Cell Stem Cell. 2012; 10(3): 244-258.
19. Huang P, Tian X, Li Q, Yang Y. New strategies for improving stem cell therapy in ischemic heart disease. Heart Fail Rev. 2016; 21(6): 737-752.
20. Carotenuto F, Teodori L, Maccari AM, Delbono L, Orlando G, Di Nardo P. Turning regenerative technologies into treatment to repair myocardial injuries. J Cell Mol Med. 2020; 24(5): 2704-2716.
21. Toh WS, Lai RC, Zhang B, Lim SK. MSC exosome works through a protein-based mechanism of action. Biochem Soc Trans. 2018; 46(4): 843-853.
22. Liu M, Wang Y, Zhu Q, Zhao J, Wang Y, Shang M, et al. Protective effects of circulating microvesicles derived from ischemic preconditioning on myocardial ischemia/reperfusion injury in rats by inhibiting endoplasmic reticulum stress. Apoptosis. 2018; 23(7-8): 436-448.
23. Sharma S, Mishra R, Bigham GE, Wehman B, Khan MM, Xu H, et al. A deep proteome analysis identifies the complete secretome as the functional unit of human cardiac progenitor cells. Circ Res. 2017; 120(5): 816-834.
24. Yu B, Zhang X, Li X. Exosomes derived from mesenchymal stem cells. Int J Mol Sci. 2014; 15(3): 4142-4157.
25. Adamiak M, Cheng G, Bobis-Wozowicz S, Zhao L, Kedracka-Krok S, Samanta A, et al. Induced pluripotent stem cell (iPSC)-derived extracellular vesicles are safer and more effective for cardiac repair than iPSCs. Circ Res. 2018; 122(2): 296-309.
26. Chistiakov DA, Orekhov AN, Bobryshev YV. Cardiac extracellular vesicles in normal and infarcted heart. Int J Mol Sci. 2016; 17(1): 63.
27. Kishore R, Khan M. More than tiny sacks: stem cell exosomes as cell-free modality for cardiac repair. Circ Res. 2016; 118(2): 330-343.
28. Gallet R, Dawkins J, Valle J, Simsolo E, de Couto G, Middleton R, et al. Exosomes secreted by cardiosphere-derived cells reduce scarring, attenuate adverse remodelling, and improve function in acute and chronic porcine myocardial infarction. Eur Heart J. 2017; 38(3): 201-211.
29. Ma J, Zhao Y, Sun L, Sun X, Zhao X, Sun X, et al. Exosomes derived from Akt-modified human umbilical cord mesenchymal stem cells improve cardiac regeneration and promote angiogenesis via activating platelet-derived growth factor D. Stem Cells Transl Med. 2017; 6(1): 51-59.
30. Khan M, Nickoloff E, Abramova T, Johnson J, Verma SK, Krishnamurthy P, et al. Embryonic stem cell-derived exosomes promote endogenous repair mechanisms and enhance cardiac function following myocardial infarction. Circ Res. 2015: 117(1): 52-64.
31. Mentkowski KI, Lang JK. Exosomes engineered to express a cardiomyocyte binding peptide demonstrate improved cardiac retention in vivo. Sci Rep. 2019; 9(1): 10041.
32. Yamashita T, Takahashi Y, Takakura Y. Possibility of exosome-based therapeutics and challenges in production of exosomes eligible for therapeutic application. Biol Pharm Bull. 2018; 41(6): 835-842.
33. Tian T, Zhang HX, He CP, Fan S, Zhu YL, Qi C, et al. Surface functionalized exosomes as targeted drug delivery vehicles for cerebral ischemia therapy. Biomaterials. 2018; 150: 137-149.
34. Migault M, Donnou-Fournet E, Galibert MD, Gilot D. Definition and identification of small RNA sponges: Focus on miRNA sequestration. Methods. 2017; 117: 35-47.
35. Wu G, Huang ZP, Wang DZ. MicroRNAs in cardiac regeneration and cardiovascular disease. Sci China Life Sci. 2013; 56(10): 907-913.
36. Shrestha S, Ren L, Vaidya R. miRNAs as biomarkers for diagnosis and assessment of prognosis of coronary artery disease. Open J Intern Med. 2018; 08(01): 54-63.
37. Samanta S, Balasubramanian S, Rajasingh S, Patel U, Dhanasekaran A, Dawn B, et al. MicroRNA: a new therapeutic strategy for cardiovascular diseases. Trends Cardiovasc Med. 2016; 26(5): 407-419.
38. Zhu K, Liu D, Lai H, Li J, Wang C. Developing miRNA therapeutics for cardiac repair in ischemic heart disease. J Thorac Dis. 2016; 8(9): E918-E927.
39. Wang X, Shang Y, Dai S, Wu W, Yi F, Cheng L. MicroRNA-16-5p aggravates myocardial infarction injury by targeting the expression of insulin receptor substrates 1 and mediating myocardial apoptosis and angiogenesis. Curr Neurovasc Res. 2020; 17(1): 11-7.
40. Zhao Z, Du S, Shen S, Wang L. microRNA-132 inhibits cardiomyocyte apoptosis and myocardial remodeling in myocardial infarction by targeting IL-1β. J Cell Physiol. 2020; 235(3): 2710-2721.
41. Bai Y, Bai L, Zhou J, Chen H, Zhang L. Sequential delivery of VEGF, FGF-2 and PDGF from the polymeric system enhance HUVECs angiogenesis in vitro and CAM angiogenesis. Cell Immunol. 2018; 323: 19-32.
42. Rebouças JS, Santos-Magalhães NS, Formiga FR. Cardiac regeneration using growth factors: advances and challenges. Arq Bras Cardiol. 2016; 107(3): 271-275.
43. Thavapalachandran S, Grieve SM, Hume RD, Le TYL, Raguram K, Hudson JE, et al. Platelet-derived growth factor-AB improves scar mechanics and vascularity after myocardial infarction. Sci Transl Med. 2020; 12(524): eaay2140.
44. Hajjar RJ, Hulot JS. Myocardial delivery of stromal cell-derived factor 1 in patients with ischemic heart disease: safe and promising. Circ Res. 2013; 112(5): 746-747.
45. Timmers L, Lim SK, Hoefer IE, Arslan F, Lai RC, van Oorschot AA, et al. Human mesenchymal stem cell-conditioned medium improves cardiac function following myocardial infarction. Stem Cell Res. 2011; 6(3): 206-214.
46. Gunawardena TNA, Rahman MT, Abdullah BJJ, Abu Kasim NH. Conditioned media derived from mesenchymal stem cell cultures: the next generation for regenerative medicine. J Tissue Eng Regen Med. 2019; 13(4): 569-586.
47. Yamaguchi S, Shibata R, Yamamoto N, Nishikawa M, Hibi H, Tanigawa T, et al. Dental pulp-derived stem cell conditioned medium

reduces cardiac injury following ischemia-reperfusion. Sci Rep. 2015; 5: 16295.
48. Ellison-Hughes GM, Madeddu P. Exploring pericyte and cardiac stem cell secretome unveils new tactics for drug discovery. Pharmacol Ther. 2017; 171: 1-12.
49. He J, Cai Y, Luo LM, Liu HB. Hypoxic adipose mesenchymal stem cells derived conditioned medium protects myocardial infarct in rat. Eur Rev Med Pharmacol Sci. 2015; 19(22): 4397-4406.
50. Ylä-Herttuala S, Bridges C, Katz MG, Korpisalo P. Angiogenic gene therapy in cardiovascular diseases: dream or vision? Eur Heart J. 2017; 38(18): 1365-1371.
51. Eibel B, Rodrigues CG, Giusti II, Nesralla IA, Prates PRL, Sant'Anna RT, et al. Terapia gênica para cardiopatia isquêmica: revisão de ensaios clínicos. BJCVS. 2011; 26: 635-646.
52. Lavu M, Gundewar S, Lefer DJ. Gene therapy for ischemic heart disease. J Mol Cell Cardiol. 2011; 50(5): 742-750.
53. Esmaeilzadeh A, Mohammadzadeh A, Bahmaie N. New generation of promising immunotherapeutics approaches for psoriasis dilemma; IL-35 gene as a potentiated candidate. Inflammation and Cell Signaling. 2018; 5: e1635.
54. Lin M, Liu X, Zheng H, Huang X, Wu Y, Huang A, et al. IGF-1 enhances BMSC viability, migration, and anti-apoptosis in myocardial infarction via secreted frizzled-related protein 2 pathway. Stem Cell Res Ther. 2020; 11(1): 22.
55. Su G, Liu L, Yang L, Mu Y, Guan L. Homing of endogenous bone marrow mesenchymal stem cells to rat infarcted myocardium via ultrasound-mediated recombinant SDF-1α adenovirus in microbubbles. Oncotarget. 2018; 9(1): 477-487.
56. Johnson T, Zhao L, Manuel G, Taylor H, Liu D. Approaches to therapeutic angiogenesis for ischemic heart disease. J Mol Med (Berl). 2019; 97(2): 141-151.
57. Bauzá MDR, Giménez CS, Locatelli P, De Lorenzi A, Hnatiuk A, Capogrossi MC, et al. High-dose intramyocardial HMGB1 induces long-term cardioprotection in sheep with myocardial infarction. Drug Deliv Transl Res. 2019; 9(5): 935-944.
58. Hadjizadeh A, Ghasemkhah F, Ghasemzaie N. Polymeric scaffold based gene delivery strategies to improve angiogenesis in tissue engineering: a review. Polym Rev. 2017; 57(3): 505-556.
59. Yin ZQ, Xing WH. Progress in gene therapy for chronic heart failure. Heart Surg Forum. 2018; 21(2): E075-E083.
60. Laakkonen JP, Ylä-Herttuala S. Recent advancements in cardiovascular gene therapy and vascular biology. Hum Gene Ther. 2015; 26(8): 518-524.
61. Yang L, Zhu J, Zhang C, Wang J, Yue F, Jia X, et al. Stem cell-derived extracellular vesicles for myocardial infarction: a meta-analysis of controlled animal studies. Aging (Albany NY). 2019; 11(4): 1129-1150.
62. Liu C, Wang J, Hu J, Fu B, Mao Z, Zhang H, et al. Extracellular vesicles for acute kidney injury in preclinical rodent models: a meta-analysis. Stem Cell Res Ther. 2020; 11(1): 11.
63. Willis GR, Kourembanas S, Mitsialis SA. Toward exosome-based therapeutics: isolation, heterogeneity, and fit-for-purpose potency. Front Cardiovasc Med. 2017; 4: 63.
64. Meng H, Chen B, Tao Z, Xu Z, Wang L, Weizhu J, et al. Safety and efficacy of adenovirus carrying hepatocyte growth factor gene by percutaneous endocardial injection for treating post-infarct heart failure: a phase iia clinical trial. Curr Gene Ther. 2018; 18(2): 125-130.
65. Gross L, Theiss HD, Grabmaier U, Adrion C, Mansmann U, Sohn HY, et al. Combined therapy with sitagliptin plus granulocyte-colony stimulating factor in patients with acute myocardial infarction - Long-term results of the SITAGRAMI trial. Int J Cardiol. 2016; 215: 441-445.
66. Kukuła K, Urbanowicz A, Kłopotowski M, Dąbrowski M, Pręgowski J, Kądziela J, et al. Long-term follow-up and safety assessment of angiogenic gene therapy trial VIF-CAD: Transcatheter intramyocardial administration of a bicistronic plasmid expressing VEGF-A165/bFGF cDNA for the treatment of refractory coronary artery disease. Am Heart J. 2019; 215: 78-82.
67. Anttila V, Saraste A, Knuuti J, Jaakkola P, Hedman M, Svedlund S, et al. Synthetic mRNA encoding VEGF-A in patients undergoing coronary artery bypass grafting: design of a phase 2a clinical trial. Mol Ther Methods Clin Dev. 2020; 18: 464-472.
68. Greenberg B, Butler J, Felker GM, Ponikowski P, Voors AA, Desai AS, et al. Calcium upregulation by percutaneous administration of gene therapy in patients with cardiac disease (CUPID 2): a randomised, multinational, double-blind, placebo-controlled, phase 2b trial. Lancet. 2016; 387(10024): 1178-1186.
69. Chung ES, Miller L, Patel AN, Anderson RD, Mendelsohn FO, Traverse J, et al. Changes in ventricular remodelling and clinical status during the year following a single administration of stromal cell-derived factor-1 non-viral gene therapy in chronic ischaemic heart failure patients: the STOP-HF randomized phase II trial. Eur Heart J. 2015; 36(33): 2228-2238.
70. Penn MS, Mendelsohn FO, Schaer GL, Sherman W, Farr M, Pastore J, et al. An open-label dose escalation study to evaluate the safety of administration of nonviral stromal cell-derived factor-1 plasmid to treat symptomatic ischemic heart failure. Circ Res. 2013; 112(5): 816-825.

Original Article

# Extremely Low Frequency Magnetic Fields Induce *mTOR* and *Hsa_Circ_100338* Expression Changes in Gastric Cancer and Normal Fibroblast Cell Lines

**Fereshteh Mansoury, Ph.D.[1], Nahid Babaei, Ph.D.[1], Soheila Abdi, Ph.D.[2*], Maliheh Entezari, Ph.D.[3, 4], Abbas Doosti, Ph.D.[5]**

1. Department of Cell Biology and Genetics, Bushehr Branch, Islamic Azad University, Bushehr, Iran
2. Department of Physics, Safadasht Branch, Islamic Azad University, Tehran, Iran
3. Department of Genetics, Faculty of Advanced Science and Technology, Tehran Medical Sciences Branch, Islamic Azad University, Tehran, Iran
4. Farhikhtegan Medical Convergence, Science Research Center, Farhikhtegan Hospital, Tehran Medical Sciences, Islamic Azad University, Tehran, Iran
5. Biotechnology Research Center, Shahrekord Branch, Islamic Azad University, Shahrekord, Iran

**Corresponding address: P.O.Box: 3164348658, Department of Physics, Safadasht Branch, Islamic Azad University, Tehran, Iran*
*Email: soheilaabdi@safaiau.ac.ir*

**Received: 29/December/2020, Accepted: 24/May/2021**

Abstract

**Objective:** Extremely low-frequency magnetic field (ELF-MF) exposure, as a targeted tumor therapy, presents several potential advantages. In this research, we investigated effects of different ELF-MF intensities on cell viability and expression levels of the mammalian target of rapamycin (mTOR) and hsa_circ_100338 in the normal fibroblast (Hu02) and human gastric adenocarcinoma (AGS) cell lines.

**Materials and Methods:** In this experimental study, cell lines of AGS and Hu02, were cultured under the exposure of ELF-MF with magnetic flux densities (MFDs) of 0.25, 0.5, 1 and 2 millitesla (mT) for 18 hours. The 3-(4, 5-dimethylthiazoyl-2-yl)-2, 5-diphenyltetrazolium bromide (MTT) assay was used to evaluate the cell viability. Relative expression of mTOR and hsa_circ_100338 RNAs was estimated by quantitative real-time polymerase chain reaction (qRT-PCR) technique.

**Results:** Viability of the normal cells was significantly increased at MFDs of 0.5, 1 and 2 mT, while viability of the tumor cells was significantly decreased at MFD of 0.25 and increased at MFD of 2 mT. Expression level of mTOR was significantly increased at the all applied MFDs in the normal cells, while it was significantly decreased at MFDs of 0.25 and 0.5mT in the tumor cells. MFDs of 1 and 2 mT in tumor cells inversely led to the increase in mTOR expression. hsa_circ_100338 was downregulated in MFD of 0.25 mT and then it was increased parallel to the increase of MFD in the normal and tumor cells.

**Conclusion:** Results of the present study indicated that ELF-MF at MFDs of 0.25 and 0.5 mT can lead to decrease in the both mTOR and hsa_circ_100338 expression levels. Given the role of mTOR in cell growth, proliferation and differentiation, in addition to the potential role of hsa_circ_100338 in metastasis, expression inhibition of these two genes could be a therapeutic target in cancer treatment.

***Keywords:*** Circulating MicroRNA, Gastric Cancer, Gene Expression, Magnetic Field, mTOR Protein

Cell Journal(Yakhteh), Vol 24, No 7, July 2022, Pages: 364-369

**Citation:** Mansoury F, Babaei N, Abdi S, Entezari M, Doosti A. Extremely low frequency magnetic fields induce mTOR and Hsa_Circ_100338 expression changes in gastric cancer and normal fibroblast cell lines. Cell J. 2022; 24(7): 364-369. doi: 10.22074/cellj.2022.7922.
This open-access article has been published under the terms of the Creative Commons Attribution Non-Commercial 3.0 (CC BY-NC 3.0).

## Introduction

Today, due to the increasing presence of electromagnetic fields in daily life, its effects on health have received much attention. It has been found that magnetic fields can affect living systems, but their beneficial or harmful effects have not been fully investigated (1). Association of electromagnetic fields with risk of various cancers, including postmenopausal breast cancer (2), childhood leukemia (3) and lung cancer (4) has been demonstrated by some studies. It has been found that electromagnetic fields affects a variety of physiological processes (5), while such effects depend on extremely low-frequency magnetic field (ELF-MF) frequency and duration (6).

Plasma membrane structure, intracellular signal transduction pathways and gene transcription could be changed following the exposure of electromagnetic fields (7, 8).

Applying the electromagnetic field as a non-invasive technique was used in the oncology field to treat cancer cells. In EMF therapy micro-currents are exposed locally to the specific tissue or the entire body. ELF-MF is used for the treatment of several diseases like Parkinson disease (9). EMF therapy, in the wave range of 0-300 Hz can help reduce dosage, harmful side-effects of chemotherapy and radiotherapy, further to enhancing prognosis of the disease (10).

During the last few years, the mammalian target of rapamycin (*mTOR*) has received significant attention for its importance in treating cancer. *mTOR* plays an important role in cancer cell growth through affecting the activity of elF4F complex. This enzyme increases translation by phosphorylating two targets of ribosomal p70S6 kinase

(S6K1) and initiation factor 4E binding protein 1 (4E-BP1) (11). Stimulating expression of the membrane surface carriers is one of the most important roles of *mTOR* in the body, leading to the increase access to nutrients for cell growth and proliferation (12). Moreover, *mTOR* also enhances expression of hypoxia-inducible factor-1α (HIF-1α), which plays a key role in angiogenesis. Therefore, mutations in the upstream components of the *mTOR* pathway are implicated in cancer progression (13). Some studies indicated that *mTOR* dysfunction is applied as a therapeutic target in gastric cancer (GC). Additionally, increased *mTOR* activity is directly related to tumor progression and low patient survival (14).

Circular RNAs (circRNAs) are non-coding RNAs with stable structure and tissue-specific expression (15). Unlike other RNAs, circRNAs are resistant to degradation and they are highly ubiquitous in the transcriptome of eukaryotes (16). Some studies have shown that circRNAs can act as microRNA (miRNA) sponges, regulators of splicing and transcription, as well as altering gene expression (15). Changes in circRNA expression could induce abnormal cellular functions and various diseases including cardiovascular diseases and various cancers (17, 18). A recent study showed the clinical significance of *hsa_circRNA_100338* in hepatocellular carcinoma (HCC) and suggested that this circRNA could be a potential biomarker for HCC. The report also revealed that *hsa_circRNA_100338* could act as a sponge for miR-141-3p and increase potential of the liver cancer cells to metastases (19). Although some studies were done to provide *hsa_circRNA_100338* as a biomarker of cancer cells, there is no evidence to assay the expression level of *hsa_circRNA_100338* on GC cells at different electromagnetic flux densities.

The aim of this study was to investigate effect of magnetic flux densities (MFDs) of 0.25, 0.5, 1 and 2 millitesla (mT) on the expression level of *mTOR* and *hsa_circRNA_100338* in a human gastric cancer cell line (AGS) and human normal fibroblast (Hu02) cells after 18 hours.

## Materials and Methods

In this experimental research, expression levels of *mTOR* and *hsa_circ_100338* were determined in AGS cell line, as tumor cell and Hu02 cell line, as normal cells, following the exposure to MFDs of 0.25, 0.5, 1 and 2 mT in comparison to the unexposed cells.

This study was approved by the Ethics Committee of Bushehr University of Medical Sciences (IR.BPUMS.REC.1339.180).

### Cell culture

Human gastric adenocarcinoma (AGS) and human normal fibroblast (Hu02) cell lines were purchased from the National Genetic Resources Center of Iran, and then according to their instructions, the cells were seeded monolayer in the 25 ml flasks. AGS cells were cultured in Ham's F12 (Gibco, USA) medium as described in the previous study (20). The cells were exposed to ELF-MF with MFDs of 0.25, 0.5, 1 and 2 mT continuously for 18 hours.

### Exposure system

Electromagnetic fields were produced by the system consisted of a solenoid cylinder of diameter 12 cm, length 30 cm and 1200 turns (21). To produce various electromagnetic intensities with a frequency of 50 Hz, an alternative current power supply (TDGC2, 220v, 50-60 Hz; Delta International Electric, China) was applied. The electromagnetic field generated inside the solenoid is uniform and in the direction of the cylindrical axis. The solenoid cylinder was placed horizontally at the center of the $CO_2$ incubator and flasks of cells were placed in the middle of the cylinder. The sham groups were incubated at the same condition inside the solenoid cylinder, while the circuit was interrupted. A digital teslameter with a 3-D sensor (Holaday, USA) was used to estimate the electromagnetic flux density at the middle of the solenoid cylinder.

### MTT assay

The cell viability was determined by the 3-(4, 5-dimethylthiazoyl-2-yl)-2, 5-diphenyltetrazolium bromide (MTT) assay. For this purpose, the medium was removed from the cultured cells in the 96 well plates. Then, the MTT solution was added to each well after which the plate was incubated for 4 hours at 37°C with 5% $CO_2$. After removing supernatant, 100 µl Dimethylsulfoxide (DMSO) was added to each well and shaken well to dissolve all formazan crystals. Finally, the absorption was measured at 570 nm by a microplate reader (Synegry HT, USA).

### RNA extraction, cDNA synthesis and real-time-polymerase chain reaction

To measure expression changes of *mTOR* and *hsa_circRNA_100338*, real-time PCR (qRT-PCR) was used. Briefly, total RNA was extracted by using TRIzol reagent (TRI Sigma-Aldrich, Germany) according to the manufacturer's instruction. Takara RNA PCR Kit was used to synthesize cDNA. Quantitative real-time PCR (qRT-PCR) was performed by Bioneer Exicycler™ 96 Detection System. Detail of the PCR steps have been described in our previous studies (20, 22). The primer sequences are listed in Table 1.

Delta threshold cycle value (ΔCt) was measured for each sample to determine the relative expression of genes to the housekeeping gene and then the delta delta threshold cycle value (ΔΔCt) which is the difference between ΔCt of the exposed tumor or normal cells and control group was determined. Fold changes of gene and miRs expression was calculated by $2^{-\Delta\Delta Ct}$ formula.

**Table 1:** The sequences of *GAPDH*, *mTOR*, and *hsa _circ_100338* primers used in the current study

| Genes | Primer sequences (5′-3′) |
|---|---|
| *hsa_circ_100338* | F: AAAAGCAAGCAGTGCCCATA |
| | R: GCTCGAATCAGGTCCACCA |
| *mTOR* | F: AGCATCGGATGCTTAGGAGTGG |
| | R: CAGCCAGTCATCTTTGGAGACC |
| *GAPDH* | F: GCACCGTCAAGGCTGAGAAC |
| | R: GGATCTCGCTCCTGGAAGATG |

### Statistical analysis

SPSS software version 25 was used to analysis the data. The results were shown as mean ± standard deviation (mean ± SD). To compare significant differences among the groups, one-way and two-way analyses of variance and Tukey Post hoc test were used. The level of probability for the significant differences among the groups was considered as P<0.05.

## Results

### Cell viability measurement

ELF-MF with MFD of 0.25 mT did not affect cell viability of the normal cells while exposure to MFDs of 0.5, 1 and 2 mT lead to a significant increase in cell viability (P<0.0001).

Exposure of tumor cells to 0.25 mT MFD led to a significant decrease in cell viability, but the cell viability was increased in parallel with the increase of MFD and this increase was significant at MFD of 2 mT (Fig.1). Sidak analysis showed a significant decrease in tumor cells in comparison with normal cells in terms of viability at MFDs of 0.25 (P=0.02), 0.5 (P<0.0001), 1 (P<0.0001), and 2 mT (P<0.0001, Fig.1).

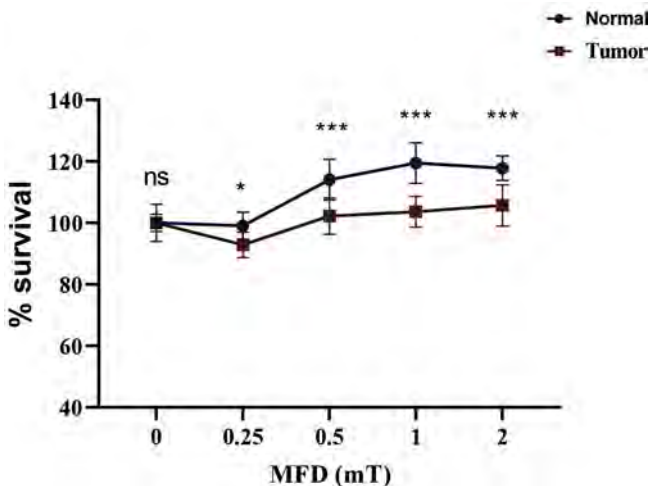


**Fig.1:** Mean viability percentage of the normal cells and tumor cells, following the exposure to continuous MFDs of 0.25, 0.5, 1 and 2 mT for 18 hours in comparison to the unexposed cells. *; P<0.05, ***; P<0.001, MFDs; Magnetic flux densities, and ns; Non significant.

### Relative expression of *mTOR*

Expression level of the *mTOR* gene in the normal cells exposed to different intensities of ELF-MF was significantly higher than that of the unexposed normal cells (P<0.001). The highest and lowest expression level of this gene was observed at 2 mT and 0.5 mT respectively (Fig.2A). However, pattern of *mTOR* expression level in tumor cells was different from that in normal cells. By that means the expression level of the gene in exposed tumor cells at MFDs of 0.25 mT and 0.5 mT was downregulated and at MFDs of 1 and 2 mT was upregulated compared to unexposed tumor cells (Fig.2B). Expression level of the *mTOR* gene in the exposed and unexposed tumor cells, as well as the exposed and unexposed normal cells, was analyzed using the sidak test. As evident from the data shown in Figure 2C, the unexposed tumor cells showed no significant difference compared to unexposed normal cells concerning the relative expression of *mTOR* mRNA (P>0.05). However, relative expression of mTOR mRNA was significantly downregulated in the exposed tumor cells at MFDs of 0.25 (P<0.0001, 0.03 FC), 0.5 (P<0.0001, 0.05 FC), 1 (P<0.0001, 0.38 FC) and 2 (P=0.003, 0.68 FC) mT in comparison with the exposed normal cells (Fig.2C).

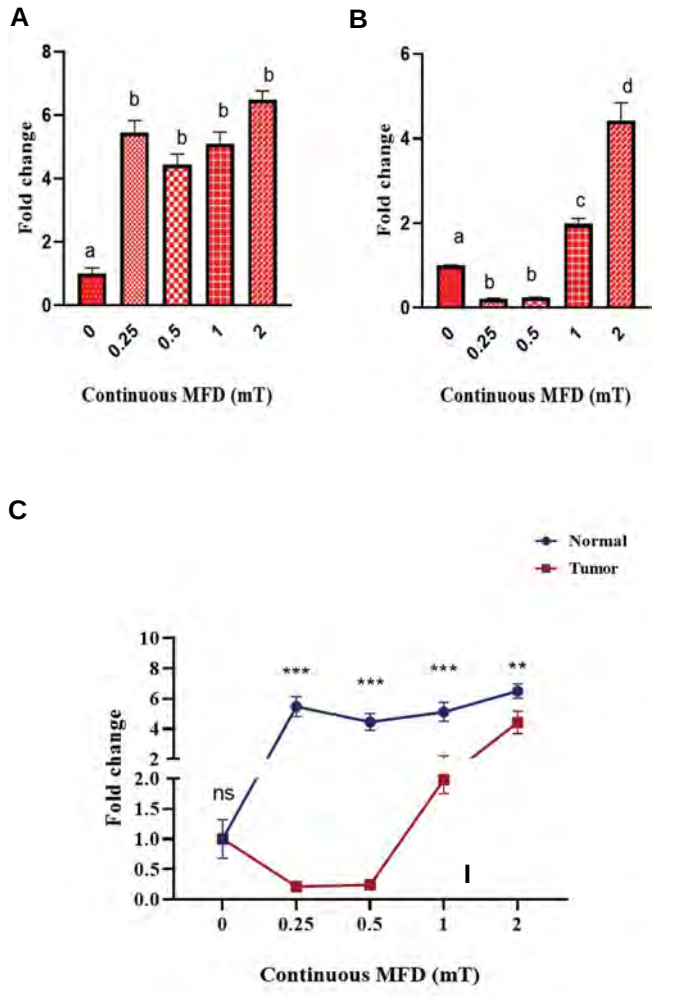


**Fig.2:** Comparison of *mTOR* expression levels in normal and tumor cells in different MFDs. mRNA expression level of *mTOR* in the **A.** Exposed normal and **B.** Gastric tumor cells at various MFDs. **C.** Comparison of the mRNA expression level of *mTOR* in the exposed, unexposed normal and tumor cells. Different letters on each column show statistically significant difference, and the same letters on each column has no difference. ***; P<0.001 and MFD; Magnetic flux densities.

### Relative expression of *hsa_circ_100338*

Expression level of *hsa_circ_100338* in the exposed normal cells significantly down regulated at MFD of 0.25 mT (0.18 FC, P=0.0005) compared to the unexposed normal cells. At the other intensities, no significant change was observed (Fig.3A). However, relative expression of *mTOR* mRNA was significantly down-regulated in the exposed tumor cells at MFDs of 0.25 (0.002 FC, P<0.0001), 0.5 (0.013 FC, P<0.0001), 1 (0.19 FC, P=0.0016) and 2 mT (0.31 FC, P=0.017) in comparison with the unexposed tumor cells (Fig.3B). Sidak test was used to analyze expression level of the *hsa_circ _100338* in the all groups of tumor and normal cells. As shown in Figure 3C, the obtained data showed no significant difference between the unexposed tumor cells and unexposed normal cells. Concerning the expression level of *has-circ-0005986* (P>0.05). However, expression level of the *hsa _circ_100338* was significantly increased in the exposed tumor cells at MFDs of 0.25 (P<0.0001, 0.013 FC), 0.5 (0.024 FC, P<0.0001), 1 (0.16 FC, P<0.0001) and 2 (0.22 FC, P<0.0001) mT.

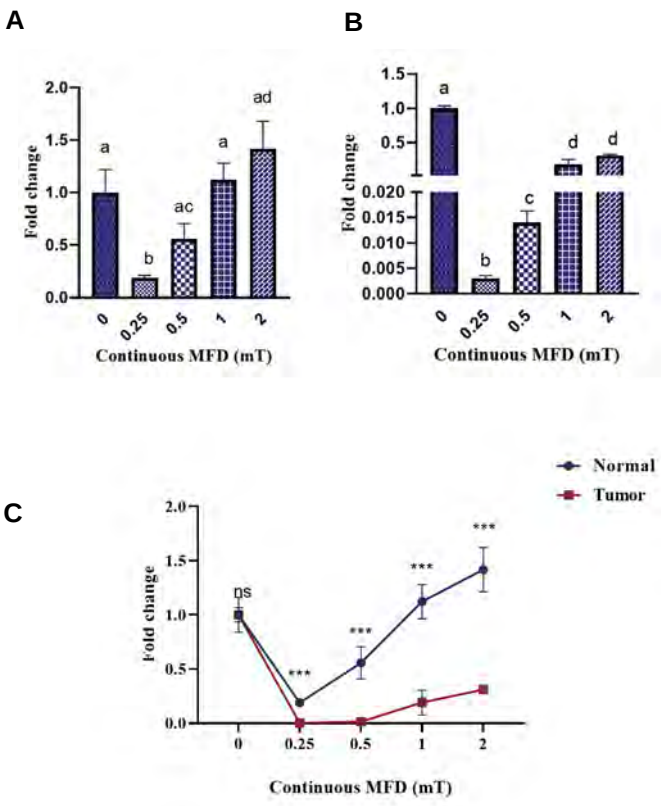


**Fig.3:** Comparison of *hsa_circ_100338* expression levels in normal and tumor cells in different MFDs. Relative expression level of *hsa_circ_100338* in the **A.** Tumor and **B.** Normal cells with different MFDs. **C.** Comparison of mRNA expression level of *hsa_circ_100338* in the exposed and unexposed normal cells with tumor cells. Different letters on each column show statistically significant differences, the columns having common letters show statistically no significant difference. ***; P<0.001, ns; Non significant, and MFDs; Magnetic flux densities.

### Correlation analysis

A significant positive correlation (r=0.799, 95% CI=0.4866 to 0.9306, P=0.0003) was observed between expression level of the *hsa_circ_100338* and *(mTOR)* genes in the tumor cells exposed to extremely low frequency magnetic fields (ELF-MF). As shown in Figure 4, no significant correlation was observed between expression level of the *hsa_circ_100338* and mTOR genes in the normal cells exposed to ELF-MF (P=0.540).

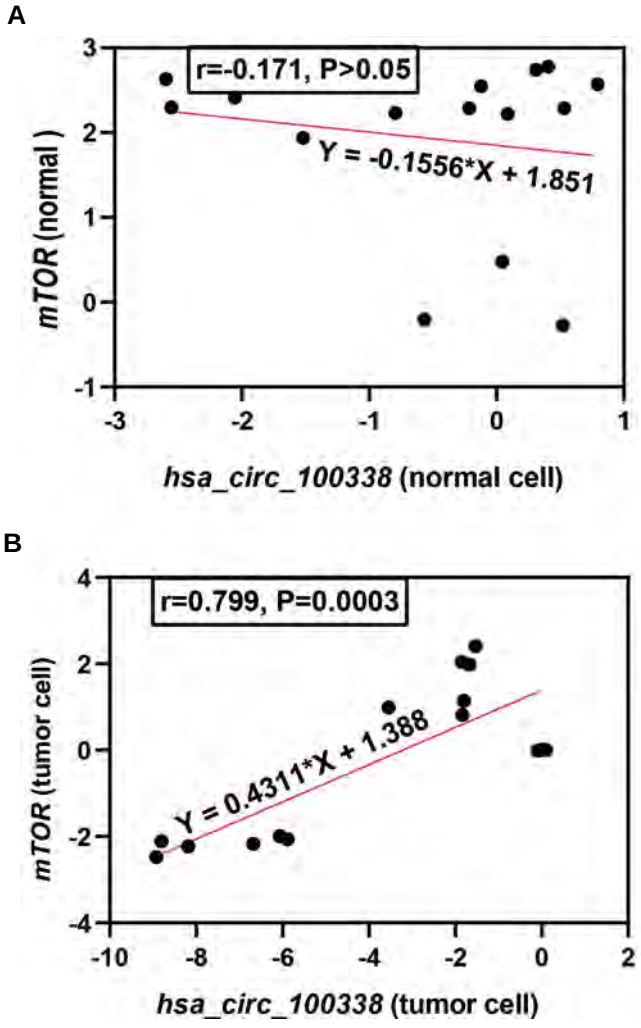


**Fig.4:** Correlation analysis between *mTOR* and *hsa_circ_100338* gene expressions in **A.** Normal cells and **B.** Gastric cancer cell lines exposed to extremely low frequency magnetic fields (ELF-MF).

## Discussion

In the present study, effects of ELF-MF with MFDs of 0.25, 0.5, 1; and 2mT on AGS and Hu02 cell lines were investigated. Our finding indicated that ELF-MF can affect the cell viability and change the expression levels of *mTOR* and *hsa_circRNA_100338* in the both tumor and normal cells. Expression levels of *mTOR* were significantly increased at all applied MFDs in the normal cells while it was significantly decreased at MFDs of 0.25 and 0.5 mT in tumor cells. MFDs of 1 and 2 mT in tumor cells inversely lead to the increase in *mTOR* expression. *Hsa_circ_100338* was down-regulated in MFD of 0.25 mT and then was increased parallel to the increase in

MFD in normal and tumor cells.

Interaction of ELF-MF with living organisms could induce different biological effects that depend on the type, MFD, frequency and time of exposure (1, 23). There are some studies that indicated antitumor effect of EMFs (24). Release of intracellular proteases that alter the integrity of cancer cell membrane was reported in A549 human lung cancer cells exposed to 50 and 385 Hz electromagnetic fields (25). Decreased growth of breast cancer tumor cells under the influence of magnetic fields has been reported (26). These cytotoxic effects have been attributed to changes in plasma membrane properties, impaired $Ca^{+2}$ penetration (27) and changes in cytoskeletal structure (28). In the present study, cytotoxic effects of the ELF-MF with MFD of 0.25 mT on gastric cancer cells were observed. However, some conflicting researches have been reported in this regard. Some researchers reported inducing effects of cell proliferation (29, 30) and the others demonstrated cytotoxic effects of EMFs (31, 32). Different results of magnetic fields in this study can be explained by EMFs window effects hypothesis. The window effect is a biological response that only occurs at certain criteria of the frequency, amplitude, intensity and time of exposure, while outside of these criteria, the biological system does not respond to EMFs (33). The intensities of 0.5-2 mT showed no decrease in cell viability of tumor cells but a relative increase in it, which indicate the anti-apoptotic effects of ELF-MF (34). It was shown that ELF-MF protected cancer cells from apoptosis due to heat shock (35). It was demonstrated that *PI3K/AKT/mTOR* pathway activation in GC could impair cell growth and proliferation as well as, metabolism and angiogenesis (14). In this study, it was shown that *mTOR* gene was overexpressed in the GC cell lines at 2 mT ELF-MF, but at MFDs of 0.25 and 0.5 mT, this gene was down-regulated in comparison with the unexposed GC cell lines. Phosphorylation of Ser2448 *mTOR* enzyme activates eukaryotic initiation factor 4E (elF4E) and ribosomal S6 kinase p70 (p70S6 kinase 1) and inactivates eIF4E inhibitor 4E-BO.1. In other words, overexpression of the *mTOR* gene upregulated expression level of cell growth and cell division mediators including cyclin D1, and down-regulated expression level of cell cycle progression regulators (36). Therefore, MFDs of 0.25 and 0.5 mT, which caused a sharp decrease in *mTOR* expression level of GC cell lines, can be considered as a treatment for gastric cancer.

Moreover, according to the results, expression level of *hsa_circ_100338* in AGS cell lines showed significant differences at different MFDs and this led to the downregulation of *hsa_circ_100338* expression level in an intensity-dependent manner. So that, the lowest expression level of *hsa_circ_100338* was seen at 0.25 mT ELF-MF. Nevertheless, by increasing, MFD of the electromagnetic field, its expression level was also increased. Few studies have been performed to determine the role of circRNAs in cancer. Our results suggested that *hsa_circ_100338* could be a good biomarker for diagnosis of gastric cancer. The biomarker role of *hsa_circ_100338* has been reported in HCC. It has been shown that *hsa_circ_100338* acted as a miR-141-3p sponge in HCC tissue (19). The other study revealed that circRNA-100338 was involved in regulation of angiogenesis and HCC metastasis (37). In the current study, therefore, *hsa_circ_100338* in AGS cells may also interact with miRNAs. Downregulation of *hsa_circ_100338* expression level was observed in AGS cells exposed to MFD of 0.25 mT.

*Hsa_circ_100338* expression level had positive correlation with *mTOR* in the tumor cells following exposure of ELF-MF, whereas the normal cells treatment with ELF-MF showed no significant correlation. A study showed that *hsa_circ_100338* regulated protein kinase activity of *mTOR* in HCC patients and operated as a key regulator in promoting the *mTOR* signaling pathway. The study indicated that not only gene expression level of *hsa_circ_100338* was increased in HCC cells compared to the normal cells, but also knockdown of *hsa_circ_100338* gene affected cell proliferation ability (37).

ELF-EMFs can alter gene expression by several mechanisms, including alteration of cell membrane channels like calcium channels (38), increase in free radicals formation and stability (39), in addition to direct interaction with DNA (40). Overall, decrease of *mTOR* and *hsa_circ_100338* expressions as well as cell viability decrease in tumor cells, following the exposure to MFD of 0.25 mT in this study, indicated that this MFD had the most beneficial effects and it can be considered as an adjutant therapeutic method in cancer treatment.

## Conclusion

Results of the present study indicated that ELF-MF at MFDs of 0.25 and 0.5 mT can down-regulated both *mTOR* and *hsa_circ_100338* expressions. Given the role of *mTOR* in cell growth, proliferation, differentiation and the potential role of *hsa_circ_100338* in metastasis, the expression inhibition of these two genes could be a therapeutic target in cancer treatment. However, more *in vitro* and *in vivo* researches are needed to find suitable MFD and exposure protocols to suppress and control cancer cell with fewer side-effects.

## Acknowledgments

This research project was approved by the Bushehr Branch of Islamic Azad University with the code number 14648657964033213981205 46. The authors would like to thank Ms. Hadiseh Mohammadpour and Ms. Neda Tekiyemaroof, from Cancer Institute, Tehran University of Medical Sciences and Razi Drug Research Center of Iran University of Medical Sciences (Tehran, Iran). There is no conflict of interest in this study.

## Authors' Contributions

S.A.; Was the designer of the project and responsible for overall supervision. N.B.; Was involved in experimental studies and data analysis. F.M.; Carried out all experimental works, including primer design, cell culture,

qRT-PCR, and data analysis. M.E., A.D.; Were involved in experimental studies and drafting the manuscript. The authors have read and approved the final manuscript.

## References


1. Abdi S, Dorranian D, Razavi AE, Naderi GA, Boshtam M, Ghorannevis M. Evaluation of the effects of weak and moderate static magnetic fields on the characteristics of human low density lipoprotein in vitro. Bioelectromagnetics. 2013; 34(5): 397-404.
2. Labreche F, Goldberg MS, Valois MF, Nadon L, Richardson L, Lakhani R, et al. Occupational exposures to extremely low frequency magnetic fields and postmenopausal breast cancer. Am J Ind Med. 2003; 44(6): 643-652.
3. Schüz J, Ahlbom A. Exposure to electromagnetic fields and the risk of childhood leukaemia: a review. Radiat Prot Dosim. 2008; 132(2): 202-211.
4. Xu Y, Wang Y, Yao A, Xu Z, Dou H, Shen S, et al. Low frequency magnetic fields induce autophagy-associated cell death in lung cancer through miR-486-mediated inhibition of Akt/mTOR signaling pathway. Sci Rep. 2017; 7(1): 1-14.
5. Saliev T, Begimbetova D, Masoud AR, Matkarimov B. Biological effects of non-ionizing electromagnetic fields: two sides of a coin. Prog Biophys Mol Biol. 2019; 141: 25-36.
6. Abdi S, Dorranian D, Naderi GA, Razavi AE. Changes in physicochemical charachteristics of human low density lipoprotein nanoparticles by electromagnetic field exposure. Stud U Babes-Bol Che. 2016; 61(1): 185-197.
7. Grassi C, D'Ascenzo M, Torsello A, Martinotti G, Wolf F, Cittadini A, et al. Effects of 50 Hz electromagnetic fields on voltage-gated Ca2+ channels and their role in modulation of neuroendocrine cell proliferation and death. Cell Calcium. 2004; 35(4): 307-315.
8. Phillips JL. Effects of electromagnetic field exposure on gene transcription. J Cell Biochem. 1993; 51(4): 381-386.
9. Vadala M, Vallelunga A, Palmieri L, Palmieri B, Morales-Medina J C, Iannitti T. Mechanisms and therapeutic applications of electromagnetic therapy in Parkinson's disease. Behav Brain Funct. 2015; 11: 26.
10. Crocetti S, Beyer C, Schade G, Egli M, Frohlich J, Franco-Obregon A. Low intensity and frequency pulsed electromagnetic fields selectively impair breast cancer cell viability. PLoS One. 2013; 8: e72944.
11. Petroulakis E, Mamane Y, Le Bacquer O, Shahbazian D, Sonenberg N. mTOR signaling: implications for cancer and anticancer therapy. Br J Cancer. 2006; 94(2): 195-199.
12. Wullschleger S, Loewith R, Hall MN. TOR signaling in growth and metabolism. Cell. 2006; 124(3): 471-484.
13. Patel PH, Chadalavada RS, Chaganti R, Motzer RJ. Targeting von Hippel-Lindau pathway in renal cell carcinoma. Clin Cancer Res. 2006; 12(24): 7215-7220.
14. Yu G, Wang J, Chen Y, Wang X, Pan J, Li G, et al. Overexpression of phosphorylated mammalian target of rapamycin predicts lymph node metastasis and prognosis of chinese patients with gastric cancer. Clin Cancer Res. 2009; 15(5): 1821-1829.
15. Memczak S, Jens M, Elefsinioti A, Torti F, Krueger J, Rybak A, et al. Circular RNAs are a large class of animal RNAs with regulatory potency. Nature. 2013; 495(7441): 333-338.
16. Hentze MW, Preiss T. Circular RNAs: splicing's enigma variations. EMBO J. 2013; 32(7): 923-925.
17. Qu S, Yang X, Li X, Wang J, Gao Y, Shang R, et al. Circular RNA: a new star of noncoding RNAs. Cancer Lett. 2015; 365(2): 141-148.
18. Jiang S, Guo C, Zhang W, Che W, Zhang J, Zhuang S, et al. The integrative regulatory network of circRNA, microRNA and mRNA in atrial fibrillation. Front Genet. 2019; 10: 526.
19. Huang X-Y, Huang Z-L, Xu Y-H, Zheng Q, Chen Z, Song W, et al. Comprehensive circular RNA profiling reveals the regulatory role of the circRNA-100338/miR-141-3p pathway in hepatitis B-related hepatocellular carcinoma. Sci Rep. 2017; 7(1): 1-12.
20. Mansoury F, Babaei N, Abdi S, Entezari M, Doosti A. Changes in NOTCH1 gene and its regulatory circRNA, hsa_circ_0005986 expression pattern in human gastric adenocarcinoma and human normal fibroblast cell line following the exposure to extremely low frequency magnetic field. Electromagn Biol Med. 2021; 40(3): 375-383.
21. Bahar M, Majd A, Abdi S. Effects of (ELF) extremely low frequency (50 Hz) AC and DC magnetic fields on lentil germination and seedlings growth. J Theor Appl Phys. 2009; 3(2): 12-16.
22. Mehrara Sh, Mohammadpour H, Miri SR, Abdi S. Plasmacytoma variant translocation 1 and nicotinamide phosphoribosyl-transferase long noncoding RNAs promote colorectal cancer. Gene Rep. 2021; 21: 101-113.
23. Eder SH, Cadiou H, Muhamad A, McNaughton PA, Kirschvink JL, Winklhofer M. Magnetic characterization of isolated candidate vertebrate magnetoreceptor cells. Proc Natl Acad Sci USA. 2012; 109(30): 12022-12027.
24. Zimmerman JW, Pennison MJ, Brezovich I, Yi N, Yang CT, Ramaker R, et al. Cancer cell proliferation is inhibited by specific modulation frequencies. Br J Cancer. 2012; 106(2): 307-313.
25. Ashdown CP, Johns SC, Aminov E, Unanian M, Connacher W, Friend J, et al. Pulsed low-frequency magnetic fields induce tumor membrane disruption and altered cell viability. Biophys J. 2020; 118(7): 1552-1563.
26. Crocetti S, Beyer C, Schade G, Egli M, Fröhlich J, Franco-Obregón A. Low intensity and frequency pulsed electromagnetic fields selectively impair breast cancer cell viability. PLoS One. 2013; 8(9): e72944.
27. Pessina G, Aldinucci C, Palmi M, Sgaragli G, Benocci A, Meini A, et al. Pulsed electromagnetic fields affect the intracellular calcium concentrations in human astrocytoma cells. Bioelectromagnetics. 2001; 22(7): 503-510.
28. Sulpizio M, Falone S, Amicarelli F, Marchisio M, Di Giuseppe F, Eleuterio E, et al. Molecular basis underlying the biological effects elicited by extremely low-frequency magnetic field (ELF-MF) on neuroblastoma cells. J Cell Biochem. 2011; 112(12): 3797-3806.
29. Trillo MÁ, Martínez MA, Cid MA, Leal J, Úbeda A. Influence of a 50 Hz magnetic field and of all-trans-retinol on the proliferation of human cancer cell lines. Int J Oncol. 2012; 40(5): 1405-1413.
30. Martínez MA, Úbeda A, Cid MA, Trillo MÁ. The proliferative response of NB69 human neuroblastoma cells to a 50 Hz magnetic field is mediated by ERK1/2 signaling. Cell Physiol Biochem. 2012; 29(5-6): 675-686.
31. Huang CY, Chang CW, Chen CR, Chuang CY, Chiang C-S, Shu WY, et al. Extremely low-frequency electromagnetic fields cause G1 phase arrest through the activation of the ATM-Chk2-p21 pathway. PLoS One. 2014; 9(8): e104732.
32. Jung IS, Kim HJ, Noh R, Kim SC, Kim CW. Effects of extremely low frequency magnetic fields on NGF induced neuronal differentiation of PC12 cells. Bioelectromagnetics. 2014; 35(7): 459-469.
33. Litovitz T, Montrose C, Wang W. Dose-response implications of the transient nature of electromagnetic-field-induced bioeffects: Theoretical hypotheses and predictions. Bioelectromagnetics. 1992; 13(S1): 237-246.
34. Feng B, Ye C, Qiu L, Chen L, Fu Y, Sun W. Mitochondrial ROS release and subsequent Akt activation potentially mediated the anti-apoptotic effect of a magnetic field on FL cell. Cell Physiol Biochem. 2016; 38(6): 2489-2499.
35. Robison JG, Pendleton AR, Monson KO, Murray BK, O'Neill KL. Decreased DNA repair rates and protection from heat induced apoptosis mediated by electromagnetic field exposure. Bioelectromagnetics. 2002; 23(2): 106-112.
36. Chiang GG, Abraham RT. Phosphorylation of mammalian target of rapamycin (mTOR) at Ser-2448 is mediated by p70S6 kinase. J Biol Chem. 2005; 280(27): 25485-25490.
37. Huang XY, Huang ZL, Zhang PB, Huang XY, Huang J, Wang HC, et al. CircRNA-100338 is associated with mTOR signaling pathway and poor prognosis in hepatocellular carcinoma. Front Oncol. 2019; 9: 392.
38. Panagopoulos D.J, Karabarbounis A, Margaritis LH. Mechanism for action of electromagnetic fields on cells. Biochem Biophys Res Commun. 2002; 298(1): 95-102.
39. Consales C, Merla C, Marino C, Benassi B. Electromagnetic fields, oxidative stress, and neurodegeneration. Int J Cell Biol. 2012; 1-17.
40. Mihai CT, Rotinberg P, Brinza F, Vochita G. Extremely low-frequency electromagnetic fields cause DNA strand breaks in normal cells. J Environ Health Sci Eng. 2014; 12(1): 15.

Original Article

# Optimizing Tenogenic Differentiation of Equine Adipose-Derived Mesenchymal Stem Cells (eq-ASC) Using TGFB3 Along with BMP Antagonists

**Asiyeh Shojaee, Ph.D.[1], Fatemeh Ejeian, Ph.D.[2], Abbas Parham, D.V.M., Ph.D.[1, 3]***

**Mohammad Hossein Nasr-Esfahani, Ph.D.[2]***

1. Division of Physiology, Department of Basic Sciences, Faculty of Veterinary Medicine, Ferdowsi University of Mashhad, Mashhad, Iran
2. Department of Animal Biotechnology, Cell Science Research Center, Royan Institute for Biotechnology, ACECR, Isfahan, Iran
3. Stem Cell Biology and Regenerative Medicine Research Group, Institute of Biotechnology, Ferdowsi University of Mashhad, Mashhad, Iran

**Corresponding Addresses: P.O.Box: 9177948974, Division of Physiology, Department of Basic Sciences, Faculty of Veterinary Medicine, Ferdowsi University of Mashhad, Mashhad, Iran*

*P.O.Box: 8159358686, Department of Animal Biotechnology, Reproductive Biomedicine Research Center, Royan Institute for Biotechnology, ACECR, Isfahan, Iran*

*Emails: parham@um.ac.ir, mh.nasr-esfahani@royaninstitute.org*

**Received: 19/December/2020, Accepted: 28/April/2021**

Abstract

**Objective:** Tendon repair strategies usually are accompanied by pathological mineralization and scar tissue formation that increases the risk of re-injuries. This study aimed to establish an efficient tendon regeneration method simultaneously with a reduced risk of ectopic bone formation.

**Materials and Methods:** In this experimental study, tenogenic differentiation was induced through transforming growth factor- β3 (TGFB3) treatment in combination with the inhibiting concentrations of bone morphogenetic proteins (BMP) antagonists, gremlin-2 (GREM2), and a Wnt inhibitor, namely sclerostin (SOST). The procedure's efficacy was evaluated using real-time polymerase chain reaction (qPCR) for expression analysis of tenogenic markers and osteo-chondrogenic marker genes. The expression level of two tenogenic markers, *SCX* and *MKX*, was also evaluated by immunocytochemistry. Sirius Red staining was performed to examine the amounts of collagen fibers. Moreover, to investigate the impact of the substrate on tenogenic differentiation, the nanofibrous scaffolds that highly resemble tendon extracellular matrix was employed.

**Results:** Aggregated features formed in spontaneous normal culture conditions followed by up-regulation of tenogenic and osteogenic marker genes, including *SCX, MKX, COL1A1, RUNX2,* and *CTNNB1. TGFB3* treatment exaggerated morphological changes and markedly amplified tenogenic differentiation in a shorter period of time. Along with TGFB3 treatment, inhibition of BMPs by GREM2 and SOST delayed migratory events to some extent and dramatically reduced osteo-chondrogenic markers synergistically. Nanofibrous scaffolds increased tenogenic markers while declining the expression of osteo-chondrogenic genes.

**Conclusion:** These findings revealed an appropriate *in vitro* potential of spontaneous tenogenic differentiation of eq-ASCs that can be improved by simultaneous activation of TGFB and inhibition of osteoinductive signaling pathways.

***Keywords:*** Bone Morphogrnic Protein, Horse, Mesenchymal Stem Cells, Tenogenic Differentiation, Transforming Growth Factor Beta

Cell Journal(Yakhteh), Vol 24, No 7, July 2022, Pages: 370-379

**Citation:** Shojaee A, Ejeian F, Parham A, Nasr-Esfahani MH. Optimizing tenogenic differentiation of equine adipose-derived mesenchymal stem cells (eq-ASC) using TGFB3 along with BMP antagonists. Cell J. 2022; 24(7): 370-379. doi: 10.22074/cellj.2022.7892.

This open-access article has been published under the terms of the Creative Commons Attribution Non-Commercial 3.0 (CC BY-NC 3.0).

## Introduction

Tendon injuries are considered the most frequent orthopedic challenges of all musculoskeletal injuries in horses. Among them, superficial digital flexor tendon (SDFT) injuries commonly occur in racehorses, which is associated with considerable time and cost (1). Tendon is a hypo-vascular and hypo-cellular tissue naturally leading to a low metabolic activity rate which, in turn, slows down spontaneous tendon repair. Autonomous tendon regeneration is accompanied by abnormalities, not only in cellular phenotypes but also in extracellular matrix (ECM) composition. These abnormalities may result in scar formation and ectopic calcification, leading to elastic mismatch and mechanical complications followed by tendon rupture (2).

Conventional medical interventions are mainly intended to control pain or destroy damaged tissue that results in loss of functionality. In recent years, cell therapy strategies using stem or progenitor cells have received a great deal of attention to improve the efficiency of tendon regeneration, particularly in horses (3). However, the relatively high risk of ectopic bone formation, and potential migration of transplanted mesenchymal stem cells (MSCs) from the site of transplantation, suggests that *in vitro* tenogenic induction before transplantation can improve the healing process and avoid the risks mentioned above (4). Adipose-derived mesenchymal stem cells (ASCs) have attracted a great deal of attention

for cell-based regeneration strategies because of their abundance and easy accessibility and their ability to secrete both tendon ECM components and cytokines (5). Indeed, different growth factors [such as TGFB, platelet-derived growth factor (PDGF), vascular endothelial growth factor (VEGF), basic fibroblast growth factor (bFGF), and insulin-like growth factor-I (IGF1)] have been applied extensively to overcome challenges of routine cell therapy strategies (6). Platelet-rich plasma (PRP) has become a popular approach in cell-based therapies, both in humans and animals, because of its exceptional level of growth factors (7).

Several lines of evidence support the pivotal regulatory role of transforming growth factor B (TGFB) superfamily either during the development of musculoskeletal differentiation or tissue repair via TGFB and/or bone morphogenetic proteins (BMP) signaling pathways. Three well-known ligand isoforms of the TGFB family (TGFB1, TGFB2, and TGFB3) affect cellular activities via canonical (SMADs 2/3-dependent) or non-canonical pathways (8). The precise regulation of these alternative pathways is highly dependent on cell type, culture conditions, and possible cross-talk with other signaling pathways, which in turn control the overall performance of stem cells (9).

TGFB is a pivotal factor for tendon generation in such a way that mutation in either the ligands (TGFB2 and TGFB3) or the receptor (TBR2) prevents tenogenesis during the early stages of embryogenesis (10). During natural tendon healing, TGFB1 normally reaches the peak of expression earlier, while TGFB3 is expressed through the late stages (11). Given the importance of the TGFB family in tendon development and repair, most of the applied regenerative approaches trigger the TGFB signaling pathway as the critical regulator of musculoskeletal lineage (12). All three known isoforms of TGFB revealed a positive effect on viability and cologne synthesis during tendon healing (13). Furthermore, it is evident that TGFB1 causes scar tissue formation, whereas TGFB3 reduces its creation (14).

Although TGFB has many important roles in tendon development and differentiation, it also regulates chondrogenic and osteogenic differentiation in which the balance between TGFB and BMP signaling is important (15). In general, BMP signaling restricts SCX expression as the key trigger signal for tenogenic differentiation. Phosphorylation of BMP receptors activates intracellular downstream SMADs (SMADs 1/5/8) that form a stable complex associated with SMAD4, which then translocate into the nucleus and regulate several target genes such as runt-related transcription factor 2 (*RUNX2*). BMP signaling plays a crucial role in bone formation, and the knockdown of its receptor (*BMPR2*) inhibits osteogenesis in MSCs (16). The positive impact of some BMP family members (BMP11, 12, and 13) on tendon differentiation is also reported (17).

*BMP* antagonizing appears to increase *SCX* expression, accompanied by reduced calcification (18). Among various BMP antagonists, gremlin-2 (GREM2) presents the notable potential to bind and inhibit BMP-2 and BMP-4 efficiently and block the activation of Smad1/5/8. Furthermore, sclerostin (SOST) is also a BMP antagonist with a higher binding affinity to BMP 5/6/7 than BMP2/4 (19). However, SOST is not accepted as a classical BMP inhibitor but more propounded as an antagonistic ligand for Wnt coreceptor LDL-receptor-related protein5 and 6 (LRP5 and LRP6). Indeed, SOST can effectively promote catenin beta1 destruction and down-regulation of the canonical Wnt target genes (20). Wnt signaling pathway provides effective crosstalk with the BMPs and is involved in bone formation and homeostasis. It has also been reported that canonical Wnt mediators are overexpressed along with tendinopathy injuries (21).

Besides chemical stimulation, scaffolds also provide a promising strategy for regulating various cellular behaviors, such as survival, proliferation, and differentiation (22). There are two common members of the poly (hydroxyalkanoates) (PHAs): Poly (3-hydroxybutyrate) (PHB) and its copolymer with 3-hydroxyvalerate (PHBV). They are known as biological polyesters produced by microorganisms and used as the intracellular energy source. So far, PHB/PHBV nanofibrous membranes have been widely investigated to regenerate connective tissues (23). In fact, PHB /PHBV nanofibrous scaffolds attract significant attention to tendon tissue engineering due to their adaptable mechanical properties, long-term biodegradation, and relatively similar structure to tendon ECM (24). It has also been reported that incorporating collagen into nanofibrous scaffolds effectively improves the biological responses involved in tenogenesis (22).

Our recent data demonstrated that eq-ASCs had propounded inherent potential to differentiate towards musculoskeletal lineage amplified in response to TGFB3 treatment (25). Regarding the critical role of TGFB during the tendon development and repair, we investigated how inhibition of the BMP signaling pathway along with TGFB activation can modulate the exclusive tenogenic differentiation of eq-ASCs with the elimination of undesirable osteo-chondrogenesis. This goal was followed through the stepwise treatment of eq-ASCs by TGFB3 and a combination of GREM2 and SOST. Furthermore, we investigated the impact of PHB /PHBV/ COL1 nanofibrous scaffold on improving the tenogenic differentiation status of eq-ASCs.

## Materials and Methods

### Eq-ASCs isolation, Culture, and Characterization

Subcutaneous adipose tissue samples were obtained from a 2-years-old female horse, and ASCs were isolated, characterized, and cultured under normal conditions (5% $CO_2$ and 37°C), as previously described. Briefly, harvested fat tissue was washed with PBS solution and enzymatically digested using 0.075% collagenase type I. Cell suspension were filtered through the 40 μm nylon

mesh and cultured under Dulbecco's Modified Eagle's Medium (DMEM) supplemented with 10% fetal bovine serum (FBS) and 1% P/S. Eq-ASCs were characterized in passage 3, considering the minimal criteria of MSCs (25). For further analysis, ADSCs in passages 3–5 were applied. The procedures used in this study to obtain primary adipose stem cells from the horse were approved by the Ethics Committee of the Royan Institute (IR.ACECR.ROYAN.REC.1395.9). All methods were performed in accordance with relevant guidelines and regulations. Unless otherwise noted, all chemical reagents were obtained from Gibco (Paisley, UK).

### Appropriate dose selection for bioactive factors

The effective dosages of recombinant human TGFB3 (R&D System, Minneapolis, Minnesota, USA) were assessed based on its ability to induce *SXC* expression following one and three days treatment with 2.5-10 ng/ml of TGFB3 (26). Also, to determine the proper concentration of BMP antagonists for eq-ASCs, dose-response studies were conducted concerning related reports on the different types of MSCs (27, 28). Following one day of treatment with TGFB3 (2.5 ng/ml), the inhibitory potential of recombinant mouse GREM2 (R&D System, Minneapolis, Minnesota, USA) was evaluated at concentrations of 100 and 200 ng/ml. Also, recombinant human SOST (R&D System, Minneapolis, Minnesota, USA) was treated at the range of 250 to 2250 ng/ml for further two days following TGFB treatment.

### Tenogenic induction in eq-ASCs

In order to induce tenogenic differentiation, cells were plated at a density of $2\times10^4$ cells/cm$^2$ in standard culture conditions. On a sub-confluent state (70-80% confluency), eq-ASCs were treated with the various combination of factors described in Table S1 (See Supplementary Online Information at www.celljournal.org). The morphological feature of cells was precisely monitored during 10 days of induction using an inverted microscope (Olympus, Tokyo, Japan), and cells were harvested for further analysis after 3, 7, and 10 days.

### RNA isolation and gene expression analysis

RNA extraction of the cells was carried out using TRI reagent (Thermo Fisher Scientific, Waltham, Massachusetts, USA), and complementary DNA (cDNA) was synthesized by cDNA Synthesis kit (Fermentas, Waltham, Massachusetts, USA) according to the manufacturer's description. Subsequently, the qRT-PCR assay was performed on the ABI Step One Real-Time PCR System (Applied Biosystem, Foster City, California, USA) with SYBR green master mix (TaKaRa Bio Inc, Kusatsu, Shiga Prefecture, Japan). Data analysis was conducted using the $2^{-\Delta\Delta Ct}$ method. *GAPDH* was used as the internal control gene, and the gene expression level was normalized to untreated cells (day 0). The information for specific primers used to evaluate the target genes is provided in Table S2 (See Supplementary Online Information at www.celljournal.org) .

### Immunocytochemical assay

Cells were fixed in 4% paraformaldehyde on days 3, 7, and 10,, permeabilized with 0.2% triton x-100, and were blocked with 10% goat serum prior to incubation. So, they were washed and incubated with the primary antibodies against SCX (Abcam, Cambridge, UK), MKX (Aviva Systems Biology, San Diego, California, USA) as well as control immunoglobulin G (Abcam, Cambridge, UK). Specific stained antigens were then labeled with FITC-conjugated secondary antibody (Sigma-Aldrich, St. Louis, Missouri, USA). In addition, nuclei were counterstained with 4, 6-diamidino-2-phenylindole (DAPI, Sigma-Aldrich, St. Louis, Missouri, USA). Further imaging was performed under fluorescence microscopy (BX51, Olympus, Tokyo, Japan). For quantitative SCX and MKX, corrected total cell fluorescence (CTCF) was determined using Image J and calculated through subtracting the background using the following formula:

CTCF=Integrated density-(area of interest×mean background fluorescence).

### Western blotting

T/G and T/G/S treated cells were lysed after 3, 7, and 10 days using TRI reagent (Thermo Fisher Scientific, Waltham, Massachusetts, USA), according to the manufacturer protocol. Total protein concentration was measured by Bradford assay. Afterward, equal amounts of each sample (30 μg) were run on sodium dodecyl sulfate–polyacrylamide gel electrophoresis (SDS-PAGE) gel and blotted onto PVDF membrane (Bio Rad). Blots were blocked with 10% skim milk (Millipore) and incubated with anti-SCX (Abcam, ab58655), anti-MKX (Aviva Systems Biology, ASB-ARP32574-P050), and anti-β-Actin (Santa Cruz, sc-47778) antibodies for 2 hours at room temperature. Then, membranes were incubated for 1 hour at room temperature with an appropriate secondary antibody: horseradish peroxidase (HRP)-conjugated goat anti-mouse IgG (Dako) or HRP-conjugated mouse anti-rabbit IgG (Santa Cruz). Finally, the protein bands were visualized by an Amersham ECL Advance Western Blotting Detection Kit (GE Healthcare).

### Sirius red staining

For Sirius Red staining, induced eq-ASCs at three-time points (3, 7, and 10 days) were rained with PBS and fixed with 4 % paraformaldehyde. Next, deposited collagens were stained with 0.1% Sirius Red F 3B (Direct Red 80, Sigma-Aldrich, St. Louis, Missouri, USA) in a saturated aqueous solution of picric acid for 1 hour at room temperature. In order to quantify, nodules were solubilized with 1:1 (v/v) 0.1% NaOH and absolute methanol for 30 minutes at room temperature, and related absorbance was measured at 540 nm by a spectrophotometric plate reader (Stat Fax 3200, Awareness Technology, Inc., Palm City, Florida, USA).

### Phalloidin staining

The morphology of the eq-ASCs on the scaffolds was evaluated with phalloidin staining of the actin cytoskeleton. Briefly, cells were fixed in formaldehyde 4%, permeabilized using triton 0.2%, and sequentially stained with the phalloidin-TRITC label (Tetramethylrhodamine B isothiocyanate; Sigma) and 4′, 6-diamidino-2-phenylindole (DAPI, Sigma). Finally, fluorescence images were obtained using fluorescence microscopy (Olympus, BX51, Japan).

### MTS assay

The viability and proliferation rate of the cells on the nanofiber scaffold was evaluated using MTS assay after one, three, and five days. To assess the metabolic activity at each time point, the medium was replaced with the fresh medium containing 10% MTS stock solution (Promega, WI, USA) and incubated at 37˚C for 3.30 hours. Finally, net absorbance was measured at 450 nm with a Microplate Reader (Fluostar Optima, BMG Lab Technologies, Germany).

### Cell seeding on the scaffold

A previously characterized aligned PHB /PHBV/Col electrospun nanofiber scaffold (a kind gift from Dr. Elaheh Masaeli, Royan institute for biotechnology, Isfahan, Iran) (29) was used to mimic the natural microenvironment of tendon tissue. The scaffolds were sterilized by immersion in 70% ethanol for 2 hours, washed twice with PBS, and incubated overnight in the basic cell culture medium. To evaluate the potential of scaffolds for amplifying tenogenic response in eq-ASCs, the cells were seeded at a density of $2.5\times10^4$ cells/cm$^2$ and induced with the optimum concentrations of T/G/S factors. The eq-ASCs cultured on the tissue culture plate (TCP) and treated under similar conditions were considered as control. Tenogenesis was assessed after 10 days via analysis of the expression of specific tenogenic markers (*SCX*, *MKX*, *COL1A1*) and osteo-chondrogenic genes (*SOX9*, *BMPR2*, *RUNX2*, *CTNNB*).

### Statistical analysis

At least three independent experiments were performed for all assays. Statistical analysis was carried out using SPSS 16.0 software (Inc., Chicago, USA) by two-way analysis of variance (ANOVA) followed by 'Tukey's post hoc test. P<0.05 were considered statistically significant for all the experiments.

## Results

### Finding the proper concentration of inducing factors

Regarding the specific function of TGFB3 in triggering musculoskeletal specification, we assessed the most effective concentration of TGFB3 on eq-ASCs based on the expression of *SCX*. 2.5 ng/ml was defined as the optimal dose for TGFB3, resulting in maximal expression of *SCX* on dayone (Fig.1A). In addition, we demonstrated that pre-treatment with 2.5 ng/ml of TGFB3 followed by 200 ng/ml of GREM2 preserves the increased *SCX* expression level on day 3 (Fig.1B). In contrast, in the absence of this pre-treatment with TGFB3, GREM2 significantly reduced the *SCX* expression (P<0.05, Fig.S1A, See Supplementary Online Information at www.celljournal.org). Moreover, a high *SCX* level was achieved by 1250 ng/ml SOST treatment accompanied by significant inhibition of *CTNNB1*, as a sign of osteogenesis (Fig.1C, D). Therefore, treatment with 2.5 ng/m of TGFB3, 200 ng/m of GREM2, and 1250 ng/ml of SOST were chosen as the optimal condition to achieve the highest *SCX* expression and used for the remaining experiments.

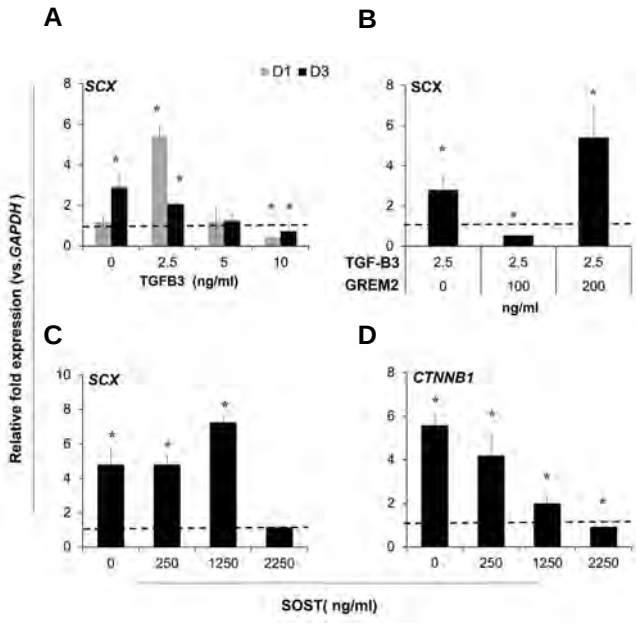


**Fig.1:** Concentration-dependent effect of bioactive factors used to induce tenogenic differentiation. **A.** qRT-PCR analysis of *SCX* following treatment of eq-ASCs with different concentrations of TGFB3 (0-10 ng/ml) for one and three days and **B.** GREM2 (100 and 200 ng/ml) for a further two days, **C.** *SCX* revealed the highest expression level in 2.5 ng/ml TGFB3 and 200 ng/ml of GREM2. In response to serial five-fold dilution of SOST (250-2250 ng/ml), *SCX* peaked at 1250 ng/ml, and **D.** The expression level of *CTNNB1* gradually decreased. All data were normalized to *GAPDH* and presented as mean ± SD. *; Present significant changes vs. day 0 untreated cells (dashed line), P<0.05 and qRTPCR; Real-time polymerase chain reaction.

### Effect of different factors on tenogenic differentiation of eq-ASCs

The untreated cells started to migrate on day 7 and formed compact aggregations after 10 days of being cultured under normal conditions (Fig.2A). However, after TGFB3 treatment (T) the aggregates were observed on day 3, and followed by cell death. In contrast, following pre-treatment for one day with TGFB3 and then with GREM2 treatment (T/G), cells spread out of aggregates and formed a monolayer. We also found that following pre-treatment with TGFB3

for one day and then with GREM2 and SOST (T/G/S), an intermediate morphological feature between T and T/G was observed after 10 days.

Assessment of expression of genes related to tenogenesis showed a significant up-regulation of *SCX* on day 3 in T/G group (P<0.05), which gradually declined over time (Fig.2B). *MKX* expression on day 3 was significantly lower in T compared to the control group (0.2 vs. 0.86, P<0.05), while *MKX* expression significantly increased in T/G and T/G/S compared to the control group (2.23 vs. 0.86, P<001; 3.8 vs. 0.86, P<0.0001 respectively, Fig.2C). *MKX* expression was also significantly reduced on days 7 and 10 in T/G/S group compared to the control group (0.35 vs. 1.6 P<0.0001, and 0.21 vs. 0.99 P<0.004). *COL1A1* expression was significantly increased on days 3, 7, and 10 in the T/G/S group in comparison with the control group (1.3 vs. 0.2, P<0.0001; 1.35 vs. 0.37, P<0.000, 0.79 vs. 1.27, P<0.002). While, COL1A1 expression in T/G group was significantly higher than the control group on day 3 (0.84 vs. 0.2, P<0.0001), the expression of this gene gradually declined by days 7 and 10. Despite this reduction, *COL1A1* expression was still significantly higher than the control group on day 7 (0.73 vs. 0.37, P<0.05). Although, it was significantly decreased and reached to a values lower than the control group by day 10 (0.02 vs. 1.27, P<0.000, Fig.2D). Nevertheless, *TNMD* expression could not be detected in any of the groups.

Regarding chondrogenic markers, *SOX9* expression level remained just below the baseline in standard culture conditions at all-time points. Although its expression fluctuated in response to TGFB3, except for a slight increase in T/G group on day 3, the value of *SOX9* did not markedly change in T/G and T/G/S (Fig.2E). The expression of *CTNNB* showed a gradual increase in the control and T/G group, while it dropped sharply in the T group and relatively in T/G/S group (Fig.2F). Figure 2G reveals a low level of *BMPR2* expression with a periodic mode in the control group, while it leveled out in the T group and dramatically decreased in T/G. Surprisingly, we found a primary increase in *BMPR2* in response to T/G/S induction, which returned to its basal level before induction. *RUNX2* exhibited a similar expression pattern to *BMPR2* in standard culture conditions, which was amplified by TGFB3 treatment and leveled out in response to GREM2 (T/G group). In addition, it was strongly inhibited by T/G/S treatment over time from day 3 to day 10 (Fig.2H).

Interestingly, treatment of cells with GREM2 without pre-treating with TGFB3, not only reduced the expression level of *SCX*, as a tenogenic marker (Fig. S1A, See Supplementary Online Information at www.celljournal.org), but also significantly increased osteo-chondrogenic markers as the time went by (Fig.S1B, See Supplementary Online Information at www.celljournal.org). Additionally, cellular aggregation in this group (Fig.S1C, See Supplementary Online Information at www.celljournal.org) was more than that in the control group, while it was delayed compared to the other groups like T, T/G, and T/G/S (Fig.2A).

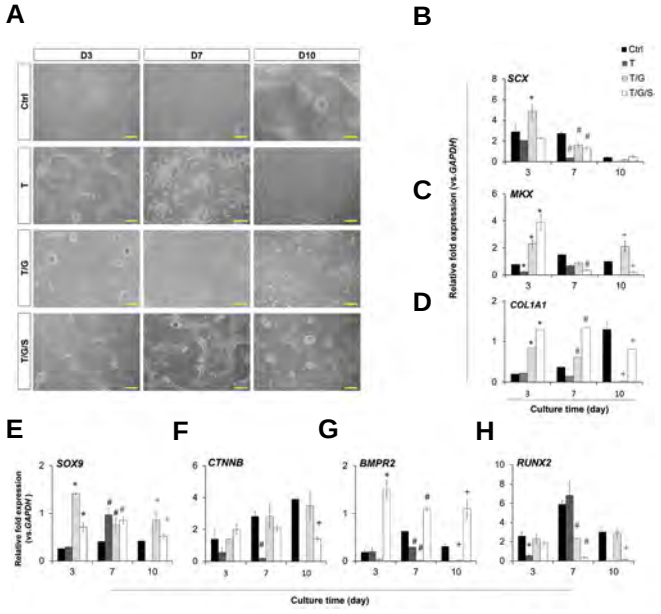


**Fig.2:** Morphological and gene expression analysis in response to the various combination of inducing factors. **A.** Phase-contrast photographs on three-time points (day 3, 7, and 10) presented notable morphological changes in eq-ASCs in all test groups (T, T/G, and T/G/S) as well as in control (scale bar: 400 µm). **B-D.** Commonly, migratory features consist of aggregate formation and appearance of empty spaces, which were different between groups and at different times. qPCR analysis for the evaluation of tenogenic-related genes (*SCX*, *MKX,* and *COL1A1*) in eq-ASCs cultured under different conditions revealed a remarkable expression level, particularly in T/G/S group. **E-H.** Analysis of the expression of chondrogenic (*SOX9*) and osteogenic-related genes (*CTNNB*, *RUNX2,* and *BMPR2*) showed a dramatic reduction in response to T/G/S treatment, except for *BMPR2*. Data were normalized to *GAPDH* and presented as mean ± SD. *, #, +; Present significant (P<0.05) changes vs. T/G group at the day 3, 7, and 10, respectively, T; Treatment with TGFB3 (2.5 ng/ml) for one day, T/G; Pretreatment with TGFB3 (2.5 ng/ml) followed by GREM2 (200 ng), T/G/S; Pretreatment with TGFB3 (2.5 ng/ml) followed by GREM2 (200 ng/ml) and SOST (1250 ng/ml), and qPCR; Real-time polymerase chain reaction.

## Expression of tendon-associated proteins in T/G vs. T/G/S culture conditions

In addition, the protein profile of two specific markers related to tenogenesis, SCX, and MKX, were investigated following T/G and T/G/S treatment which had the most significant effect on the tenogenic differentiation status of eq-ASCs. Figure 3A, B shows the strong nucleus signal (green stain) of SCX on day 3, both in T/G and T/G/S groups, which gradually declined until day 10; this reduction appeared to delay in the T/G/S. On the other hand, the expression of MKX was facilitated in T/G/S compared to the T/G group (Fig.4A, B), which was verified by quantification of SCX and MKX intensity (Figs.C3, C4). The results are consistent with the expression pattern of SCX and MKX presented by western blot analysis (Figs.3D, 4D). The targeted protein bands were visualized at 22 KDa for SCX and 39 KDa in the case of MKX and β-actin.

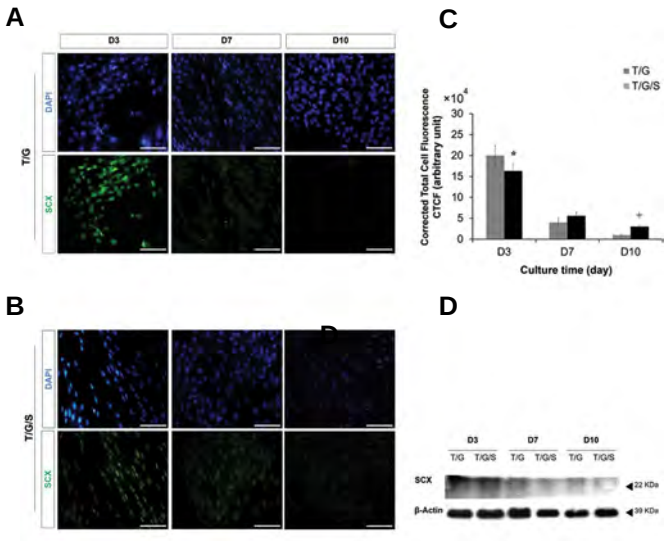


**Fig.3:** Immunocytochemistry assay to assess expression pattern of SCX. **A, B.** Immunofluorescence images showed a considerable level of SCX (green) positive cells, especially on day 3, in both T/G and T/G/S treated groups, which was gradually reduced by day 10. **C.** Nuclei were counterstained with DAPI (scale bar: 50 µm). Quantification assay results are presented as corrected total cell fluorescence (CTCF) for SCX in both T/G and T/G/S treated groups and presented as mean ± SD, *, +; Present significant (P<0.05) changes vs. T/G group at the day3 and 10, respectively. **D.** Western blotting analysis confirmed the expression pattern of SCX in T/G and T/G/S during the treatment period. T/G; Pretreatment with TGFB3 (2.5 ng/ml) for one day followed by GREM2 (200 ng/ml), T/G/S; Pretreatment with TGFB3 (2.5 ng/ml) followed by GREM2 (200 ng/ml) and SOST (1250 ng/ml).

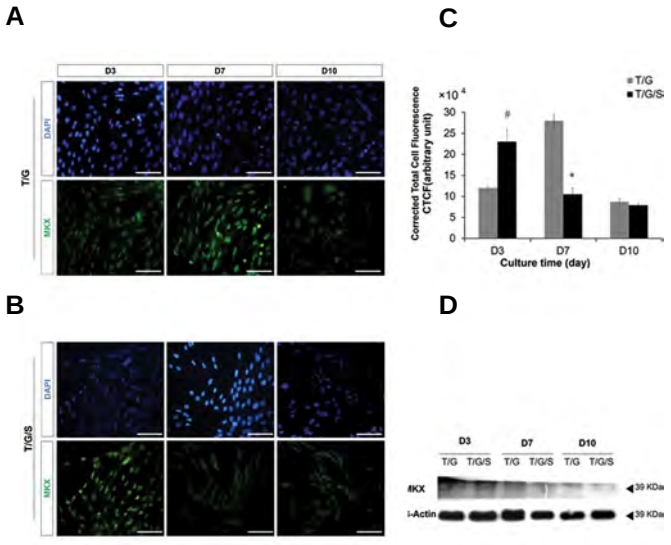


**Fig.4:** Immunocytochemistry assay to assess expression pattern of MKX. **A.** Immunofluorescence images showed that MKX (green) reached the maximum level on day 7 in T/G group (scale bar: 100 µm), **B.** but was extensively expressed on day 3 in T/G/S treated eq-ASCs. Nuclei were counter-stained with DAPI (scale bar: 100 µm). **C.** Quantification assay results are presented as corrected total cell fluorescence (CTCF) for MKX in both T/G and T/G/S treated groups(c) and presented as mean ± SD. *, #, +; Present significant (P<0.05) changes vs. T/G group at days 3, 7 and 10 respectively. **D.** The western blotting analysis confirmed the expression pattern of MKX in T/G and T/G/S during the treatment period. T/G; pretreatment with TGFB3 (2.5 ng/ml) for one day followed by GREM2 (200 ng/ml), T/G/S; pretreatment with TGFB3 (2.5 ng/ml) followed by GREM2 (200 ng/ml) and SOST (1250 ng/ml).

Moreover, Sirius Red staining was applied to investigate the collagen content as the major component of the tendon matrix. All groups were positive for this staining (Fig.5A). However, the quantitative analysis of the stained imagesrevealed that the maximum collagen content was observed in the T/G/S group, which was significantly higher than the control group on days 3 and 7 (P<0.05). In contrast, collagen content significantly decreased in the T/G group compared to the control group by day 10 (Fig.5B). Furthermore, the considerable amount of collagen accompanied by results of gene expression profile analysis in the control group confirmed the spontaneous tenogenic differentiation potential of eq-ASCs. Expression of tenogenic markers in the control group showed up-regulation of tendon progenitor marker (*SCX*) at mRNA level on day 3 versus day 1 (1.17 vs. 2.8, P<0.02) and late differentiation marker (*MKX)* on day 3 versus day 7 (0.77 vs. 1.6, P<0.002) followed by increasing of *COL1A1* expression on day 10. However, their tenogenic potential is limited due to the up-regulation of osteo- chondrogenic genes (Fig.2F-H).

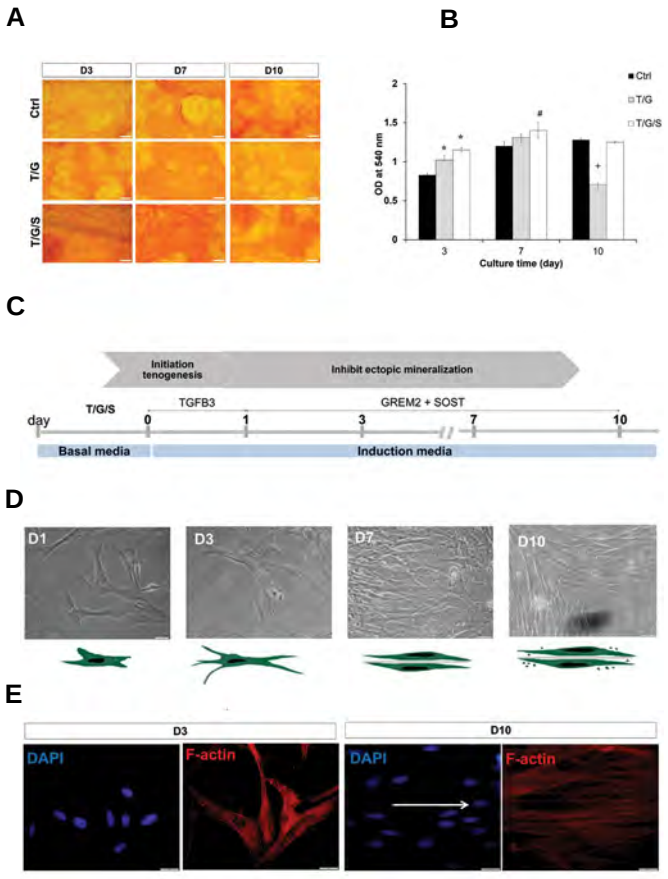


**Fig.5:** Eq-ASCs during stepwise tenogenic differentiation. **A.** Accumulation of collagen fibers in the extracellular matrix was shown in red, which was gradually increased over induction time, specifically in T/G/S group (scale bar: 200 µm). **B.** Quantification analysis of Sirius Red stained samples at 540 nm by spectrophotometric plate reader significantly showed the highest collagen secretion in T/G/S. Data are presented as mean ± SD. *; Present significant changes vs. control sample of the same day, P<0.05. Ctrl; control, T/G; Pretreatment with TGFB3 (2.5 ng/ml) followed by GREM2 (200 ng), T/G/S; Pretreatment with TGFB3 (2.5 ng/ml) followed by GREM2 (200 ng/ml) and SOST (1250 ng/ml). **C.** Flow chart illustrates the experimental design for stepwise induction of Eq-ASCs into tenocytes through biological factors stimulation. **D.** Morphological changes of eq-ASCs during differentiation to tenocytes under an inverted microscope with their schematic presentation. **E.** Fluorescence images of TRITC-phalloidin staining showed morphological changes of eq-ASCs at the early (day 3) and late (day 10) time point of induction. The arrow highlights the alignment of the cell (scale bar: 20 µm).

### Expression of tendon-specific markers is associated with morphological changes of eq-ASCs

In addition to tenogenic marker expression, the morphologic features for tenocytes were also assessed in the best group (T/G/S) according to mRNA and protein expression profiles. Phase-contrast photographs at different time points (day 1, 3, 7, and 10) indicated that we achieved tenocytes based on cell shape appearance within 7 days of induction by treatment with 2.5 ng/m of TGFB3 for one day, followed by 200 ng/m of GREM2 and 1250 ng/ml of SOST, as stepwise tenogenic differentiation approach (Fig.5C, D). Furthermore, phalloidin staining exhibited an ovoid nucleus with large cytoplasmic and protrusive structures at the early stage of induction (day 3). Elongated nuclei and thin cytoplasmic are observed at the late time point (day 10). The cells displayed a few prolonged stress fibers on day 3 which gradually became longer along with the aligned cell morphology (Fig.5E), which confirmed morphological changes under inverted microscopy (Fig.5D).

### Cell - cytotoxicity assay for scaffold using eq-ASCs

The cell viability, cell growth, and cell morphology were used as parameters to determine the cytotoxic effect of the scaffolds. Visualization of the F-actin cytoskeleton to assess the morphology was done by phalloidin staining after 3 days of culture. The fluorescence images demonstrated that eq-ASCs had well attached and spread on the scaffold; additionally, an aligned cell orientation was observed (Fig.6A,B). Interestingly, MTS assay after 1, 3, 5 days of cell culture on nanofiber displayed no significant difference ($P<0.05$) compared with tissue culture plates (TCP) (Fig.6C).

### Effect of scaffold on the expression of tenogenic markers in eq-ASCs treated with T/G/S

To evaluate the influence of the substrate on the tenogenic differentiation status, we analyzed the expression levels of the genes mentioned above in eq-ASCs treated with T/G/S in the presence and absence of scaffold. According to our findings, tenogenesis was induced on PHB/PHBV/COL1 membranes under sequential treatment with T/G/S factors. In comparison with T/G/S group, we showed a relatively lower level of expression of tenogenic markers at the earliest time point (day 3) in the scaffold group, while it provided higher and more stable expression on days 7 and 10 (Fig.6D-F). It is also interesting to note that the expression of osteo-related genes (BMPR2, RUNX2, and CTNNB) had significantly reduced in the scaffold group. The only exception was the expression of the chondrogenic marker *SOX9* which had fluctuated (Fig.6G-J).

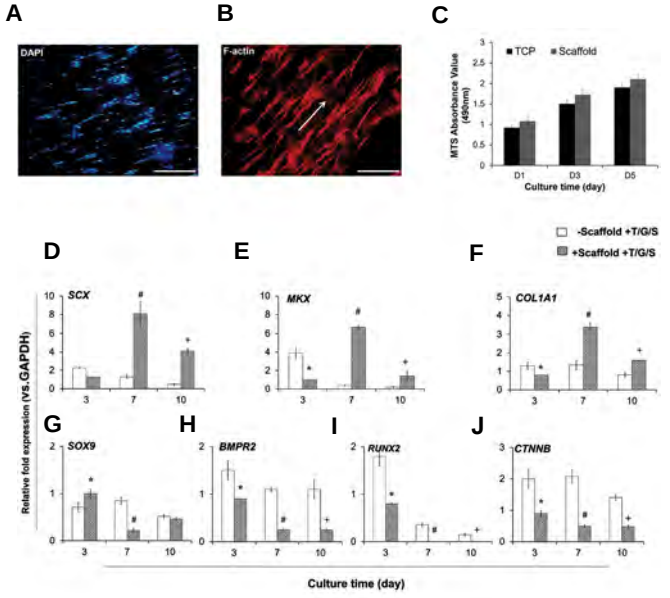


**Fig.6:** Cell culture and tenogenic differentiation of eq-ASCs on nanofibrous PHB/PHBV/COL1 scaffold. **A, B.** The phalloidin staining of the actin cytoskeleton (red) after 3 days of culture showed the attachment and growth of the eq-ASCs on the scaffolds. Nuclei were counterstained with DAPI (blue) (scale bar: 200 µm). **C.** MTS assay indicated that there was no significant difference in viability of eq-ASCs in the presence and absence of nanofiber scaffold on day 1, 3, and 5 of the culture. The arrow highlights the alignment of cells. Data were normalized to the ratio absorbance of scaffold and medium without cells and presented as mean ± SD. *P<0.05. **D-F.** QPCR analysis of tenogenic markers expression and **G-J.** The osteochondrogenic markers in eq-ASCs treated with T/G/S for 10 days. eq-ASCs were seeded on the scaffold and treated with T/G/S showed increased expression of *SCX*, *MKX*, *COL1A1, SCX*, *MKX,* and *COL1A1,* and decreased expression of *SOX9, CTNNB*, BMPR2, and *RUNX2* compared to T/G/S group without scaffold. Data are presented as mean ± SD. *, #, +; Present significant (P<0.05) changes *vs.* control at days 3, 7, and 10, respectively. T/G/S; Pretreatment with TGFB3 (2.5 ng/ml) followed by GREM2 (200 ng/ml) and SOST (1250 ng/ml).

## Discussion

Despite recent advances in cell therapy for tendon injuries, conventional strategies for regenerating functional tendons are often inefficient. Therefore, *in vitro* modification for improving the efficacy of cell therapy appears to be highly reasonable before clinical application. We recently showed that eq-ASCs have inherent differentiation capacity to musculoskeletal-lineage (26). In the present study, we focused on investigating an efficient procedure for specific tenogenic induction of eq-ASCs with particular attention to reducing the chance of osteogenesis.

During embryogenesis, transcription factors, such as scleraxis (SCX) and sex-determining region Y-box 9 (SOX9), play a crucial role in the formation of tendon progenitors, whereas Mohawk (MKX) and early growth response protein 1/2 (EGR1/2) are required for terminal tendon differentiation. These transcription factors are involved in tenocyte specification and coding ECM components such as collagen type I (*COL1A1*) and tenomodulin (*TNMD*) as a late marker of tendon development (30). Therefore, we initially estimate the effective concentration of TGFB3 that induced higher expression of *SCX*. Since the highest expression level of

*SCX* was achieved on day 1, for further experiments, we treated the cells with TGFB3 only for one day.

Literature supports the critical impact of TGFB3 ligands on the up-regulation of tendon-associated markers, including *MKX* and *COL1,* via up-regulation of SCX (31). The relative expression of these markers was decreased upon the continuation of treatment with TGFB3 within the following days. This is not unexpected as the expression of SCX was reduced by further treatment with TGFB3 (after day one). Indeed, similar to our results, it has been shown that a high concentration of TGFB over time negatively affects tenogenesis (32). Therefore, we decided to treat the eq-ASCs only with TGFB3 for one day based on these results.

These results confirmed that TGFB3 efficiently triggered tendon specification of eq-ASCs while achieving a stable and final tenogenic differentiation status requires complementary signals. It is important to note that ectopic mineralization, as a major hurdle to tendon regeneration, takes place in the absence of these secondary signals. Besides, BMP treatment has an inhibitory effect on *SCX* expression, which was almost reversed by noggin (18). Hence, we focused on inhibiting the BMP signaling pathway by using two well-known BMP antagonists, GREM2 and SOST, following one-day treatment or induction with TGFB3.

Initially, we showed that short-term treatment with GREM2 for one day and assessment of SCX on day 3 did not improve SCX expression compared to the control group. Therefore, we decided to evaluate the effect of TGFB3 for one day, followed by GREM2 from days 2-10. Our result revealed that the expression of SCX, MKX, and COL1A1 was increased on day 3, followed by a reduction during additional days. The only signal in osteo-chondrogenic differentiation was reduced through treatment with TGFB3 followed by GREM2 was RUNX2. Therefore, these results suggest that other secondary signals are required to improve tenogenic differentiation.

Several lines of evidence verified SOST as an impressive BMP antagonist, which also negatively regulates the Wnt signaling pathway and inhibits osteogenesis (32). Therefore, it was not surprising that the severe inhibition of BMPR2 induced by GREM2 was partially reversed in the presence of SOST, which seemed to recover the BMP pathway to some extent. This is consistent with the observed drastic down-regulation of *RUNX2* by the combinational treatment with G/S over time (day 10), along with the reduced *CTNNB* level. Although SOX9 is known as a cartilage-associated marker, previous studies have suggested that a basal level of *SOX9* expression is required in a distinct subtype of tendon progenitor cells (33). We also found a primary overexpression of *SOX9* in T/G and T/G/S groups, which declined over time.

Regarding tenogenic related genes, T/G treated cells showed the highest expression level of SCX, while MKX showed its highest expression in T/G/S group, both on day 3. Considering the primary high COL1A1 expression level in untreared cells, T/G/S showed aoitential to keep this level constant which underscored the importance of SOST in tenogenic induction. These results are consistent with the data obtained by Sirius Red staining showing almost the same manner for the secretion of collagen fibers as the major extracellular content in the tendon.

SCX is a basic helix-loop-helix transcription factor that plays a critical role in the early stage of development in tenocytes and other dense connective tissues, like periodontal ligaments and heart valve (34). Regarding the force transmitting function of these cells, SCX is required for modulating cytoskeletal tension via triggering the expression of proteins linked between actin filaments and integrin molecules (35). Nichols et al. (36) reported that equine tenocytes transfected with *SCX* siRNA faced a remarkable decrease in cytoskeletal stiffness and inability to migrate on soft surfaces. Moreover, several tendon-specific genes, such as *MKX*, *COL1,* and *TNMD,* are positively regulated in tenocytes by SCX (37).

Unlike SCX, different studies have noticed some severe issues with using TNMD as a reliable marker for tenogenic differentiation in equines, especially at mRNA level. For instance, an almost similar expression level of *TNMD* was detected by Taylor et al. (38) in the ‘horse’s bone and tendon. Also, Barsby and Guest (26) provided some valuable evidence about the high degradation of TNMD mRNA in TGFB -treated equine ESCs. Similarly, we also did not find TNMD expression in the control and tested groups.

Gene expression analysis was further confirmed at the protein level, which revealed a more stable expression of SCX and facilitated the expression of MKX as the result of T/G/S treatment compared to T/G treatment. Since the morphological feature of cells is still noted as an important sign of their state, the spindle-like shape and aligned arrangement are typically considered for tenocytes, in contrast with the more rounded shape of tenoblasts with a large and oval nucleus. At the end of the induction time, we observed spindle-like cells with elongated nuclei and thin cytoplasmic protrusions.

Overall, based on the results of gene expression analysis, protein expression data, and morphological analysis, we propose a stepwise protocol to induce tenogenic differentiation of eq-ASCs within 7 days which is far shorter than what has been previously reported (14 days) by transient induction with TGFB3 followed by co-inhibition of BMP and Wnt signaling pathways. In addition, one of the main strengths of this procedure was a severe reduction in levels of ectopic osteo and chondrogenesis markers. It has been highlighted in several studies in which the expression of tendon-associated markers were shown to be down-regulated in mature tenocytes (39). However, reaching stable mature tenocytes with proper function in the long term and preventing cellular dedifferentiation requires further modification of the protocol. Therefore, we subsequently examined the effects of nanofibrous PHB /PHBV/COL1 scaffolds on the efficiency and long-

term stability of reported sequential tenogenic induction on eq-ASCs.

Both enhanced and more stable expression of tenogenic markers and the potent inhibition of osteo-chondrogenesis on PHB /PHBV/COL1 membrane proposed the scaffold as a suitable substrate for cell transplantation and tendon regeneration. It seems that incorporating collagen type 1, as the major content of natural tendon ECM, in addition to the fibrous and porous topology of PHB/PHBV, provides a positive impact on tenogenesis (24).

It is interesting to note that the most successful cell therapy approaches were reported in the cases of intra-lesional injection of a cell suspension due to granular tissue and the enclosed nature of core lesions. The use of MSC-derived tenocyte progenitors revealed a notable positive impact on increasing the efficacy of cell therapy for tendon repair (40). Although, for other forms of tendon-related disorders (like eccentric lesions), further studies are required to optimize the condition ,including the use of different types of scaffolds or self-organizing tendon structures (3D tendon-like tissue constructs).

For the first time, we investigated the tenogenic differentiation of equine adipose stem cells under the stepwise inductive approach which provides a safe, valuable alternative for un-induced MSCs for future intra-lesional injection. This result was verified mainly by using the scaffold to maintain a tenogenic status. However, future studies need to be conducted regarding the damaged condition to choose a scaffold which can be practicaly delivered into equine tendon injury.

## Conclusion

The present study demonstrated a fast and effective procedure for reducing the risk of ectopic osteogenesis in tendon regeneration strategies. We recently provided evidence that confirmed the remarkable potential of eq-ASCs for spontaneous differentiation towards musculoskeletal lineage due to the high expression of endogenous TGFB1. Here, we established a stepwise inductive approach to induce tenogenesis of eq-ASCs using TGFB3, GREM2, and SOST to overcome this limitation to some degree and achieve tenocytes in a short time. The current study provides new findings for future cell-based therapies to avoid the risk of ectopic bone formation after injection of MSCs in tendon injuries.

## Acknowledgments

The authors would like to thank Dr. Elahe Masaeli (Royan Institute for Biotechnology) for kindly gifting the PHB/PHBV/COL1 membranes. We are also grateful to all members of the Royan Institute for Biotechnology for their kind support and help. This study was financially supported by Ferdowsi University of Mashhad and Royan institute. The authors declare that they have no conflict of interest.

## Authors' Contributions

A.Sh., Carried out the experiments and analyzed data. F.E., Conceived the project, interpreted the data, and drafted the manuscript. A.P., M.H.N.-E.; Supervised the research, interpreted the data, and critically revised the manuscript. All authors read and approved the final manuscript.

## References

1. Ortved KF. Regenerative Medicine and rehabilitation for tendinous and ligamentous injuries in sport horses. Vet Clin North Am Equine Pract. 2018; 34(2): 359-373.
2. Yang G, Rothrauff BB,Tuan RS. Tendon and ligament regeneration and repair: clinical relevance and developmental paradigm. Birth Defects Res C Embryo Today. 2013; 99(3): 203-222.
3. Conrad S, Weber K, Walliser U, Geburek F, Skutella T. Stem cell therapy for tendon regeneration: current status and future directionsSeries. Adv Exp Med Biol. 2019; 1084: 61-93.
4. Becerra P, Valdes Vazquez MA, Dudhia J, Fiske-Jackson AR, Neves F, Hartman NG, et al. Distribution of injected technetium (99m)-labeled mesenchymal stem cells in horses with naturally occurring tendinopathy. J Orthop Res. 2013; 31(7): 1096-1102.
5. Burk J, Gittel C, Heller S, Pfeiffer B, Paebst F, Ahrberg AB, et al. Gene expression of tendon markers in mesenchymal stromal cells derived from different sources. BMC Res Notes. 2014; 7(1): 826.
6. Molloy T, Wang Y, Murrell G. The roles of growth factors in tendon and ligament healing. Sports Med. 2003; 33(5): 381-394.
7. Mishra A, Woodall Jr, Vieira A. Treatment of tendon and muscle using platelet-rich plasma. Clin Sports Med. 2009; 28(1): 113-125.
8. Nourissat G, Berenbaum F, Duprez D. Tendon injury: from biology to tendon repair. Nat Rev Rheumatol. 2015; 11(4): 223-233.
9. Wang MK, Sun HQ, Xiang YC, Jiang F, Su YP, Zou ZM. Different roles of TGF- β in the multi-lineage differentiation of stem cells. World J of Stem Cells. 2012; 4(5): 28-34.
10. Chien C, Pryce B, Tufa SF, Keene DR, Huang AH. Optimizing a 3D model system for molecular manipulation of tenogenesis. Connect Tissue Res. 2018; 59(4): 295-308.
11. Docheva D, Müller SA, Majewski M, Evans CH. Biologics for tendon repair. Adv Drug Deliv Rev. 2015; 84: 222-239.
12. Kaji DA, Howell KL, Balic Z, Hubmacher D, Huang AH. Tgfβ signaling is required for tenocyte recruitment and functional neonatal tendon regeneration. Elife. 2020; 9: e51779.
13. Hou Y, Mao Z, Wei X, Lin L, Chen L, Wang H, et al. The roles of TGF-beta1 gene transfer on collagen formation during achilles tendon healing. Biochem Biophys Res Commun. 2009; 383(2): 235-239.
14. Campbell BH, Agarwal C, Wang JH. TGF-beta1, TGF-beta3, and PGE(2) regulate contraction of human patellar tendon fibroblasts. Biomech Model Mechanobiol. 2004; 2(4): 239-245.
15. Grafe I, Alexander S, Peterson JR, Snider TN, Levi B, Lee B, et al. TGF-β family signaling in mesenchymal differentiation. Cold Spring Harb Perspect Biol. 2018; 10(5): a022202.
16. Cao Y, LV Q, LV C. MicroRNA-153 suppresses the osteogenic differentiation of human mesenchymal stem cells by targeting bone morphogenetic protein receptor type II. Int J Mol Med. 2015; 36(3): 760-766.
17. Shen H, Gelberman RH, Silva MJ, Sakiyama-Elbert SE, Thomopoulos S. BMP12 induces tenogenic differentiation of adipose-derived stromal cells. PLoS One. 2013; 8(10): e77613.
18. Chen X, Yin Z, Chen JL, Shen WL, Liu HH, Tang QM, et al. Force and scleraxis synergistically promote the commitment of human ES cells derived MSCs to tenocytes. Sci Rep. 2012; 2: 977.
19. Chang C. Agonists and antagonists of TGF-β family ligands. Cold Spring Harb Perspect Biol. 2016; 8(8): a021923.
20. Semënov M, Tamai K, He X. SOST is a ligand for LRP5/LRP6 and a Wnt signaling inhibitor. J Biol Chem. 2005; 280(29): 26770-26775.
21. Lui PP. Histopathological changes in tendinopathy-potential roles of BMPs? Rheumatology (Oxford). 2013; 52(12): 2116-2126.
22. Zhang X, Bogdanowicz D, Erisken C, Lee NM, Lu HH. Biomimetic scaffold design for functional and integrative tendon repair. J Shoulder Elbow Surg. 2012; 21(2): 266-277.
23. Webb WR, Dale TP, Lomas AJ, Zeng G, Wimpenny I, El Haj AJ, et al. The application of poly(3-hydroxybutyrate-co-3-hydroxyhex-

anoate) scaffolds for tendon repair in the rat model. Biomaterials. 2013; 34(28): 6683-6694.
24. Rathbone S, Furrer P, Lübben J, Zinn M, Cartmell S. Biocompatibility of polyhydroxyalkanoate as a potential material for ligament and tendon scaffold material. J Biomed Mater Res A. 2010; 93(4): 1391-1403.
25. Shojaee A, Parham A, Ejeian F, Nasr Esfahani MH. Equine adipose mesenchymal stem cells (eq-ASCs) appear to have higher potential for migration and musculoskeletal differentiation. Res Vet Sci. 2019; 125: 235-243.
26. Barsby T, Guest D. Transforming growth factor beta3 promotes tendon differentiation of equine embryo-derived stem cells. Tissue Eng Part A. 2013; 19(19-20): 2156-2165.
27. Winkler DG, Sutherland MS, Ojala E, Turcott E, Geoghegan JC, Shpektor D, et al. Sclerostin inhibition of Wnt-3a-induced C3H10T1/2 cell differentiation is indirect and mediated by bone morphogenetic proteins. J Biol Chem. 2005; 280(4): 2498-2502.
28. Yeung CY, Gossan N, Lu Y, Hughes A, Hensman JJ, Bayer ML, et al. Gremlin-2 is a BMP antagonist that is regulated by the circadian clock. Sci Rep. 2014; 4: 5183.
29. Masaeli E, Morshed M, Nasr-Esfahani MH, Sadri S, Hilderink J, van Apeldoorn A, et al. Fabrication, characterization and cellular compatibility of poly(hydroxy alkanoate) composite nanofibrous scaffolds for nerve tissue engineering. PLoS One. 2013; 8(2): e57157.
30. De Schauwer C, Van de Walle GR, Van Soom A, Meyer E. Mesenchymal stem cell therapy in horses: useful beyond orthopedic injuries? Vet Q. 2013; 33(4): 234-241.
31. Bavin EP, Atkinson F, Barsby T, Guest DJ. Scleraxis is essential for tendon differentiation by equine embryonic stem cells and in equine fetal tenocytes. Stem Cells Dev. 2017; 26(6): 441-450.
32. Kishimoto Y, Ohkawara B, Sakai T, Ito M, Masuda A, Ishiguro N, et al. Wnt/β-catenin signaling suppresses expressions of Scx, Mkx, and Tnmd in tendon-derived cells. PLoS One. 2017; 12(7): e0182051.
33. Soeda T, Deng JM, de Crombrugghe B, Behringer RR, Nakamura T, Akiyama H. Sox9-expressing precursors are the cellular origin of the cruciate ligament of the knee joint and the limb tendons. Genesis. 2010; 48(11): 635-644.
34. Levay AK, Peacock JD, Lu Y, Koch M, Hinton RB Jr, Kadler KE, et al. Scleraxis is required for cell lineage differentiation and extracellular matrix remodeling during murine heart valve formation in vivo. Circ Res. 2008; 103(9): 948-956.
35. Murchison ND, Price BA, Conner DA, Keene DR, Olson EN, Tabin CJ, et al. Regulation of tendon differentiation by scleraxis distinguishes force-transmitting tendons from muscle-anchoring tendons. Development. 2007; 134(14): 2697-2708.
36. Nichols AEC, Settlage RE, Werre SR, Dahlgren LA. Novel roles for scleraxis in regulating adult tenocyte function. BMC Cell Biol. 2018; 19(1): 14.
37. Shukunami C, Takimoto A, Oro M, Hiraki Y. Scleraxis positively regulates the expression of tenomodulin, a differentiation marker of tenocytes. Dev Biol. 2006; 298(1): 234-247.
38. Taylor SE, Vaughan-Thomas A, Clements DN, Pinchbeck G, Macrory LC, Smith RK, et al. Gene expression markers of tendon fibroblasts in normal and diseased tissue compared to monolayer and three dimensional culture systems. BMC Musculoskelet Disord. 2009; 10: 27.
39. Theiss F, Mirsaidi A, Mhanna R, Kümmerle J, Glanz S, Bahrenberg G, et al. Use of biomimetic microtissue spheroids and specific growth factor supplementation to improve tenocyte differentiation and adaptation to a collagen-based scaffold in vitro. Biomaterials. 2015; 69: 99-109.
40. Gomiero C, Bertolutti G, Martinello T, Van Bruaene N, Broeckx SY, Patruno M, et al. Tenogenic induction of equine mesenchymal stem cells by means of growth factors and low-level laser technology. Vet Res Commu. 2016; 40(1): 39-48.

**Original Article**

# Redesigning of 3-Dimensional Vascular-Muscle Structure Using ADSCs/HUVECs Co-Culture and VEGF on Engineered Skeletal Muscle ECM

**Abbas Heidari Moghadam, Ph.D.[1, 2], Vahid Bayati, Ph.D.[1, 2*], Mahmoud Orazizadeh, Ph.D.[1, 2], Mohammad Rashno, Ph.D.[1]**

**1. Cellular and Molecular Research Center, Medical Basic Sciences Research Institute, Ahvaz Jundishapur University of Medical Sciences, Ahvaz, Iran**
**2.Department of Anatomical Sciences, Faculty of Medicine, Ahvaz Jundishapur University of Medical Sciences, Ahvaz, Iran**

***Corresponding Address: P.O.Box: 45, Cellular and Molecular Research Center, Medical Basic Sciences Research Institute, Ahvaz Jundishapur University of Medical Sciences, Ahvaz, Iran***
***Email: bayati-v@ajums.ac.ir***

**Received: 05/June/2021, Accepted: 22/August/2021**

Abstract

**Objective:** The main objective of this study is to determine the myogenic effects of skeletal muscle extracellular matrix, vascular endothelial growth factor and human umbilical vein endothelial cells on adipose-derived stem cells to achieve a 3-dimensional engineered vascular-muscle structure.

**Materials and Methods:** The present experimental research was designed based on two main groups, i.e. monoculture of adipose tissue-derived stem cells (ADSCs) and co-culture of ADSCs and human umbilical vein endothelial cells (HUVECs) in a ratio of 1:1. Skeletal muscle tissue was isolated, decellularized and its surface was electrospun using polycaprolactone/gelatin parallel nanofibers and then matrix topography was evaluated through H&E, trichrome staining and SEM. The expression of *MyHC2* gene and tropomyosin protein were examined through real-time reverse transcription polymerase chain reaction (RT-PCR) and immunofluorescence, respectively. Finally, the morphology of mesenchymal and endothelial cells and their relationship with each other and with the engineered scaffold were examined by scanning electron microscopy (SEM).

**Results:** According to H&E and Masson's Trichrome staining, muscle tissue was completely decellularized. SEM showed parallel Polycaprolactone (PCL)/gelatin nanofibers with an average diameter of about 300 nm. The immunofluorescence proved that tropomyosin was positive in the ADSCs monoculture and the ADSCs/HUVECs co-culture in horse serum (HS) and HS/VEGF groups. There was a significant difference in the expression of the *MyHC2* gene between the ADSCs and ADSCs/HUVECs culture groups ($P<0.05$) and between the 2D and 3D models in HS/VEGF differentiation groups ($P<001$). Moreover, a significant increase existed between the HS/VEGF group and other groups in terms of endothelial cells growth and proliferation as well as their relationship with differentiated myoblasts ($P<0.05$).

**Conclusion:** Co-culture of ADSCs/HUVECs on the engineered cell-free muscle scaffold and the dual effects of VEGF can lead to formation of a favorable engineered vascular-muscular tissue. These engineered structures can be used as an acceptable tool for tissue implantation in muscle injuries and regeneration, especially in challenging injuries such as volumetric muscle loss, which also require vascular repair.

***Keywords:*** Engineered Scaffold, Extracellular Matrix, Human Umbilical Vein Endothelial Cells, Mesenchymal Stem Cells, Vascular Endothelial Growth Factor

Cell Journal(Yakhteh), Vol 24, No 7, July 2022, Pages: 380-390

**Citation:** Heidari Moghadam A, Bayati V, Orazizadeh M, Rashno M. Redesigning of 3-dimensional vascular-muscle structure using ADSCS/HUVECS CO-culture and VEGF on engineered skeletal muscle ECM. Cell J. 2022; 24(7): 380-390. doi: 10.22074/cellj.2022.8098.
This open-access article has been published under the terms of the Creative Commons Attribution Non-Commercial 3.0 (CC BY-NC 3.0).

## Introduction

This experimental study continues our previous research which investigated 2D co-culture in muscle tissue challenges such as volumetric muscle loss (VML) (1). VML refers to the special volumetric, contractive, and non-returnable injury of the muscle tissue that can arise due to various causes such as severe trauma, cancer, surgery, and accident (2). Skeletal muscle, like other tissues, has a significant regenerative ability following injury; a process in which a part of the muscle can grow and develop (3). However, this regenerative response is ineffective when a large volume of the muscle is lost. According to recent studies, there is a limited treatment options for VML and no favorable, effective, and definitive treatment is found for this challenge so far (4). New methods, such as regenerative medicine with its high potential for regeneration and substitution of damaged tissues and organs, have attracted the attention of researchers in recent years (5).

*In vitro* designing of favorable tissue models for use in tissue engineering is considered an acceptable therapeutic option for important challenges such as VML (6). The use of stem cells in research has received attention in the last two decades. Adipose tissue-derived stem cells (ADSCs) are one of the special stem cells that have gradually found their place in these studies. They are ideal options in regenerative medicine as their favorable features such as easy isolation and culture and their control, high growth and differentiation potential, non-invasiveness, and lack of ethical consideration have attracted the attention of most researchers (7). It has been founded that decellularization is as an effective strategy in tissue

engineering, and decellularized tissues have been used in recent years in biomedical applications such as research on physicochemical properties of the extracellular matrix (ECM) and providing a special tissue scaffold with native mixture, consisting of tissue-specific macromolecules within a 3D structure, for redesigning the functional tissues of the body (8). ECM is a complex of proteins and polysaccharides as well as a combination of tissue- or organ-specific scaffold basic components. In the skeletal muscle tissue, the large part of the ECM consists of collagen fibers, different types of ECM components such as laminin, elastin, and glycosaminoglycans, growth factors, and a high number of proteoglycans and glycoproteins that are necessary for cell adhesion, permeability, migration, and differentiation (9).

Numerous studies have shown that in muscular tissue engineering, homologue tissues play a key role in the growth, differentiation, and regeneration processes of damaged tissues (10).

On the other hand, various studies have reported that differentiation of stem cells to myoblasts and formation of muscle fibers requires scaffolds with parallel and unidirectional fibers. Due to lack of certain superficial direction in biological scaffolds such as muscle ECM, the use of parallel electrospun nanofibers has gained a particular importance as an acceptable strategy for induction and improvement of myogenesis.

Numerous studies have shown that the combination of the synthetic and natural polymers of Polycaprolactone (PCL) and gelatin has a crucial role in adhesion, growth, and organization of ADSCs (11), tendon engineering advancement (12), regeneration of cardiac muscle tissue, and proliferation and differentiation of myoblasts to skeletal muscle myotubes (13).

Despite all mentioned issues, creation of an ideal engineered structure for differentiation and formation of parallel muscular myofibrils has been always associated with development of neurovascular structures as an inseparable part of normal tissues and a challenge against muscular tissue engineering. Co-culture of endothelial cells with other cell types has been used in recent years for formation of vascular structures in engineered structures as a novel method and trustable strategy to solve this challenge. For instance, it was shown that co-culture of endothelial cells with primary osteoblasts, fibroblasts or smooth muscle cells can significantly improve vascular bifurcations and buds *in vitro* (14). In addition, as the third factor in muscle tissue engineering, it seems necessary to use factors which, besides formation of vascular structures, can affect the differentiation of myoblasts. Vascular endothelial growth factor (VEGF) is a key angiogenesis regulating factor during embryogenesis that can also affect many adult cells. Studies have shown that this factor has inductive roles in endothelial cells, myoblasts, hepatocytes, and neurons in cellular migration, cellular protection against apoptosis, and induction of myoblasts for formation of myofibrils (15).

Given the existing challenge, the main objective of this experimental study is to evaluate the myogenic effects of skeletal muscle ECM, VEGF and human umbilical vein endothelial cells (HUVECs) on adipose-derived stem cells (ADSCs) to achieve a 3-dimensional engineered vascular-muscle structure.

## Materials and Methods

### ADSCs isolation and culture

In this experimental research, ADSCs were isolated according to a previous study (1). Briefly, the adipose tissue was removed from the gonadal region of Wistar rats, washed with PBS containing 1% penicillin/streptomycin, and fragmented to facilitate the enzymatic digestion. The specimens were incubated with collagenase type I at 37°C for 30-40 minutes and then the enzyme effect was neutralized using the culture medium [Dulbecco's Modified Eagle Medium (DMEM), 10% fetal bovine serum (FBS)]. (DMEM, 10% FBS). To separate adipocytes from the stromal vascular fraction (SVF), the cell suspension was centrifuged at 2000 rpm for 5 minutes. The supernatant was then discarded and the cellular palate was immersed in a culture medium containing DMEM, 10% FBS, 1% L-glutamine, and 1% penicillin/streptomycin. The cells were plated at $2.5\times10^4$ cells/$cm^2$ per 25 $cm^2$ cell culture flasks and incubated at 37˚C in 5% $CO_2$. After 2 days, the non-adherent cells were discarded, and the cellular passage stages were performed 4 times on adheerent cells. After 4 passages, for ADSCs characterization, the surface antigens of ADSCs including CD73, CD44, and CD90 as positive markers and CD45 as the negative marker were evaluated through flow cytometry assay. To induce myogenesis of the mesenchymal cells, ADSCs were cultured in the DMEM culture medium containing 10% FBS and 3 M 5-Azacytidine (Sigma, NY, USA) for 24 hours and then in the DMEM supplemented with 5% horse serum (HS, Gibco, NY, USA) for 7 days. Supplemented media was replaced every 48 hours.

### Decellularization of skeletal muscle

Muscle tissue decellularization was performed according to previous protocols, as shown in Figure 1. After euthanization of Wistar rats, the anterior abdominal muscles (external and internal oblique) were removed. To further improve the quality of the decellularization process, the muscle layers were separated. Samples were washed in phosphate-buffered saline (PBS) with 1% antifungal and antibiotic solution, and then the muscle tissue was purified from all vascular, fat and connective tissue and washed out for 1 hour in deionised water. These samples were then treated with 0.5 M NaCl for 4 hours, followed by 1 M NaCl for 4 hours, and washed in ultra-pure water for 48 hours. After being treated with 0.25% trypsin/EDTA at 37°C for 2 hours, the samples were washed in dhen samples were processed with DNAase at 37°C for 3 hours, washed in ultra-pure water for 2 days,

rinsed in PBS for 24 hours and finally kept at 4°C till use (Fig.2A).

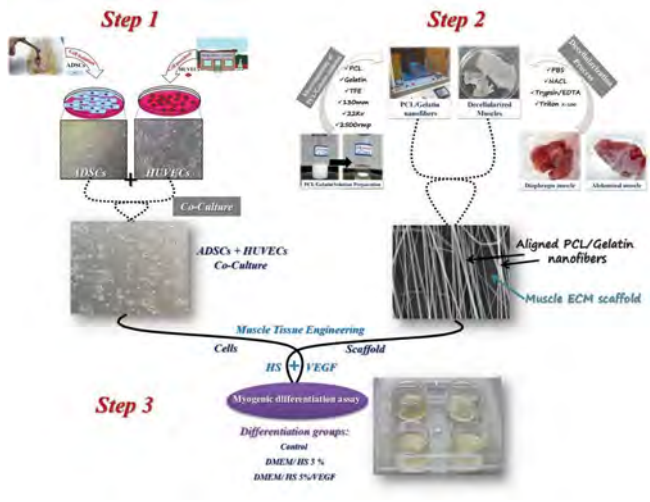


**Fig.1:** Schematic diagram representing the different steps of this study. Step 1; Monoculture and co-culture of stem cells and endothelial cells. Step 2; Decellularization of the muscle tissue according to the protocol (briefly) and electrospinning of the PCL/gelatin parallel nanofibers on the decellularized muscle scaffold. Step 3; Represents triad of muscle tissue engineering including scaffold (engineered ECM), cells (ADSCs/HUVECs co-culture) and factors (HS and VEGF) for evaluation of myogenic differentiation in 3 experimental groups. PCL; Polycaprolactone, ADSCs; Adipose-derived stem cells, HUVECs; Human umbilical vein endothelial cells, ECM; Extracellular matrix, HS; Horse serum, and VEGF; Vascular endothelial growth factor

## Evaluation of muscle decellularization

Immediately after the muscle cell removal process, the accuracy of decellularized muscles were determined by visual examination, tissue staining and also by scanning electron microscopy (SEM) (Fig.2B). For tissue staining, a part of the prepared tissue was fixed in 10% formalin. Samples were then embedded in paraffin to provide microscopic sections and then stained with H&E and Masson's Trichrome at different magnifications.

## Scanning electron microscopy

SEM evaluation was done based on previous protocols (19). First the scaffolds were washed three times with PBS and then fixed with 2.5% glutaraldehyde solution (Sigma, USA) for 30 minutes. The samples were dehydrated in different percentages of ethanol aqueous solutions from 30% to 100% successively for 10 minutes each and dried at room temperature under sterile conditions under the hood. After preparing the samples, SEM (SEM, Zeiss Evo 50, Germany) examination was used to determine the surface topography (with and without PCL/Gelatin nanofibers), arrangement of ECM fibers and structure and porosity of decellularized muscle tissue.

In addition, after fabrication of parallel PCL/Gelatin nanofibers on the ECM surface and cell culture, the samples were prepared in the same way in order to visualize the orientation and diameter of the nanofibers, surface topography of the electrospun nanofibers, cell morphology, attachment and interaction with other cells by SEM. Fiber diameters and size distribution were measured from the SEM images using Image J software version 1.46 (NIH, MD).

## Fabrication of of polycaprolactone/gelatin nanofibers

PCL (Sigma-Aldrich, USA, Mw: 80000 g/mol) and gelatin type A (from porcine skin in powder form, Sigma-Aldrich, USA) scaffold were prepared by the electrospinning method as described previously (16). Briefly, to prepare a 10% (w/v) concentration solution, PCL, and gelatin in a 50/50 (w/w) ratio was dissolved separately in 2, 2, 2-trifluoroethanol (TFE, Sigma-Aldrich, USA) and stirred overnight until the mixture was dissolved completely at room temperature. Before stirring, 1% acetic acid (Fisher Scientific, USA) was added to the final solution to improve miscibility.

For the electrospinning process, PCL/gelatin solution was loaded into a 10-mL syringe with a 21-Gauge needle that was located at a distance of 130 mm from the collector. The solution flow rate, applied voltage, collector rotation speed and duration were set to 1 mL/hour, 22 kV, 2,500 rmp and 4 minutes, respectively. Moreover, before the electrospinning process, decellularized muscle ECM was placed on the collector (Fig.1). The process was carried out at room temperature within a range of relative humidity (45-50%). The PCL/Gelatin solvent turned to nanofibers and was collected in parallel orientation on decellularized muscle ECM on the collector. Before using the engineered scaffolds, in order to dry and stabilize the nanofibers, they were kept in a sterile environment at room temperature overnight.

## Mechanical tensile test

The tensile strength of the decellularized muscle scaffolds, with or without parallel PCL/gelatin electrospun nanofibers, was evaluated in dry and wet conditions (Cultivated for 10 days in DMEM culture medium) by the material test device (Wance, China) equipped with a 5 kN load cell. Initially, strip-shaped pieces were prepared at a 12 mm width×30 mm length from both types of scaffolds. Tensile tests and their analysis were performed after setting the crosshead speed at 10 mm/minutes. At least three samples were investigated. Finally, using the tensile stress curve obtained from the test device, we examined the tensile strength and scaffold elastic modulus (17).

## MTT assay

MTT (3-(4, 5-Dimethylthiazol-2-yl)-2, 5-diphenyltetrazolium-bromide) assays were used to evaluate the effects of engineered muscle scaffold on ADSCs/HUVECs co-culture viability and proliferation. Briefly, ADSC and HUVEC cells were seeded in 96-well plates ($1\times10^4$ cells/well) and were then maintained with culture media for 48 h. Then the cells were further incubated with MTT (0.5 mg/mL) for 4 hours at 37°C. After removal of the super-

natants, 700 µL of dimethyl sulfoxide (DMSO) was added to each well to dissolve the formazan product. Then using a microplate reader (BioRad, Hercules, CA) absorbance was measured at 540 nm. Optical density values of the control cells were calculated as 100% viability. Because absorbance is in proportion to the number of living cells in a sample, the MTT assay reflects the extent of cell proliferation (17).

### Co-culture models

The HUVECs were obtained from the Iranian Biological Resource Center and cultured in their special culture medium (1). To track HUVECs in co-culture with ADSCs, they were labeled with C7000 according to the cell tracking guideline CellTrackerTM CM-DiI (C7000) (Sigma-Aldrich, USA). Briefly, HUVEC cells were plated at $2.5\times10^4$ cells/cm$^2$ per 25 cm$^2$ cell culture flasks. Then 15 µl of CM-DiI (C7000) was added for every 4 ml of culture medium and incubated at 37˚C in 5% $CO_2$ for 24 to 48 hours. After removal the supernatants, the attached cells could be seen in red light using fluorescence microscopy. The cell tracker was still detectable up to 2 passages.

Similar to our previous study, 2 experimental groups were designed in this research, so that each group was evaluated in 3 different culture media including the control group, the horse serum (HS) differentiation culture medium group, and the HS/VEGF differentiation culture medium group. Table S1 represents a brief description of the experimental groups (See Supplementary Online Information at www.celljournal.org).

Co-culture of HUVECs and mesenchymal cells was performed at a ratio of 1:1. The dose of VEGF used in the experimental groups was 50 ng/µL. The main points of this study are shown in Figure 1.

### Cell labeling

HUVECs were marked with CM-DiI (Invitrogen, USA) according to manufacturer's instructions and then confirmed by fluorescence microscopy after 1 day.

### Real-time reverse transcriptase-polymerase chain reaction analysis

Immediately after completion of the experiment on day 7, real-time reverse transcription polymerase chain reaction (RT-PCR) was used to confirm the expression of *MyHC2* according to the manufacturer's instructions. At first, for RNA extraction, cultured cells were lysed using the RNeasy plus Mini Kit (Qiagen, Gaithersburg, MD, USA). Then, by using a NanoDrop 2000c spectrophotometer (Thermo Scientific, USA) the cells were quantified. cDNA synthesis using a QuantiTect Reverse Transcription Kit (Qiagen, Gaithersburg, MD, USA) was performed. The following primer sequences for amplification were used:

*MyHC2*-

F: 5′-GGCTGGCTGGACAAGAACA-3′
R: 5′-CCACCACTACTTGCCTCTGC-3′

*GAPDH*-

F: 5′-TGCTGGTGCTGAGTATGTCGTG-3′
R: 5′-CGGAGATGATGACCCTTTTGG-3′

### Immunofluorescence analysis

Immediately after conclusion of the experiment on day 7, the scaffolds were washed three times with PBS and then fixed with paraformaldehyde 4% for 20 minutes. Then, the scaffolds with their surface cells became permeable using Triton X-100 for 10 minutes and were rinsed again with PBS. To prevent any non-specific adherence, they were impregnated in BSA 3% for 2 hours. Experimental groups were stained with primary antibody against anti-tropomyosin antibody (1:100, Sigma, USA) overnight at 4˚C. Then, the cultured cells on muscle scaffold were rinsed with PBS and incubated with goat anti-mouse fluorescein isothiocyanate (FITC)-conjugated secondary antibody (1:150, Sigma, USA) for 1 hour. Using 4′, 6-diamidino-2-phenylindole (DAPI, 1:400, Sigma, USA), nuclear staining was done for 15 minutes at room temperature. Ultimately, the scaffolds were washed three times with PBS and then examined by an invert fluorescent microscope (IX 71, Olympus, Japan).

### Ethical considerations

This research was approved by the Ethics Committee of Ahvaz Jundishapur University of Medical Sciences (IR.AJUMS.REC.1396.282). All protocols such as animal care, anesthesia, and euthanasia were performed in accordance with the guidelines of the moral committee of this university.

### Statistical analysis

All data was expressed as the mean ± standard deviation and performed in triplicate and repeated three times with similar results. The data was analyzed using different techniques including one-way analysis of variance (ANOVA) followed by Tukey's test for each paired experiment. All analyses were done using GraphPad Prism Software (version 5.1, Graphpad Software Inc., La Jolla, CA, USA). Moreover, $P<0.05$ was considered statistically significant.

## Results

### Characterisation of decellularized muscle ECM

Macroscopic evaluation indicates discoloration of muscle tissue due to elimination of the muscle cells. Figure 2B shows that decellularized muscle scaffold was obtained, as a transparent sheet-like layer after completing all the steps of cell removal, washing and drying (for 6 days).

Images obtained from light microscope with H&E,

Masson's Trichrome staining, and SEM showed cell-free muscle tissue ECM. In addition, SEM indicated the porous space and intertwined fibers appearance of the decellularized muscle tissue. Different sections and views of the decellularized muscle ECM are shown in Figure 2B.

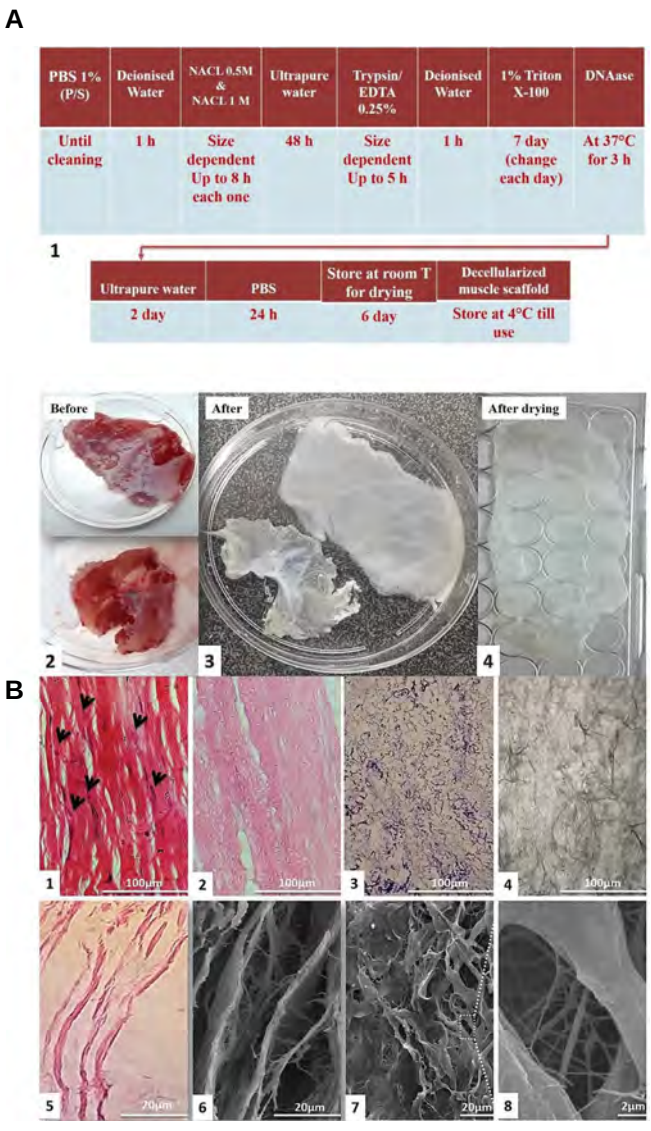


**Fig.2:** Macroscopic and microscopic assessment of the muscle tissue decellularization. **A.** The skeletal muscle tissue decellularization steps using Trypsin and Triton X-100 (as the important step), **A1.** Duration of each step depended on the size and thickness of the muscle tissue, **A2.** The diaphragm and the anterior abdominal wall muscles before decellularization, **A3.** After complete decellularization color clearness can be easily detected macroscopically, **A4.** The dried state of the decellularized muscle (ECM of the muscle tissue) prepared as a transparent layer. **B.** Light microscopic view and SEM of the normal and decellularized muscle tissue, **B1.** The normal abdominal wall anterior muscle of the rats in which the nuclei positions are shown with arrows (scale bar: 100 µm), **B2, B3.** The decellularized muscle tissue stained with H&E) Trichrome (scale bar: 100 µm), **B4.** Non-stained with light microscope (scale bar: 100 µm), **B5.** The longitudinal cross-section of the decellularized muscle tissue with light microscope (scale bar: 20 µm), **B6.** And with SEM (scale bar: 20 µm), **B7.** The surface view of the decellularized muscle tissue with SEM indicating the lack of any specific surface orientation (scale bar: 20 µm), and **B8.** A part of image B7 after magnification (scale bar: 2 µm). ECM; Extracellular matrix and SEM; Scanning electron microscope.

Viability of ADSCs/HUVECs Co-cultured on the scaffold engineered with PCL/gelatin nanofibers was evaluated through measurement of the cells' metabolic activity using the MTT test. The results indicate the relative improvement of ADSCs/HUVECs viability in comparison with the control group. Although the difference was insignificant, the similarity of culture conditions in 3D and 2D culture in growth, proliferation, and viability indicated the lack of toxicity of the decellularized muscle ECM. The results of mechanical tests showed a noticeable difference between the tensile strength of wet scaffolds compared to dry scaffolds. Also, ECM engineered with PCL/Gelatin were more resistant than ECM engineered without PCL/Gelatin nanofibers in dry and wet conditions, respectively (Fig.3).

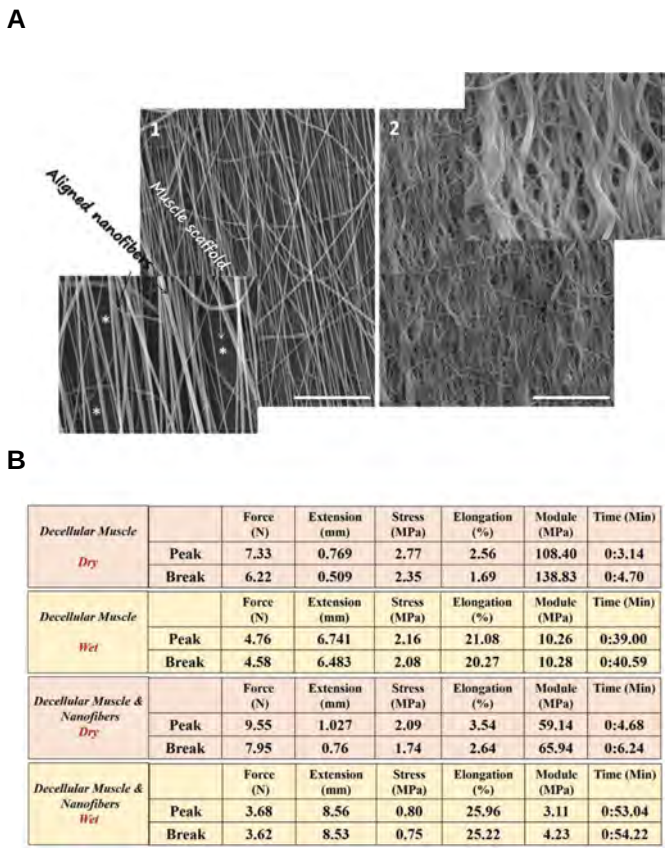


| | | Force (N) | Extension (mm) | Stress (MPa) | Elongation (%) | Module (MPa) | Time (Min) |
|---|---|---|---|---|---|---|---|
| *Decellular Muscle Dry* | Peak | 7.33 | 0.769 | 2.77 | 2.56 | 108.40 | 0:3.14 |
| | Break | 6.22 | 0.509 | 2.35 | 1.69 | 138.83 | 0:4.70 |
| | | Force (N) | Extension (mm) | Stress (MPa) | Elongation (%) | Module (MPa) | Time (Min) |
| *Decellular Muscle Wet* | Peak | 4.76 | 6.741 | 2.16 | 21.08 | 10.26 | 0:39.00 |
| | Break | 4.58 | 6.483 | 2.08 | 20.27 | 10.28 | 0:40.59 |
| | | Force (N) | Extension (mm) | Stress (MPa) | Elongation (%) | Module (MPa) | Time (Min) |
| *Decellular Muscle & Nanofibers Dry* | Peak | 9.55 | 1.027 | 2.09 | 3.54 | 59.14 | 0:4.68 |
| | Break | 7.95 | 0.76 | 1.74 | 2.64 | 65.94 | 0:6.24 |
| | | Force (N) | Extension (mm) | Stress (MPa) | Elongation (%) | Module (MPa) | Time (Min) |
| *Decellular Muscle & Nanofibers Wet* | Peak | 3.68 | 8.56 | 0.80 | 25.96 | 3.11 | 0:53.04 |
| | Break | 3.62 | 8.53 | 0.75 | 25.22 | 4.23 | 0:54.22 |

**Fig.3:** Morphological and mechanical characterization of engineered muscle scaffold. **A.** Arrangement and bio-degradation behavior of the PCL/gelatin nanofibers; the images show SEM of the PCL/gelatin parallel nanofibers on the decellularized muscle scaffold; **A1.** The initial state (*) indicates the underneath muscle tissue covered by the parallel nanofibers (scale bar: 20 µm), **A2.** After culture in the incubator for 7 days to evaluate the rate of nanofibers biodegradation. The results demonstrated that the direction of the nanofibers did not change and were still in parallel, although their dimensions (swelling) and high adherence to each other show the proper bio-degradation trend of the PCL/gelatin nanofibers that can be considered a favorable feature for implantation (scale bar: 20 µm) and **B.** Stress-strain data of muscle ECM with and without PCL/Gelatin nanofibers in dry and wet status under tensile loading (scale bar 20 µm). ECM; Extracellular matrix, SEM; Scanning electron microscope, and PCL; Polycaprolactone.

## PCL/Gelatin nanofiber arrangement

SEM images of electrospun PCL/gelatin nanofibers showed the parallel and unidirectional fibers arranged

on the muscle ECM before and after immersing in culture medium (Fig.3A). The nanofibers diameter was measured in the dry and wet states using Image J software indicating a mean diameter of 350 nm and 520 nm, respectively. As shown in Figure 3A2, although nanofibers were swelled and their thickness was increased, they were still in alignment, and favorable for myogenic differentiation.

### Flow cytometry

After 4 passages, the expression of the isolated stem cell surface markers, including CD44, CD45, CD73, and CD90, was evaluated through flow cytometry; the results of which showed that CD44, CD73, and CD90 were expressed on the surface of these cells and almost a negligible number of the cells were positive for the hematopoietic cell marker CD45. All these results indicate the high purity of the isolated mesenchymal stem cells.

### Co-culture and differentiation of ADSCs/HUVECs in 3D culture

In the 3D culture, ADSCs/HUVECs were cultured on the muscle ECM engineered with PCL/gelatin nanofibers in different culture media (proliferation or differentiation) for 1 week according to the experimental groups. Each group of endothelial cells (stained with C7000 cell marker) and mesenchymal cells (stained with tropomyosin antibody) in monoculture and co-culture states were evaluated. As shown in Figure 4, the growth and cell proliferation of HUVECs in the HS group was much lower than the VEGF group. The results from ADSCs groups indicated myogenic differentiation of ADSCs to myoblast-like cells and the expression of tropomyosin on the engineered scaffold in the monoculture and co-culture. In addition, it was shown that the differentiated cells in the Co-culture/HS/VEGF group were arranged close to the HUVECs on the engineered structure. Although no geometrical vascular structure was observed, their proliferation and distribution in the VEGF-differentiated group was well observable. VEGF in the Co-culture groups also increased the myogenic induction and hence lead endothelial cells to be in close proximity with differentiated myoblast-like cells (Fig.4).

### Scanning electron microscopy

Seven days after differentiation, the position and arrangement of the ADSCs and HUVECs on the engineered scaffold with PCL/gelatin parallel nanofibers were examined through SEM. The results revealed that the ADSCs/HUVECs co-culture had a higher growth and proliferation in the VEGF-treated group. Based on the cells' dimensions, it can be concluded that the higher number of endothelial cells (signified with *) was the reason for the higher density in the VEGF group, which indicates the capacity of this cell model for providing the angiogenesis process in the engineered scaffold. These cells were located on the PCL/gelatin parallel nanofibers and attached to each other and to the scaffold underneath. In the absence of VEGF, proliferation of the cells was low which was consistent with the findings obtained from immunofluorescence technique (Fig.5).

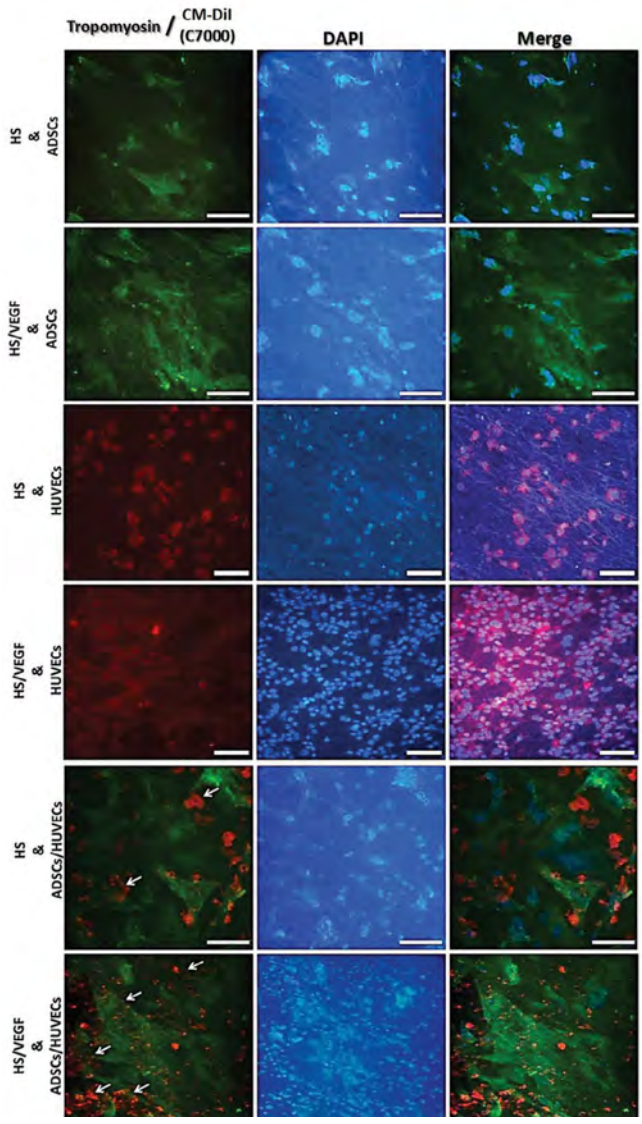


**Fig.4**: Immunofluorescence and Morphological characterization of ADSCs, HUVECs and HUVECs and ADSCs co-culture in experimental groups (HS and HS/VEGF). The expression of tropomyosin in HS and HS/VEGF groups was indicated in immunofluorescence. As shown, ADSCs proliferation was increased in HS/VEGF group and were arranged in proximity to parallel nanofibers. As shown in figures, the proliferation and distribution of HUVECs in the HS/VEGF group was increased in comparison to the HS group which indicates the predictable effect of VEGF on HUVECs. Also the orientation of the PCL/Gelatin nanofibers can be detected. In HUVECs and ADSCs co-culture, Tropomyosin-specific fluorescent staining for differentiated mesenchymal cells and endothelial cells-specific C7000 staining are shown. The density of differentiated myoblasts like cells, in particular endothelial cells, was higher in the VEGF-differentiated group compared with the HS-differentiated group after the 7 days differentiation period. The endothelial cells are signified with red. The arrows indicate the level of distribution and proliferation of HUVECs in the groups. As is obvious, like 2D culture, growth and proliferation of the endothelial cells along with myogenesis differentiation of the ADSCs on the VEGF-differentiated group is well observed (scale: 200 µm).PCL; Polycaprolactone, ADSCs; Adipose-derived stem cells, HUVECs; Human umbilical vein endothelial cells, HS; Horse serum, and VEGF; Vascular endothelial growth factor.

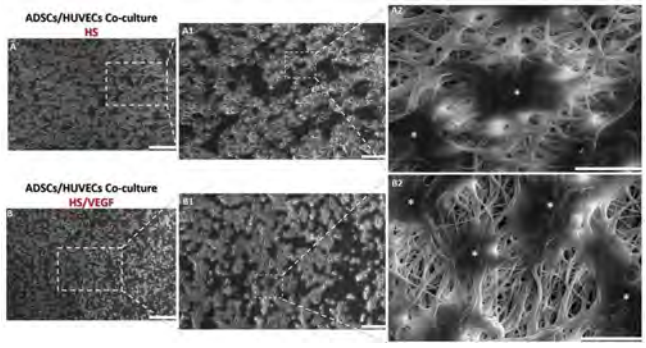


**Fig.5:** SEM of the ADSCs/HUVECs co-cultured on the muscle ECM engineered with PCL/gelatin parallel nanofibers after a-week of differentiation in 3 different magnifications. The cell density is higher in image B (VEGF group) compared to Image A (HS group). Based on the cell size, (*) indicates endothelial cells. Proliferation and distribution of these cells in the VEGF-treated group was much higher than the HS-treated group (scale bar of Fig.A, B: 200 µm, Fig.A1, B2: 20 µm, Fig.A2, B2: 10 µm). PCL; Polycaprolactone, ADSCs; Adipose-derived stem cells, HUVECs; Human umbilical vein endothelial cells, ECM; Extracellular matrix, HS; Horse serum, SEM; Scanning electron microscope, and VEGF; Vascular endothelial growth factor.

### Results of real-time RT-PCR in the 3D culture

The quantitative data obtained from real-time RT-PCR in the 3D culture on nanofibers proved that the expression of *MyHC2* was significantly higher in the VEGF and HS groups as compared with the control group (P<0.001). In addition, there was a significant difference between the VEGF and HS groups in terms of expression of this gene (P<0.05). As an important point of these findings, expression of *MyHC2* in the presence of VEGF was increased in the ADSCs/HUVECs co-culture in comparison with the ADSCs monoculture (P<0.05). However, there was no significant difference between the HS-treated group in co-culture and ADSCs monoculture groups in *MyHC2* expression. These results indicated that VEGF along with HUVECs can increase the expression of *MyHC2* in the mesenchymal differentiated group as compared with the other groups (Fig.6). It should be mentioned that although HUVECs monoculture (without VEGF) were unable to significantly improve *MyHC2* gene expression, the co-culture along with VEGF resulted in a significant difference in comparison with ADSCs monoculture (P<0.05). This finding indicates the effective role of ADSCs/HUVECs co-culture along with the use of VEGF in increased expression of the myogenic differentiation genes. The results of comparison between 2D and 3D cultures in different groups showed that the *MyHC2* gene had a significantly higher expression in the 3D culture in comparison with the 2D culture, so that its expression was significantly increased in the HS/3D group compared to the HS/2D group (P<0.05) and in the HS/VEGF/3D group compared to the HS/VEGF/2D and other groups (P<0.05, Fig.6).

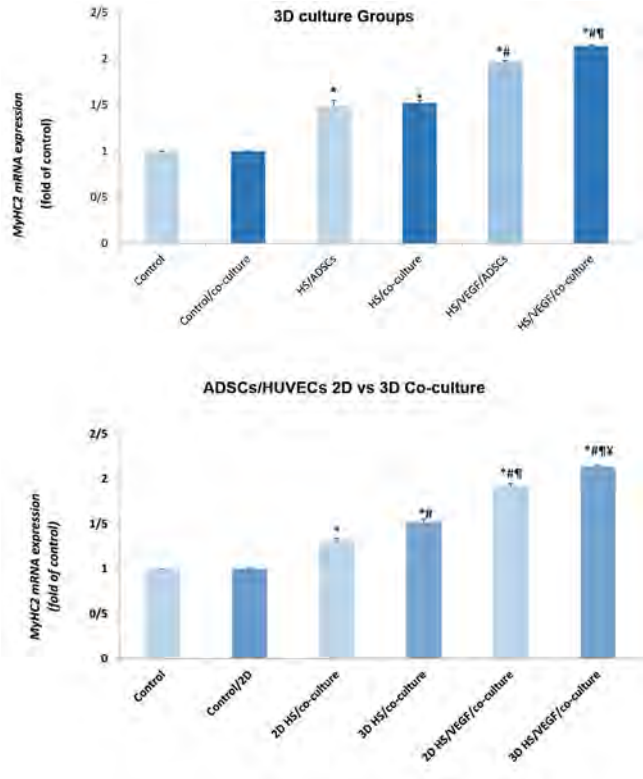


**Fig.6:** Gene expression in experimental groups. Expression of *MyHC2* mRNA in different experimental groups which was 1.49 ± 0.06 in the HS/ADSCs group, 1.52 ± 0.03 in the HS/Co-culture group, 1.96 ± 0.02 in the HS/VEGF/ADSCs group, and 2.14 ± 0.01 in the HS/VEGF/co-culture group, *; P<0.001, #¶; P<0.05; *; Indicate the comparison between the control groups. #; Indicate the comparison between the HS groups, and ¶; Indicate the comparison between the HS/VEGF groups. Expression of *MyHC2* mRNA in 2D and 3D cultures which was 1.32 ± 0.02 in the HS/2D group, 1.52 ± 0.03 in the HS/3D group, 1.92 ± 0.03 in the HS/VEGF/2D group, and 2.14 ± 0.01 in the HS/VEGF/3D group. *; P<0.001, #&¶&¥; P<0.05, *; Indicate the comparison between the control groups, #; Indicate the comparison between the HS/2D groups, ¶; Indicate the comparison between the HS/3D groups, ¥; Indicate the comparison between the HS/VEGF/2D groups, ADSCs; Adipose-derived stem cells, HUVECs; Human umbilical vein endothelial cells, HS; Horse serum, and VEGF; Vascular endothelial growth factor.

## Discussion

Skeletal muscle tissue engineering is a complex process and achievement of a favorable and contractive tissue requires some prerequisites such as formation of myofibrils, development of vascular structures, innervation, and improvement and organization of the ECM (18).

In this study, the effects of endothelial cells (HUVECs), VEGF, and engineered muscle ECM with PCL/gelatin nanofibers was investigated on myogenic differentiation of the ADSCs. The use of such a scaffold along with ADSCs/HUVEC co-culture in evaluation of myogenic differentiation and their mutual roles to improve angiogenesis have not been investigated so far. The muscle scaffold or ECM was used given numerous studies performed in this regard. ECM is usually obtained through decellularization of the tissues and organs of mammals. For example, ECM of intestine, dermis, bladder, pericardium, heart valves, amniotic membrane, muscle, and fascia are approved by FDA to be used for soft tissue regeneration (19). Li et al. (20) reported that the

use of dehydrated amniotic membrane in damaged biceps femoris of rats caused migration of a higher number of myoblasts to the affected area. In another study, Merritt et al. (21) evaluated the role of muscle-derived ECM in the improvement of the gastrocnemius muscle function in Lewis mice and showed a function improvement rate of 85% after a period of 42 days, indicating the effective therapeutic role of the ECM and BMSCs combination in regeneration of skeletal muscle. In this regard, Badylak et al. (22) used a medical regeneration approach on 13 patients with muscle defects and showed that the contractive force increased by 37.3% and muscle motility improved by 27.1% after using muscle ECM in the damaged area and physiotherapy exercises. According to previous studies and the confirmed effective role of decellularized scaffold, abdominal muscle tissue ECM was used in this study, so that after decellularization of the tissue, a clear cell-free structure was obtained and used for *in vitro* experiments. In this study, a transparent muscle scaffold was obtained that had a significant role in myogenic differentiation (as increased expression of the *MyHC2* gene) in ADSCs compared with 2D culture. The muscle ECM is an ideal option in muscle tissue engineering due to its specific properties.

Wang et al. (17) compared the decellularized muscle and fascia tissues in their study and showed that both tissues not only maintained their 3D optimal structure, mechanical properties, and biologic compounds, but also were non-toxic and well retained their ability to induce the integrity of human adipose stem cells (hASCs). In addition, they reported that the muscle scaffold has a significant role in induction of angiogenesis and the pro-myogenic properties in comparison with the fascia scaffold, which can be considered as a favorable scaffold for engineering muscle and fascia tissues.

It should be noted that in addition to the scaffold material and ECM properties, the surface topography is an important parameter for muscle tissue engineering. Regular and unidirectional scaffolds are more potent to form myotubes and regular arrangement of myofibers than scaffolds with multidirectional fibers on their surface. Chen et al. (23) used a new type of 3D porous collagen scaffold with special microgrooves in their research, which formed a structure similar to the muscle basement membrane for skeletal muscle tissue engineering. In our study, the topography of the muscle scaffold due to lack of no specific direction was engineered to create a favorable and parallel shape for myogenic differentiation using PCL/gelatin parallel nanofibers electrospinning. PCL/gelatin is an ideal compound for tissue engineered, because PCL increases the structural strength and gelatin can improve cell attachment. Kim et al. (13) showed that the expression rate of myosin heavy chain and troponin T in C2C12 cells and their proliferation rate increased significantly when the PCL/gelatin scaffold was used as compared with the PCL scaffold. Likewise, Yang et al. (12) showed that human ADSCs were arranged longitudinally in parallel with the electrospun PCL/gelatin nanofibers and were able to acquire tendon cell phenotypes under the influence of TGF-β3. Our research indicated a better arrangement of ADSCs unidirectional with the parallel nanofibers and expression of differentiation factors, in particular the expression of *MyHC2* gene in the HS and HS/VEGF differentiation groups both in the monoculture and co-culture as compared with the 2D culture (lacking the parallel nanofibers). It seems that using VEGF could be helpful in the muscular-vascular differentiation process. VEGF is a key regulator of angiogenesis, but its effect on restoration of muscular force and musculoskeletal damages regeneration has not yet been properly identified. Recent studies have shown that VEGF may affect a lot of different cells including neurons, hepatocytes, osteoblasts, hematocytes, and myoblasts (24). In addition, it was proven that in vitro administration of VEGF can stimulate migration of myoblasts, improvement of cell life critical conditions, protection of myogenic cells against apoptosis, and progression of myoblast growth (15). Chen et al. (25) and Song et al. (26) reported in two independent studies that VEGF is the main factor in differentiation of embryonic stem cells (ESCs) and ADSCS to cardiomyocyte, respectively.

The results of this study showed that VEGF significantly increased the myogenic differentiation of ADSCs in monoculture or co-culture as compared with other differentiation or control groups.

Shvartsman et al. (27) implanted VEGF- and IGF1-including alginate gels to the skeletal muscle ischemic damage area and showed that they were able to increase the regeneration speed and progression of angiogenesis process and helped viability of myoblasts. Kim et al. (28) showed that VEGF associated with ADSCs can be used as an angiogenesis strategy in tissue engineering specially the complex muscle tissue.

The results of this study are consistent with those of other studies in this field, so that based on our study, VEGF induced myogenic differentiation in ADSCs and endothelial tube formation in the co-culture groups under the influence of HS/VEGF. The endothelial tube was observed as a regular pentagon shape initiating the angiogenesis process in the co-culture groups in the 2D culture. This information followed a scientific fact, that angiogenesis is the prerequisite of favorable myogenesis so that myogenesis seems to be increased in groups where VEGF was used due to improved vascular structure (although primitive). As an important point, angiogenesis and myogenesis were induced by VEGF. This was also mentioned in previous studies, so that increased angiogenesis by VEGF improves the muscle function in ischemic tissues (37). The findings of this study are similar with previous studies regarding the relationship between angiogenesis and more effective regeneration of muscle tissue (29).

In this study, endothelial cells were co-cultured with ADSCs with two objectives: first, to evaluate their roles

in myogenesis differentiation of ADSCs and second, to provide conditions for angiogenesis and vascular organizations by HUVECs using VEGF (or paracrine effects of ADSCs) in the engineered structure. Co-culture of ADSCs and HUVECs was performed at a ratio of 1:1. This ratio was chosen according to previous studies on mesenchymal cells and HUVECs (30) as well as myoblasts and HUVECs (31). Accordingly, the cell-to-cell interaction and the paracrine effect of endothelial cells on differentiation, morphology, and direction of ADSCs and vice versa was investigated. This subject was raised based on the idea that cell-to-cell interactions between ADSCs and HUVECs may improve myogenesis differentiation. In this regard, Lin and Lilly (32) reported that co-culture of endothelial cells and bone marrow-derived stem cells (BMSCs) can guide BMSCs toward smooth muscle cells due to their role in advancement of contractive phenotype, decrease in proliferation, and increase in synthesis and release of collagen fibers. Accordingly, Gholobova et al. (33) indicated that co-culture of endothelial cells and skeletal muscle precursor cells on engineered ECM can improve the parallel and dense arrangement of muscle fibers which led to expansion of the endothelial vascular network (in particular in a high cell density).

Similarly, Chen et al. (31) reported that myoblasts and HUVECs co-culture could cause a significant increase in the myosin heavy chain expression rate and parallel formation of myoblasts along with regular arrangement of vascular endothelial tubular cells in the porous scaffold.

Koffler et al. (34) used a triple culture system consisting of myoblasts, HUVECs, and fibroblasts and observed the formation of muscle tissue and vascular network, organization, and integrity of the host tissue 3 weeks after implantation. Other studies have shown that co-culture of myoblasts with endothelial cells in a sandwich-like structure improved the formation of vascular structures (35). Criswell et al. (18) investigated the co-culture of HUVECs and precursors of 10T1/2 myoblasts on an acellular bladder scaffold *in vitro* and *in vivo* and showed that the rate of angiogenesis, innervations, and myogenesis significantly increased in comparison with scaffolds cultured with only myoblasts.

The present study proved that although VEGF-free HUVECs were not able to significantly improve the expression of *MyHC2* gene, their simultaneous co-culture with the use of VEGF led to significant difference in comparison with the ADSCs monoculture. This finding indicates the effective role of ADSCs and HUVECs co-culture on the expression of differentiation genes especially when VEGF was used. It should be noted that there are scarce information about co-culture of ADSCs/HUVECs in the myogenic differentiation process, and most studies focused on the muscle precursor cells. As another important point, this study investigated the role of HUVECs on myogenic differentiation and ADSCs direction as well as the mutual connection of these cells aiming to develop an engineered vascular-muscle cellular model, a process that has not been studied yet. This study intended to design a favorable cell model using a cell-free muscle scaffold aiming to develop a vascular-muscle structure and take a step toward solving the extensive challenges of muscle tissue.

Angiogenesis and formation of vascular network in engineered tissues has been always an important challenge in recent years. Therefore, this study evaluated the formation of vascular structures of endothelial tube formation in 2D Co-culture. We assumed that the interaction between ADSCs and HUVECs may result in proliferation and improvement of cell arrangement as well as angiogenesis by the endothelial cells, and all these processes may improve myogenic differentiation. It is believed that endothelial cells are induced to initiate the angiogenesis process, as endothelial tube formation, during regeneration of vascular structures *in vitro*.

Recent studied have reported that the co-culture of ADSCs/ECs can induce the formation of vascular sprouts and significantly increase the number of connections and vascular tubules. According to studies, induction of these vascular structures may arise from factors produced by ADSCs and released in the culture medium. Using ELISA technique, Holnthoner et al. (36) showed that an increased number of ADSCs in the co-culture results in an increase in the VEGF concentration in the culture medium. It has been proven that ADSCs release a large amount of VEGF into their culture medium (25). Numerous studies have reported that simultaneous induction of muscle precursor cells and formation of vascular tubules can be stimulated due to the paracrine effects of VEGF as well as IGF-1, HGF, bFGF, and PDGF-BB (37). Contrary to our findings, Kook et al. (38) did not observe any capillary network after Co-culture of ADSCs/HUVECs in cell plates. They reported a slight increase in proliferation, expression of adhesion proteins, and vascular branches originating from HUVECs in the VEGF-treated co-culture group. In contrast to the results of Kook et al. (38) our findings confirmed that ADSCs can induce the formation of endothelial tube formation in the VEGF-treated co-culture group (in 2D culture) significantly more than other groups (lacking VEGF). This finding was similar to that of Park and Gerecht (39), probably due to direct cellular interaction and more importantly due to the effects of ADSCs paracrine secretions such as VEGF, angiopoietin 1 and 2, and interleukin 6 which result in cell proliferation and endothelial tube formation in HUVECs. Finally, after accurately reviewing all aspects in this study, it can be concluded that this research confirms other studies in this regard: on the one hand, its provides a favorable cellular model in the framework of an engineered ECM muscle scaffold and on the other hand, it was able to take a step towards designing an effective engineered vascular-muscle structure.

## Conclusion

It can be generally concluded that muscle ECM engineered scaffolds can be used as a desirable strategy in muscle tissue engineering. Also, ADSCs / HUVECs

cell interaction and dual effects of VEGF can result in the myogenic differentiation of ADSCs in close proximity to endothelial cells and vascular network. Co-culture of ADSCs/HUVECs can be an ideal option for achieving a favorable cellular model for use in the engineered vascular-muscular tissues. Redesigning such engineered structures can be used in challenging muscle injuries such as VML, where muscle and vascular structures regeneration are required.

## Acknowledgments

This manuscript is second part of a Ph.D. thesis, funded by grant no. 9625, from the Cellular and Molecular Research Center (CMRC-9625), of the Ahvaz Jundishapur University of Medical Sciences (AJUMS), Ahvaz, Iran. The authors sincerely thank all individuals who cooperated with this study. The authors declared no conflicts of interest.

## Authors' Contributions

A.H.M., V.B., M.O.; Participated in study design, data collection and evaluation, drafting and statistical analysis. A.H.M., V.B., M.R.; Contributed to all experimental work such as muscle decellularization, cell culture, immunofluorescence staining, and interpretation of data. A.H.M., M.R.; Conducted molecular experiments and RT-qPCR analysis. V.B., M.O.; Were responsible for overall supervision. A.H.M.; Drafted the manuscript, which was revised by V.B., M.O. All authors read and approved the final manuscript.

## References

1. Heidari-Moghadam A, Bayati V, Orazizadeh M, Rashno M. Role of vascular endothelial growth factor and human umbilical vein endothelial cells in designing an in vitro vascular-muscle cellular model using adipose-derived stem cells. Cell J. 2020; 22 Suppl 1: 19.
2. Jia W, Hu H, Li A, Deng H, Hogue CL, Mauro JC, et al. Glass-activated regeneration of volumetric muscle loss. Acta Biomater. 2020; 103: 306-317.
3. Chen B, Shan T. The role of satellite and other functional cell types in muscle repair and regeneration. J Muscle Res Cell Motil. 2019; 40(1): 1-8.
4. Shayan M, Huang NF. Pre-Clinical Cell Therapeutic Approaches for Repair of Volumetric Muscle Loss. Bioengineering. 2020; 7(3): 97.
5. Kesireddy V. Evaluation of adipose-derived stem cells for tissue engineered muscle repair construct-mediated repair of a murine model of volumetric muscle loss injury. Int J Nanomedicine. 2016; 11: 1461-1473.
6. Lee E, Kim HJ, Shaker MR, Ryu JR, Ham MS, Seo SH, et al. High-performance acellular tissue scaffold combined with hydrogel polymers for regenerative medicine. ACS Biomater Sci Eng. 2019; 5(7): 3462-3474.
7. Gorecka A, Salemi S, Haralampieva D, Moalli F, Stroka D, Candinas D, et al. Autologous transplantation of adipose-derived stem cells improves functional recovery of skeletal muscle without direct participation in new myofiber formation. Stem Cell Res Ther. 2018; 9(1): 195.
8. Gillies AR , Smith LR, Lieber RL, Varghese S. Method for decellularizing skeletal muscle without detergents or proteolytic enzymes. Tissue Eng Part C Methods. 2011; 17(4): 383-389.
9. Wassenaar JW, Boss GR, Christman KL. Decellularized skeletal muscle as an in vitro model for studying drug-extracellular matrixinteractions. Biomaterials. 2015; 64: 108-114.
10. Machingal MA, Corona BT, Walters TJ, Kesireddy V, Koval CN, Dannahower A, et al. A tissue-engineered muscle repair construct for functional restoration of an irrecoverable muscle injury in a murine model. Tissue Eng Part A. 2011; 17(17-18): 2291-2303.
11. Yao R, He J, Meng G, Jiang B, Wu F. Electrospun PCL/Gelatin composite fibrous scaffolds: mechanical properties and cellular responses. J Biomater Sci Polym Ed. 2016; 27(9): 824-838.
12. Yang G, Lin H, Rothrauff BB, Yu S, Tuan RS. Multilayered polycaprolactone/gelatin fiber-hydrogel composite for tendon tissue engineering. Acta Biomater. 2016; 35: 68-76.
13. Kim MS, Jun I, Shin YM, Jang W, Kim SI, Shin H. The development of genipin-crosslinked poly (caprolactone) (PCL)/gelatin nanofibers for tissueengineering applications. Macromol Biosci. 2010; 10(1): 91-100.
14. Ucuzian AA, Bufalino DV, Pang Y, Greisler HP. Angiogenic endothelial cell invasion into fibrin is stimulated by proliferating smooth muscle cells. Microvasc Res. 2013; 90: 40-47.
15. Germani A, Di Carlo A, Mangoni A, Straino S, Giacinti C, Turrini P, et al. Vascular endothelial growth factor modulates skeletal myoblast function. Am J Pathol. 2003; 163(4): 1417-1428.
16. Fu W, Liu Z, Feng B, Hu R, He X, Wang H, et al. Electrospun gelatin/PCL and collagen/PLCL scaffolds for vascular tissue engineering. Int J Nanomedicine. 2014; 9: 2335-2344.
17. Wang L, Johnson JA, Chang DW, Zhang Q. Decellularized musculofascial extracellular matrix for tissue engineering. Biomaterials. 2013; 34(11): 2641-2654.
18. Criswell TL, Corona BT, Wang Z, Zhou Y, Niu G, Xu Y, et al. The role of endothelial cells in myofiber differentiation and the vascularization and innervation of bioengineered muscle tissue in vivo. Biomaterials. 2013; 34(1): 140-149.
19. Crapo PM, Gilbert TW, Badylak SF. An overview of tissue and whole organ decellularization processes. Biomaterials. 2011; 32(12): 3233-3243.
20. Li MT, Willett NJ, Uhrig BA, Guldberg RE, Warren GL. Functional analysis of limb recovery following autograft treatment of volumetric muscle loss in the quadriceps femoris. J Biomech. 2014; 47(9): 2013-2021
21. Merritt EK, Cannon MV, Hammers DW, Le LN, Gokhale R, Sarathy A, et al. Repair of traumatic skeletal muscle injury with bone-marrow-derived mesenchymal stem cellsseeded on extracellular matrix. Tissue Eng Part A. 2010; 16(9): 2871-2881.
22. Badylak SF, Dziki JL, Sicari BM, Ambrosio F, Boninger ML. Mechanisms by which acellular biologic scaffolds promote functional skeletal muscle restoration. Biomaterials. 2016; 103: 128-136.
23. Chen S, Nakamoto T, Kawazoe N, Chen G. Engineering multilayered skeletal muscle tissue by using 3D microgrooved collagen scaffolds. Biomaterials. 2015; 73: 23-31.
24. Ferrara N, Gerber HP, LeCouter J. The biology of VEGF and its receptors. Nat Med. 2003; 9(6): 669-676.
25. Chen Y, Amende I, Hampton TG, Yang Y, Ke Q, Min JY, et al. Vascular endothelial growth factor promotes cardiomyocyte differentiation of embryonic stem cells. Am J Physiol Heart Circ Physiol. 2006; 291(4): H1653-H1658.
26. Song YH, Gehmert S, Sadat S, Pinkernell K, Bai X, Matthias N, et al. VEGF is critical for spontaneous differentiation of stem cells into cardiomyocytes. Biochem Biophys Res Commun. 2007; 354(4): 999-1003.
27. Shvartsman D, Storrie-White H, Lee K, Kearney C, Brudno Y, Ho N, et al. Sustained delivery of VEGF maintains innervation and promotes reperfusion in ischemic skeletal muscles via NGF/GDNF signaling. Mol Ther. 2014; 22(7): 1243-1253.
28. Kim MH, Hong HN, Hong JP, Park CJ, Kwon SW, Kim SH, et al. The effect of VEGF on the myogenic differentiation of adipose tissue derived stem cells within thermosensitive hydrogel matrices. Biomaterials. 2010; 31(6): 1213-1218.
29. Ochoa O, Sun D, Reyes-Reyna SM, Waite LL, Michalek JE, McManus LM, et al. Delayed angiogenesis and VEGF production in CCR2-/- mice during impaired skeletal muscleregeneration. Am J Physiol Regul Integr Comp Physiol. 2007; 293(2): R651-R661.
30. Carter RN, Casillo SM, Mazzocchi AR, DesOrmeaux JS, Roussie JA, Gaborski TR. Ultrathin transparent membranes for cellular barrier and Co-culture models. Biofabrication. 2017; 9(1): 015019.
31. Chen S, Kawazoe N, Chen G. Biomimetic assembly of HUVECs and muscle cells in microgrooved collagen porous scaffolds. Tissue Eng Part C Methods. 2017; 23(6): 367-376.
32. Lin CH, Lilly B. Endothelial cells direct mesenchymal stem cells toward a smooth muscle cell fate. Stem Cells Dev. 2014; 23(21): 2581-2590
33. Gholobova D, Decroix L, Van Muylder V, Desender L, Gerard M, Carpentier G, et al. Endothelial network formation within human tissue-engineered skeletal muscle. Tissue Eng Part A. 2015; 21(19-20): 2548-2558.

34. Koffler J, Kaufman-Francis K, Shandalov Y, Egozi D, Pavlov DA, Landesberg A, et al. Improved vascular organization enhances functional integration of engineered skeletal muscle grafts. Proc Natl Acad Sci USA. 2011; 108(36): 14789-24794.
35. Sasagawa T, Shimizu T, Sekiya S, Haraguchi Y, Yamato M, Sawa Y, et al. Design of prevascularized three-dimensional cell-dense tissues using a cell sheet stacking manipulation technology. Biomaterials. 2010; 31(7): 1646-1654.
36. Holnthoner W, Hohenegger K, Husa AM, Muehleder S, Meinl A, Peterbauer-Scherb A, et al. Adipose-derived stem cells induce vascular tube formation of outgrowth endothelial cells in a fibrin matrix. J Tissue Eng Regen Med. 2015; 9(2): 127-136.
37. Walgenbach KJ, Gratas C, Shestak KC, Becker D. Ischemia-induced expression of bFGF in normal skeletal muscle: a potential paracrine mechanism for mediating angiogenesis in ischemic skeletal muscle. Nat Med. 1995; 1: 453-459.
38. Kook YM, Kim H, Kim S, Heo CY, Park MH, Lee K, et al. Promotion of vascular morphogenesis of endothelial cells Co-cultured with human adipose-derived mesenchymal stem cells using polycaprolactone/gelatin nanofibrous scaffolds. Nanomaterials. 2018; 8(2): 117.
39. Park KM, Gerecht S. Harnessing developmental processes for vascular engineering and regeneration. Development. 2014; 141(14): 2760-2769.

Original Article

# Fungal Infected Adipose Stem Cells: The Effects of Novel Lipo-Niosome Nanoparticles Loaded with Amphotericin B and Thymus Essential Oil

**Fardin Rahimi, M.Sc.[1, 2], Ghasem Amoabediny, Ph.D.[2, 3, 4*], Hossein Sabahi, Ph.D.[1], Behrouz Zandieh-Doulabi, Ph.D.[2, 5]**

1. Department of Life Science Engineering, Faculty of New Sciences and Technologies, University of Tehran, Tehran, Iran
2. Department of Biomedical Engineering, Research Center for New Technologies in Life Science Engineering, University of Tehran, Tehran, Iran
3. School of Chemical Engineering, College of Engineering, University of Tehran, Tehran, Iran
4. Department of Oral and Maxillofacial Surgery/Oral Pathology, Amsterdam University Medical Centers-location Vumc and Academic Centre for Dentistry Amsterdam (ACTA), Vrije Universiteit Amsterdam, Amsterdam Movement Sciences, Amsterdam, The Netherlands
5. Department of Oral Cell Biology, Academic Centre for Dentistry Amsterdam (ACTA), The University of Amsterdam and Vrije Universiteit Amsterdam, Amsterdam Movement Sciences, Amsterdam, The Netherlands

**Corresponding Address: P.O.Box: 14155-6619, School of Chemical Engineering, College of Engineering, University of Tehran, Tehran, Iran*
*Email: amoabediny@ut.ac.ir*

**Received: 06/February/2021, Accepted: 23/October/2021**

Abstract

**Objective:** In this study, we aimed to develop new Lipo-niosomes based nanoparticles loaded with Amphotericin B (AmB) and Thymus Essential Oil (TEO) and test their effectiveness in the treatment of fungal-infected human adipose stem cells (hASCs).

**Materials and Methods:** In this experimental study, optimal formulation of AmB and TEO loaded lipo-niosome (based on lipid-surfactant thin-film hydration method) was chemically, and biologically characterized. Therefore, encapsulation capacity, drug release, size, and the survival rate of cells with different concentrations of free and encapsulated AmB/TEO were evaluated using the MTT method, and its antifungal activity was compared with conventional AmB.

**Results:** Lipo-Niosome containing Tween 60 surfactant: cholesterol: Dipalmitoyl phosphatidylcholine (DPPC): Polyethylene glycol (PEG) with a ratio of 20:40:60:3 were chosen as optimal formulation. Lipo-Niosomes entrapment efficiency was 94.15%. The drug release rate after 24 hours was 52%, 54%, and 48% for Lipo-AmB, Lipo-TEO, and Lipo-AmB/TEO, respectively. Physical and chemical characteristics of the Lipo-Niosomes particles indicated size of 200 nm and a dispersion index of 0.32 with a Zeta potential of -24.56 mv. Furthermore, no chemical interaction between drugs and nano-carriers was observed. The cell viability of adipose mesenchymal stem cells exposed to 50 µg/ml of free AmB, free TEO, and free AmB/TEO was 13.4, 58, and 36.9%, respectively. Whereas the toxicity of the encapsulated formulas of these drugs was 48.9, 70.8, and 58.3% respectively. The toxicity of nanoparticles was very low (8.5%) at this concentration. Fluorescence microscopic images showed that the antifungal activity of Lipo-AmB/TEO was significantly higher than free formulas of AmB, TEO, and AmB/TEO.

**Conclusion:** In this study, we investigated the efficacy of the TEO/AmB combination, in both free and encapsulated-niosomal form, on the growth of fungal infected-hASCs. The results showed that the AmB/TEO-loaded Lipo-Niosomes can be suggested as a new efficient anti-fungal nano-system for patients treated with hASCs.

***Keywords:*** AmB and TEO, Fungal Infection, Lipo-Niosomes, Stem Cells

Cell Journal(Yakhteh), Vol 24, No 7, July 2022, Pages: 391-402

**Citation:** Rahimi F, Amoabediny Gh, Sabahi H, Zandieh-Doulabi B. Fungal infected adipose stem cells: the effects of novel lipo-niosome nanoparticles loaded with amphotericin B and thymus essential oil. Cell J. 2022; 24(7): 391-402. doi: 10.22074/cellj.2022.7967.
This open-access article has been published under the terms of the Creative Commons Attribution Non-Commercial 3.0 (CC BY-NC 3.0).

## Introduction

Today, the world needs new methods to treat diseases, especially fungal diseases to increase the effectiveness of drugs and reduce their side effects. Fungal diseases are important in three aspects: infection, mortality, and economic losses. These infections threaten almost all patients, especially children who use stem cell transplants. The prevalence of invasive candidiasis in these patients is about 70-80%, and the resulting mortality is reported to be about 60-90% (1).

Mesenchymal stem cells (MSCs) are multipotent stem cells that are important for making and repairing skeletal tissues, such as cartilage, bone, and nerve cell lineages. The MSC is found in various tissues such as bone marrow, amniotic fluid, cord blood, and other mesoderm tissues. These types of cells can grow, multiply, and differentiate for generations in the laboratory while maintaining the stable morphology and natural state of their chromosomes (2). Patients with MSC transplant recipients are at high risk for invasive fungal infections (IFIs). Over the past two decades, the number of patients at risk of fungal infections has increased after using MSC to treat cancer. Dominant organisms that cause IFIs include *Candida spp.*, *Aspergillus spp.*, and Mucorales molds (3, 4). Among the allogeneic hematopoietic stem cell transplantation (HSCT) recipients, about 86% were due to molds, and 14% were due to yeasts. The majority of mold infections, about 94%, were caused by Aspergillus species (5).

One of the most common complications of stem cell transplantation is the suppression of the immune system following the administration of corticosteroids

and nosocomial infections, which can lead to a variety of diseases, especially bacterial and fungal infections. To prevent and treat these diseases, especially fungal agents, Amphotericin B (AmB) is used. Although free administration of this drug has several side effects on kidney, liver, lungs, and the body's hematopoietic system, yet AmB is considered a golden treatment against these fungal infections in the patient treated with hASCs. The drug binds to the fungal cell membrane and induces the pores in the membranes leading to ions leakage, and microorganisms death (6).

One possible approach to reduce the side effects of AmB is to use the essential oils of herbs. In recent years, there has been a growing tendency toward herbal medicines. The main advantages of cost-effective herbal medicines are good safety and their fewer side effects (7). The essential oils of medicinal plants, especially thyme, can be a good alternative to chemical drugs with antifungal and antibacterial properties. It has been also shown that Essential Oil (TEO) can inhibit the pathogenicity of microorganisms such as Candida albicans, Clostridium, and Bactericides fragilis (8).

Another way to reduce the side effects of these drugs is to use drug delivery nanocarriers. The goal of researchers in the synthesis and optimization of drug delivery is to design a system for proper drug loading, optimal release properties, short half-life, and less toxicity (9). Nanocarrier containing AmB bind to the fungal cell and facilitate the slow release of drug molecules into the fungus cell membrane as well as infected hASCs (10). Diezi and Kwon (11), fabricated cholesterol-combined AmB PEG-DSPE micelles that met the safety and solubility requirements of AmB and reduced toxicity at the membrane level for the treatment of life-threatening systemic fungi. Walsh et al. (12), also encapsulated AmB in liposomal and found that the nano-drug delivery system increased its therapeutic effect and decreased its side effects.

Using advanced *in vitro* methods, Mostafavi et al. (13), investigated the effect of AmB in combination with selenium, free and loaded inside the nano niosome, on *Leishmania tropica (L. tropica)*. Using the MTT method, macrophage model, flow cytometry, and quantitative polymerase chain reaction (qPCR), cytotoxicity and efficiency of the niosomic formula were investigated, and no toxicity was found for niosomal forms of the compound. Alam et al. (14), also developed a niosomal drug nanosystem containing diallyl sulfide in combination with garlic oil, and the results showed that the niosomic form of the drugs significantly reduced the activity of Candida albicans and animal death compared to its free form. In addition, histopathological studies showed that the niosomal showed no toxic effects, and fewer hyphae were observed in C. Albicans biosystems treated with SL-AmB niosomes compared to free AmB (15).

Nano-carrier of liposomal amphotericin B (LAmB) in the transplantation setting has increased the rate of therapeutic achievement of fungal infections with a suitable safety profile (12). In recent decades, niosomes have been considered by researchers as a suitable carrier for drug delivery, and in some cases, it has been reported that this carrier can be a suitable alternative to liposomal nanocarriers (16). A promising method for reducing side effects and effective drug treatment is the use of nano niosomes, which are an excellent alternative to trapping hydrophobic drugs due to their high efficiency, biodegradation, and biocompatibility. In addition, they have good stability, low preparation cost and are easy to store (17).

Sharma et al. (17) used the Niosome system to study the effect of co-delivery of curcumin and doxorubicin on the Hela (human cervical cancer) cell line. Studies of two combinations of curcumin and doxorubicin showed that curcumin is located in the lipid layer, while doxorubicin is trapped in the hydrophilic part of the noisome. Molecular dynamics simulations confirmed that in the membrane environment, AmB interacts with ergosterol, 3-4 times stronger interactions than in solution. The AmB-cholesterol bonding is weaker compared with ergosterol not only because of the weaker van der Waals (vdW) interactions but also because of entropy decrease associated with a reduction in the structural flexibility of the sterol side-chain (8). Zhou et al. (18), examined the effectiveness of umbilical cord mesenchymal stem cells (uMSCs) on corneal scarring. They used natamycin for the prevention and treatment of fungal keratitis. Although liposomes have been widely studied as promising carriers of proteins, drugs, and DNA, one of the major problems with using these nanocarriers for drug delivery is their non-specificity, which causes their removal by reticuloendothelial systems (19).

Studies of mineral and metal-based nanoparticles for drug delivery have shown that some nanoparticles cause toxicity to normal cells. For example, amorphous silica nanoparticles can cause inflammatory reactions on target organs resulting in apoptotic cell death (20). Carbon nanotubes (CNTs) have been reported to cause toxicity in normal cells. CNTs react with living cells to produce reactive oxygen species causing mitochondrial dysfunction and lipid peroxidation (21). It has been shown that mesoporous silica nanoparticles (MSNs) for targeted drug delivery in the size range of 50-100 nm with a positive charge accumulate mainly in the liver after intravenous injection (22).

Therefore, we aimed to evaluate the effectiveness of AmB and TEO loaded in Lipo-Niosomes on fungal-infected stem cells. In the present study, the lipid-based lipo-Niosome formula was optimized for further binding to the fungal wall ergosterol and the co-delivery of two antifungal drug combinations including AmB and TEO based on diffusion parameters, size, and trapping percentage. This model is for the transfer of hydrophobic compounds (especially the use of essential oils of medicinal plants) to reduce the dose and side effects of the chemical drug AmB and to increase their effectiveness on fungal-infected hASCs.

The experiment aimed to develop Lipo-Niosomes nanoparticles loaded with AmB and TEO and test their effectiveness for the development of an anti-fungal system favorable for hASCs. We hypothesized that due to their poor stability and low solubility in water, the AmB and TEO will be loaded in the hydrophobic part of the Lipo-Niosomes and be released slowly after contacting the fungal cells.

## Materials and Methods

Ethics approval for the current laboratory study was given by the Ethics Committee at Shahed University, Tehran, Iran (IR.SHAHED.REC.1399.164). All procedures were in accordance with the ethical guidelines of responsible institutional and national committees. Cholesterol (Sigma-Aldrich USA, C3045), Tween 60 (Sigma-Aldrich USA, P1629), Dipalmitoyl phosphatidylcholine (DPPC), derivatized distearyl phosphatidylethanolamine (mPEG2000-DSPE) were obtained from Lipoid GmbH (Ludwigshafen, Germany). AmB (India, B. No. GI50253), Thymus (Yazd, Iran), and human adipose-derived mesenchymal stem cells (hASCs) were provided by the Hazrat Rasool Hospital (Tehran, Iran). For cell culture, DMEM (21969035), fetal bovine serum (FBS, 26140), Trypsin/EDTA (R001100), and penicillin-streptomycin 1%10000) U/ml, 15140122), were purchased from Thermo Fisher Scientific, USA. MTT (3[4,5dimethyl-thiazol-2-yl]-2,5-diphenyl tetrazo- liumb bromide were (Sigma-Aldrich, Darmstadt, Germany ,1146500700), Candida Albicans ATCC 10231 [Shahed University of Medical Sciences, Tehran, Iran), Dialysis bags (MWCO 12000-14000) were supplied by Jingkehongda Biotechnology Co, Ltd. (Beijing, China). Chloroform and ethanol were purchased form Merck, Germany.

### Preparation of Lipo-Niosomes

Lipo-Niosomes containing AmB$1.08\times10^{-6}$ mol, TEO $1.8\times10^{-6}$ mol, cholesterol $9.8\times10^{-5}$ mol, Tween 60 $6.9\times10^{-5}$ mol, DPPC $1.4\times10^{-4}$ mol, and PEG $1.6\times10^{-5}$ mol, were prepared (Table 1). After weighing the required materials, they were dissolved in chloroform in a round bottom pot, and rotated (150 rpm/minute), to form a thin lipid film. Then, to prepare the Nanocarrier, the lipid film was hydrated with distilled water at 60°C for 30 minutes. Finally, 10 mol of Lipo-Niosomes with different concentrations were formed to load hydrophobic drugs. To reduce the size of the Lipo-Niosomes, the probe of the sonication device was placed in the colloidal solution of the niosomes in the ice bath, and then the sonication process was performed to produce smaller niosomes for 55 minutes (15 seconds: on and 10 seconds: off with a power of 100 watts). To separate the larger particles from the smaller particles and sterilize the Nanocarrier, a syringe filter was used (23). The prepared Lipo-Niosome was stored at 4°C for further studies. The ratio of materials composition to each material of cholesterol, Tween 60, DPPC, and PEG has been calculated (equal to 3.2, 4.6, 2.3, and 20.1 mol, respectively) and the ratio of drug composition to each drug has been calculated, AmB 2.6 mol and TEO equal 1.6 mol (Table 1).

### Essential oil extraction method

After purchasing thyme seeds, 100 g of seeds were used for the extraction of three milliliters of essential oil. The essential oil was extracted by water distillation (Hydrodistilation) using Clevenger for 2 hours and stored at 4°C. Finally, the separation and identification of essential oil compounds were performed by the gas chromatography method connected to a mass spectrometer (24).

**Table 1: Combination of drugs and materials in the Lipo-Niosomes used**

| Materials Name | Hydrophobic drug and materials (mol) | Moles ration [C/drugs (mol)] | Moles ration [H/materials (mol)] | Moles ration [H/drugs (mol)] |
|---|---|---|---|---|
| (A). AmB | $1.08 \times 10^{-6}$ | 2.6 | __ | 299 |
| (B). Thymus | $1.8 \times 10^{-6}$ | 1.6 | __ | 179 |
| (C). Total (A, B) | $2.88 \times 10^{-6}$ | __ | 3.2 | 112.15 |
| (D). Cho | $9.8 \times 10^{-5}$ | __ | 4.6 | __ |
| (E). Tween 60 | $6.9 \times 10^{-5}$ | __ | 2.3 | __ |
| (F). DPPC | $1.4 \times 10^{-4}$ | __ | 20.1 | __ |
| (G). PEG | $1.6 \times 10^{-5}$ | __ | __ | __ |
| (H). Total (D, E, F, G) | $3.23 \times 10^{-4}$ | __ | __ | __ |

AmB; Amphotericin B, Cho; Cholesterol, DPPC; Dipalmitoyl phosphatidylcholine, and PEG; Polyethylene glycol.

### Chemical and physical characterization, and morphology of Lipo-Niosomes

The morphology of hydrated Lipo-Niosomes loaded with AmB and TEO dispersions was examined by transmission electron microscopy (TEM, Zeiss EM10C-100 VK). The Lipo-Niosomes size and distribution were determined by dynamic light scattering (DLS, Malvern zen-3600-England). Fourier transform infrared (FTIR) spectroscopy (Model 8300, Shimadzu Corporation, Tokyo, Japan) was used to analyze molecular interaction between drugs and Nanocarrier for AmB, TEO, blank Lipo-Niosomes, and Lipo-Niosomes-AmB/TEO.

### Entrapment efficiency and drug release study

Spectrophotometric measurements were performed to evaluate entrapment efficacy and drug release characteristics over time. Nanocarriers containing drugs were calculated after preparation by UV spectroscopy at 330, 378, and 407 nm (Lmax). To evaluate the encapsulation efficiency, the following formula was used:

Encapsulation efficiency (%)=(The amount of AmB and Thymus encapsulated within niosomes)/(Total amount of AmB and Thymus added )×100

*In vitro* release of AmB/TEO from Lipo-Niosomes was investigated using a dialysis bag (MW=12 kDa) against phosphate-buffered saline (PBS) for 72 hours at 37°C and pH=7.4. Afterward, 2 ml of the samples were collected from the incubation medium at specific times, and immediately substituted with an equal volume of fresh PBS to maintain the environment's balance. Then, the release rate was evaluated by UV-vis spectrometer at 370, 388, and 407 nm for AmB and 275 nm for TEO.

### Isolation of stem cells from adipose tissue

The adipose tissue sample was cut into small pieces with sterile scissors in the culture room and under the laminar hood. To remove blood cells and impurities, the fat sample was washed several times with PBS solution and then the supernatant solution was removed from the environment. The remaining adipose tissue was transferred to the falcon tube at the bottom of the plate and 5-6 ml of 0.1% collagenase enzyme was added to it and placed in a 37°C hot water bath for 1.5-3 hours. The tubes containing the sample were then removed from the hot water bath and centrifuged at 2000 rpm for 5 minutes (repeated three times). The cells were transferred into a culture flask containing DMEM with 10% FBS. Finally, a flask containing cells was placed in an incubator at 37°C and 5% $CO_2$ (25).

### Cytotoxicity assay

Human Adipose-derived mesenchymal stem cells (hASCs) were cultured in DMEM supplemented with 10% FBS and 1% penicillin-streptomycin under standard conditions (37°C and 5% $CO_2$ in a humidified incubator). Cytotoxicity (MTT) assay was done to evaluate *in vitro* toxicity of free AmB/TEO and conjugated with Lipo-Niosomes. They were cultivated at a congestion of $5\times10^3$ cells in a 96-well culture plate in DMEM including 10% FBS at 37°C, and 5% $CO_2$ overnight. Cells were incubated with different drug concentrations (free and encapsulated) for 24 and 72 hours. They were incubated for with 5000 cells in a 96-well plate before assessment with the colorimetric MTT assay. After 72 hours of cell seeding in a medium, the control wells and samples were removed and washed with PBS and then incubated with 20 mL of 5 mg $mL^{-1}$ MTT in PBS for 3 hours. The resultant formazan crystals were dissolved in DMSO. Cytotoxicity was determined using an MTT reagent and specified spectrophotometrically at 570 nm using a microplate reader (Multiskan MS, Lab System Helsinki, Finland).

### Anti-fungal activity

*In vitro*, anti-fungal activity of free and loaded drugs in Lipo-Niosomes was assessed on various yeast strains Candida [Candida (C), Albicans (A), Dubliniensis (D), Parapsilosis (P), and Glabrata (G)]. Fungal strains were treated with free and drugs loaded Lipo-Niosomes concentrations ranging from 0.23 to 500 µg/ml at 36°C for 24, 48, and 72 hours. The diameter of the fungal region was determined to study the effectiveness of free AmB, TEO, and encapsulated against standard strains of Candida albicans. The standard strain of Candida albicans ATCC 10231 was sensitive (26, 27). The anti-fungal activities of AmB/TEO and their complex in Lipo-Niosomes were assessed against yeast different yeast strains of Albicans. The yeasts were grown in yeast mold broth (YMB). The optical density of the fungal growth was performed using a spectrophotometer at 520 nm to efficiency turbidity equal to 0.7 McFarland standards. The strains of fungal were treated with AmB/TEO and AmB-Niosome-TEO loaded at different concentrations from 0.12 to 500 µg/ml. Drug-free medium and yeast culture were only considered as controls. Finally, the plates were incubated at 36°C at different times, and growth in each well was appraised using an ELISA plate reader.

### Determining minimum inhibitory concentration

In this experiment, 96 wells microplates, were used. In the beginning, 100 µl of the culture medium sabouraud dextrose broth (SDB) was placed in the first row of wells. Then 100 µl of it was transferred to the second well, and this procedure was repeated. Finally, 100 µL of the volume of the final well solution was discarded, and 10 microliters of suspension fungus yeast were added to all wells. The microplate was then incubated in a shaker incubator at 150 rpm for 24 hours, and the lowest yeast growth inhibition concentration was considered in that MIC (26).

### Fungal Infection of stem cells

Human Adipose-derived mesenchymal stem cells (hASCs) were transferred to 96-well plates and seeded at a congestion of $5\times10^3$ cells per well and incubated

for 48 hours. Due to the sensitivity of stem cells and the lethality of Candida fungal strains, first, Lipo-Niosomes containing AmB and TEO with different concentrations (5, 10, 25, 50, 100, 150, 250, 500 μg/ml) in cells culture medium were added. Candida was then added to the cell-containing medium, free drugs, and nanocarriers containing the drug. In this method, the effect on cells was evaluated in different ways for 24 to 72 hours. The Alomar Blue colorimetric assay was used to evaluate drug sensitivity to fungal strains and cell viability. The optimized nanocarrier structure includes cholesterol, DPPC, and PEG, which play an important role in binding to fungal cells and stem cell membranes. The higher the percentage of these compounds, especially cholesterol and phospholipid, the connection will be longer and more stable.

### Statistical analysis

Statistical data analyses were performed using the student t-test to compare the differences between groups. The quality of fitting was performed by R2 (28), and nonlinear regression analysis was evaluated via MATLAB software (version 7.8). The relative standard deviation was calculated to determine the accuracy. The amount of standard solutions in the concentration range was analyzed by UV spectroscopy at the characteristic value of λ max with the standard curve of drugs. On the other hand, drug entrapment and drug release, the effect of fungi on cells and the effect of drugs on fungal growth in different groups were performed for 24 to 72 hours. The results of the analysis showed that in all triplicate experiments, significant differences were noted at $P \leq 0.05$ and $P \leq 0.01$, respectively.

## Results

### Preparation of Lipo-Niosomes

In this study, we used different formulas for optimization (data not shown). For finding the optimal formulation capable of high drug trapping efficiency, controlled release at 37°C physiological pH=7.4, and increasing the effectiveness of optimization were performed. After forming a thin lipid film for nanocarrier, it was exposed to 4°C for 24 hours to ensure complete removal of the solvent, the lipid thin film was exposed to 4°C for 24 hours. The AmB and TEO were encapsulated as antifungal agents in Lipo-Niosomes-based vesicles. The structure of Lipo-Niosomes including Tween 60: cholesterol: DPPC: PEG at 20:40:60:3 ratio was considered as a model for the delivery of several hydrophobic drugs.

In this study, Lipo-Niosomes contained AmB$1.08\times10^{-6}$ mol, TEO $1.8\times10^{-6}$ mol, cholesterol $9.8\times10^{-5}$ mol, Tween 60 $6.9\times10^{-5}$ mol, DPPC $1.4\times10^{-4}$ mol, and PEG $1.6\times10^{-5}$ mol were formed. The ratio of materials composition to each material of Cholesterol, Tween 60, DPPC, and PEG was calculated (equal to 3.2, 4.6, 2.3, and 20.1 mol, respectively). To prepare Lipo-Niosomes with hydrophobic molecules, AmB $1.08\times10^{-6}$ mol and TEO $1.8\times10^{-6}$ mol was added to the initial chloroform solution. Lipo-Niosomes formulations were formed with controlled release, and high entrapment efficiency parameters. Details of the Lipo-Niosomes preparation were: $2.88\times10^{-6}$ mol total weight of drugs, $3.23\times10^{-4}$ mol Lipo-Niosomes empty, and 112.15 mol is the vesicle ratio to drugs (Table 1). AmB and TEO molecules were placed in the hydrophobic part of the lipo-Niosome due to their hydrophobic properties. As a result, the drug entrapment rate in the nanocarrier was 94.15% and the release of AmB and TEO in the first 24 hours was 52% and 54%, respectively Their combined release from the nanocarrier was 48% in 24 hours, the nanosystem size was 200 nm and the zeta potential was -24.56 mv .This formula was selected as the most suitable formula. The Co-encapsulation of both hydrophobic drugs increased the total antifungal molecules loaded into the Nano-carrier bilayers, entrapment efficiencies and the effectiveness of the AmB/TEO in Lipo-Niosomes increased compared to the free samples. Optimized formulations after 60 days of storage, did not change significantly from the freshly prepared samples confirming stability after long-term storage. Finally, after choosing the optimal formula, their effects on Candida and fungal-infected hASCs were evaluated *in vitro*.

### Morphology and evaluation of drug interactions

The morphology of hydrated Lipo-Niosomes dispersions was examined by TEM. The structures of Nano-carriers were spherical with a core-shell structure. The particle size observed by TEM, blank Lipo-Niosome (100 nm), and Co-drugs loaded in lipo-Niosome [AmB-TEO, 200 nm)] was slightly smaller than that measured by DLS (220 nm, Fig.1A-C). To investigate the presence of chemical interactions between Multi-drugs Nanocarrier AmB, TEO, and unloaded Lipo-Niosomes, FTIR spectral data were obtained. The FTIR template for Lipo-Niosomal AmB-TEO showed different characteristic peaks of DPPC, cholesterol, Tween 60, and DSPE-MPEG in the range of 3400-1115 $cm^{-1}$. All peaks were repeated in the FTIR spectrum of blank Lipo-Niosomes, Lipo-Niosomes AmB, and Lipo-Niosomes TEO. peak of 1070 $cm^{-1}$ is due to the C=O asymmetrical stretching vibrations of AmB (29). All peaks were also observed in the spectrum of the single drug encapsulation of AmB and TEO; As a result, the FTIR results confirmed the conjugation of AmB and TEO with Lipo-Niosomes.

### Entrapment efficiency and drug release study

UV-visible spectroscopy for the determination of the free drugs was used in Lipo-Niosomes vesicles (Fig.2A). Free drugs have typical absorptions in the UV-visible region, concentration, and characteristic peaks of AmB at 370,388,407 nm, TEO 225 nm, and AmBisome® 325 nm (AmB Liposomal as standard, Fig.2B). UV-visible of AmB at 380, 400, 417 nm, and TEO 275 nm in Lipo-Niosomes were determined. As a result of the increase in the wavelength of the nanocarrier, it indicated that the

drugs have been loaded into the Lipo-Niosomes. UV-spectra of AmBisome® 325 nm and Lipo-Niosomes AmB/TEO compositions (295, 380, 405 nm) are shown, and considering the wavelengths of the drug compound loaded in the lipo-Niosome and the AmBisome, it is concluded that the present nanocarrier is similar to the standard nanocarrier [AmBisome (Fig.2C)]. As a result, the UV-visible spectra can be employed to analyze the degree of aggregation of AmB/TEO in Lipo-Niosomes conjugate (30).

The *in vitro* release of AmB and TEO from Lipo-Niosomes was investigated using a dialysis method and PBS as a running buffer at different time points at 37°C and pH=7.4 (Fig.2D). The percentage of released AmB and TEO alone in Lipo-Niosomes was 52% and 54%, after 24 hours and 54%, and 57% after 72 hours, respectively. Whereas, co-drugs were released after 24 hours 48% and after 72 hours 52%. As a result, the release of drugs loaded into the Nanocarrier showed a slow release and a prolonged effect

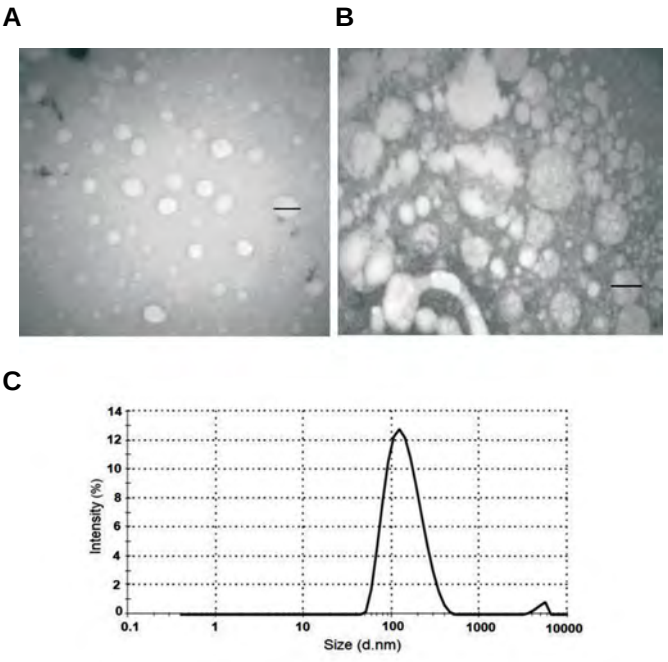


**Fig.1:** Microscopic images (TEM). Determination of morphology, structure and particle size distribution of lipo-Niosomes hydrated by TEM, and drugs loaded into nanocarriers by DLS. **A.** Blank Lipo-Niosome (100 nm), **B.** Co-drugs loaded in lipo-Niosome [AmB-TEO (200 nm)], and **C.** Size distribution of Lipo-Niosome containing AmB-TEO (220 nm) was slightly smaller than that measured by DLS. DLS; Dynamic light scattering, AmB; Amphotericin B, and TEO; Thymus essential oil.

## Cytotoxic effect of drugs on hASCs

As shown in Figure 2E, free and combination drugs, especially AmB, increase toxicity, and cell death with increasing concentration. Free drug molecules, Lipo-Niosomes, AmB, TEO, and their combination at a concentration of 50 µg/ml caused cell death. The survival rates of cells were 91.5, 13.4, 58%, and 36.88%, respectively (Lipo-Niosomes without drugs are safe and show low toxicity). On the other hand, the toxicity of free drugs (AmB, TEO, and their combination) with a concentration of 50 micrograms per ml were: 61, 80, and 56%, respectively, and by trapping drugs with the same concentration, the toxicity of 11, 19, and 26% were determined (Fig.2F). Thus, the toxicity has been significantly reduced.

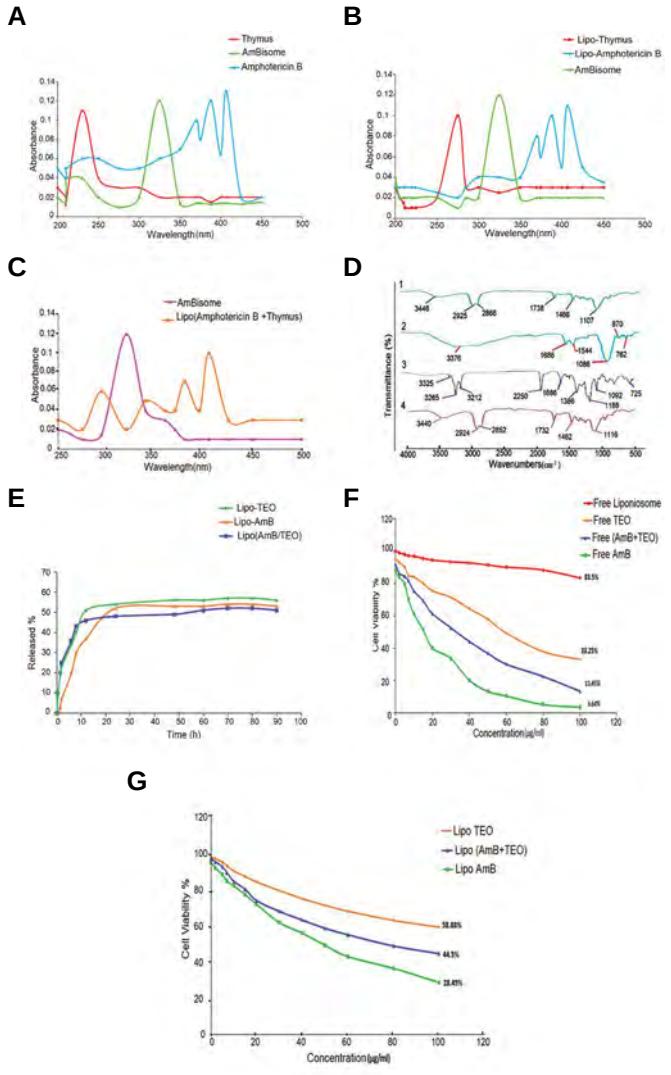


**Fig.2:** UV-visible spectrum: Morphology and evaluation of drug interactions, entrapment efficiency and release study and cytotoxic effect of drugs on hASCs. **A.** Free drugs (AmB and TEO), **B.** Lipo-Niosomes (AmB/TEO), and **C.** Combination drugs in Nanocarriers and AmBisome® (Liposomal AmB as standard). Free drugs had typical absorptions in the UV-visible region, concentration, and characteristic peaks, and UV-visible spectroscopy of AmB with a lower concentration in Lipo-Niosomes. **D.** FTIR spectra of Lipo-Niosomes (AmB-TEO) conjugate, AmB, TEO and Lipo-Niosomes. To investigate the presence of chemical interactions between co- drugs Nanocarrier, AmB, TEO, and blank Lipo-Niosomes the FTIR spectral data were obtained. **E.** Release of Lipo-Niosome AmB, Lipo-Niosome TEO, Lipo-Niosome AmB/TEO at 24 hours was 52, 54, 48%, and after 72 hours were 54, 57, and 52% respectively. **F, G.** Free and combination drugs, especially AmB, increase toxicity, and cell death with increasing concentration. But, with trapping drugs (AmB, TEO, and their combination) in the nanocarrier, their toxicities were reduced compared to free drugs.

## Anti-fungal Activity

### Effect on Candida fungi in culture medium

The diameters of the growth inhibition zone of different species of Candida were determined after 24, 48, and 72

hours. This experiment was performed in two parts. In the first stage, post-culture fungal strains were treated with free and combined AmB and TEO (Fig.3A). Free drugs had the greatest effect on the diameter of the growth inhibition zone in the first 24 hours. Drug concentrations decreased over time and as a result, the diameter of the fungal area decreased. Candida albicans growth aura diameter, which is more prevalent, after prescription of AmB, TEO, and their combination were 45,40, and 51 mm in the first 24 hours, 42.5, 37.6, and 47.8 mm in 48 hours:, and, 40.5, 36.6, and 44.8 mm in 72 hours, respectively.

This shows that free drugs affect quickly, and their effect soon wears off, so the fungi grow again ($P<0.05$). In the second stage, Candida strains were treated with encapsulated drugs (Fig.3B). In the first 24 hours, the drugs were less effective, but over time, the effectiveness increased. The diameters of the inhibition zone of different Candida species increased. After the prescription of AmB and TEO encapsulated in lipo-Niosome, the diameter of the Candida albicans area in the first 24 hours was 20.7mm and after 72 hours reached 22.7mm ($P<0.05$). Therefore, the drugs were slowly released from the nanocarrier (Fig.3) (26). For MIC, free drugs used in the cultured medium were in the range of 0.56 to 0.86 µg/ml (AmB) and 0.98 to 1.46 µg/ml (TEO), but when placed in Lipo-Niosomes, their MIC was about 0.83 to 1.42 µg/ml, while for MIC AmBisome was 0.78 to 1.5 µg/0 ml (30). With the increase of free drug concentration, their antifungal effects increased in the early hours, and after 72 hours due to dose reduction, these effects decrease.

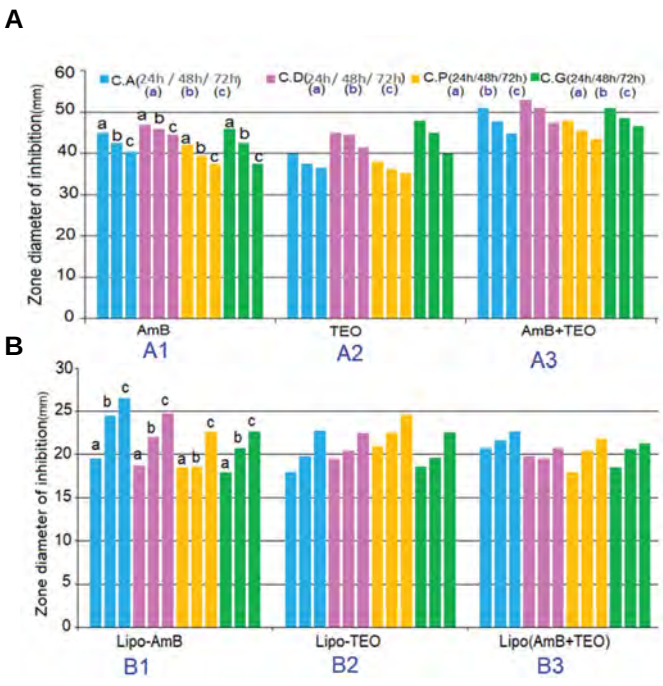


**Fig.3:** Efficacy of free and encapsulated AmB and TEO on Candida strains (C.A, C.D, C.P, and C.G). **A.** Free AmB (A1), free TEO (A2), and free AmB/TEO combined (A3). **B.** Lipo-Niosome AmB (B1), Lipo-Niosome TEO (B2), Lipo-Niosome AmB/TEO combined (B3) during 24 (a), 48 (b), and 72 (c) hours. AmB; Amphotericin B and TEO; Thymus Essential Oil.

In lipo-Niosome binding to cells and fungus wall, the effect of free and encapsulated AmB/TEO on fungal-infected hASCs was evaluated. These molecules are released slowly after attaching the Lipo-Niosomes to the fungus wall, but free drugs affect quickly, and their effect wears off quickly (Fig.4).

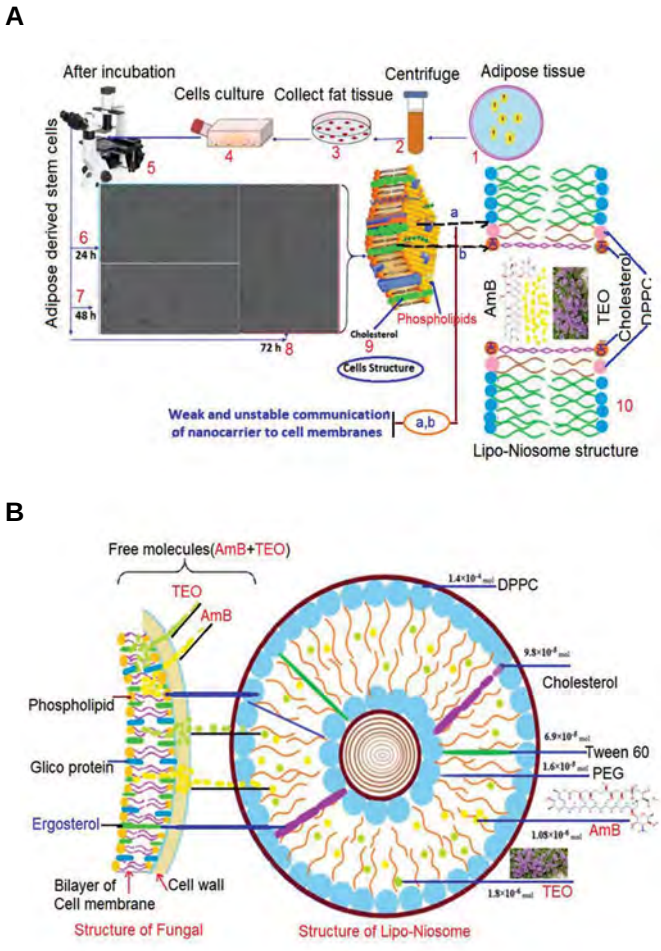


**Fig.4:** Lipo-Niosomes binding: Effect of free and encapsulated AmB/TEO on fungal-infected hASCs, the AmB and TEO molecules are released slowly after attaching the Lipo-Niosomes to the fungus wall, but free drugs affect quickly, and their effect wears off quickly. **A.** Stem cell wall, the structure of stem cells contains cholesterol and phospholipids that bind to Lipo-Niosomes. **B.** fungal cell wall, Lipo-Niosome containing drugs bind to phospholipids, beta-glucan, and especially ergosterol in the fungal wall. This bonding is due to the triple connection of the Nanocarrier to the fungal wall, it is stable and causes a slow release of drugs. This formulation has the ability to bonding to the fungal wall sterol, especially ergosterol, but its ability to connect to cholesterol in the stem cell membrane is weaker. The attachment to the cell wall is a van der Waals connection, But ergosterol binding is a covalent bond (10, 31). AmB; Amphotericin B, TEO; Thymus Essential Oil, and hASCs; Human adipose stem cells.

## Effect of free and encapsulated AmB/TEO on fungal-infected hASCs

In this study, the effect of free AmB, TEO, and compounds on hASCs was evaluated. The combined use of free drugs at a concentration of 50 µg/ml (equivalent to 1.5 µg/ml AmB and 1.5 µg/ml TEO) caused toxicity in these cells. The cell death rates due to AmB, TEO, and a

combination of AmB/TEO were 85%, 35%, and 70%, respectively. At this stage, the rate of cell death was compared with the control group (cells and fungi) and this mortality increased with higher doses of drugs. On the other hand, over time from 24 to 72 hours, as the concentration of the drugs decreased, the cells began to grow again (Fig.5A1, 2), which is consistent with the study of Kamiński et al. (10).

As shown in Figure 5B1, the fungus has begun to grow and occupy the entire cellular environment, and drugs have not been able to prevent the growth of fungi in the early hours. But over 72 hours, the drugs stopped the fungi from growing and killed them, and the stem cells got an opportunity to grow again. By comparing Figure 5B2 and reducing the concentration of fungi, the cells were marked. In the second stage, cells and drugs encapsulated were examined with fungi. At this stage, the cells become infected with the fungus, and during the first 24 hours, the fungi stop growing, but after some time (72 hours) and the slow release of the drugs, we see a decrease in the concentration of the fungus (Fig.5C, D). This is consistent with the studies of Moen et al. (32), and Tollemar et al. (33). Lipo-Niosome containing drugs at a concentration of 100 µg / ml (equivalent to ~ 3 µg AmB and 3 µg essential oil) showed much less toxicity.

A comparison of cell viability by the MTT method showed that the survival percentage of stem cells treated with concentrations of AmB and TEO, especially AmB in the first days was significantly reduced compared to the control sample ($P<0.01$). In addition, the results showed that the lethal effect of TEO on cells during the experiment was less than that of AmB. However, observations about the use of higher concentrations of AmB and TEO encapsulated in the lipo-Niosome had very little lethal effect compared to the control group, and over time, their effect on fungi increased. This process was performed with three repetitions in 24 to 72 hours.

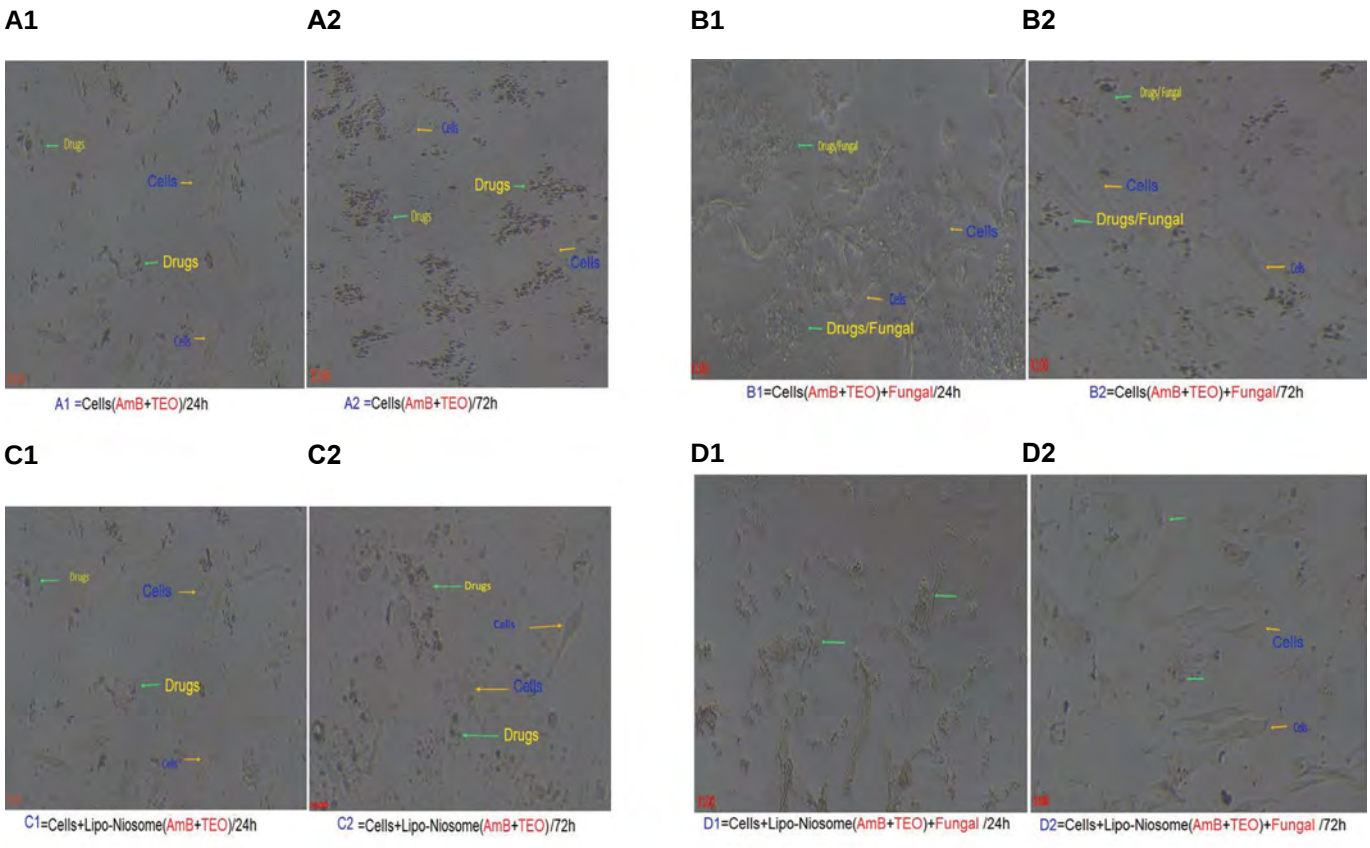


**Fig.5:** Effect of free and encapsulated AmB/TEO on fungal-infected hASCs. **A.** The effect of free drugs on cells over 24 to 72 hours. In the first 24 hours, drugs at a concentration of 50 µg /ml affected the cells and caused cell toxicity, and over time, as the dose of the drug decreased, the cells began to grow again after 72 hours. And it was found that different concentrations had different effects on cells (comparison of Figures A1 and A2). **B.** The cells became infected with the fungus after growing in a culture medium. The effect of free drugs on fungal-infected cells was investigated. As shown in Figure B1, the fungus has begun to grow and occupy the entire cellular environment. But over 72 hours, the drugs stopped the fungi from growing and killed them, and the stem cells got an opportunity to grow again. By comparing Fig. B1 and B2 and reducing the concentration of fungi, the cells were marked. **C.** At this stage, we placed the drugs inside the lipo-Niosome and then measured their effects on the cells. At this stage, the effect of drugs encapsulated in Lipo-Niosomes on cells was tested. Free drugs at a concentration of 50 micrograms, were not toxic when placed in nanocarriers. in the first 24 hours, the drugs are released late, and the structure of the cells is obvious, but after 72 hours, when the drugs are released slowly, they affect the cells and we see no the growth of cells. **D.** Encapsulated drugs were tested on fungal infected cells. The drugs were released slowly and over time from 24 to 72 hours, their effects increased and caused the fungus to die. In the first hours before 24 hours, we see that the growth of fungi has covered the surface of the cells, but in 72 hours, it is observed that with the release of drugs, the concentration of fungal strains decreases and the cells begin to grow. AmB; Amphotericin B, TEO; Thymus Essential Oil, and hASCs; Human adipose stem cells.

## Discussion

Patients with mesenchymal stem cell (MSC) receptors are at high risk for IFIs. Candida is one of the predominant organisms that cause these infections. Despite the diagnosis of these risk factors, attention to IFI in stem cell transplantation is underestimated, because several patients die without identifying the causes of the disease, especially fungal agents (34). It is worth noticing that all IFIs appeared in autologous hematopoietic stem cell transplant (*HSCT*) recipients immediately after transplantation, while patients receiving allogeneic HSCT are at risk even after 100 days (5). IFI is one of the leading causes of increased morbidity and mortality among patients with hematologic malignancies, particularly in those affected by acute myeloid leukemia, and in those who do hematopoietic stem cell transplant. Although more attention has been focused on identifying risk factors or prognosis in recipients of HSCT, few efforts have been made to assess the true IFI incidence (35).

Liposomal nanocarriers containing AmB (LAmB) have been used for many years to treat fungal infections and have been approved by the FDA, but have challenges such as instability, maintenance, and cost-effectiveness, while optimized Lipo-Niosomes are less challenging. As a result, the nanocarrier easily attaches to the fungal wall, and after the ions removing from the fungal membrane, it destroys them, these results are similar to studies by, Walsh et al. (12), Cordonnier et al. (36), Alam et al. (14), Mostafavi et al. (13). The advantage of this nanocarrier is its low toxicity and effectiveness because TEO essential oil has good antifungal activity and can be a good alternative to amphotericin.

Due to the stated challenges liposomes, Lipo-Niosomes have attracted the attention of many researchers and pharmaceutical companies. They are biocompatible, biodegradable, non-immunogenic, and non-toxic and can entrapment lots of material in relatively smaller volumes compared to other vesicles. The use of this nanocarrier improves the stability and pharmacokinetics of the drug, reduces the side effects of drugs, and increases the therapeutic effects. Also, they are easier and cheaper to prepare, store, and transport (37). The present Lipo-Niosomes are non-toxic, stable, biodegradable and inexpensive compared to liposomes.

Antifungal molecules attach to ergosterol after being exposed to the fungal membrane and extract it. The drug-ergosterol interaction is stronger and more stable than the drug-cholesterol because it is attributed to the double bond and the methyl group in sterol (10). The use of this nanocarrier improves the stability and pharmacokinetics of the drug, reduces the side effects of the drugs, and increases the effectiveness. Also, they are easier to prepare, store, transport, and trap a wider range of drugs (37). We tried to use the essential oils of medicinal plants with a similar and suitable effect. On the other hand, abundance, cheaper, fewer side effects are some of the advantages of these plant metabolites. They reduce the concentration of AmB, and even after release from the nanocarrier do not affect healthy cells in the body.

The morphology of cultured stem cells was assessed. According to a study by Kamiński (10), although the lipo-Niosome may bind to the membrane of these cells, the ability of the lipo-Niosome to bind to the ergosterol of the fungal wall is stable and stronger. On the other hand, the AmB drug forms a large agglomerate after being exposed to fungal membranes, then binds to ergosterol and extracts it. In this process, strong interaction between ergosterol and AmB drug is very important and based on the surface absorption of AmB drug in which antibiotic molecules are oriented parallel to the surface of the lipid, causing separation of ergosterol from the membrane surface of fungi and their structural instability. According to a study by Diezi and Kwon (11) the AmB-ergosterol interaction is stronger than AmB-cholesterol because it is attributed to the double bond and the methyl group in this sterol, and this particular atomic pattern is responsible for the better matching of the AmB heptane chain to ergosterol.

The amphiphilic nature of niosomes also causes permeability, solubility, increased absorption, reduced toxicity, and other side effects. UV-visible spectroscopy was used to determine the formation of the AmB-Liponiosome-TEO combination. Co-encapsulation of AmB and TEO have typical absorptions in the UV-visible region with characteristic peaks at 295, 380, and 405 nm with different concentrations (0.06,0.07, and 0.1). The AmBisome® (Standard liposomal AmB) spectrum also shows a characteristic peak at 325 nm with a concentration of 0.12. As a result, the almost identical wavelengths and concentrations of the two nanocarriers confirm the formation of the Liponiosome.

In this research, the main limitations associated with the use of AmB and TEO, especially amphotericin B, for antifungal therapy such as low water solubility, toxicity, and hemolytic potential were eliminated by conjugating the drug to Lipo-Niosome. It was found that these molecules were monomers in the conjugate and did not aggregate. The slow and continuous release of AmB and TEO from nanocarrier has a considerable role in increasing its half-life if used systemically which corresponds with the study of Gurudevan et al. (38).

Due to the structure of the fungal wall, the lipo-Niosome with compounds including Dppc: Chol: Tween60: PEG for proper and stable binding to the ergosterol of the fungal wall was investigated and finally an optimal formulation was obtained. The morphology of the selected nanocarriers containing a complex of two drug compounds, Am B and TEO, was performed by TEM. The size of the drug-free nanocarrier is close to 100 nanometers, but when the drug molecules were loaded into it, the size of the nanosystem reached about 200 nanometers, indicating that the drugs were properly loaded into the lipo-Niosome. In this case, the morphology of the nanocarrier is visible as a sphere with separate borders and a smooth surface.

Drug release from the optimized lipo-Niosome was

evaluated at pH=7.4 and 37°C by the physiological conditions of the body. As demonstrated, the essential oil has more release due to higher loading, and this release of drug molecules and essential oil during different hours shows that the nanosystem can release slowly and in a controlled manner. Also, the formulation prepared under physiological conditions has a favorable, continuous, and slow release. The release of AmB and TEO from Lipo-Niosome was very similar to the release observed in the case of AmBisome® and the study of Gurudevan et al. (38), suggesting that the conjugated pharmacokinetic profile in case of intravenous injection, would probably be similar to AmBisome®. Drug release rates after 24 hours were 48% for AmB-Lipo-TEO, whereas the release of AmB in AmBisome® and AmB-albumin conjugates was 45% and 48% at 24 hours, respectively. As a result, this optimized model was much similar to the release from AmBisome® and the study of Gurudevan et al. (38), and therefore could be fitted into this model.

Since the encapsulation in the present study has a similar *in vitro* release profile as that of AmBisome® and AmB-albumin conjugates, it is reasonable to assume that the conjugated pharmacokinetic properties in vivo are similar to AmBisome®. Although, this formulation must be confirmed by *in vivo* studies. Also, in this study, for early detection of the effectiveness of drugs loaded in this nanocarrier, for the treatment of candidiasis, the antifungal disk diffusion method was used, which is consistent with the results of studies by M.T. Blanco et al. (26). The antifungal susceptibility of AmB-Liponiosome-TEO than AmBisome® was evaluated as a reference for Candida strains. Since AmB is widely used against fungal infections of candidiasis, the AmB-Liponiosome-TEO combination was evaluated for its anti-fungal efficacy against this strain. The minimum inhibitory concentration (MIC) for AmB-Liponiosome-TEO combination (0.83 to 1.42 µg/ml), and AmBisome® (0.78 to 1.50) µg/ml) against the candida were determined. Interestingly, MIC values of AmB/TEO in the conjugate were similar to the MIC values of AmBisome® (38), as a result, the present nanocarrier has a good antifungal effect.

Due to the chemical structure of AmB and TEO, they were placed in the hydrophobic section of nano-carriers. Hydrophobic molecules are non-polar and therefore tend to other non-polar molecules and solvents. Interestingly, free and encapsulated molecules of TEO showed less toxicity than AmB with and without loading in Lipo-Niosomes (30). The diameters of the growth inhibition zone of different Candida species were determined in 24, 48, and 72 hours *in vitro*. Fungal strains were assayed after culture with AmB, TEO, and their combination in liposuction. In the first 24 hours the encapsulated drugs showed the least effect due to the lack of release from the nanocarrier and after 72 hours with the release of the drugs, they showed the greatest effectiveness, while free drugs had the greatest effect in the first 24 hours and their effectiveness disappeared after 72 hours. Growth area diameter was after prescription of Lipo-Niosomal (AmB/TEO combination) in 24 hours, 20.7 mm, 24.5 mm in 48 hours, and 72 hours, 26.5 mm were determined. This indicates that the encapsulated drugs have a long effect, so the fungi do not have a chance to grow again. In this study, the effect of Candida fungus on stem cells and the effectiveness of AmB and TEO drugs, and encapsulated in Lipo-Niosome with concentrations different were evaluated. Free drugs were quick to take effect and their effects soon disappeared, but loaded drugs due to slow-release, continuous effects, as well as more appropriate efficacy appeared. After the effectiveness of the drugs, the diameter of fungi decreased significantly and showed that the drug and essential oil have a good effect on these fungi. As a result, the standard strain of Candida Albicans had a certain sensitivity and according to the results, obtained in disk diffusion, TEO has similar antifungal effects as AmB. It is concluded that the TEO contains an effective substance capable of preventing the growth of fungal compared to the drug AmB.

*In vitro*, their toxicity, cell viability, and efficacy on fungal-infected stem cells were investigated. Nano-carriers containing drugs are attached to the ergosterol in the fungal cell wall by cholesterol, and drug molecules are slowly released into the fungus cell membrane (8, 39, 40). The AmB and TEO molecules are placed in the hydrophobic part of the Nano-carrier due to poor stability and low solubility in water. They are released slowly after attaching the Lipo-Niosomes to the fungus wall, but free drugs affect quickly, and their effect wears off quickly. The morphology of cells and fungi underwent significant changes, including a decrease and increase in volume, Spherical and spindle-shaped, cell transplantation, decrease and increase in the concentration of fungi. Images obtained using a reverse microscope showed that in early culture the cells had a spindle and polyhedral morphology (spindle-shaped cells had a higher growth rate than other cells and formed the highest cell percentage after the first passage).

Our goal is to produce nanoparticles based on Lipo-Niosome loaded with AmB, thymus essential oil, and evaluated their effectiveness in treating human adipose-derived stem cells infected with the fungus. As a result, study and imaging of the effects of drugs on fungal infected cells, reduction of fungal strain concentration after drug administration, and stem cell regrowth show that this nanocarrier is effective in inhibiting the growth of fungi in cell culture medium. Similar to the present system, the liposome nanocarrier contains AmB (LAmB), which has been used for many years to treat fungal infections and has been approved by the FDA. On the other hand, inspired by the LAmB nanocarrier that treats them after attaching to the fungal wall, the lipo-Niosome nanocarrier (27, 32-36) which has a liposome-like structure can attach to the fungal wall. As a result, the use of this nanocarrier *in vitro* causes growth inhibition, reduction of fungal concentration and cell regrowth (microscopic results). In this study, Am B which has many side effects, was loaded complex with TEO in a new nanocarrier, to reduce the

dose, reduce the side effects of this chemical drug, and reducing cellular stress. This review tried to compensate for the deficiency of various vitamins and minerals created by cell transplantation through the essential oil of the medicinal plant, and also increased the effectiveness or synergy of the drug with this process.

Therefore, it can be concluded that the present system, after the animal and clinical tests and FDA approval can be a good alternative to liposome containing AmB, because we tried to use the essential oil of a medicinal plant with similar and suitable effectiveness, more abundant, cheaper, with fewer side effects, and reduce the concentration of AmB which has side effects on the body cells even after release from the nanocarrier. Innovation of present study, Optimization of a new formulation for Co-delivery of two antifungal drug combinations including AmB and TEO based on release parameters, size, and percentage of entrapment has been done. This model is for the delivery of hydrophobic combinations (especially the use of medicinal plant essential oil) to reduce the dose and side effects of the chemical drug AmB for the effectiveness on fungal-infected stem cells. We introduce a model similar to LAmB.

## Conclusion

One of the side effects of AmB is moderate to severe anemia and cessation of red blood cell production, which can be solved by the prescription of TEO. In this optimized formula, we optimized the Lipid level in such a way that in addition to transferring the Multi-drug compounds, it could be properly attached to the ergosterol of the fungal cell membrane. And causes the stability of Nanocarriers during the binding and slow release of drug molecules. The proposed formula provided potential benefits, including smooth spherical surface morphology, sustained release, high entrapment efficiency (94.15%), the release of Lipo-AmB/TEO (24 hours=48%), and size (200 ± 20 nm), polydispersity index (0.32 ± 3), and Zeta (-24.56 mv). Free drug molecules, at a concentration of 50 μg/ml cause cell death, however by encapsulating them at a concentration of 100 micrograms per milliliter, the survival rate of the cells is increased. The proposed nanocarrier provides an obvious understanding of the Lipo-Niosomes formulation as a successful system based on surfactant and lipid for the Co-delivery of antifungal agents in stem cells. This method can be an appropriate alternative to AmB liposomal.

## Acknowledgments

The authors are grateful to Dr. Naeini Head of the Mycology Department, Shahed University Tehran, Iran for scientific assistance during the project. The authors also wish to thank the Department of Nanobiotechnology, Research Center for New Technologies in Life Science Engineering, University of Tehran, Tehran, Iran and Department of The Cell Therapy Center of Hazrat Rasool Hospital, Tehran, Iran. This study did not receive any special grant from funding agencies in the general, mercantile, or non-profit organizations. There is no conflict of interest in this research. It is noteworthy that this research is being patented.

## Authors' Contributions

F.R., Gh.A., H.S., B.Z.-D.; Participated in study design, data collection and evaluation, drafting and statistical analysis. F.R., Gh.A.; Contributed to all experimental work, and interpretation of data. F.R., Gh.A., H.S.; Were responsible for overall supervision. H.S., B.Z.-D.; Conducted molecular experiments and stem cells analysis. All authors read and approved the final manuscript.

## References

1. Hedayati MT, Khodavaisy S, Alialy M, Omran SM, Habibi MR. Invasive aspergillosis in intensive care unit patients in Iran. Acta Medica (Hradec Kralove). 2013; 56(2): 52-56.
2. da Silva Meirelles L, Caplan AI, Nardi NB. In search of the in vivo identity of mesenchymal stem cells. Stem Cells. 2008; 26(9): 2287-2299.
3. Otto WR, Green AM. Fungal infections in children with haematologic malignancies and stem cell transplant recipients. Br J Haematol. 2020; 189(4): 607-624.
4. Bays DJ, Thompson GR 3rd. Fungal infections of the stem cell transplant recipient and hematologic malignancy patients. Infect Dis Clin North Am. 2019; 33(2): 545-566.
5. Pagano L, Caira M, Nosari A, Van Lint MT, Candoni A, Offidani M, et al. Fungal infections in recipients of hematopoietic stem cell transplants: results of the SEIFEM B-2004 study--Sorveglianza Epidemiologica Infezioni Fungine Nelle Emopatie Maligne. Clin Infect Dis. 2007; 45(9): 1161-1170.
6. Schneemann M, Schaffner A. Host defense mechanism in aspergillus fumigatus infections. Contrib Microbiol. 1999; 2: 57-68.
7. Singh N, Limaye AP, Forrest G, Safdar N, Muñoz P, Pursell K, et al. Combination of voriconazole and caspofungin as primary therapy for invasive aspergillosis in solid organ transplant recipients: a prospective, multicenter, observational study. Transplantation. 2006; 81(3): 320-326.
8. Yazgi M, Awad D, Jreikous B. Screening of the antifungal activity of plant Mentha longifolia crude extracts against two fungi Alternaria citri and Fusarium moniliforme. J Entomol Zool Stud. 2015; 3(2): 359-364.
9. Arias JL. Nanotechnology and drug delivery. Nanoplatforms in drug delivery. 1st ed. CRC Press; 2014.
10. Kamiński DM. Recent progress in the study of the interactions of amphotericin B with cholesterol and ergosterol in lipid environments. Eur Biophys J. 2014; 43(10-11): 453-467.
11. Diezi TA, Kwon G. Amphotericin B/sterol co-loaded PEG-phospholipid micelles: effects of sterols on aggregation state and hemolytic activity of amphotericin B. Pharm Res. 2012; 29(7): 1737-1744.
12. Walsh TJ, Finberg RW, Arndt C, Hiemenz J, Schwartz C, Bodensteiner D, et al. Liposomal amphotericin B for empirical therapy in patients with persistent fever and neutropenia. National institute of allergy and infectious diseases mycoses study group. N Engl J Med. 1999; 340(10): 764-771.
13. Mostafavi M, Sharifi I, Farajzadeh S, Khazaeli P, Sharifi H, Pourseyedi E, et al. Niosomal formulation of amphotericin B alone and in combination with glucantime: In vitro and in vivo leishmanicidal effects. Biomed Pharmacother. 2019; 116: 108942.
14. Alam M, Dwivedi V, Khan AA, Mohammad O. Efficacy of niosomal formulation of diallyl sulfide against experimental candidiasis in Swiss albino mice. Nanomedicine (Lond). 2009; 4(7): 713-724.
15. Haque F, Sajid M, Cameotra SS, Battacharyya MS. Anti-biofilm activity of a sophorolipid-amphotericin B niosomal formulation against Candida albicans. Biofouling. 2017; 33(9): 768-779.
16. Kopermsub P, Mayen V, Warin C. Potential use of niosomes for encapsulation of nisin and EDTA and their antibacterial activity enhancement. Int Food Res. 2011; 44(2): 605-612.
17. Sharma V, Anandhakumar S, Sasidharan M. Self-degrading niosomes for encapsulation of hydrophilic and hydrophobic drugs: An efficient carrier for cancer multi-drug delivery. Mater Sci Eng C Mater Biol Appl. 2015; 56: 393-400.

18. Zhou Y, Chen Y, Wang S, Qin F, Wang L. MSCs helped reduce scarring in the cornea after fungal infection when combined with anti-fungal treatment. BMC Ophthalmol. 2019; 19(1): 226.
19. Higashi N, Sunamoto J. Endocytosis of poly(ethylene oxide)-modified liposome by human lymphoblastoid cells. Biochim Biophys Acta. 1995; 1243(3): 386-392.
20. McCarthy J, Inkielewicz-Stępniak I, Corbalan JJ, Radomski MW. Mechanisms of toxicity of amorphous silica nanoparticles on human lung submucosal cells in vitro: protective effects of fisetin. Chem Res Toxicol. 2012; 25(10): 2227-2235.
21. Manke A, Wang L, Rojanasakul Y. Mechanisms of nanoparticle-induced oxidative stress and toxicity. Biomed Res Int. 2013; 2013: 942916.
22. Rosenholm JM, Sahlgren C, Lindén M. Towards multifunctional, targeted drug delivery systems using mesoporous silica nanoparticles--opportunities & challenges. Nanoscale. 2010; 2(10): 1870-1883.
23. Heyes J, Hall K, Tailor V, Lenz R, MacLachlan I. Synthesis and characterization of novel poly(ethylene glycol)-lipid conjugates suitable for use in drug delivery. J Control Release. 2006; 112(2): 280-290.
24. Haghiroalsadat F, Azhdari M, Oroojalian F, Omidi M, Azimzadeh M. The chemical assessment of seed essence of three native medicinal plants of Yazd Province (Bunium Premium, Cuminum Cyminum, Trachyspermum Copticum) and the comparison of their antioxidant properties. Journal of Shahid Sadoughi University of Medical Sciences and Health Services. 2015; 2(6): 1592-1603.
25. Raposio E, Bertozzi N. isolation of ready-to-use adipose-derived stem cell (ASC) pellet for clinical applications and a comparative overview of alternate methods for ASC isolation. Curr Protoc Stem Cell Biol. 2017; 41: 1F.17.1-1F.17.12.
26. Blanco MT, Pérez-Giraldo C, Blanco J, Morán FJ, Hurtado C, Gómez-García AC. In vitro studies of activities of some antifungal agents against candida albicans ATCC 10231 by the turbidimetric method. Antimicrob Agents Chemother. 1992; 36(4): 898-901.
27. Upton A, Kirby KA, Carpenter P, Boeckh M, Marr KA. Invasive aspergillosis following hematopoietic cell transplantation: outcomes and prognostic factors associated with mortality. Clin Infect Dis. 2007; 44(4): 531-540.
28. Naderinezhad S, Amoabediny G, Haghiralsadat F. Co-delivery of hydrophilic and hydrophobic anticancer drugs using biocompatible pH-sensitive lipid-based nano-carriers for multidrug-resistant cancers. RSC Adv. 2017; 7(48): 30008-30019.
29. Gagoś M, Arczewska M. FTIR spectroscopic study of molecular organization of the antibiotic amphotericin B in aqueous solution and in DPPC lipid monolayers containing the sterols cholesterol and ergosterol. Eur Biophys J. 2012; 41(8): 663-673.
30. Jain S, Valvi PU, Swarnakar NK, Thanki K. Gelatin coated hybrid lipid nanoparticles for oral delivery of amphotericin B. Mol Pharm. 2012; 9(9): 2542-2553.
31. Silva L, Coutinho A, Fedorov A, Prieto M. Competitive binding of cholesterol and ergosterol to the polyene antibiotic nystatin. A fluorescence study. Biophys J. 2006; 90(10): 3625-3631.
32. Moen MD, Lyseng-Williamson KA, Scott LJ. Liposomal amphotericin B: a review of its use as empirical therapy in febrile neutropenia and in the treatment of invasive fungal infections. Drugs. 2009; 69(3): 361-392.
33. Tollemar J, Höckerstedt K, Ericzon BG, Sundberg B, Ringdén O. Fungal prophylaxis with AmBisome in liver and bone marrow transplant recipients: results of two randomized double-blind studies. Transplant Proc. 1994; 26(3): 1833.
34. Kume H, Yamazaki T, Abe M, Tanuma H, Okudaira M, Okayasu I. Increase in aspergillosis and severe mycotic infection in patients with leukemia and MDS: comparison of the data from the annual of the pathological autopsy cases in Japan in 1989, 1993 and 1997. Pathol Int. 2003; 53(11): 744-750.
35. Marr KA, Seidel K, White TC, Bowden RA. Candidemia in allogeneic blood and marrow transplant recipients: evolution of risk factors after the adoption of prophylactic fluconazole. J Infect Dis. 2000; 181(1): 309-316.
36. Cordonnier C, Mohty M, Faucher C, Pautas C, Robin M, Vey N, et al. Safety of a weekly high dose of liposomal amphotericin B for prophylaxis of invasive fungal infection in immunocompromised patients: PROPHYSOME Study. Int J Antimicrob Agents. 2008; 31(2): 135-141.
37. Wadhwa S, Paliwal R, Paliwal SR, Vyas SP. Nanocarriers in ocular drug delivery: an update review. Curr Pharm Des. 2009; 15(23): 2724-2750.
38. Gurudevan S, Francis AP, Jayakrishnan A. Amphotericin B-albumin conjugates: synthesis, toxicity and anti-fungal activity. Eur J Pharm Sci. 2018; 115: 167-174.
39. Kim J, Sudbery P. Candida albicans, a major human fungal pathogen. J Microbiol. 2011; 49(2): 171-177.
40. Li WR, Shi QS, Dai HQ, Liang Q, Xie XB, Huang XM, et al. Antifungal activity, kinetics and molecular mechanism of action of garlic oil against Candida albicans. Sci Rep. 2016; 6: 22805.

**Original Article**

# Study of The Correlation between miR-106a, miR-125b, and miR-330 on Multiple Sclerosis Patients by Targeting TNFSF4 and SP1 in NF-êb/TNF-α Pathway: A Case-Control Study

**Nasrin Hadi, M.Sc.[1], Seyed Morteza Seifati, Ph.D.[1], Behnaz Nateghi, M.Sc.[2, 3], Parisa Ravaghi, M.Sc.[4], Farinaz Khosravian, M.Sc.[2, 3], Faezeh Namazi, M.Sc.[1], Maryam Fotouhi Firouzabad, M.Sc.[1], Vahid Shaygannejad, M.D.[5], Mansoor Salehi, Ph.D. [2, 3, 6*]**

**1. Medical Biotechnology Research Center, Ashkezar Branch, Islamic Azad University, Ashkezar, Yazd, Iran**
**2. Medical Genetics Research Center of Genome, Isfahan University of Medical Sciences, Isfahan, Iran**
**3. Cellular, Molecular, and Genetics Research Center, Isfahan University of Medical Sciences, Isfahan, Iran**
**4. Department of Biology, Faculty of Science, Shahid Chamran University of Ahvaz, Ahvaz, Iran**
**5. Department of Neurology, Isfahan Neurosciences Research Center, Isfahan University of Medical Sciences, Isfahan, Iran**
**6. Department of Genetics and Molecular Biology, School of Medicine, Isfahan University of Medical Sciences, Isfahan, Iran**

***Corresponding Address: P.O.Box: 81746-73461, Department of Genetics and Molecular Biology, School of Medicine, Isfahan University of Medical Sciences, Isfahan, Iran***
***Email: m_salehi@med.mui.ac.ir***

**Received: 21/ October/ 2020, Accepted: 20 /April/2021**

Abstract

**Objective:** Multiple sclerosis (MS) is a complex multifactorial neuro-inflammatory disorder. This complexity arises from the evidence suggesting that MS is developed by interacting with environmental and genetic factors. This study aimed to evaluate the *miR-106a*, *miR-125b,* and *miR330-* expression levels in relapsing-remitting multiple sclerosis (RRMS) patients. The miRNAs' impact on *TNFSF4* and *Sp1* genes through the NF-κB/TNF-α signaling pathway was analyzed by measuring the expression levels in case and controls.

**Materials and Methods**: In this in silico-experimental study, we evaluated the association of *miR-106a*, *miR-125b,* and *miR330-* with *TNFSF4* and *SP1* gene expression levels in 60 RRMS patients and 30 healthy controls by real-time polymerase chain reaction (PCR).

**Results:** The expression levels of *miR-330, miR-106a,* and *miR125-b* in blood samples of RRMS patients were predominantly reduced. The expression of *TNFSF4* in patients demonstrated a significant enhancement, in contrast to the diminishing *Sp1* gene expression level in controls.

**Conclusion:** Our findings indicated an association between *miR-106a* and *miR-330* and *miR125-b* expression and RRMS in our study population. Our data suggested that the *miR106-a, miR125-b,* and *mir330-* expression are correlated with *TNFSF4* and *Sp1* gene expression levels.

***Keywords:*** Biomarker, *microRNA*, Multiple Sclerosis

Cell Journal(Yakhteh), Vol 24, No 7, July 2022, Pages: 403-409

**Citation:** **Hadi N, Seifati SM, Nateghi B, Ravaghi P, Khosravian F, Namazi F, Fotouhi Firouzabad M, Shaygannejad V, Salehi M. Study of the correlation between miR-106a, miR-125b, and miR-330 on multiple sclerosis patients by targeting TNFSF4 and SP1 in NF-κb/TNF-α pathway: a case-control study. Cell J. 2022; 24(7): 403-409. doi: 10.22074/cellj.2022.7835.**

**This open-access article has been published under the terms of the Creative Commons Attribution Non-Commercial 3.0 (CC BY-NC 3.0).**

## Introduction

Multiple sclerosis (MS) disorders are developed due to chronic inflammation of the central nervous system (CNS) and can increase focal lesions in the white matter of the spinal cord and brain (1). Clinical studies have shown that MS affects women 2-fold higher than men, and the progressive phase was between 5 and 35 years after the first onset (2). Relapsing-remitting MS (RRMS) is the typical primary type of MS and accounts for about 85% of MS patients (3). There is no standardized method of how to pursue MS patients to detect disease activity (4). Although MS's exact etiology remains enigmatic, the identification of genetic variations affecting MS disease development has grown in the last few years (5).

Immense evidence has indicated that tumor necrosis factor alpha (TNF-α) plays a pivotal role in MS development (6-8). Consecutive TNF-α expression could induce chronic inflammatory demyelinating disorder, synaptic instability in the brain, and subsequently sensory and cognitive damage (9). It has been demonstrated that the damaging role of TNF-α in MS might significantly relate to its transmembrane receptors tumor necrosis factor receptor type II (TNF-RII) or receptors, tumor necrosis factor (TNFR-I) (10). TNF receptors are present at the cell surface as monomers, while the monomers' ligand-induced homodimerization activates TNF-α signaling. OX40L is recognized as a ligand for OX40, also known as tumor necrosis factor ligand superfamily member 4 (TNFSF4) and CD252 (Cluster of differentiation 252), and is a type II transmembrane protein that might have a pivotal role in the differentiation and stimulation of T-cells. TNFSF4 is mainly expressed on the surface of T-cell antigen-presenting cell (APC) cells (11). The encoded protein of this gene is primarily expressed on activated CD4+ and CD8+ T-cells and various B-cells, microglia, vascular endothelial cells, and dendritic cells

(12). The encoded protein is involved in APC interactions and facilitates the adhesion of T-cells to endothelial cells. Interaction between TNFSF4 and CD4+ T-cells by TNFSF4 stimulates nuclear factor-kappa B (NF-κB) through TNF-R related TRAF1 and TRAF2. Besides, this signaling pathway is related to several immune functional activities, which include the intensification of Th2 responses and the production of Th2 and Th1 cytokines (13).

Sp1 is a transcription factor that binds to many promoters. Moreover, SP1 could involve in many processes such as apoptosis and immune responses. It has been proved that there is a relationship between Sp1 expression and the activity of the inflammatory cytokine TNF (14). Sp1 sites are frequently observed in NF-κB related genes, which can activate specific promoters in NF-κB over its binding sites. Sp1 acts through NF-κB by activating the NF-κB promoter sites (15).

The association of miRNA with components of the RNA-induced silencing complex (RISC) results in the degradation or translational repression and/or destabilization of their relevant mRNA. It occurs through miRNA binding to the 3′-untranslated region (UTR) of target genes (16). Growing evidence has shown the abnormal miRNA activity in CNS glial cells of patients with MS and peripheral blood immune cells compared with normal individuals, suggesting that miRNA expression could be correlated with MS pathogenesis and immunological features (17).

Honardoost et al. (18) have proposed that miR-106a probably has an inductive function in Th17 differentiation. Sanctuary et al. (19) have revealed that Mir-106a may have a crucial function in inflammatory bowel disease through the TNF-α pathway. Also, the biological role of miR-330-5p has been offered in some cells and cancers (20). According to Mao et al. (21) study on prostate cancer cells, microRNA-330 suppresses cell motility by decreasing the expression of Sp1, which plays the role of a transcription factor through the TNF-α pathway. Furthermore, miR-125b was demonstrated to bind the 3′UTR of TNF-α; therefore, MicroRNAs could reduce the expression of TNF-α in the innate immune response pathway. In this study, we examined whether the dysregulated expression of miR-106a, miR-125b, and mir-330 can be considered a diagnostic biomarker in RRMS patients with recurrent disease symptoms two months after relapse. This study evaluated the correlation of miRNAs with the TNFSF4 and SP1 mRNA and its pathogenicity by examining the expression levels of miR-106a and miR-125b, and miR-330 in normal and MS samples.

## Materials and Methods

### Ethical Issue

All experimental procedures were approved by the Ethic Committee of the Isfahan University of Medical Sciences (289271) .

### miRNA prediction

In this in silico-experimental study, we collected lists of microRNA target genes using miRWalk (22) and a list of gene-disease association export of DisGeNET (23). We chose genes that overlapped between these lists. These genes were studied in several databases for data mining. In this search, we evaluated Reactome (24), DAVID, STRING, and KEGG analysis. Interactions between genes, microRNAs, and pathways are illustrated in the designed network using Cytoscape software (25).

### Patients and controls

The Informed consent was taken from all subjects before sample collection. Briefly, we collected 4mL of blood from 90 participants (both male and female), including 60 RRMS patients and 30 healthy subjects. Overall, 30 healthy controls were recruited from Kashani Hospital (Isfahan, Iran), and 60 patients with RRMS were divided into two groups, including 30 who were recurrent and 30 who had recurrences for at least two months. Based on medical examinations, the healthy participants had no family history of autoimmune disease. The RRMS patients were diagnosed by a specific neurologist based on McDonald's criteria (26). 32 of these patients had solely received interferon (IFN)-β treatment two months before sampling, and the rest had not received any treatments. In the next step, we collected.

### Preparing peripheral blood human mononuclear cells from blood

Blood samples were isolated through a gradient of density Lymphoprep Peripheral Blood Human Mononuclear Cells (PBMCs, Bio Sera, USA). The cells remained in an intermediate phase after centrifugation, although other cells were deposited. In the next step, we gradually diluted the lymphoprep solution in a falcon tube with physiological saline at a ratio of 1:1, and then the solution was centrifuged at 800 g for 30 minutes (27). Afterward, Peripheral Blood Human Mononuclear Cells were transferred into a 2 ml RNAase-free microtube from the middle phase.

### Evaluating the expression of genes and MicroRNAs

RNA extraction from PBMCs was conducted by TRIzol reagent (Invitrogen, USA). The purity of the RNA was evaluated by a NanoDrop spectrometer. Furthermore, cDNA was prepared by a cDNA Synthesis Kit (TaKaRa, Japan). Additionally, the miRNA synthesis of RNA was done using a standard kit (Pars Genome, Tehran, Iran). *U6* was selected as the housekeeping gene for the normalization of the miRNAs data. Also, For the normalization of genes, *GAPDH* was considered a reference gene. The quantitative real-time polymerase chain reaction (qPCR) was accomplished by the Rotor-Gene 6000 (Corbett Life Science, Australia), and the repetition of samples was duplicated. Moreover, the amount of cycle threshold of real-time was determined by $2^{-\Delta\Delta Ct}$ methods. Primers purchased from micro-gene (Korea) are indicated in Table 1.

**Table 1:** The primer genes list

| Genes | Primer sequence (5′→3′) | Temperature (°C) |
|---|---|---|
| *SP1* | F: TTG AAA AAG GAG TTG GTG GC | 60 |
| | R: TGC TGG TTC TGT AAG TTG GG | |
| *TNFSF4* | F: GAAGAAGGTCAGGTCTGTCAAC | 58 |
| | R: AATCAGTTCTCCGCCATTCAC | |
| *GAPDH* | F: TGCCGCCTGGAGAAACC | 60 |
| | R: TGAAGTCGCAGGAGACAACC | |

### Statistical analysis

The GraphPad Prism Ver.9 (San Diego, USA) was applied to analyze the real time polymerase chain reaction (PCR) results. The Kolmogorov-Smirnov test was used to evaluate the normal distribution of the data. The one-way ANOVA test was used to analyze expression levels between two case and control groups. $P<0.05$ was considered statistically significant for the tests.

## Results

### Clinical and biological features

Sixty RRMS patients participated in this study, of which 30 subjects were selected 2-months after relapse. Furthermore, 30 healthy subjects joined the study as the control group. Patients and controls were sufficiently matched in terms of age and sex. According to the expression analysis results, there was no statistically significant difference in sex and taking interferon and non-interferon drugs between patients and controls (P=0.619 and P=0.388, respectively). The biological characteristics of two groups of patients (recurrent and recurrences for at least two months) are shown in Table 2.

**Table 2:** Biological and Clinical characteristics of patients and healthy individuals

| Characteristics | Control | Recurring patients | Two months after relapse patients |
|---|---|---|---|
| Number of subjects | 30 | 30 | 30 |
| Sex | | | |
| Males | 10 | 9 | 9 |
| Females | 20 | 21 | 21 |
| Drug | | | |
| Interferon | - | 11 | 11 |
| Non-interferon | - | 19 | 19 |
| Age (Y) | | | |
| Mean age | 1.843 ± 38.60 | 1.522 ± 33.7 | 1.522 ± 33.7 |
| Range | 21-58 | 21-45 | 21-45 |

### *In-silico* analysis

We provided a list including 178 genes that had overlap between microRNAs and genes associated with multiple sclerosis, and we presented these results using a VENN Diagram (Fig.1). Based on the enrichment of these genes, we found that these genes are correlated with NF-κB and TNF-α signaling pathways as vital pathways in MS. (Fig.S1, See Supplementary Online Information at www.celljournal.org). Also, the enrichment results pointed to the relationship between genes and MS in DisGeNET. We reported an interaction between genes, pathways, and microRNAs targeted genes in the cytoscape network (Fig.2).

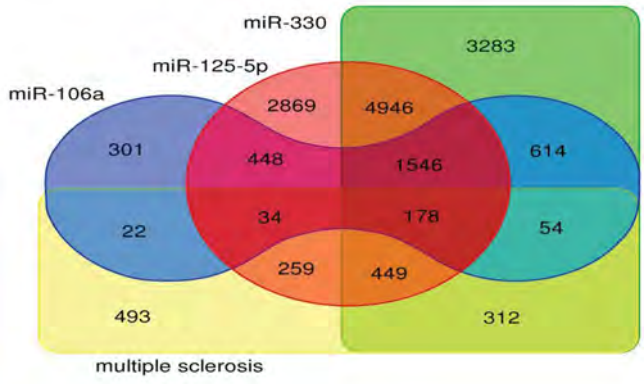


**Fig.1:** miRNA targets. Venn diagrams were employed to acquire the prediction of miRNAs that target *SP1* and *TNFSF4* genes. The number of 178 indicated the quantity of the selective miRNAs which target the genes.

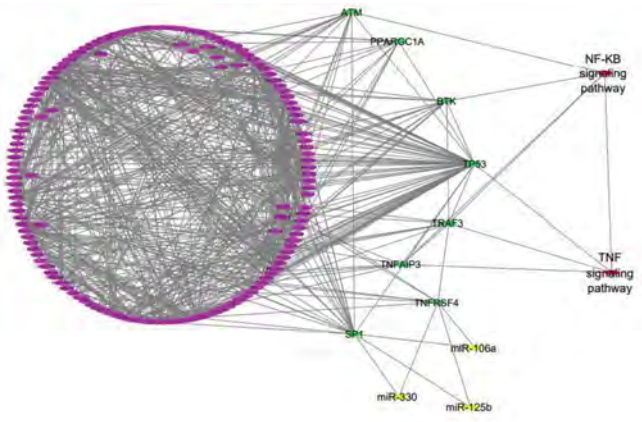


**Fig.2:** The network mapping. Interaction and correlation of mir and hub genes indicating *miR-330-5p, miR-106a,* and *miR-125b* are associated with *SP1*, *TNFSF4* genes in NF-κB/TNF-α pathway.

### miR-330-5p is up-regulated in RRMS patients

miR-330-5p expression was assessed by qRT-PCR in

two groups: The patients, including 30 patients with recurrent presentations and 30 patients two months after relapse (n=60) and healthy subjects (n=30). The results indicated a significant growth (by 3-fold) in the expression of this miRNA in patients (both recurrence and two months after relapse) compared with healthy subjects (P<0.0001 and P<0.0002, respectively, Fig.3A).

### Down-regulation of miR-125b and miR-106a expression in RRMS patients

To determine the potential roles of miR-125b and miR-106a in RRMS patients, we investigated both miRNAs' expression levels in patients (two months after relapse and recurrence) versus control individuals. Our results demonstrated that miR-106a expression was significantly down-regulated (by 0.5-fold) in the recurrence and two months after relapse patients compared with the control group (P<0.0001 and P<0.006, respectively). Moreover, data demonstrated that miR-125b was significantly diminished (by 0.7-fold) in both recurrence and two months after relapse patients (P<0.0001 and P<0.0005, respectively) and probably plays an essential role in RRMS patients (Fig.3B, C).

### Analysis of the expression level of *TNFSF4* and *SP1*

In this study, two potential targets of *miR-330-5p*, *miR-106a* and *miR-125b* were selected for further analyses. *TNFSF4* and *SP1* were selected as mentioned in the methods. Our data indicated decreased expression of *SP1* (by 0.5- fold) (P<0.0017 and P<0.003, respectively). In contrast, *TNFSF4* expression was increased significantly in recurrence and patients two months after relapse (by 3-fold) (P<0.004 and P<0.02, respectively) compared with healthy (Fig.3D, E).

### Analysis of the expression relationship of miR-106a, mir-125b, and miR-330 with selected targets

To assess the hypothesis's validity, we compared the expression level differences between miR-106a and miR-125b in patients and control samples with the expression level differences in *TNFSF4* between patient and control samples. According to data analysis, there was a significant inverse relationship between the reduced expression levels of miR-106a and miR-125b with the increase in *TNFSF4* expression. The Pearson correlations for the association of miR-106 and miR-125b with *TNFSF4* were equal to -0.4970 and -0.6284, respectively, and P values showed significant relationships (P=0.0052 and P=0.0002, respectively, Fig.4).

Moreover, the increase in miR-330 expression was inversely correlated with a decrease in *Sp1* gene expression. The Pearson correlation r was -0.7280, while the P<0.0001 showed the significance of the association (Fig.4).

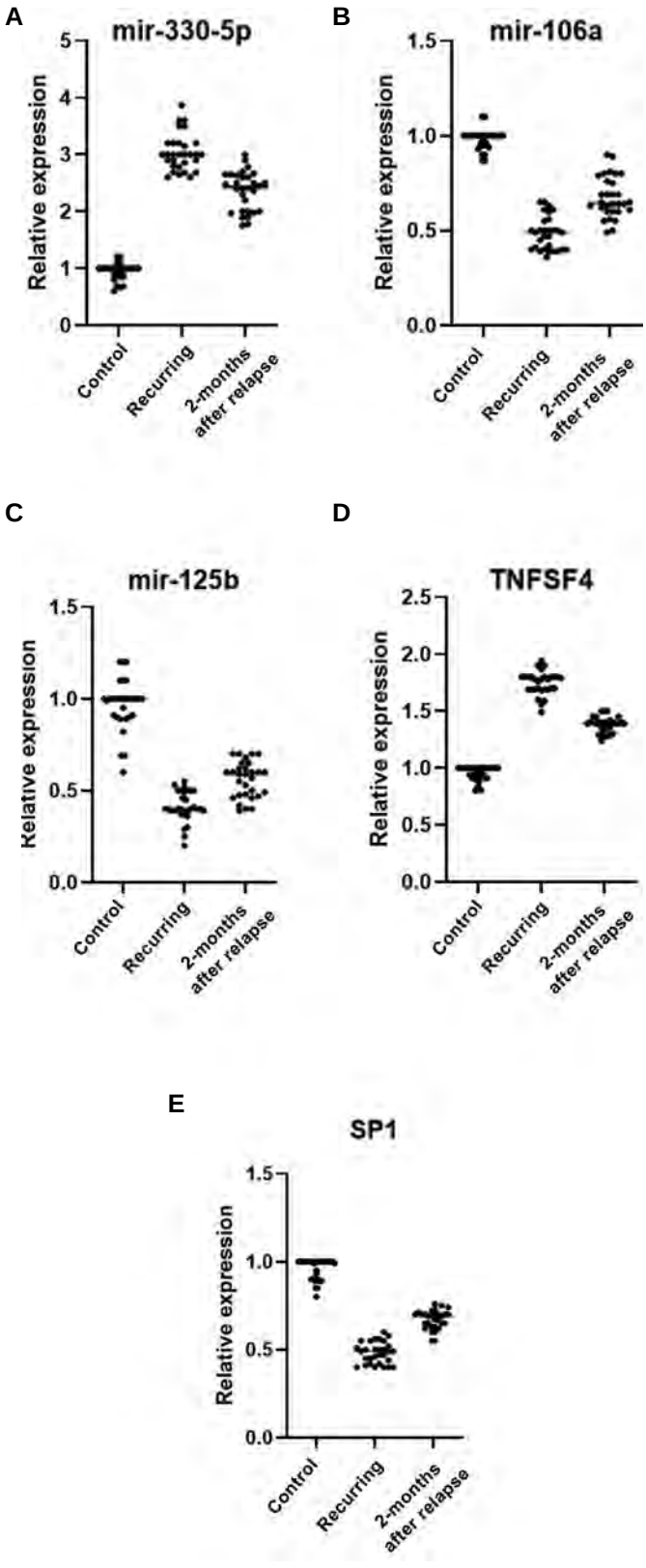


**Fig.3:** Quantitative real-time polymerase chain reaction (PCR) analysis results. **A.** Relative expression of *miR-330-5p,* **B.** *miR-106a,* and **C.** *miR-125b* in recurring patients and two months after relapse patients and healthy individuals. Relative quantification for the *miR-330-5p* (P<0.0001 and 0.0002, respectively), *miR*-106a (P<0.0001 and P<0.006, respectively) and *miR-125b* (P<0.0001 and P<0.0005, respectively) and **D.** *TNFSF4* (P<0.004 and P<0.02, respectively), and **E.** *SP1* (P<0.0017 and P<0.003, respectively) were significantly different between patients and the control group. All Data were presented as mean ± SD (n=30 per group). Data were calculated using a one-way analysis of variance (ANOVA) and Tukey's post hoc test.

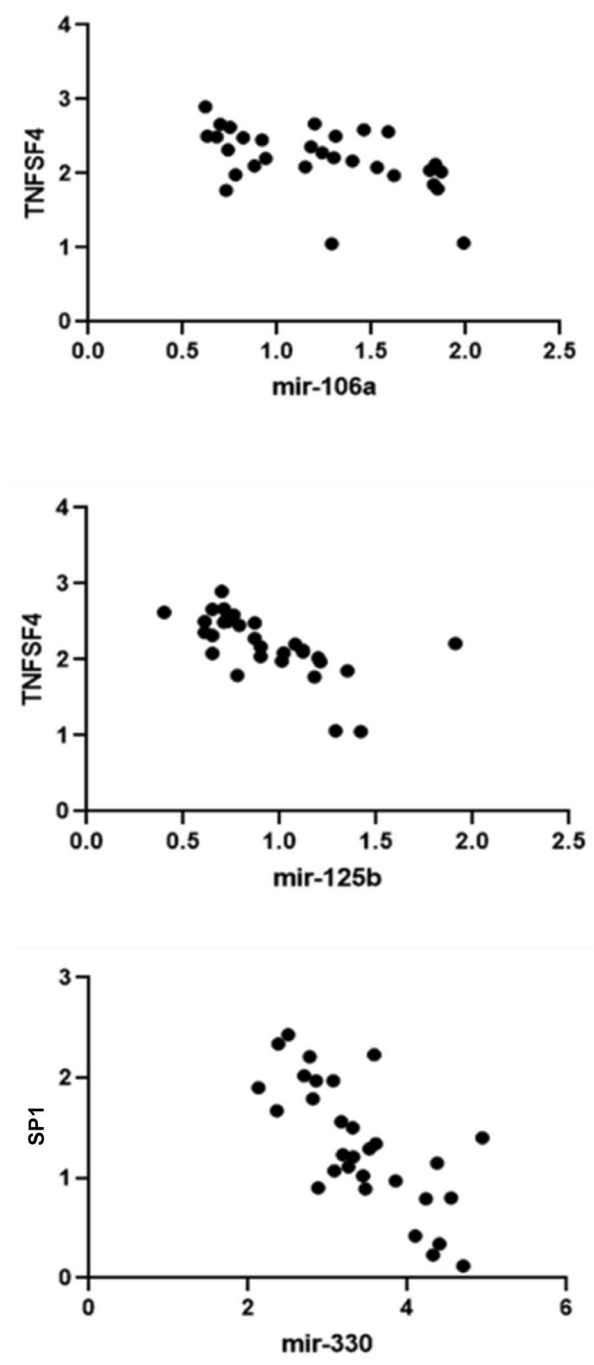


**Fig.4:** Graphs plotted from the Pearson correlation analysis showed a significant relationship between microRNAs and their targets. This correlation between genes and their targets is inverse. The Pearson correlation for associating miR-106 and *TNFSF4* was equal to -0.497 and P<0.0052 and miR-125b with *TNFSF4* was equal to -0.6284 and P<0.0002. The Pearson correlation for miR-330 and *SP1* was -0.7280, with a P<0.0001. All data were presented as mean ± SD (n=30 per group).

## Discussion

MS's clinical pathophysiology is diverse to the extent that despite the accessibility of therapeutics for the relapsing type of MS, patients have clinical disease activity and neurologic inability within months after disease onset. Due to the need for more effective treatments, biomarkers recruited for predicting inability and therapeutic response assessment are desirable in managing patients (28). In MS, dysregulation of miRNAs has been indicated in various immune cells. Immense evidence has demonstrated changes in miRNA expression in immune cells and brain tissue of MS patients. Therefore, we explored the correlation between MS progression and the expression of miRNAs (29).

In this study, the correlation of three miRNAs, such as miR-125b, miR-330-5p, and miR-106a expression with MS disease, was investigated. We indicated significantly higher expression of miR-330-5p in both RRMS groups than in healthy subjects. In contrast, a decrease was revealed in the miR-125b and miR-106a expression in RRMS patients. According to the Choi et al. (30) study, the expression of miR-330 increased during brain development and NSC (Neural stem cells) differentiation. In a miRNA microarray analysis, it was indicated that miR-106a was significantly reduced in MS patients (31). It has been proposed that the down-regulated miR-125b expression could serve as a helpful noninvasive biomarker for Alzheimer's disease (32). We investigated these three miRNAs' potential roles via in-silico molecular enrichment analysis, and we found a correlation between miRNA and gene roles in biological processes involved in MS pathology. Notably, we indicated that miR-330-5p, miR-106a, and miR-125b were directly associated with the inflammation pathway. These data are supported our hypothesis that there is a correlation between miR-106a, miR-125b, and miR-330 in MSpatients by targeting TNFSF4 and *SP1* in NF-κb/TNF-α pathway.

The regulation of immune system responses to nerve cell myelin sheaths is a fundamental matter in MS development. TNF-α/NF-κB signaling pathway has a crucial role in autoimmune responses regulated by various factors, and Sonar et al. indicated an association between TNFSF and autoimmune disease (33, 34).

Another gene examined in this study is a transcription factor called SP1, which was predicted to be targeted by miR-330 (21). SP1 is a transcription factor regulated by the TNF-α/ NF-κB signaling pathway. This transcription factor is activated after binding to the GC-box at NF-κB binding sites. We found an association between SP1 and miR-106a, miR-125b, and miR-330 in MS based on the bioinformatic analysis. Moreover, in-silico data have demonstrated that SP1 could target the NF-κb/ TNF-α pathway. Based on the evidence, NF-κb decreases through increasing miR-330 expression and subsequently with reduced expression of SP1. Contrariwise, it can increase apoptosis in autoimmune diseases such as MS and deteriorate the symptoms. Mao et al. (21) confirmed that miR-330 was downregulated and inversely associated with SP1 expression. Also, they induced miR-330 expression by transfection of miR-330 mimic, and the outcome was a reduction in expression levels of the *SP1* gene, but the results of SP1-knockdown were contrary to previous. Based on their research, miR-330 could target SP1 directly (14, 15).

Recently, primary MS therapies have been based on the

inhibition of the TNF-α/ NF-κB signaling pathway. Thus, tumor factor α-necrosis factor (α) blockers are a treatment of interest in many inflammatory and autoimmune diseases (35). This therapeutic target can control the demyelination of nerve cells in MS and its recurrence. Therefore, regulatory inhibiting factors such as miR-330 might be acceptable candidates. However, miR-106a and miR-125b are inhibitory candidates for treating MS and other autoimmune conditions.

## Conclusion

Our findings illustrated that low miR-106a and miR-125b expression contributes to high TNFSF4 expression, whereas increased miR-330 expression activates the TNF-α signaling pathway by targeting and reducing the *SP1* gene expression. Subsequently, the activated TNF-α signaling pathway may lead to the initiation and progression of autoimmune diseases such as MS.

## Acknowledgments

There is no financial support and conflict of interest in this study.

## Authors' Contributions

N.H., S.M.S.; Contributed to the conception and design. N.H., F.Kh., F.N., B.N.; Contributed to all experimental work and molecular experiments. F.Kh., P.R.; Contributed to the conception, and design of the database and bioinformatic analysis, statistical analysis, and data interpretation. N.H.; Drafted the manuscript, which was revised by M.S.V.Sh., M.F.F.; Resources and methodology. M.S.; Conceptualization, validation, visualization, and supervision. All authors read and approved the final manuscript.

## References

1. Lassmann H. Multiple sclerosis pathology. Cold Spring Harb Perspect Med. 2018; 8(3): a028936.
2. Montalban X, Hauser SL, Kappos L, Arnold DL, Bar-Or A, Comi G, et al. Ocrelizumab versus placebo in primary progressive multiple sclerosis. N Engl J Med. 2017; 376(3): 209-220.
3. Goldenberg MM. Multiple sclerosis review. P T. 2012; 37(3): 175-84.
4. Stangel M, Penner IK, Kallmann BA, Lukas C, Kieseier BC. Towards the implementation of 'no evidence of disease activity' in multiple sclerosis treatment: the multiple sclerosis decision model. Ther Adv Neurol Disord. 2015; 8(1): 3-13.
5. Patsopoulos NA. Genetics of multiple sclerosis: an overview and new directions. Cold Spring Harb Perspect Med. 2018; 8(7): a028951.
6. Kahl KG, Kruse N, Faller H, Weiss H, Rieckmann P. Expression of tumor necrosis factor-alpha and interferon-gamma mRNA in blood cells correlates with depression scores during an acute attack in patients with multiple sclerosis. Psychoneuroendocrinology. 2002; 27(6): 671-681.
7. Ribeiro CM, Oliveira SR, Alfieri DF, Flauzino T, Kaimen-Maciel DR, Simão ANC, et al. Tumor necrosis factor alpha (TNF-α) and its soluble receptors are associated with disability, disability progression and clinical forms of multiple sclerosis. Inflamm Res. 2019; 68(12): 1049-1059.
8. Fiedler SE, George JD, Love HN, Kim E, Spain R, Bourdette D, et al. Analysis of IL-6, IL-1β and TNF-α production in monocytes isolated from multiple sclerosis patients treated with disease modifying drugs. J Syst Integr Neurosci. 2017; 3(3): 10.
9. Yang G, Parkhurst CN, Hayes S, Gan WB. Peripheral elevation of TNF-α leads to early synaptic abnormalities in the mouse somatosensory cortex in experimental autoimmune encephalomyelitis. Proc Natl Acad Sci USA. 2013; 110(25): 10306-10311.
10. Dong Y, Dekens DW, De Deyn PP, NaudéPJW, Eisel ULM. Targeting of tumor necrosis factor alpha receptors as a therapeutic strategy for neurodegenerative disorders. Antibodies. 2015; 4(4): 369-408.
11. An J, Ding S, Hu X, Sun L, Gu Y, Xu Y, et al. Preparation, characterization and application of anti-human OX40 ligand (OX40L) monoclonal antibodies and establishment of a sandwich ELISA for autoimmune diseases detection. Int Immunopharmacol. 2019; 67: 260-267.
12. van Wanrooij EJ, van Puijvelde GH, de Vos P, Yagita H, van Berkel TJ, Kuiper J. Interruption of the Tnfrsf4/Tnfsf4 (OX40/OX40L) pathway attenuates atherogenesis in low-density lipoprotein receptor-deficient mice. Arterioscler Thromb Vasc Biol. 2007; 27(1): 204-210.
13. Takahashi Y, Tanaka R, Yamamoto N, Tanaka Y. Enhancement of OX40-induced apoptosis by TNF coactivation in OX40-expressing T cell lines in vitro leading to decreased targets for HIV type 1 production. AIDS Res Hum Retroviruses. 2008; 24(3): 423-435.
14. Ping D, Boekhoudt G, Zhang F, Morris A, Philipsen S, Warren ST, et al. Sp1 binding is critical for promoter assembly and activation of the MCP-1 gene by tumor necrosis factor. J Biol Chem. 2000; 275(3): 1708-1714.
15. Hirano F, Tanaka H, Hirano Y, Hiramoto M, Handa H, Makino I, et al. Functional interference of Sp1 and NF-kappaB through the same DNA binding site. Mol Cell Biol. 1998; 18(3): 1266-1274.
16. Shende VR, Kim SM, Neuendorff N, Earnest DJ. MicroRNAs function as cis- and trans-acting modulators of peripheral circadian clocks. FEBS Lett. 2014; 588(17): 3015-3022.
17. Tufekci KU, Oner MG, Genc S, Genc K. MicroRNAs and multiple sclerosis. Autoimmune Diseases. 2011; 807426.
18. Honardoost MA, Naghavian R, Ahmadinejad F, Hosseini A, Ghaedi K. Integrative computational mRNA-miRNA interaction analyses of the autoimmune-deregulated miRNAs and well-known Th17 differentiation regulators: An attempt to discover new potential miRNAs involved in Th17 differentiation. Gene. 2015; 572(2): 153-162.
19. Sanctuary MR, Huang RH, Jones AA, Luck ME, Aherne CM, Jedlicka P, et al. miR-106a deficiency attenuates inflammation in murine IBD models. Mucosal Immunol. 2019; 12(1): 200-211.
20. Kim BK, Yoo HI, Choi K, Yoon SK. miR-330-5p inhibits proliferation and migration of keratinocytes by targeting Pdia3 expression. FEBS J. 2015; 282(24): 4692-4702.
21. Mao Y, Chen H, Lin Y, Xu X, Hu Z, Zhu Y, et al. microRNA-330 inhibits cell motility by downregulating Sp1 in prostate cancer cells. Oncol Rep. 2013; 30(1): 327-333.
22. Sticht C, De La Torre C, Parveen A, Gretz N. miRWalk: An online resource for prediction of microRNA binding sites. PLoS One. 2018; 13(10): e0206239.
23. Piñero J, Ramírez-Anguita JM, Saüch-Pitarch J, Ronzano F, Centeno E, Sanz F, et al. The DisGeNET knowledge platform for disease genomics: 2019 update. Nucleic Acids Res. 2020; 48(D1): D845-D855.
24. Jassal B, Matthews L, Viteri G, Gong C, Lorente P, Fabregat A, et al. The reactome pathway knowledgebase. Nucleic Acids Res. 2020; 48(D1): D498-D503.
25. Shannon P, Markiel A, Ozier O, Baliga NS, Wang JT, Ramage D, et al. Cytoscape: a software environment for integrated models of biomolecular interaction networks. Genome Res. 2003; 13(11): 2498-2504.
26. Lu Q. The critical importance of epigenetics in autoimmunity. J Autoimmun. 2013; 41: 1-5.
27. Fathullahzadeh S, Mirzaei H, Honardoost MA, Sahebkar A, Salehi M. Circulating microRNA-192 as a diagnostic biomarker in human chronic lymphocytic leukemia. Cancer Gene Ther. 2016; 23(10): 327-332.
28. Hauser SL, Bar-Or A, Comi G, Giovannoni G, Hartung HP, Hemmer B, et al. Ocrelizumab versus interferon beta-1a in relapsing multiple sclerosis. N Engl J Med. 2017; 376(3): 221-234.
29. Regev K, Healy BC, Khalid F, Paul A, Chu R, Tauhid S, et al.

Association between serum microrna and magnetic resonance imaging measures of multiple sclerosis severity. JAMA Neurol. 2017; 74(3): 275-285.
30. Choi I, Woo JH, Jou I, Joe EH. PINK1 deficiency decreases expression levels of mir-326, mir-330, and mir-3099 during brain development and neural stem cell differentiation. Exp Neurobiol. 2016; 25(1): 14-23.
31. Cox MB, Cairns MJ, Gandhi KS, Carroll AP, Moscovis S, Stewart GJ, et al. MicroRNAs miR-17 and miR-20a inhibit T cell activation genes and are under-expressed in MS whole blood. PLoS One. 2010; 5(8): e12132.
32. Tan L, Yu JT, Liu QY, Tan MS, Zhang W, Hu N, et al. Circulating miR-125b as a biomarker of Alzheimer's disease. J Neurol Sci. 2014; 336(1-2): 52-56.
33. Sicotte NL, Voskuhl RR. Onset of multiple sclerosis associated with anti-TNF therapy. Neurology. 2001; 57(10): 1885-1888.
34. Sonar S, Lal G. Role of tumor necrosis factor superfamily in neuroinflammation and autoimmunity. Front Immunol. 2015; 6: 364.
35. Kemanetzoglou E, Andreadou E. CNS demyelination with TNF-α blockers. Curr Neurol Neurosci Rep. 2017; 17(4): 36.

Original Article

# *TGFß* Gene Members and Their Regulatory Factors in Granulosa Compared to Cumulus Cells in PCOS: A Case-Control Study

**Faezeh Alvandian, M.Sc.[1, 2, 3], Elham Hosseini, Ph.D.[4, 5], Zohre Hashemian, M.Sc.[2], Mona Khosravifar, M.Sc.[2], Bahar Movaghar, Ph.D.[6], Maryam Shahhoseini, Ph.D.[2, 7, 8], Marzieh Shiva, M.D.[9]*, Parvaneh Afsharian, Ph.D.[1, 2]***

**1. Faculty of Sciences and Advanced Technologies in Biology, University of Science and Culture, Tehran, Iran**
**2. Department of Genetics, Reproductive Biomedicine Research Center, Royan Institute for Reproductive Biomedicine, ACECR, Tehran, Iran**
**3. Deputy of Research and Technology, Hamadam University of Medical Sciences, Hamadan, Iran**
**4. Department of Obstetrics and Gynecology, Mousavi Hospital, School of Medicine, Zanjan University of Medical Sciences, Zanjan, Iran**
**5. Zanjan Metabolic Diseases Research Center, Zanjan University of Medical Sciences, Zanjan, Iran**
**6. Department of Embryology, Reproductive Biomedicine Research Center, Royan Institute for Reproductive Biomedicine, ACECR, Tehran, Iran**
**7. Reproductive Epidemiology Research Center, Royan Institute for Reproductive Biomedicine, ACECR, Tehran, Iran**
**8. Department of Cell and Molecular Biology, School of Biology, College of Science, University of Tehran, Tehran, Iran**
**9. Department of Endocrinology and Female Infertility, Reproductive Biomedicine Research Center, Royan Institute for Reproductive Biomedicine, ACECR, Tehran, Iran**

***Corresponding Address: P.O.Box: 16635-148, Department of Endocrinology and Female Infertility, Reproductive Biomedicine Research Center, Royan Institute for Reproductive Biomedicine, ACECR, Tehran, Iran***
***Department of Genetics, Reproductive Biomedicine Research Center, Royan Institute for Reproductive Biomedicine, ACECR, Tehran, Iran***
***Emails: m.shiva@royan-rc.ac.ir, p.afsharian@royan-rc.ac.ir***

**Received: 20/April/2021, Accepted: 23/August/2021**

Abstract

**Objective:** Transforming growth factor-beta (TGF-β) superfamily and its members that include bone morphogenetic protein 15 (BMP15), anti-Mullerian hormone (AMH), growth /differentiation factor-9 (GDF9), and their respective receptors: BMPR1A, BMPR1B, and BMPR2 have been implicated as key regulators in various aspects of ovarian function. The abnormal function of the ovaries is one of the main contributing factors to polycystic ovarian syndrome (PCOS), so this study aimed to investigate the mRNA expression profile of these factors in granulosa (GCs) and cumulus cells (CCs) of those patients.

**Materials and Methods:** The case-control research was conducted on 30 women (15 infertile PCOS and 15 normo-ovulatory patients, 22≤age ≤38 years old) who underwent ovarian stimulation for *in vitro* fertilization (IVF)/ intracytoplasmic sperm injection (ICSI) cycle. GCs/CCs were obtained during ovarian puncture. The expression analysis of the aforementioned genes was quantified using real-time polymerase chain reaction (PCR).

**Results:** *AMH* and *BMPR1A* expression levels were significantly increased in GCs of PCOS compared to the control group. In contrast, *GDF9, BMP15, BMPR1B,* and *BMPR2* expressions were decreased. PCOS' CC showed the same expression patterns. *GDF9* and *AMH* were effectively expressed in normal CCs, and *BMP15* and *BMPR1B* in normal GCs (P<0.05).

**Conclusion:** Differential gene expression levels of *AMH* and its regulatory factors and their primary receptors were detected in granulosa and cumulus cells in PCOS women. Since the same antagonist protocol for ovarian stimulation was used in both PCOS and control groups, the results were independent of the protocols. This diversity in gene expression pattern may contribute to downstream pathways alteration of these genes, which are involved in oocyte competence and maturation.

***Keywords:*** Cumulus Cell, Granulosa Cell, Polycystic Ovarian Syndrome, TGF-Beta Superfamily

Cell Journal(Yakhteh), Vol 24, No 7, July 2022, Pages: 410-416

**Citation:** **Alvandian F, Hosseini E, Hashemian Z, Khosravifar M, Shiva M, Movaghar B, Shahhoseini M, Afsharian P. TGFβ gene members and their regulatory factors in granulosa compared to cumulus cells in PCOS: a case-control study. Cell J. 2022; 24(7): 410-416. doi: 10.22074/cellj.2022.8051.**
**This open-access article has been published under the terms of the Creative Commons Attribution Non-Commercial 3.0 (CC BY-NC 3.0).**

## Introduction

Polycystic ovary syndrome (PCOS), one of the most common causes of an-ovulatory, is a heterogeneous endocrine disorder in infertile women, affecting up to 6-20% of women of reproductive age (1).

PCOS is confirmed by existing at least two of three special features based on the Rotterdam criteria: clinical/ biochemical evidence of hyperandrogenism, oligomenorrhea/ anovulation, and polycystic ovaries (2). A wide variety of genetic alterations in differential tissues and cell types impact normal follicular development in this syndrome. Imbalanced follicle-stimulating hormone (FSH), luteinizing hormone (LH), and some key factors that are involved in the inappropriate progression of folliculogenesis are the main molecular features associated with impaired and arrested development of the germinal vesicle stage of oocytes toward the dominant and mature follicles in polycystic ovaries (3, 4).

The delicate communication process between different types of cells in the mammalian follicles, namely oocyte and its surrounding somatic cells, granulosa (GCs), and cumulus cells (CCs), has a pivotal impact on the oogenesis process, oocyte maturation, cumulus expansion, and ovulation (5, 6). Paracrine signals of the oocyte are the potent stimulators in GCs/CCs, which regulate the above physiological processes and consequently affect female fertility (7).

Among the secreted factors by the oocyte or follicle somatic cells, transforming growth factor-beta (TGF-β) superfamily and its members, including anti-mullerian hormone (*AMH*), growth and differentiation factor 9 (*GDF9*), and bone morphogenetic protein 15 (*BMP15*) which are expressed in follicular stage-related manner, have been implicated as key regulators in various aspects of intra-ovarian development (8). On the other hand, alteration in expression of these factors, especially *AMH*, is related to pathological ovarian conditions, such as PCOS and Endometriosis (9).

AMH is now a quantitative marker of ovarian reserve as well as a diagnostic factor for PCOS (10). TGF-β family members bind to their receptors in GCs/CCs which induces a cascade of several downstream protein-coding genes. Even though GCs are differentiated into CCs and both of them have a common progenitor during folliculogenesis, the mentioned genes show different expression and even regulation patterns in those specialized cell types (11, 12).

Based on previous studies, alterations in the gene expression pattern of granulosa-cumulus cells play a definite role in the impaired final maturation of antral follicles to later-stage growth, which is one of the main contributing factors and underlying causes of polycystic ovaries (13).

AMH is secreted from ovarian cells in the growing follicles and can regulate the FSH-dependent follicle development. Previous studies showed that the expression and secretion of AMH from granulosa-cumulus cells are increased in preovulatory follicles, which contain atretic oocytes (14, 15).

GDF-9 and BMP-15, as other members of the TGF-β superfamily, are known as growth promoters during normal folliculogenesis (16). A study of intraovarian interactions, regulatory mechanisms, and possible abnormalities which interfere with the balance between these molecular factors in patients suffering PCOS compared to women with normal oogenesis can provide a better overview of controlling and monitoring ovarian function that may be resulted in improving the fertility of such patients.

This study aimed to investigate the mRNA expression profile of *BMP15, GDF9, AMH* genes, and their respective receptors, which include: *BMPR1A*, *BMPR1B*, and *BMPR2*, in GCs and CCs of PCOS patients, compared to women with normal oogenesis undergoing controlled ovarian stimulation (COS) treatment cycles.

## Materials and Methods

The case-control research was endorsed by the Royan Institute Ethics Boards (IR.ACECR.ROYAN.REC.1394.86). Thirty patients (15 PCOS patients with infertility and 15 normo-ovulatory patients, 22≤age≤38 years old) were recruited to the study between November 2014 and April 2016 who underwent COS for IVF/ICSI at the Infertility Clinic (Royan Institute, Iran). Informed consent were obtained from all subjects.

Patients who met the following criteria were included in the control group: absence of clinical/ biochemical signs of hyperandrogenism or other endocrine diseases, polycystic ovaries, diabetes, with regular menstrual cycles (26<cycle length<32), having normal hormone profile (TSH, FSH, and LH). All controls were undergoing ovarian stimulation treatment due to their tubal factor infertility.

Rotterdam diagnostic criteria are routinely used for PCOS phenotyping which includes: chronic oligo and/ or anovulation (<26 or >35 days of cycle length), biochemical or clinical evidence of hyperandrogenism (total testosterone concentration >0.5 ng/ml, hirsutism, acne, and alopecia), and the presence of 12 or more ovarian cysts with 2-10 mm diameter per cyst and/or ovarian volume ≥10 $cm^3$ on ultrasound (polycystic ovaries).

Inclusion criteria for all women (PCOS and control) were including the first IVF/ICSI cycle, ovarian stimulation by antagonist protocol, 22≤age≤38 years, and body mass index (BMI) of 18-28 $kg/m^2$. The severe male factor, including oligo-astheno-teratozoospermia, retrieved sperm from testis, and semen freeze was excluded. The semen was analyzed in accordance with the criteria of the $5^{th}$ edition of the World Health Organization (WHO) in 2010.

All hormone tests (FSH and LH levels) were carried out on days 2 to 3 of the menstrual cycle using electro-chemiluminescence immunoassay kits (ECLIA kits, Roche Diagnostics GmbH, Germany). Further evaluation of total testosterone concentrations in PCOS patients was performed by using ELISA kits (Monobind Inc., USA), and serum AMH levels were assessed using an electro-chemiluminescence immunoassay by Elecsys® and Cobas Immunoassay Analyzers (Roche GmbH).

### Control ovarian stimulation protocol

Down-regulation of the pituitary gland with GnRH antagonist protocol [the administration of 75–150 IU recombinant FSH (Gonal F; Merck Serono, or Puregon; MSD, the Netherlands)] was done for all women up to the day of human chorionic gonadotropin (hCG, Ovitrelle®, Merck-Serono) injection. The COS was performed considering the age of the women and the antral follicle count (AFC).

### Granulosa and cumulus cells isolation

The following steps were taken to isolate the follicular fluid and extract cumulus and granulosa cells from collected cumulus-oocyte complex (COC) as described previously (17, 18). Briefly, follicular fluid (FF) was obtained after hCG injection (34-36 hours) during ovarian puncture. COCs were collected from FF and repeatedly washed in culture medium G1V5™ (Vitrolife AB, Sweden), then incubated at 37°C and 5% $CO_2$. Just before ICSI, the COC was denuded with hyaluronidase enzyme, then CCs washed in free enzyme medium, and cold phosphate buffered saline (PBS), then the cells were pelleted by centrifugation twice for 8 minutes at 3000

rpm; the pellet was snap-frozen in liquid nitrogen then stored at -80°C (17).

After retrieval of COCs, aspirated FF was centrifuged for 10 minutes at 2000 rpm. The clear supernatant (without blood) was isolated, the pellet was solved in Tyrode's solution, and the suspension was added on Sill select gradient and centrifuged at 3000 rpm for 13 minutes. Granulosa cells (The layer formed between Sill select gradient and supernatant) were removed and washed with 3 ml of DMEM / HamF12 medium 10%. In the next step, the suspensions were centrifuged at 3000 rpm for 13 minutes. Afterward, the diluted hyaluronidase enzyme was added, and the suspension was incubated for 3 minutes; a culture medium was added to neutralize the effect of the enzyme, then the suspension was centrifuged for 5 minutes at 1500 rpm; Red blood cell lysing buffer was added to the cell suspension and incubated for 5 minutes, the solution was removed; granulosa cells were taken for extraction of RNA.

### RNA extraction, cDNA synthesis, and reverse transcription-polymerase chain reaction (RT-PCR)

Total RNA was extracted, then purified by removing DNA genomic from the samples using the RNeasy Micro Kit (Qiagen, cat. no: 74004) as per the ' 'manufacturer's protocol which is also previously described (18).

After assessment of RNA quantity and quality by using the NanoDrop spectrophotometer (NanoDrop 2000 spectrophotometer), cDNA was synthesized using 20 nanograms of total RNA according to QuantiTect Whole Transcriptome Kit (Qiagen, Cat.No:207045) instruction and stored at -20°C until molecular analysis.

For granulosa cells' RNA extraction, TRIzol Reagent (Sigma-Aldrich) was used following the ' 'manufacturer's protocol. Genomic DNA contaminations were removed from all extracted RNA samples by treating them by DNaseI (Fermentas, Thermo Scientific, Germany). DNase I enzyme was inactivated by incubation for 7 minutes at 65°C with EDTA (50 mM, Fermentas, Germany). The purity of RNA was detected by NanoDrop spectrophotometer to determine A260/A280 ratio. RNA (1 μg) was reverse transcribed to cDNA using first-strand cDNA synthesis kit (K1632- Fermentas, Thermo Scientific, Germany) instruction, then stored at -20°C until molecular analysis.

### Quantitative real time-polymerase chain reaction

A quantitative mRNA analysis was performed using the Step-One RT-PCR system for doing qRT-PCR (Applied Biosystems, USA). All reactions were run in duplicate. Evaluation of mRNA gene expression of *GDF9*, *BMP15*, *AMH*, *BMPR1A*, *BMPR1B*, *BMPR2* between the patient and control groups was done by calculation of $\Delta C_t$ and $2^{-\Delta Ct}$. To perform this analysis, cDNAs were synthesized from granulosa and cumulus cells of patients and healthy individuals. The qPCR was performed with human-specific primers. The product size and primer sets are listed in Table 1. *GAPDH* primer was used as a control gene expression. PCR products were visualized using Gel Red ZellBio, Germany) staining and electrophoreses (1.7%-2% agarose, Paya pazhoh pars, Iran) under UV light by Molecular Imager® Gel Doc™ XR+ (BioRad, USA).

**Table 1:** Sequence of the primers used for quantitative polymerase chain reaction (qPCR) experiments

| Gene | Primer sequence (5′→3′) | Annealing temperature (°C) | Size (bp) |
|---|---|---|---|
| *GDF9* | F: AGAAGTCACCTCTACAACACTG<br>R: AACGGTAGTAATGCGATCCA | 60 | 132 |
| *BMP15* | TGTGAACTCGTGCTTTTCATG<br>R: CTCAATCAGGGGCAAAGTAGG | 60 | 102 |
| *AMH* | AAGCTGCTCATCAGCCT<br>R: TGCTTGCTGGTCTTTATTGG | 60 | 194 |
| *BMPR1A* | GAACTATTGCCAAACAGATTCAGA<br>R: TGCCGCTATGAAACCAAGTAT | 60 | 200 |
| *BMPR1B* | ATTTGCAGCACAGACGGATATTGTT<br>R: GAGGCAGTGTAGGGTGTAGGTCTT | 60 | 199 |
| *BMPR2* | TGCCGCTATGAAACCAAGTAT<br>R: GACTCACCTATCTGTATACTGCT | 60 | 184 |
| *GAPDH* | AGAAGGCTGGGGCTCATTTG<br>R: TGATGGCATGGACTGTGGT | 60 | 228 |

### Statistical analysis

Data obtained were analyzed using the Independent Samples t test, using IBM SPSS software version 22. The one-sample Kolmogorov-Smirnov (K-S) test was used to determine whether the variables come from the normal distribution in each group. Data are presented as mean ± SD at the level of P<0.05.

## Results

### Demographic information

Table 2 presents all the demographic data. Age, BMI, and duration of infertility were similar between the PCOS and control groups (P>0.05). However, there were significant differences among them considering the main PCOS features and characteristics, such as the ratio of LH/FSH, LH and AMH levels (Table 2). The PCOS subjects showed higher LH level than normo-ovulatory females (control group) (P<0.01).

### The expression level of *GDF9, BMP15, AMH* and their receptors in GCs and CCs from PCOS women compared to non-PCOS women

As shown in Figure 1, all amplified RT-PCR products were at the expected size for *GDF9, BMP15, AMH, BMPR1B, BMPR1A,* and *BMPR2* genes.

In GCs isolated from PCOS subjects, an overexpression of *AMH* (P<0.001) and *BMPR1A* (P<0.001) was observed. In contrast, the level of *GDF9* (P>0.001), *BMP15*, *BMPR1B*, and *BMPR2* gene expression were significantly decreased (P<0.001, Fig.2A).

On the other hand, CCs from PCOS patients display the same patterns as observed in GCs genes expression increased expression of *AMH* (P<0.001) and *BMPR1A* (P<0.038); decreased expression of *GDF9* (P<0.001), *BMP15* (P=0.005), *BMPR1B* (P<0.004), and *BMPR2* (P<0.001) mRNA significantly (Fig.2B).

**Table 2:** Demographic information

| Parameters | PCOS group | Control group | P value |
|---|---|---|---|
| Age (Y) | 28.87 ± 6.5 | 28.87 ± 6.5 | 0.9 |
| BMI (kg/m$^2$) | 24.5 ± 4.5 | 25.82 ± 4.5 | 0.2 |
| Infertility duration (Y) | 2.5-10 | 3-15 | 0.6 |
| Number of oocyte | 11.5 ± 4.5 | 8 ± 3 | 0.7 |
| AMH (ng/µl) | 12.43 ± 5.9* | 4.7 ± 2.9 | 0.0001 |
| FSH (IU/I) | 6.71 ± 3.3 | 6.42 ± 3.15 | 0.6 |
| LH (IU/I) | 14.35 ± 11.55* | 3.85 ± 3.35 | 0.01 |
| TSH (IU/I) | 2.23 ± 1.65 | 2.45 ± 2.15 | 0.5 |

The results are reported as mean ± SD. AMH; Anti-mullerian hormone, BMI; Body mass index, FSH; Follicle-stimulating hormone, TSH; Thyroid stimulating hormone, and *; P<0.05.

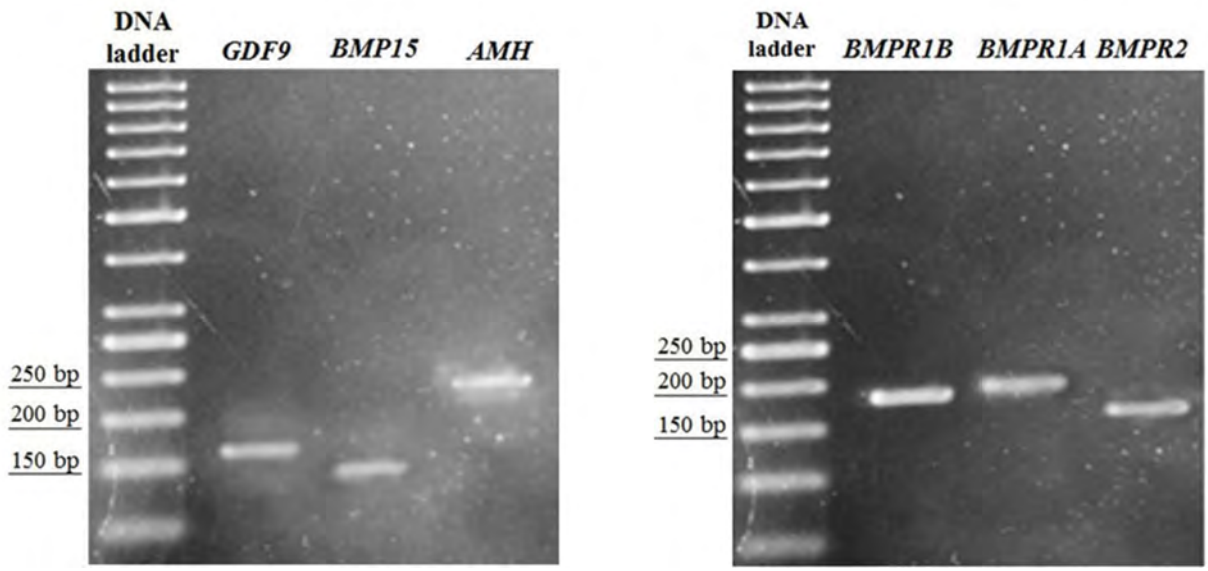


**Fig.1:** Results of RT-PCR for mRNA expression of *GDF9, BMP15, AMH, BMPR1B, BMPR1A,* and *BMPR2* genes (DNA ladder 50 base pair). RT-PCR; Reverse transcription polymerase chain reaction.

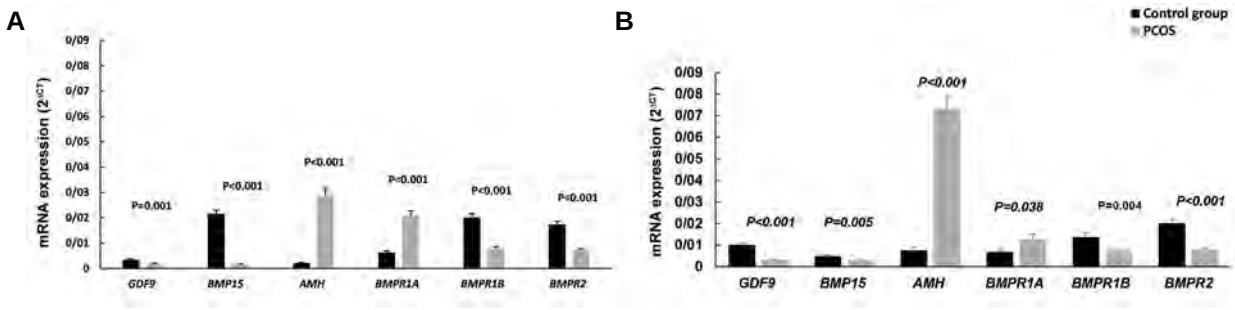


**Fig.2:** Expression level of *GDF9*, *BMP15*, *AMH* and their receptors in polycystic ovarian syndrome (PCOS) women and control group. **A.** Gene expression of granulosa cell from PCOS women compared to control group. **B.** Gene expression of cumulus cells from PCOS women compared to control group.

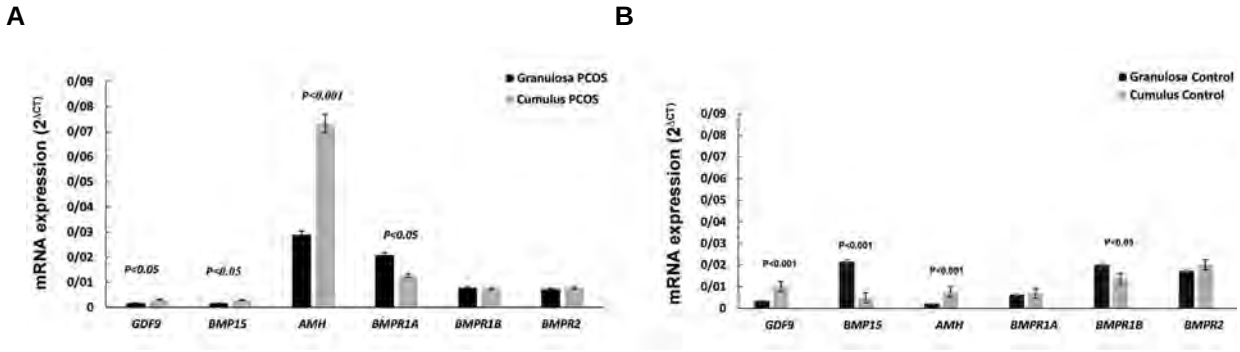


**Fig.3:** Differential gene expression profile in granulosa compared to cumulus cells. **A.** Gene expression profile in granulosa cells compared to cumulus cells in polycystic ovarian syndrome (PCOS) group. **B.** Gene expression profile in granulosa cells compared to cumulus cells in control groups.

### Differential gene expression profile in GCs compared to CCs in control and PCOS women

Comparing CCs and GCs from PCOS patients revealed GDF9, BMP15 ($P<0.05$) and AMH ($P<0.001$) have higher expression in cumulus cells; in contrast, BMPR1A ($P<0.05$) expression level is higher in GCs of such patients (Fig.3A). On the other hand, BMP15 ($P<0.001$) and BMPR1B ($P<0.03$) are effeΔively expressed in normal granulosa cells compared to normal CCs, and AMH ($P<0.001$) and GDF9 ($P<0.001$) have higher mRNA expression in CCs of control than PCOS patients (Fig.3B).

## Discussion

The differential gene expression levels of *AMH* and its regulatory factors that include *BMP15* and *GDF9*, as well as their primary receptors: *BMPR2*, *BMPR1B*, and *BMPR1A*, were detected in granulosa and cumulus cells in PCOS women compared to the control group. In addition, these genes showed different expression patterns in two ovarian cells (GCs and CCs).

Granulosa cells show phenotypic heterogeneity in the developing ovarian Follicle. During folliculogenesis, the heterogeneous GC populations differentiate and divide into mural GCs and CCs. Their function is associated with their position in the follicles and proximity to the oocyte resulting in different properties and gene expression patterns (19, 20). The mural GCs have a great steroidogenic function, a high level of LH receptors, and mainly are involved in the acquisition of signals from outside Follicle; however, the cumulus cells provide essential regulatory factors for oocytes to promote final cytoplasmic and nuclear maturation (21, 22).

The resumption of oocyte meiosis is regulated by activating some genes in the oocyte itself and a broad signaling network in other follicular cells (23). The increased expression of *BMP15* and *BMPR1B* receptors in the periovulatory phase of ovarian cells showed their implication in the ovulatory process. On the other hand, these BMP proteins, the largest subfamily belonging to the TGFβ superfamily, regulate numerous main biological processes in the ovarian follicle, including cell differentiation, proliferation, and apoptosis (24). Also, the expression of *BMPR1B* is correlated with serum oestradiol (E2) level in normal folliculogenesis (25). Alterations in BMPs signaling are involved in some folliculogenesis disorders such as PCOS (24). In *Bmp15* knockout mice, uni- and bi-lateral cysts developed, ovulation rate was decreased and female mice were subfertile due to reduced developmental potential of oocytes and ovulation (26). The reduced expression of this ligand and its receptor in

PCOS patients, as shown in the present study, has revealed the association mechanism of PCOS-related anovulation and impaired oocyte competency and maturation.

The study performed by Kedem-Dickman et al. (27) showed a reverse association between GC -cumulus *AMH* expression and oocyte maturity in preovulatory follicles. It means that corresponding GC-cumulus cells of the Germinal Vesicle oocyte stage express higher AMH mRNA levels than the Metaphase stage ones. They suggested that AMH meiosis inhibition, which had been confirmed previously (28), was the mechanism by which the oocytes may fail to resume meiosis.

Some recent studies showed that high levels of AMH decrease the FSH receptors number and reduces the sensitivity of GC to FSH, which consequently prevents the provoke activation of critical genes in steroidogenesis processes such as *P450scc* and *CYP19A1* genes (29).

PCOS is a disease in which AMH has putative roles in its pathophysiology (30). Usually, it is the first cause of anovulation infertility in women (31). It seems that AMH contributes to the mechanisms leading to antral follicle arrest, anovulation, and oligomenorrhoea/ amenorrhoea (32, 33). Taken together, these studies suggest that increased AMH levels in PCOS women create an AMH-dominated microenvironment, which counteracts the action of FSH on follicles selection (34). The increased pre-antral follicle number, which is the primary source of AMH, is not merely contributing factor, but also elevated AMH concentration in PCOS is largely due to increased AMH production by individual follicles (35).

These studies have shown indirect confirmation of AMH's role in PCOS. Further observations elucidated the mechanism by which *AMH* expression is up-regulated in GCs. A limited number of BMPs such as BMP15 can bind to BMPR1B and BMPR2 receptors, and the activated receptors recognize SMAD1, which is translocated to the AMH promoter sequence. This mechanism significantly causes the *AMH* expression induction in human GCs (36, 37). In our study, mRNA expression of BMP15 in cumulus cells of PCOS patients is higher than in granulosa ones, and *AMH* expression was also higher in these cells. However, when CCs/GCs of PCOS are compared to normal oogenesis ones, this pattern was not observed. The high level of *AMH* expression in PCOS may be due to an additional source of BMP15 secretion, especially from the corresponding oocyte, which could induce *AMH* expression in CCs/GCs of such patients.

In PCOS, however, *BMPR1A* in GCs and *GDF9*, *BMP15* and *AMH* in CCs have a substantial expression. These distinct alterations in the follicular microenvironment of PCOS patients may negatively interfere with intra-follicular signals such as the follicle sensitivity to FSH, compromise the dominant follicle selection and the other functions of the GC/CC cells from the viewpoint of the oocyte maturation aspect and reproductive processes (38, 39).

On the other hand, in ovarian cells, the most important receptor for AMH is BMPR-1A. Therefore some members of the TGF-β superfamily share their signaling pathway with AMH, and target genes involved in folliculogenesis and GCs differentiation could also be regulated by AMH (40).

To explore whether gene expression pattern is diverse between cumulus cells and granulosa cells, we analyzed the expression profile. Data showed a differential overexpression of GDF9, *BMP15*, and *AMH* in infertile PCOS cumulus cells in comparison to PCOS granulosa cells. However, *AMH* and *GDF9* have the same pattern in normal cyclic cumulus cells, but *BMP15* and *BMPR1B* significantly decreased in granulosa cells of normal patients. Therefore, the gene expression profile in both GC and CC cells showed interesting diversity. Since the same antagonist protocol for ovarian stimulation was used in both PCOS and control groups, the results were independent of the protocols.

## Conclusion

To conclude, based on the previous results, increased gene expression of *AMH* and *BMPR1A* and decreased gene expression of *GDF9*, *BMP15*, and *BMPR1B* may contribute to alterations in the downstream pathway, which are involved in ovulatory function, follicular growth, and oocyte maturation. The results of the current study are important for understanding the mechanisms of follicular growth arresting and anovulation cycles in patients suffering from PCOS. It will be considered to screen the epigenetic regulatory mechanism of the promoter regions of the TGFβ family members and corresponding receptors in future studies.

## Acknowledgements

This study was financially sponsored by the Genetics Department of Royan Institute Tehran, Iran. The authors dedicate this article to the memory of Dr. Saeid Kazemi Ashtiani, the late founder of Royan Institut. There is no conflict of interest.

## Authors' Contributions

F.A., P.A., M.Shi, M.Sha, E.H.; Contributed to conception and design. F.A.; Contributed to all experimental work, data and statistical analysis, and interpretation of data. P.A., M.Shi.; Were responsible for overall supervision. B.M., M.Shi.; Cooperated in the sampling section. M.Shi.; Was responsible for patients assessment and diagnosis, also for patient recruitment to study. F.A.; Collected the sample. Z.H., M.Kh.; Cooperated with some experimental tests. F.A., E.H.; Drafted the initial manuscript and wrote the manuscript. P.A., E.H., M.Shi.; Contributed to revise and edit the manuscript. All authors read and approved the final manuscript.

## References

1. Lizneva D, Atabiekov I, Azziz R. Polycystic ovary syndrome. In: skinner MK, editor. Encyclopedia of reproduction. 2nd ed. Oxford:

Academic Press; 2018: 59-69.
2. Alzamil H, Aloraini K, AlAgeel R, Ghanim A, Alsaaran R, Alsomali N, et al. Disparity among Endocrinologists and Gynaecologists in the Diagnosis of Polycystic Ovarian Syndrome. Sultan Qaboos Univ Med J. 2020; 20(3): e323-e329.
3. Arroyo A, Kim B, Yeh J. Luteinizing hormone action in human oocyte maturation and quality: signaling pathways, regulation, and clinical impact. Reprod Sci. 2020; 27(6): 1223-1252.
4. Albu D, Albu A. The ratio of exogenous Luteinizing hormone to Follicle stimulating hormone administered for controlled ovarian stimulation is associated with oocytes' number and competence. Biosci Rep. 2020; 40(1): BSR20190811.
5. Burnik Papler T, Vrtacnik Bokal E, Lovrecic L, Kopitar AN, Maver A. No specific gene expression signature in human granulosa and cumulus cells for prediction of oocyte fertilisation and embryo implantation. PLoS One. 2015; 10(3): e0115865.
6. Feuerstein P, Cadoret V, Dalbies-Tran R, Guerif F, Bidault R, Royere D. Gene expression in human cumulus cells: one approach to oocyte competence. Hum Reprod. 2007; 22(12): 3069-3077.
7. Belli M, Shimasaki S. Molecular aspects and clinical relevance of GDF9 and BMP15 in ovarian function. Vitam Horm. 2018; 107: 317-348.
8. Raja-Khan N, Urbanek M, Rodgers RJ, Legro RS. The role of TGF-β in polycystic ovary syndrome. Reprod Sci. 2014; 21(1): 20-31.
9. Romanski PA, Brady PC, Farland LV, Thomas AM, Hornstein MD. The effect of endometriosis on the antimüllerian hormone level in the infertile population. J Assist Reprod Genet. 2019; 36(6): 1179-1184.
10. van Houten EL, Themmen AP, Visser JA. Anti-Müllerian hormone (AMH): regulator and marker of ovarian function. Ann Endocrinol (Paris). 2010; 71(3): 191-197.
11. Rybska M, Knap S, Stefańska K, Jankowski M, Chamier-Gliszczyńska A, Popis M, et al. Transforming growth factor (TGF) – is it a key protein in mammalian reproductive biology? Med J Cell Biol. 2018; 6(3): 125-30.
12. Zhao B, Wu X, Yuan Y, Gao Y, Li X, Du R, et al. Gene expression of granulosa and cumulus cells: The prospect in predicting the quality and developmental competence of oocytes in vitro maturation. Biocell. 2020; 44(4): 487-499.
13. Dumesic DA, Meldrum DR, Katz-Jaffe MG, Krisher RL, Schoolcraft WB. Oocyte environment: follicular fluid and cumulus cells are critical for oocyte health. Fertil Steril. 2015; 103(2): 303-316.
14. Field SL, Dasgupta T, Cummings M, Orsi NM. Cytokines in ovarian folliculogenesis, oocyte maturation and luteinisation. Mol Reprod Dev. 2014; 81(4): 284-314.
15. Lv P-P, Jin M, Rao J-P, Chen J, Wang L-Q, Huang C-C, et al. Role of anti-Müllerian hormone and testosterone in follicular growth: a cross-sectional study. BMC Endocr Disord. 2020; 20(1): 101.
16. Sanfins A, Rodrigues P, Albertini DF. GDF-9 and BMP-15 direct the follicle symphony. J Assist Reprod Genet. 2018; 35(10): 1741-1750.
17. Hosseini E, Shahhoseini M, Afsharian P, Karimian L, Ashrafi M, Mehraein F, et al. Role of epigenetic modifications in the aberrant CYP19A1 gene expression in polycystic ovary syndrome. Arch Med Sci. 2019; 15(4): 887-895.
18. Hosseini E, Mehraein F, Shahhoseini M, Karimian L, Nikmard F, Ashrafi M, et al. Epigenetic alterations of CYP19A1 gene in Cumulus cells and its relevance to infertility in endometriosis. J Assist Reprod Genet. 2016; 33(8): 1105-1113.
19. Andrei D, Nagy RA, van Montfoort A, Tietge U, Terpstra M, Kok K, et al. Differential miRNA expression profiles in cumulus and mural granulosa cells from human pre-ovulatory follicles. MicroRNA. 2019; 8(1): 61-67.
20. Turathum B, Gao EM, Chian RC. The function of cumulus cells in oocyte growth and maturation and in subsequent ovulation and fertilization. Cells. 2021; 10(9): 2292.
21. Huang Z, Wells D. The human oocyte and cumulus cells relationship: new insights from the cumulus cell transcriptome. Mol Hum Reprod. 2010; 16(10): 715-725.
22. Ouandaogo ZG, Haouzi D, Assou S, Dechaud H, Kadoch IJ, De Vos J, et al. Human cumulus cells molecular signature in relation to oocyte nuclear maturity stage. PLoS One. 2011; 6(11): e27179.
23. Assidi M, Dieleman SJ, Sirard M-A. Cumulus cell gene expression following the LH surge in bovine preovulatory follicles: potential early markers of oocyte competence. Reproduction. 2010; 140(6): 835-852.
24. Khalaf M, Morera J, Bourret A, Reznik Y, Denoual C, Herlicoviez M, et al. BMP system expression in G.C.s from polycystic ovary syndrome women and the in vitro effects of BMP4, BMP6, and BMP7 on GC steroidogenesis. Eur J Endocrinol. 2013; 168(3): 437-444.
25. Paradis F, Novak S, Murdoch GK, Dyck MK, Dixon WT, Foxcroft GR. Temporal regulation of BMP2, BMP6, BMP15, GDF9, BMPR1A, BMPR1B, BMPR2 and TGFBR1 mRNA expression in the oocyte, granulosa and theca cells of developing preovulatory follicles in the pig. Reproduction. 2009; 138(1): 115 -129.
26. Yan C, Wang P, DeMayo J, DeMayo FJ, Elvin JA, Carino C, et al. Synergistic roles of bone morphogenetic protein 15 and growth differentiation factor 9 in ovarian function. Mol Endocrinol. 2001; 15(6): 854-866.
27. Kedem-Dickman A, Maman E, Yung Y, Yerushalmi G.M., Hemi R, Hanochi M, et al. Anti-Müllerian hormone is highly expressed and secreted from cumulus granulosa cells of stimulated preovulatory immature and atretic oocytes. Reprod Biomed Online. 2012; 24(5): 540-546.
28. Nilsson EE, Schindler R, Savenkova MI, Skinner MK. Inhibitory actions of Anti-Müllerian Hormone (AMH) on ovarian primordial follicle assembly. PLoS One. 2011; 6(5): e20087.
29. Sacchi S, 'D'Ippolito G, Sena P, Marsella T, Tagliasacchi D, Maggi E, et al. The anti-Müllerian hormone (AMH) acts as a gatekeeper of ovarian steroidogenesis inhibiting the granulosa cell response to both FSH and LH. J Assist Reprod Genet. 2016; 33(1): 95-100.
30. Pasquali R. New perspectives on the role of anti-Müllerian hormone (AMH) in women. Ann Transl Med. 2018; 6 Suppl 2: s94.
31. Capuzzo M, La Marca A. Use of AMH in the differential diagnosis of anovulatory disorders including PCOS. Front Endocrinol (Lausanne). 2021; 11: 616766.
32. Fréour T, Mirallié S, Colombel A, Bach-Ngohou K, Masson D, Barrière P. Anti-mullerian hormone: clinical relevance in assisted reproductive therapy. Ann Endocrinol. 2006; 67(6): 567-574.
33. Garg D, Tal R. The role of AMH in the pathophysiology of polycystic ovarian syndrome. Reprod Biomed Online. 2016; 33(1): 15-28.
34. Oh SR, Choe SY, Cho YJ. Clinical application of serum anti-Müllerian hormone in women. Clin Exp Reprod Med. 2019; 46(2): 50-59.
35. Pellatt L, Hanna L, Brincat M, Galea R, Brain H, Whitehead S, et al. Granulosa cell production of anti-mullerian hormone is increased in polycystic ovaries. J Clin Endocrinol Metab. 2007; 92(1): 240-245.
36. Ogura-Nose S, Yoshino O, Osuga Y, Shi J, Hiroi H, Yano T, et al. Anti-mullerian hormone (AMH) is induced by bone morphogenetic protein (BMP) cytokines in human granulosa cells. Eur J Obstet Gynecol Reprod Biol. 2012; 164(1): 44-47.
37. Estienne A, Pierre A, di Clemente N, Picard JY, Jarrier P, Mansanet C, et al. Anti-Müllerian hormone regulation by the bone morphogenetic proteins in the sheep ovary: deciphering a direct regulatory pathway. Endocrinology. 2015; 156(1): 301-313.
38. Li J, Chen H, Gou M, Tian C, Wang H, Song X, et al. Comprehensive molecular features of polycystic ovary syndrome revealed by transcriptome analysis of oocytes and cumulus cells. bioRxiv. 2021. Available from: https://www.biorxiv.org/content/10.1101/2021.01.30.428778v1.full (20 Apr 2021).
39. Rosenfield RL, Ehrmann DA. The pathogenesis of polycystic ovary syndrome (PCOS): the hypothesis of PCOS as functional ovarian hyperandrogenism revisited. Endocr Rev. 2016; 37(5): 467-520.
40. Sèdes L, Leclerc A, Moindjie H, Cate RL, Picard JsY, Di Clemente N, et al. Anti-Müllerian hormone recruits BMPR-IA in immature granulosa cells. PLoS One. 2013; 8(11): e81551.

Original Article

# Alginate Effects on Human Sperm Parameters during Freezing and Thawing: A Prospective Study

**Somayeh Feyzmanesh, M.Sc.[1], Iman Halvaei, Ph.D.[1]*, Nafiseh Baheiraei, Ph.D.[2]***

**1. Department of Anatomical Sciences, Faculty of Medical Sciences, Tarbiat Modares University, Tehran, Iran**
**2. Tissue Engineering and Applied Cell Sciences Division, Department of Anatomical Sciences, Faculty of Medical Sciences, Tarbiat Modares University, Tehran, Iran**

***Corresponding Addresses: P.O.Box: 14115-331, Department of Anatomical Sciences, Faculty of Medical Sciences, Tarbiat Modares University, Tehran, Iran***
***P.O.Box: 14115-331, Tissue Engineering and Applied Cell Sciences Division, Department of Anatomical Sciences, Faculty of Medical Sciences, Tarbiat Modares University, Tehran, Iran***
***Emails: ihalvaei@modares.ac.ir, n.baheiraei@modares.ac.ir***

**Received: 28/June/2021,Accepted: 09/September/2021**

Abstract

**Objective:** The main goal was to evaluate the effects of alginate on human sperm parameters during cryopreservation.

**Materials and Methods**: In this prospective study, twenty-five normozoospermic samples were divided into two groups, encapsulated with 1% alginate and the control group. The samples were then frozen by rapid freezing. Different sperm parameters including motility, normal morphology, viability, acrosome reaction, and DNA integrity, were examined before freezing and after thawing.

**Results:** All sperm parameters had a significant decrease after thawing compared to before freezing. Our data showed a significant decrease in sperm motility of the alginate group but sperm viability, normal morphology, and DNA fragmentation were similar between the two groups. However, the rates of intact acrosome and native DNA were significantly lower in the control group compared to the alginate group (45.12 ± 11.1 vs. 55.25 ± 10.69 and 52.2 ± 11.92 vs. 68.12 ± 10.15, respectively, $P<0.05$).

**Conclusion:** It seems that alginate can prevent premature acrosome reaction and protect sperm DNA from denaturation during the rapid freezing process.

***Keywords:*** Alginate, Encapsulation, Rapid Freezing, Sperm DNA

Cell Journal(Yakhteh), Vol 24, No 7, July 2022, Pages: 417-423

**Citation:** **Feyzmanesh S, Halvaei I, Baheiraei N. Alginate effects on human sperm parameters during freezing and thawing: a prospective study. Cell J. 2022; 24(7): 417-423. doi: 10.22074/cellj.2022.8122.**

**This open-access article has been published under the terms of the Creative Commons Attribution Non-Commercial 3.0 (CC BY-NC 3.0).**

## Introduction

Human sperm cryopreservation is a routine practice in assisted reproductive technology (ART) for several reasons including fertility preservation before initiation of radiotherapy, chemotherapy, and vasectomy, for patients with diabetes and autoimmune disorders (1). It could also be used for people with azoospermia without affecting ART outcomes in comparison with fresh controls (2). However, cryopreservation may have detrimental effects on spermatozoa including cold shock, formation of intracellular and extracellular ice crystals, osmotic shock, and production of reactive oxygen species (ROS) that may affect sperm motility (3-5). Spermatozoa are unique cells with a high level of polyunsaturated fatty acid in their plasma membrane, a high number of mitochondria, a low volume of cytoplasm, and antioxidant potential that make the spermatozoa vulnerable to cryopreservation (6).

Encapsulation technology has lately been suggested as a potential favorable method to preserve spermatozoa during cryopreservation. Alginate, an anionic polysaccharide derived from brown seaweed, has been extensively used for several biomedical applications because of its high biocompatibility, relatively low cost, and low toxicity (7). Supplementation with sodium alginate also helped the metal chelating capacities and free radical scavenging to preserve buffalo sperm during cryopreservation (8). More importantly, cell encapsulation in alginate is an encouraging approach during cryopreservation as cells could be protected against mechanical destruction during ice crystallization (9). It has been shown that alginate mimics the extracellular matrixes for spermatogonial stem cells supporting the potential of their stemness during the cryopreservation (10). Also, the fertilizing potential of cryopreserved sperm using alginate encapsulation did not change in buffalo (11). It was shown that microencapsulation could mechanically inhibit spermatozoa movement. However, it did not negatively impact the intracytoplasmic sperm injection results and a high rate of the vitality of immotile spermatozoa was observed. Also, alginate microencapsulation could preserve spermatozoa from the risk of contamination with foreign material, either spermatozoa or genetic material (12). Controlled-release alginate capsules having boar spermatozoa have also been utilized to increase the time of spermatozoa preservation and maximize the effectiveness of single artificial insemination (13). Also, the alginate microencapsulation method has been used successfully to cryopreserve canine sperm by extending the post-thaw motility, viability, and acrosomal integrity (14).

There are limited data about the cryoprotective effects of alginate on human spermatozoa. Herrler et al. only evaluated the effects of human cell encapsulation on sperm motility and viability (12). They showed that alginate encapsulation using a slow freezing technique decreased human sperm motility while no difference was observed for sperm viability. It seems that using sperm encapsulation in cryopreservation needs to be adjusted. This study aimed to evaluate the effects of alginate encapsulation on human sperm motility, viability, acrosome reaction, and DNA integrity during rapid freezing.

## Materials and Methods

### Collecting and preparing samples

Twenty-five normozoospermic semen samples were included in this prospective study. Heavy smokers and patients who received antioxidants were excluded from this study. The specimens were obtained from patients who were referred to the Gandhi IVF clinic for infertility workups. The abstinence period was 3-5 days. This study was approved by the Ethics Committee of Tarbiat Modares University (IR.MODARES.REC.1397.198). The direct swim-up method was used to prepare the spermatozoa. The mean age of men was 33.29 ± 3.85.

### Sperm encapsulation into alginate hydrogel

Sperm containing alginate microcapsules were prepared according to the previously described method (12). Briefly, 50 µL of sperm solution was mixed with 50 µL of Quinn`s Advantage Sperm Freeze (SAGE, USA) for 3 minutes which then was added to 100 µL sterilized alginate solution (1% w/v, sodium alginate, Sigma-Aldrich, USA). For polymerization, 50-100 µL aqueous calcium chloride (Sigma-Aldrich, Germany) with a concentration of 102 mmol/L was added dropwise to the as-prepared suspension. After 1 minute, the remaining unreacted crosslinker was removed through washing with 50 µL of 0.9% w/v sodium chloride. Finally, microcapsules were transferred into the cryotubes containing 100 µL cryoprotectant medium containing sodium chloride for 3 minutes before cryopreservation.

### Scanning electron microscopy and *in vitro* sperm release

Scanning electron microscopy (SEM) was used to evaluate the morphology of the prepared hydrogels without sperm. Samples were first freeze-dried (ALPHA 1-2 LD, UK) overnight before being sputtered with gold for SEM analysis. Evaluation of the *in vitro* rate of sperm releasing was also performed using the previously reported protocol with modification (15). This test was done to estimate the *in vitro* release of spermatozoa after gel encapsulation. For this test, alginate microcapsules were incubated in four-well plates containing 200 µL of F10 Ham's medium at 37˚C (n=3). After incubation for 2, 4, 6, and 24 hours, the entire medium was removed and checked for detection of released spermatozoa. Sperm number was detected by light microscopy with a Neubauer chamber in at least 5 fields. Three replications were assessed for each time point. The percentage of spermatozoa released versus time was calculated using the following formula:

Percentage of released sperm=(number of spermatozoa counted in the medium at a specified time/total number of encapsulated spermatozoa)×100.

### Freezing and thawing sperm

In this study, the samples were frozen using the rapid freezing method. As previously described (16), the samples inside cryotubes were first placed horizontally 3 cm above the surface of liquid nitrogen for 30 minutes in the nitrogen vapor and then immersed in the liquid nitrogen. The samples were stored in liquid nitrogen for at least two weeks. During thawing, the cryotubes were first placed in a water bath at 35°C for 2 minutes after removal from the nitrogen tank. In the control group, a pre-warmed culture medium supplemented with human serum albumin was added dropwise and centrifugated. In the alginate group, 150 µL of 119 mM/L sodium citrate solution (pH=7.5) was added to the cryotube. After 30 seconds, the pre-warmed culture medium supplemented with human serum albumin was added dropwise. After that, the samples were centrifugated. After centrifugation in both groups, the supernatant was removed and the pellet was used for analysis.

### Sperm motility, viability, and morphology

Sperm motility was examined according to the WHO guidelines. In each slide, at least 200 spermatozoa were evaluated at six microscopic fields. Each sample was evaluated twice by two different expert technicians and the mean percent was reported for rates of progressive and non-progressive motile and immotile spermatozoa and total sperm motility (progressive+non-progressive). Sperm viability was measured by evaluating sperm membrane integrity using the eosin-nigrosin staining method. The spermatozoa with red/dark pink and white heads were considered live and dead cells, respectively (light microscope 1000x). At least 200 cells were assessed and the rate of sperm viability was reported as percentage. Papanicolaou staining method was used to evaluate the sperm morphology. At least 200 spermatozoa were evaluated reporting morphological abnormalities in the head, midpiece, and tail percentages (light microscope 1000x) (17).

### Acrosome reaction

The double staining method was used to evaluate the acrosome reaction. First, samples were fixed in a 1:1 ratio with 3% glutaraldehyde for 30 minutes followed by being centrifuged at 1500 g for 5 minutes. Slides were then stained with 8% Bismarck Brown for 10 minutes, and after rinsing, were being stained with 8% Rose Bengal for 20 minutes. A minimum of 200 spermatozoa was evaluated and the cells with healthy light brown or pink acrosome areas were reported as percentages (18).

### DNA denaturation

Acridine orange staining was used to test denatured sperm DNA. First, the sperm sample was placed in Carnoy's fixative solution in a ratio of 3:1 methanol/acetic acid for 2 hours at 4°C and then stained with acridine orange for 10 minutes in the dark. Using a fluorescent microscope, the green spermatozoa were considered healthy (native), and yellow to red spermatozoa were considered abnormal (denatured). A minimum of 200 spermatozoa was examined by a fluorescent microscope (1000x, 460 nm filter) and the rate of spermatozoa with healthy DNA was reported (16).

### Sperm chromatin dispersion

Sperm chromatin dispersion (SCD) was used to evaluate the DNA integrity using Sperm DNA Fragmentation Assay [IDEH VARZAN FARDA (IVF Co.), Tehran, Iran]. First, a 20 µL of sperm suspension (15-20 million $mL^{-1}$) was added to 25 µL of low melting agarose. In the next step, a smear was prepared on a pre-coated glass slide with 65% agarose and kept in the refrigerator at 4°C for 5 minutes. The lysis buffer solution containing hydrogen chloride (HCl) was then poured on the samples in the dark for 7 minutes. After washing the lysis buffer, the slides were immersed in the mercaptoethanol lysing solution, which separates nucleoproteins, for 15 minutes. The slides were then rinsed in distilled water for 5 minutes and the dehydration process was performed with 70, 90, and 100% ethanol. After staining with Wright color, at least 200 spermatozoa were examined for each sample (light microscope 1000x). According to the size of the halo around the head of spermatozoa, the degree of DNA fragmentation was considered. Spermatozoa with no halo or small halo were considered abnormal, while spermatozoa with medium or large halo were considered normal DNA (19).

### Statistical analysis

Quantitative data were reported as mean ± standard deviation, median (maximum-minimum). Shapiro-Wilk test was used to evaluate the distribution of data. To analyze the data between the three groups before freezing, alginate, and control, one-way ANOVA with the Tukey test was used. In cases where the distribution was not normal, the Kruskal-Wallis test with the Dunn test was used. The hypothesis was considered one-tailed and the significance level was considered $P<0.05$.

## Results

### Scanning electron microscopy

SEM test was performed to evaluate the structure of prepared alginate hydrogels. Figure 1 shows images of alginate hydrogels at two different magnifications. As can be seen, hydrogels have a porous structure with interconnected porosities.

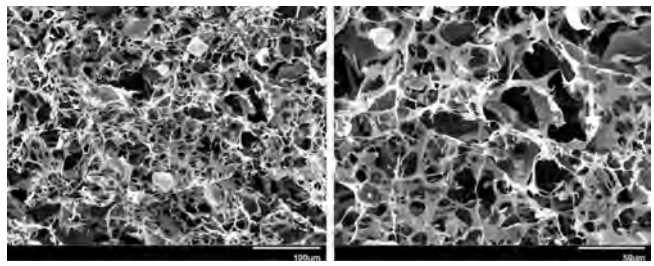

**Fig.1:** Scanning electron microscopy (SEM) images of alginate hydrogel with different magnifications. Hydrogels have porous structures with interconnected porosities (scale bars: 100 µm and 50 µm in the left and right image, respectively).

### *In vitro* examination of sperm release from alginate capsule

The profile of sperm release percentage from the alginate capsule is shown in Figure 2. Almost 0.01 % of spermatozoa were released after 2 hours. However, the corresponding value reached a constant within 24 hours.

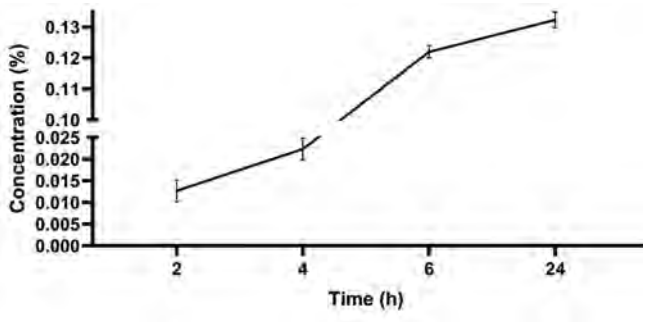


**Fig.2:** Sperm release profile from alginate microcapsules (n=3). The rate of released spermatozoa had an increasing trend by increasing time and reached a constant value after 24 hours.

### Sperm parameters

Semen characteristics included in this study are shown in Table 1. Sperm motility was significantly decreased after thawing compared to before freezing. The rates of progressive motility and total motility were significantly lower in the alginate group compared to the control group. Sperm viability had a significant decrease after thawing but there was the same in the two groups of control and alginate. The percentage of sperm normal morphology after thawing was significantly lower than before freezing. Additionally, after thawing, sperm morphology was preserved in the alginate group compared to the control group, but no significant difference was observed between the two groups. The cryopreservation induced the acrosome reaction. However, the rate of spermatozoa with intact acrosome was significantly higher in the alginate group compared to the control group. The rate of native DNA in spermatozoa after thawing was significantly lower

than before freezing. This reduction was improved in the alginate group and a significant difference was observed between the alginate and control groups. The rate of DNA fragmentation significantly decreased after thawing. This reduction improved in the alginate group but there was no significant difference between the alginate group and the control group (Table 2). Figure 3 shows acridine orange, acrosome reaction, and SCD tests.

**Table 1:** Semen characteristics included in this study

| Parameters | Mean | Minimum | Maximum | SD |
|---|---|---|---|---|
| Male age (Y) | 33.29 | 23 | 39 | 3.85 |
| Count ($10^6$/mL) | 140.25 | 90 | 182 | 26.15 |
| Progressive motility (%) | 61.45 | 43 | 70 | 6.9 |
| Non-progressive motility (%) | 16.25 | 6 | 30 | 6.27 |
| Total motility (%) | 77.7 | 54 | 89 | 8.37 |
| Immotile (%) | 22.29 | 11 | 46 | 8.37 |
| Normal morphology (%) | 7.8 | 4 | 15 | 1.32 |
| Round cell ($10^3$/mL) | 427.16 | 200 | 950 | 203.31 |

SD; Standard deviation.

**Table 2:** Comparison of the mean percentage of sperm parameters (± standard deviation) between different experimental groups

| Parameters | After swim-up | Control group | Alginate group |
|---|---|---|---|
| Progressive motility | $83.87 \pm 3.8^{ab}$ | $47.79 \pm 16.28^{bc}$ | $13.75 \pm 10.64^{ac}$ |
| | 84.5 (76-90) | 55 (13-69) | 10 (0-40) |
| Total motility | $92.83 \pm 3.62^{ab}$ | $65.33 \pm 15.67^{bc}$ | $29.91 \pm 15.01^{ac}$ |
| | 93 (85-98) | 71 (26-91) | 28.5 (7-65) |
| Viability | $97.33 \pm 1.97^{ab}$ | $89.83 \pm 4.93^{b}$ | $89.58 \pm 3.33^{a}$ |
| | 97 (91-99) | 90 (75-96) | 89 (85-97) |
| Normal morphology | $17.17 \pm 4.18^{ab}$ | $8.83 \pm 3.54^{b}$ | $11.13 \pm 3.2^{a}$ |
| | 16.5 (10-32) | 9 (4-19) | 10 (6-18) |
| Intact acrosome | $70.16 \pm 7.11^{ab}$ | $45.12 \pm 11.1^{bc}$ | $55.25 \pm 10.69^{ac}$ |
| | 70 (54-84) | 42 (29-66) | 52 (37-75) |
| Native DNA (AO) | $77 \pm 9.47^{ab}$ | $52.2 \pm 11.92^{bc}$ | $68.12 \pm 10.15^{ac}$ |
| | 76.5 (58-94) | 51 (33-80) | 67.5 (49-84) |
| Normal DNA (SCD) | $90.2 \pm 6.07^{ab}$ | $79.45 \pm 9.26^{b}$ | $81.95 \pm 7.88^{a}$ |
| | 92 (68-96) | 81 (60-92) | 85.5 (65-93) |

Data are presented as mean ± SD, median (min-max). Similar letters have significant difference. AO; Acridine orange and SCD; Sperm chromatin dispersion test.

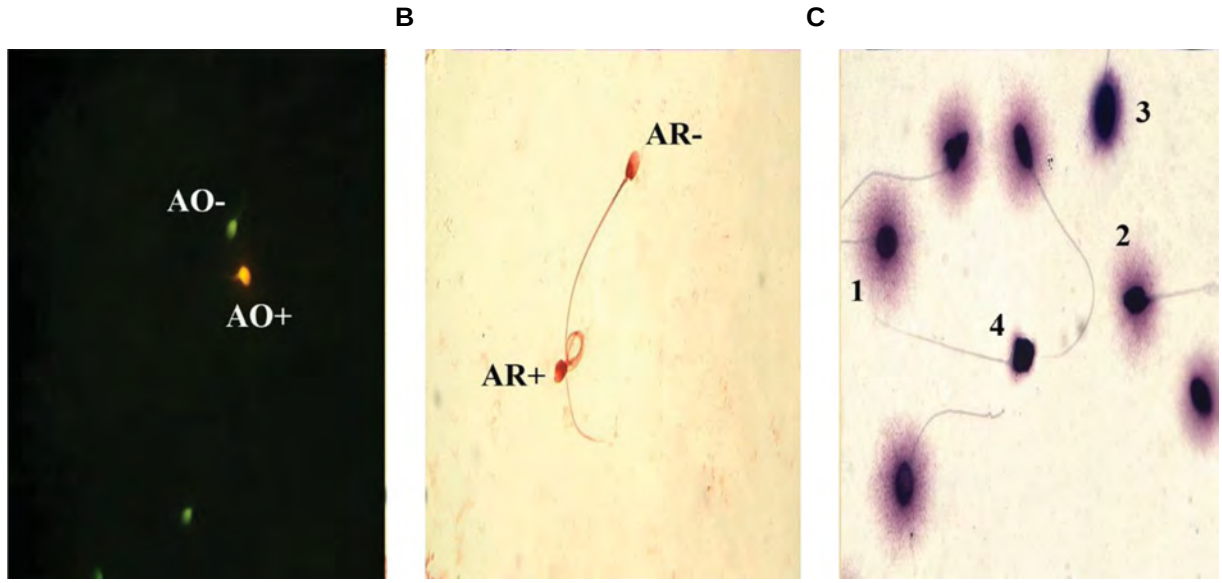


**Fig.3:** Acridine orange, acrosome reaction and sperm chromatin dispersion test. **A.** Acridine orange shows the orange sperm with DNA denaturation (AO+) and green native DNA (AO-), **B.** Double stating shows the sperm with brown head (acrosome intact, AR-) and dark brown and conical head (acrosome reacted, AR+), **C.** Sperm chromatin dispersion test shows different patterns of halos; 1; A normal DNA with a large halo, 2; A normal DNA with a medium halo, 3; Abnormal DNA with small halo, and 4; Abnormal DNA without halo (1000×).

## Discussion

Cell encapsulation with alginate is a promising method of preventing unwanted effects during cryopreservation. Our results showed that, after thawing, the rate of sperm progressive motility was significantly lower in the alginate group compared to that of the control group which was in line with a previous study that used 7 mg/dL alginate to encapsulate human sperm *in vitro* under slow freezing (12). It seems that one of the factors that decrease sperm motility may be the presence of alginate particles on the surface of sperm. The cytoskeletal structure of the sperm flagella is composed of fibrous sheaths which play an active role in sperm motility (20, 21). When the alginate residue is retained on the sperm, it may impair the active movement of the sperm tail and reduces motility. Torre et al. encapsulated porcine semen with 0.5% alginate and reported a decrease in sperm motility due to the remaining residual alginate particles on the sperm which impaired sperm motility (22). In fact, alginate hydrogel may be affected by many factors such as crosslink concentration, type of alginate, alginate concentration, cell encapsulation method, and protocol of hydrogel degradation. Each of these factors can affect sperm motility alone. Moreover, most damages occur rapidly after the thawing stage (23). During thawing, cryoprotectants inside the cell cannot leave the cell quickly, but water enters the cell faster leading to osmotic shock causing cell swelling and sperm damage. Alginate, which acts as a matrix around the spermatozoa and protects the sperm membrane, is removed during thawing.

According to the results of the present study, the sperm viability was the same between the alginate and control groups. As mentioned earlier, alginate is a biodegradable polymer with high biocompatibility, with a prominent potential to form a three-dimensional matrix around the cell similar to the extracellular matrix. This type of porous matrix can maintain the desired level of cell viability in any *in vitro* and *in vivo* environment (24). Alginate creates a unique structure that facilitates the transport of signaling molecules and nutrients. It was shown that poly (propylene fumarate)-co-alginate resists the penetration of ROS (25). However, according to Pirnia et al., spermatogonia stem cell viability in the alginate-containing group was significantly reduced compared to the control group. According to this study, the probable cause of the decrease in viability is in the thawing step after removing alginate hydrogel and exposure to ROS (10). In addition, Kumar et al. (8), supplemented semen extender of buffalo with alginate and cryopreserved the samples with a programmable biological freezer. They showed that alginate maintains membrane integrity and increases sperm viability.

Regarding sperm morphology, the rate of normal sperm morphology in the alginate group was similar to the control group. Osmotic stress may affect sperm morphology. Permeable cryoprotectant agents must penetrate the cell to play protective roles and this addition before freezing and removal in the thawing step causes severe osmotic volume changes, which in turn may cause cell injury (26). These rapid changes in cell osmolality have caused the shape and structure of the sperm membrane to change especially in the form of deformities in the sperm head and the twisting of the sperm tail. According to Torre et al. (15) the percentage of porcine sperm morphological abnormalities in both encapsulated and control groups was not significantly different concluding that the presence of sperm morphological abnormalities does not depend on the storage process in the alginate.

Based on our results, the acrosome reaction rate after the freeze-thawing process was significantly decreased in the alginate group compared to that of the control group. During the cryopreservation, due to temperature changes and increased ROS, the structure of polyunsaturated fatty acids and cholesterol is disrupted, which in turn increases the membrane's permeability to calcium and ROS, subsequently activating phospholipase A2, leading to the onset of an acrosome reaction (27). It was shown that adding sodium alginate to the cryopreservation medium prevents sperm membrane changes and maintains membrane integrity, which in turn preserves the acrosome membrane and prevents premature acrosome reaction (8).

Our data showed that acridine orange and SCD results were not in line with each other in the alginate group. In the group containing alginate, the rate of DNA denaturation and DNA fragmentation decreased compared to the control group, which significantly differed in DNA denaturation. It was shown that there was a lack of relationship between SCD and acridine orange (28). The cut-off value of acridine orange (native DNA) is greater than 50% (29) and all groups in our study had native DNA greater than the cut-off value. It suggested that acridine orange is reliable when there is a high level of DNA damage (28). Two important factors of DNA fragmentation and DNA damage are oxidative stress and apoptosis (30). In fact, the increase in ROS production during cryopreservation is the cause of oxidative stress leading to DNA fragmentation. In the thawing step, various factors such as temperature, osmotic stress, and the use of centrifuges cause defects in the sperm mitochondrial membrane and ROS production (31). Removing alginate at the thawing step makes the spermatozoa more prone to oxidative stress compared with the control group. According to Pirnia et al. (10), the use of 1% alginate hydrogel for encapsulation of spermatogonia stem cells can regulate the differentiation of these cells and maintain their pluripotency of them during slow freezing by regulating *Lin28a* and *Sall14* genes. The potential role of encapsulation is to maintain sperm viability while allowing their gradual release (32). Our data showed that *in vitro* sperm release was very low and the corresponding value reached constant within 24 hours confirming the stability of the hydrogel structure in F10 Ham's medium over time (15). Microencapsulation of semen has been suggested as a method of choice for a gradual release of spermatozoa within the female reproductive or extended storage (33). The latter was regarded in this study. Here, we did not observe the fast release and the total *in vitro* sperm release was very low. We do not expect many releases after effective crosslinking of the hydrogel as the calcium chloride is making links between the alginate branches. This observation confirms the great integrity of the prepared hydrogels preventing the burst effect of the sperm release. We also achieved gradual release which further approves the stability of the hydrogel structure. More importantly, different parameters including concentrations of calcium ions for making the capsules could affect gel strength and thickness of the alginate membrane which in turn impacts the spermatozoa release behavior (22). Further studies are required to evaluate the effect of sperm species, alginate type, and the cross-linkers as well as their concentration for optimal sperm release. In this study, we evaluated the impact of alginate encapsulation on normozoospermic samples. It should be noted that pre-cryo sperm parameters including motility and viability are useful to predict post-thaw outcomes (34). It is suggested to evaluate the probable effects of alginate encapsulation on abnormal sperm samples in the next research.

## Conclusion

According to the results of this study, alginate can prevent sperm premature acrosome reaction and protect sperm DNA from denaturation during the rapid freezing process. More studies should be performed for optimization of alginate for application in sperm cryopreservation.

## Acknowledgments

This manuscript was extracted from the M.Sc. thesis of S.F. The authors thank Tarbiat Modares University for the financial support of this study. The authors declare no competing interests.

## Authors' Contributions

I.H., N.B.; Designed the study and revised the manuscript. S.F.; Conducted experiments and wrote the manuscript. I.H.; Conducted statistics. All authors read and approved the final manuscript.

## References

1. Di Santo M, Tarozzi N, Nadalini M, Borini A. Human sperm cryopreservation: update on techniques, effect on DNA integrity, and implications for ART. Adv Urol. 2011; 2012.
2. Ammar SJ, Arfaoui R, Hammami F, Souayah N, Chibani M, Rachdi R. Does cryopreservation of testicular sperm affect icSi outcomes in azoospermia? Tunis Med. 2020; 98(07): 581-587.
3. Bahmyari R, Zare M, Sharma R, Agarwal A, Halvaei I. The efficacy of antioxidants in sperm parameters and production of reactive oxygen species levels during the freeze-thaw process: A systematic review and meta-analysis. Andrologia. 2020; 52(3): e13514.
4. Hezavehei M, Sharafi M, Kouchesfahani HM, Henkel R, Agarwal A, Esmaeili V, et al. Sperm cryopreservation: a review on current molecular cryobiology and advanced approaches. Reprod Biomed Online. 2018; 37(3): 327-339.
5. O'connell M, McClure N, Lewis S. The effects of cryopreservation on sperm morphology, motility and mitochondrial function. Hum Reprod. 2002; 17(3): 704-709.
6. Said TM, Gaglani A, Agarwal A. Implication of apoptosis in sperm cryoinjury. Reprod Biomed Online. 2010; 21(4): 456-462.
7. Gombotz WR, Wee S. Protein release from alginate matrices. Adv Drug Deliv Rev. 1998; 31(3): 267-285.
8. Kumar P, Pawaria S, Dalal J, Ravesh S, Bharadwaj S, Jerome A, et al. Sodium alginate potentiates antioxidants, cryoprotection and antibacterial activities of egg yolk extender during semen cryopreservation in buffalo. Anim Seprod Sci. 2019; 106166.
9. Swioklo S, Constantinescu A, Connon CJ. Alginate-sencapsulation for the improved hypothermic preservation of human adipose-derived stem cells. Stem Cells Transl Med. 2016; 5(3): 339-349.
10. Pirnia A, Parivar K, Hemadi M, Yaghmaei P, Gholami M. Stemness of spermatogonial stem cells encapsulated in alginate hydrogel during cryopreservation. Andrologia. 2017; 49(5): e12650.
11. Perteghella S, Gaviraghi A, Cenadelli S, Bornaghi V, Galli A, Crivelli B, et al. Alginate encapsulation preserves the quality and fertilizing ability of Mediterranean Italian water buffalo (Bubalus bubalis) and

Holstein Friesian (Bos taurus) spermatozoa after cryopreservation. J Vet Sci. 2017; 18(1): 81.
12. Herrler A, Eisner S, Bach V, Weissenborn U, Beier HM. Cryopreservation of spermatozoa in alginic acid capsules. Fertil Steril. 2006; 85(1): 208-213.
13. Vigo D, Faustini M, Villani S, Orsini F, Bucco M, Chlapanidas T, et al. Semen controlled-release capsules allow a single artificial insemination in sows. Theriogenology. 2009; 72(4): 439-444.
14. Shah S, Otsuki T, Fujimura C, Yamamoto N, Yamashita Y, Higaki S, et al. Cryopreservation of microencapsulated canine sperm. Theriogenology. 2011; 75(4): 679-686.
15. Torre M, Faustini M, Norberti R, Stacchezzini S, Maggi L, Maffeo G, et al. Boar semen controlled delivery system: storage and in vitro spermatozoa release. J Control Release. 2002; 85(1-3): 83-89.
16. Najafi L, Halvaei I, Movahedin M. Canthaxanthin protects human sperm parameters during cryopreservation. Andrologia. 2019; 51(10): e13389.
17. World Health Organization. WHO laboratory manual for the examination and processing of human semen. Geneva: WHO press; 2010.
18. Shahmoradi E, Baheiraei N, Halvaei I . Trehalose attenuates detrimental effects of freeze-drying on human sperm parameters. Biopreserv Biobank. 2022; 20(1): 31-37.
19. Nabi A, Khalili M, Halvaei I, Roodbari F. Prolonged incubation of processed human spermatozoa will increase DNA fragmentation. Andrologia. 2014; 46(4): 374-379.
20. Akbari A, Anvar Z, Jaafarinia M,Totonchi M. Genetic etiology of Asthenozoospermia: a review. Feyz. 2019; 23(3): 318-333.
21. Baccetti B, Collodel G, Gambera L, Moretti E, Serafini F, Piomboni P. Fluorescence in situ hybridization and molecular studies in infertile men with dysplasia of the fibrous sheath. Fertil Steril. 2005; 84(1): 123-129.
22. Torre M, Maggi L, Vigo D, Galli A, Bornaghi V, Maffeo G, et al. Controlled release of swine semen encapsulated in calcium alginate beads. Biomaterials. 2000; 21(14): 1493-1498.
23. Gosálvez J, Cortés-Gutierez E, López-Fernández C, Fernández J L, Caballero P, Nuñez R. Sperm deoxyribonucleic acid fragmentation dynamics in fertile donors. Fertil Steril. 2009; 92(1): 170-173.
24. Ghidoni I, Chlapanidas T, Bucco M, Crovato F, Marazzi M, Vigo D, et al. Alginate cell encapsulation: new advances in reproduction and cartilage regenerative medicine. Cytotechnology. 2008; 58(1): 49-56.
25. Finosh GT, Jayabalan M. Reactive oxygen species—Control and management using amphiphilic biosynthetic hydrogels for cardiac applications. Adv Biosci Biotech. 2013; 4(12): 41356.
26. Gao D, Liu J, Liu C, McGann L, Watson P, Kleinhans F, et al. Andrology: Prevention of osmotic injury to human spermatozoa during addition and removal of glycerol. Hum Reprod. 1995; 10(5): 1109-1122.
27. Pommer A, Meyers SA. Tyrosine phosphorylation is an indicator of capacitation status in fresh and cryopreserved stallion spermatozoa. Theriogenology. 2002; 58(2-4): 351-354.
28. Chohan KR, Griffin JT, Lafromboise M, De Jonge CJ,Carrell DT. Comparison of chromatin assays for DNA fragmentation evaluation in human sperm. J Androl. 2006; 27(1): 53-59.
29. Gopalkrishnan K, Hurkadli K, Padwal V, Balaiah D. Use of acridine orange to evaluate chromatin integrity of human spermatozoa in different groups of infertile men. Andrologia. 1999; 31(5): 277-282.
30. Aitken RJ, Koppers AJ. Apoptosis and DNA damage in human spermatozoa. Asian J Androl. 2011; 13(1): 36-42.
31. Agarwal A, Said TM. Oxidative stress, DNA damage and apoptosis in male infertility: a clinical approach. BJU Int. 2005; 95(4): 503-507.
32. Nebel RL, Vishwanath R, McMillan W, Pitt C. Microencapsulation of bovine spermatozoa: effect of capsule membrane thickness on spermatozoal viability and fertility. Anim Reprod Sci. 1996; 44(2): 79-89.
33. Nebel RL, Saacke RG. Spermatozoa microencapsulation and capsule behavior in female tract. Reprod Dom Anim. 1996; 31(1): 75–85.
34. Whaley D, Damyar K, Witek RP, Mendoza A, Alexander M, Lakey JRJCT. Cryopreservation: an overview of principles and cell-specific considerations. Cell Transplant. 2021; 30: 963689721999617.

# Hypertension in COVID-19, A Risk Factor for Infection or A Late Consequence?

**Maryam Barekat, M.D.[1#], Mohammad Amin Shahrbaf, M.D.[1, 2#], Kosar Rahi, M.Sc.[1], Massoud Vosough, M.D., Ph.D.[1, 3*]**

**1. Department of Regenerative Medicine, Cell Science Research Center, Royan Institute for Stem Cell Biology and Technology, ACECR, Tehran, Iran**
**2. Research and Development Department, Royan Stem Cell Technology Co, Tehran, Iran**
**3. Experimental Cancer Medicine, Institution for Laboratory Medicine, Karolinska Institute, Stockholm, Sweden**

***Corresponding Address: P.O.Box: 16635-148, Department of Regenerative Medicine, Cell Science Research Center, Royan Institute for Stem Cell Biology and Technology, ACECR, Tehran, Iran***
***Email: masvos@royaninstitute.org***

**#These authors contributed equally to this work.**

**Received: 27/February/2022, Accepted: 14/June/2022**

Abstract

There are a lot of data about the correlation of SARS-CoV-2 infection and hypertension (HTN), but most of them are in the increased risk of morbidity and mortality in patients with HTN. SARS-CoV-2 can interfere with host cells through the renin-angiotensin system (RAS) via the angiotensin-converting enzyme 2 (ACE2) receptor. RAS activation is associated with pro-inflammatory effects through the ACE/Ang II/ Angiotensin II type 1 receptor (AT1R) pathway or anti-inflammatory effects through ACE2/Ang1-7/Mas axis. In the current paper, we discuss the pathophysiology of newly diagnosed HTN and its effect on morbidity in patients with coronavirus disease 2019 (COVID-19).

***Keywords:*** COVID-19, Hypertension, Renin-Angiotensin-Aldosterone System

Cell Journal(Yakhteh), Vol 24, No 7, July 2022, Pages: 424-426

**Citation:** **Barekat M, Shahrbaf MA, Rahi K, Vosough M. Hypertension in COVID-19, a risk factor for infection or a late consequence? Cell J. 2022; 24(7): 424-426. doi: 10.22074/cellj.2022.8487.**

**This open-access article has been published under the terms of the Creative Commons Attribution Non-Commercial 3.0 (CC BY-NC 3.0).**

## Introduction

Coronavirus disease 2019 (COVID-19), caused by severe acute respiratory syndrome coronavirus 2 (SARS-CoV-2) firstly reported in Wuhan in 2019 (1), China, that caused more than 517 million confirmed cases and almost 6.2 million deaths until 6 May 2022 (2). It is shown that cardiovascular diseases and risk factors such as hypertension (HTN) are associated with more severe symptoms in affected individuals including dyspnea, and hypoxia. These patients need intensive care unit (ICU) that represent the increased likelihood of morbidities, and even mortality (3). On the other hand, HTN may be a consequence of COVID-19, due to the over-activity of the renin-angiotensin system (RAS) (4).

During the COVID-19 pandemic disease, especially during lockdown and quarantine, diagnostic and therapeutic interventions for HTN were reduced significantly, which deteriorates the long-term consequences of HTN and cardiovascular events (5, 6). In addition, studies reported that the COVID-19 pandemics has changed the treatment strategies of HTN in order to have a better management of this condition in patients (7). In this study, we review the association between COVID-19 and HTN as a risk factor for the infection, and a consequence of the infection.

### COVID-19 and RAS

SARS-CoV-2 penetrates host cells using surface spike protein through the angiotensin-converting enzyme 2 (ACE2) receptor that interferes with host cells via RAS (8). Recent studies showed that RAS over-activation might have pro-inflammatory, profibrotic, and vasoconstrictive effects by reactive oxygen species (ROS) production and cytokines release through ACE/Ang II/ Angiotensin II type 1 receptor ($AT_1R$) pathway (9). However, RAS can act through an alternative pathway, the ACE2/Ang1-7/Mas axis, which is a counter-regulator of classic pathway causing anti-inflammatory effects (10). It was revealed that, the ACE2/Ang1-7/Mas axis, may be downregulated in COVID-19 infection due to eliminating ACE2 expressing cells by virus. This issue may cause the over expression of ACE/Ang II/$AT_1R$ pathway (11). Since angiotensin II receptor blockers, ACE inhibitors, and mineralocorticoid receptor antagonists overexpressed the ACE2 receptor, it has been thought that these drugs can lessen the severity of the disease and cause ACE2/Ang1-7/Mas axis upregulation. These properties associated with beneficial effects on lung function. Therefore, these drugs should not be withheld during COVID-19 (12).

### Inflammation

SARS-CoV-2 infection can induce cytokine storm via different mechanisms. The activation of Ang II, which promotes production of pro-inflammatory

cytokines such as IL-6 and TNF-alpha causing an influx of inflammatory cells to the infected sites results in vascular injury, fibrosis and even thrombosis (13). In addition, SARS-CoV-2 infection can induce production of ROS, which stimulates the synthesis of NF-κB (14). This usually results in increment of cytokines and the cytokine storm (15). On the other hand, the role of inflammation in HTN has been investigated. It seems that systemic inflammation may cause arterial stiffness associated with elevating blood pressure until the rage of HTN (16). In fact, oxidative stress alongside chronic inflammation causes changing the arterial walls, increase in intima-media thickness, and endothelial dysfunction (17).

It was shown that endothelial dysfunction may be associated with essential HTN (18) and severe endothelial injury in the severe COVID-19 (19). It seems that endothelial dysfunction resulted from HTN, may exacerbate COVID-19 symptoms in patients with HTN; also, and in some patients without HTN, endothelial dysfunction resulted from COVID-19 infection may develop HTN in near future.

**Hypertension: a risk factor for COVID19 or its consequence?**

The endothelial dysfunction caused by HTN may influence the outcome of COVID-19. In the evaluation of newly onset HTN in COVID-19, there are many of studies that supported this concept. In a study in late 2021 on 211 COVID-19 patients, new onset HTN was seen in 18 patients during a 30-day follow-up (20). In another study by Chen et al. (4) on 366 patients, new onset HTN was observed in 190 patients without history of HTN, with high levels of Ang II and cardiac troponin. In addition, Bekbossynova et al. (21) observed a case of COVID-19 that was manifested as sudden HTN. However, conflicting results observed in a cohort study in China on more than 1,700 COVID-19 patients with a six months follow-up, without reports of newly diagnosed HTN (7).

According to our explorations, there is a close relationship between HTN and COVID-19 infection. Each of them can induce and exacerbate the other one; although, more studies are needed to investigate new onset HTN after COVID-19.

**How should we battle?**

It was suggested that the mortality rate is similar in adjusted model analysis, in the context of beta blocker, ACEIs or ARBs consumption in COVID-19 patients (22). Furthermore, large scale studies reduced the uncertainties in the context of medication controversies in COVID-19 patients with HTN; however, further cohort studies are needed to confirm this hypothesis.

## Conclusion

According to our explorations, there is a close association between HTN and COVID-19 infection. Each of them can induce and exacerbate the other one; although, to have a better insight, more studies are needed to investigate new onset HTN after COVID-19.

## Acknowledgments

There is no financial support and conflict of interest in this study.

## Authors' Contributions

M.B., M.V.; Contributed to conception and design. M.A.S., K.R.; Drafted the manuscript, which was revised by M.B. and M.V. All authors read and approved the final manuscript.

## References

1. Available from: https://covid19. who.int/ (13 May 2022).
2. Shahrbaf MA, Hassan M, Vosough M. COVID-19 and Hygiene Hypothesis: increment of the Inflammatory Bowel Diseases in next generation? Expert Rev Gastroenterol Hepatol. 2022; 16(1): 1-3.
3. Savoia C, Volpe M, Kreutz R. Hypertension, a moving target in COVID-19: current views and perspectives. Circ Res. 2021; 128(7): 1062-1079.
4. Chen G, Li X, Gong Z, Xia H, Wang Y, Wang X, et al. Hypertension as a sequela in patients of SARS-CoV-2 infection. PLoS One. 2021; 16(4): e0250815.
5. Weber T, Amar J, de Backer T, Burkard T, van der Giet M, Gosse P, et al. Covid-19 associated reduction in hypertension-related diagnostic and therapeutic procedures in Excellence Centers of the European Society of Hypertension. Blood Press. 2022; 31(1): 71-79.
6. Burnier M, Kjeldsen SE, Narkiewicz K, Egan B, Kreutz R. Hypertension management during the COVID-19 pandemic: what can we learn for the future? Blood Press. 2022; 31(1): 47-49.
7. Huang C, Huang L, Wang Y, Li X, Ren L, Gu X, et al. 6-month consequences of COVID-19 in patients discharged from hospital: a cohort study. Lancet. 2021; 397(10270): 220-232.
8. Yang J, Petitjean SJL, Koehler M, Zhang Q, Dumitru AC, Chen W, et al. Molecular interaction and inhibition of SARS-CoV-2 binding to the ACE2 receptor. Nat Commun. 2020; 11(1): 4541.
9. Benigni A, Cassis P, Remuzzi G. Angiotensin II revisited: new roles in inflammation, immunology and aging. EMBO Mol Med. 2010; 2(7): 247-257.
10. Capettini LS, Montecucco F, Mach F, Stergiopulos N, Santos RA, da Silva RF. Role of renin-angiotensin system in inflammation, immunity and aging. Curr Pharm Des. 2012; 18(7): 963-970.
11. Issa H, Eid AH, Berry B, Takhviji V, Khosravi A, Mantash S, et al. Combination of angiotensin (1-7) agonists and convalescent plasma as a new strategy to overcome angiotensin converting enzyme 2 (ACE2) inhibition for the treatment of COVID-19. Front Med (Lausanne). 2021; 8: 620990.
12. Brojakowska A, Narula J, Shimony R, Bander J. Clinical implications of SARS-CoV-2 interaction with renin angiotensin system: JACC review topic of the week. J Am Coll Cardiol. 2020; 75(24): 3085-3095.
13. Tay MZ, Poh CM, Rénia L, MacAry PA, Ng LFP. The trinity of COVID-19: immunity, inflammation and intervention. Nat Rev Immunol. 2020; 20(6): 363-374.
14. Shahriari-Felordi M, Alikhani HK, Hashemian SM, Hassan M, Vosough M. Mini review ATF4 and GRP78 as novel molecular targets in ER-Stress modulation for critical COVID-19 patients. Mol Biol Rep. 2022: 1-5.
15. Bhaskar S, Sinha A, Banach M, Mittoo S, Weissert R, Kass JS,

et al. Cytokine storm in COVID-19-immunopathological mechanisms, clinical considerations, and therapeutic approaches: the REPROGRAM consortium position paper. Front Immunol. 2020; 11: 1648.
16. Tomiyama H, Shiina K, Matsumoto-Nakano C, Ninomiya T, Komatsu S, Kimura K, et al. The contribution of inflammation to the development of hypertension mediated by increased arterial stiffness. J Am Heart Assoc. 2017; 6(7): e005729.
17. Castellon X, Bogdanova V. Chronic inflammatory diseases and endothelial dysfunction. Aging Dis. 2016; 7(1): 81-89.
18. Faulkner JL, Belin de Chantemèle EJ. Mineralocorticoid receptor and endothelial dysfunction in hypertension. Curr Hypertens Rep. 2019; 21(10): 78.
19. Ruhl L, Pink I, Kühne JF, Beushausen K, Keil J, Christoph S, et al. Endothelial dysfunction contributes to severe COVID-19 in combination with dysregulated lymphocyte responses and cytokine networks. Signal Transduct Target Ther. 2021; 6(1): 418.
20. Akpek M. Does COVID-19 cause hypertension? Angiology. 2022; 73(7): 682-687.
21. Bekbossynova M, Ainur T. Hypertension as a manifestation of COVID-19 pneumonia. Clin Case Rep. 2021; 9(9): e04720.
22. Tadic M, Saeed S, Grassi G, Taddei S, Mancia G, Cuspidi C. Hypertension and COVID-19: ongoing controversies. Front Cardiovasc Med. 2021; 8: 639222.